DESIGN AND ANALYSIS OF WIRELESS DIVERSITY SYSTEMS

ZHANG SONGHUA

NATIONAL UNIVERSITY OF SINGAPORE

2004

DESIGN AND ANALYSIS OF WIRELESS DIVERSITY SYSTEMS

ZHANG SONGHUA

(*B. Eng., Huazhong University of Science and Technology*)

A THESIS SUBMITTED

FOR THE DEGREE OF DOCTOR OF PHILOSOPHY

DEPARTMENT OF ELECTRICAL AND COMPUTER ENGINEERING

NATIONAL UNIVERSITY OF SINGAPORE

2004

Acknowledgement

I would like to express my gratitude to Professor Kam Pooi Yuen, my principal supervisor, and Professor Paul Ho, my co-supervisor, for their guidance, support and advice over the entire study. I have received much encouragement and stimulation from them to work in the area of research. Their knowledge and insight has inspired many of the ideas expressed in this thesis, and their efforts and patience in revising the drafts are much appreciated.

Special thanks to all my friends who have helped me in one way or another, for their advice, help and tolerance, especially my colleagues in ECE-I2R lab who have made my study here an enjoyable experience.

The support of National University of Singapore is highly appreciated.

To my dearest fiancée, Hao Ping, my mother, my father and my sister, for their everlasting love and support, I dedicate this thesis.

Contents

List of figures and tables

Abbreviations and notations

AWGN: Additive White Gaussian Noise

BEP: Bit Error Probability

BTRC: Better Than Raised Cosine (pulse)

CCI: Cochannel Interference

cdf: cumulative distribution function

CF: Characteristic Function

CGRV: Complex Gaussian Random Variable (Vector)

CSI: Channel State Information

FSK: Frequency Shift-Keying

iid: independent identically distributed

INR: Interference-to-Noise Ratio

IO: Individually Optimum

ISI: Inter-Symbol-Interference

JO: Jointly Optimum

LRT: Likelihood Ratio Test

MGF: Moment Generation Function

ML: Maximum Likelihood

MRC: Maximum Ratio Combining

MRT: Maximum Ratio Transmission

OC: Optimum Combining

pdf: probability density function

PDR: Pilot (power) to Data (power) Ratio

PEP: Pairwise Error Probability

PSAM: Pilot Symbol Assisted Modulation

- IPSAM: Implicit PSAM

PSD: Power Spectrum Density

PSK: Phase-Shift-Keying

- BPSK: Binary PSK
- CPSK: Coherent PSK
- QPSK: Quaternary PSK
- DPSK: Differential PSK
- BDPSK: Binary DPSK
- QDPSK: Quaternary DPSK

QR: Quadratic Receiver

- GQR: Generalized QR

RC: Raised Cosine (pulse)

REC: Rectangular (pulse)

Rx: Receive (diversity)

SEP: Symbol Error Probability

SINR: Signal-plus-Interference-to-Noise Ratio

SIR: Signal-to-Interference Ratio

SNR: Signal-to-Noise Ratio

Tx: Transmit (diversity)

Through out this thesis, we will use upper case boldface to represent matrix and lower case boldface to represent vector. All vectors are assumed to be column vectors unless otherwise specified.

Summary

It has been recognized that spatial diversity using multiple antennas is an efficient technique to combat the severe destructive effects of fading and interference on the performance of mobile wireless communication system. Previous works on cochannel interference normally assume that the interfering signals are synchronized with the desired signal. In the first half of this thesis we examine the more general and realistic scenario where the cochannel interference is asynchronous with the desired signal. In Chapter 2 and Chapter 3, we investigate the performance of coherent phase-shift-keying and differentially encoded and decoded phase-shift-keying with maximum-ratio-combining in nonselective Rayleigh fading channels with multiple asynchronous cochannel interferers. Through the analytical study of the effect of the timing offsets between the interferer's signal and the desired user's signal on the error performance, it is found that for system using rectangular pulse shaping, the synchronized model actually gives the worst error performance, while the best error performance is achieved when all the interferers' signals are half-symbol-duration delayed with respect to the desired user's signal. The second half of this thesis examines the performance of transmit diversity system with practical channel estimation schemes. Two types of the transmit diversity are considered in this thesis. In Chapter 4 we develop a pilot-symbol-assisted-modulation scheme for a maximum-ratio-transmission based transmit diversity system. Optimum transmit and receive strategies are derived and error performance are examined. In Chapter 5 we consider space-time block codes with orthogonal M-ary frequency-shift-keying. The error performance is examined and compared with that of differential space-time codes.

Chapter 1

Introduction

1. 1 Background

During the past few decades, the development of modern mobile communication systems has experienced a blooming era [1-3]. Many new technologies are developed and implemented to improve the quality of personal wireless communications. Stepping into the new century, mobile communication has already become an indispensable element in our fast paced modern life. New wireless mobile communication systems are expected to support more users and provide better quality of service for both voice and data applications.

A primary design objective for any commercial or military mobile communication system is to conserve the available spectrum by reusing allocated frequency channels. For this purpose, cellular systems are widely used in wireless communication networks which divide a geographical area into small cells and allow each cell to utilize specific allocated frequency channels. The same frequency channel could then be reused in other cells that are far away from a given cell so that the signal from the cochannel cells to the cell concerned would be weak enough to avoid any destructive interference. However, as the number of subscribers increases, either the size of the cell needs to be reduced or the number of the assigned frequency channels in each cell needs to be increased in order to keep up with the increased subscriber density. Therefore, with the number of the total available channels fixed, the

interference from cochannel cells could increase to a level that may cause destructive effects on communication in the concerned cell.

Another important issue in wireless mobile communication is to efficiently detect the signal that has been corrupted from channel fading. Unlike the conventional wired communication system where the received signal normally only suffers from additive white Gaussian noise (AWGN), in a wireless environment the received signal is typically a combination of many reflected replicas of the original transmitted signal with different power, delay and direction of arrival. Consequently, on top of the AWGN, wireless communication system suffers from multiplicative random amplitude attenuation and phase distortion, a phenomenon known as channel fading. Thus, developing new techniques that could reduce the severe impairment caused by channel fading is always of great importance for any practical design of high quality wireless communication system.

Among the numerous innovative wireless communication techniques, spatial diversity reception using multiple antennas is always a significant research area that has been shown to lead to tremendous improvements in system performance. In a system where multiple antennas are deployed sufficiently far from one another spatially, the received signal from these antennas can be viewed as undergoing independent channel fading process. Since deep fades seldom occur simultaneously during the same time intervals on these independent diversity branches, the effect of fading can be reduced by properly weighting and combining the received signal from these branches.

Various diversity combining schemes have been proposed in the past, varying in performance and complexity. For a system suffering only from fading and AWGN, maximum ratio combining (MRC) has been known as the optimum combining scheme

which gives the received signals from different diversity branches a weight proportional to the instantaneous channel gain of that particular branch, therefore the instantaneous signal-to-noise ratio (SNR) is maximized and the probability of error is minimized. In another case, selection combining (SC) only chooses the branch that has the largest instantaneous SNR and detects the signal based on observation from this one branch only. Although worse in performance when compared with MRC, SC only processes one diversity branch at a time and therefore the receiver structure is simpler. Besides combating fading, diversity technique can also suppress interference. For example, for systems suffering from fading, AWGN as well as cochannel interference (CCI), optimum combining (OC) is proposed to mitigate the effects of both the fading and the CCI.

In addition to diversity reception, diversity transmission has also been considered as an effective technique to improve the system performance. According to the required channel information at the transmitter, transmit diversity can be categorized into two forms – schemes that require feedback and those do not require feedback. For the first type of transmit diversity, the transmitter requires the knowledge of instantaneous channel gain so it can pre-weight the signal to compensate for the fading in the same way as a conventional diversity receiver. For the second type of the transmit diversity, channel information is only available at the receiver, and the transmitter use linear processing to spread the information across the antennas, which could also be viewed as a form of coding. One of the most-pursued form of the second type transmit diversity is space-time coding.

In general, spatial diversity is an efficient method to improve the performance of wireless mobile communication.

1. 2 Motivation

As mentioned earlier, current and future generation wireless communication are expected to support more subscribers and offer higher transmission data rate, or, in other word, higher system capacity. Therefore, cochannel interference has become an important issue that must be considered in the design of practical communication systems. Diversity systems have been shown to be an efficient method to mitigate the destructive effect of fading and interference. However, the efficiency of a practical diversity system to suppress the interference depends on the available amount of information regarding the interferers' channel information. Optimum combining has been proposed and proven to be efficient in suppressing cochannel interference, but it follows a simplified and somewhat an unrealistic assumption that the system has full channel knowledge for all the users and the signals of different users are symbol synchronized. For a more general and practical situation where the different users are asynchronous, optimum combining is no longer implementable. For other types of diversity combining schemes such as MRC, little has been done on the performance analysis for the case with asynchronous CCI. Therefore it is necessary to fully understand the effects of asynchronous CCI on performance of these systems.

More recently, much research efforts have been given to the design and analysis of new diversity schemes that offer lower error probability and higher capacity, one of which is the use of multiple antennas at the transmitter side in addition to conventional diversity at the receiver side. One potential of a combined transmit and receive (Tx-Rx) diversity system is that with the same number of antennas utilized by the system, a Tx-Rx diversity structure generally provides more transmission links than a conventional receive diversity. As mentioned earlier, there are generally two form of transmit diversity. One way is to provide the transmitter with prior-

transmission channel information, so that the transmitter could use different weights on different transmit antennas to pre-compensate for the channel fading. The optimal scheme of this type of Tx-Rx diversity is known as maximum ratio transmission plus maximum ratio combining (MRT-MRC) diversity. In most of the previous works on the performance analysis of such Tx-Rx diversity systems, a basic assumption is that the system has complete knowledge of the instantaneous channel gain. Consequently, the error performance results obtained in these works can only be viewed as lower bounds. To provide designers with more realistic results, it is important to consider more practical channel estimation strategies for Tx-Rx diversity systems, and examine their performance in the presence of channel estimation errors. Also with imperfect channel estimation, the optimum structure of this type of the transmit-receive diversity may also assume a different form other than MRT-MRC. This is an optimum design problem that worth investigating.

Another form of Tx-Rx diversity is to use space-time (ST) codes. Space-time trellis coding is a recent proposal that combines signal processing at the receiver with coding techniques appropriate to multiple transmit antennas. It has been shown that specific space-time trellis codes perform extremely well in slow-fading environment. However, the decoding complexity of space-time trellis codes increases exponentially with transmission rate. Recently, Alamouti discovered a remarkable scheme for transmission using two transmit antennas which requires much less decoding complexity. Following Alamouti's work, orthogonal space-time block codes are developed which utilize signal processing and coding technology to achieve diversity gain from both the spatially separated antennas and orthogonal codes transmitted on these antennas. Comparing with MRT-MRC diversity, space-time codes do not need any prior-transmission channel information at the transmitter. Thus, no feed back is

required for this system. However, the channel estimation at the receiver end still needs to be carefully examined.

For any communication systems undergoing fading, in order to detect the transmitted signal from the multiplicative fading corruption, certain channel estimation schemes must be employed. One popular channel estimation method is to insert pilot symbols periodically into the data symbol to continuously sample the channel and produce channel estimation for data symbol detection. Alternatively, the system can also employ a non-coherent modulation scheme such as differential encoded and decoded PSK, where the information is embedded in the phase difference of the adjacent symbols and the detection is accomplished by using the channel's memory. Although a differential system provides a simple and robust solution for data detection in fading channels, when the channel fading fluctuates fast, or, in other words, when the channel memory is short, its performance degrades fast as well. On the other hand, orthogonal signaling – another commonly considered "non-coherent" signal - has been shown [4] as a modulation scheme that possess a channel measurement component. In light of this fact, the channel estimation can be refined by exploiting the fading autocorrelation through a sequence of received symbols. This encourage us to use orthogonal signaling in transmit diversity system and compare its performance with coherent signaling and also differential system.

1. 3 Literature Review

The concept and fundamental performance analysis of diversity system are well documented in papers and books such as [2], [3,] [5,] [6]. It has been shown that in general MRC receiver provides the optimum performance by maximizing the

instantaneous SNR. However, most of these fundamental analyses concern only independent diversity systems with quasi-static fading and without CCI.

For fluctuating fading channels, the performance of coherent PSK signal remains the same as that of quasi-static fading channels because perfect channel estimation is assumed. However, for differentially encoded and detected PSK signals, the fading fluctuation plays an important role in the error performance as the differential detector relies solely on the channel autocorrelation to recover from the fading distortion. Although the performance of DPSK suffers from channel fading fluctuation, it requires no channel estimation mechanism, and thus the receiver structure can be very simple, whereas for coherent PSK, certain channel estimation scheme such as PSAM must be utilized to provide channel reference for coherent detection. The performance of DPSK signal in fluctuating fading channels is evaluated in [7] with selection combining. In [8], [9], the BEP of MDPSK is studied for fluctuating nonselective Rayleigh fading channels with MRC reception. For the Rician fading case, the exact BEP of MDPSK and NCFSK is given in [10], where an MGF based method is adopted. In [11], the same modulation schemes are considered and closed-form expressions for the SEP are obtained with post-detection equal gain combining. A simplified tight bound for the similar case can be found in [12]. In [13], [14], generalization of diversity combining scheme and optimization of the receiver structure for DPSK signaling are discussed when the fading statistics are known at the receiver, and the BEP performances are given correspondingly. More recently, with the work in [15] on calculating the error probability for two-dimensional signal constellations, new mathematical tools involving the Gaussian probability integral and Marcum Q-function are developed [16], [17]. These advancements in mathematical analysis tools and techniques make it possible to evaluate the error performance of

linearly modulated signals over generalized fading channels under a unified analytical framework [18]. However, most of the results from this approach are in complicated forms involving numerical integrals, where the effects of individual system parameters are difficult to examine.

For a cellular system with CCI, MRC no longer provides the optimum performance because only the fading of the desired user is taken into consideration and compensated for by MRC. Therefore, more research interests have been given to OC which exploits the CSI of the CCI component as well. Compared to MRC, OC has been shown to be more effective in suppressing interference [19]-[23]. Although excellent in performance, the practicality of OC is somehow questionable, as in reality it is very difficult to obtain the required CSI for both the desired user and the CCI. In most cases, MRC remains a more practical choice even for systems with CCI [24]. Most of the previous works model CCI as a signal synchronized with the desired signal [24]-[28], which is mathematically simpler in derivation and analysis, but practically hard to realize on the other hand. Among the work that considers asynchronous CCI, the characterization of asynchronous CCI can be found in [29], and its application to the performance analysis can be found in [30], [31] for coherent PSK and DPSK, respectively. The error performance of BPSK communication links with multiple asynchronous interferers is studied in [32] and its counterpart of DPSK system is given in [33], in which exact error probabilities are derived for single channel system, i.e., either non-diversity or diversity with selection combining. More recently, results for the performance of BPSK in Nakagami fading channels with asynchronous CCI is reported in [34]. Again, the approach in this work is currently limited to single channel systems, and the form of the BEP results is very complicated. For selection combining diversity system, BEP expressions of both CPSK and DPSK are given in [35]. In [36],

performance of MPSK with dual-diversity system using equal gain combining (EGC) and selection combining (SC) is studied. However, the extension of the approach to higher order diversity combining is not addressed. In [37] a general methodology for performance analysis of a system with asynchronous CCI is provided. Some new methods for evaluating the outage probability are proposed. However, the BEP analysis in their work could only be carried out using a semianalytical method which requires the help of adaptive algorithm simulation. Another interesting perspective to the CCI related research is its similarity with multiuser detection where the data detection is performed for all the cochannel users [38]. By applying the concept of multiuser detection in the CCI scenario, the work in [39], [40] has shown that a great performance improvement can be achieved over the popular OC. However, exact error performance analysis for multiuser detection remains rare. More recently, research interest has been drawn to the exact performance analysis of optimum detection for signals in the presence of cochannel interference [41]-[43], where the exact BEP for a two-user system is studied using joint-optimum (JO) (one-shot) detection. The analysis for individually-optimum (IO) (minimum error probability) remains unsolved in these works but the performance difference has been shown to be very slim for most of the commonly considered system conditions.

For transmit diversity systems assuming channel information at the transmitter side, the concept of MRT has been summarized and studied in [44]. The optimization of transmit and receive weight vectors is carried out so as to maximize the instantaneous SNR, assuming equal energies for all the entries of the receive weight vector but different phase. An approximate expression for the bit error probability (BEP) of binary phase-shift-keying (BPSK) is also obtained for the high SNR scenario. In [45], [46], improved weighting schemes are suggested which remove the

performance degradation due to the equal-energy assumption in [44]. The joint optimal weighting scheme at both the transmitter and the receiver is derived in [47], which relates the error performance analysis with the distribution of the eigenvalues of a complex Wishart matrix. The exact error performance of this optimal transmit-receive diversity system in Rayleigh fading has been studied in [48], assuming perfect CSI. In [49], the distribution of the eigenvalues of a non-central complex Wishart matrix is analyzed and the outage probability for the optimal transmit-receive diversity system is studied. This enables the performance analysis of Tx-Rx diversity systems in a Rician fading environment to be studied. Among these previous works regarding Tx-Rx diversity system, one important assumption is that perfect CSI must be available at both the transmitter and the receiver. Thus the performance analysis results obtained so far are only lower bound benchmarks which could not be achieved in a reality. Therefore, to make Tx-Rx diversity a more realizable communication technique, it is important to design a practical channel estimation scheme with the optimal transmitter/receiver structure, and study the effect of channel estimation error on the system performance.

Another form of transmit diversity as introduced earlier is space-time codes. The systematic design procedure together with performance analysis regarding Space-Time block coding can be found in [50], [51]. The performance of specific Space-Time trellis codes has been shown to perform extremely well in slow-fading environment [50]. However, the decoding complexity of this type of codes increases exponentially with transmission rate. A simple scheme using two transmit antennas is proposed in [52]. Despite a certain performance loss compared to the trellis codes in [50], this scheme offers fairly good performance and simple decoding at the same time. Later this simple scheme is extended to multiple transmit antennas in [53] using the theory

of orthogonal designs. Although excellent in performance, practical implement of these codes requires certain channel estimation scheme such as PSAM [51], or noncoherent detection such as differential detection [54], [67], [68].

1. 4 Contributions of the Thesis

This thesis provides error performance analysis for diversity systems and also develop optimum system structure for transmit diversity system with practical channel estimation schemes.

For the conventional Rx-diversity receiver, we study its error performance when asynchronous cochannel interference is presented. We consider two extreme conditions regarding the knowledge of channel information of the desired user's signal at the receiver, i.e., perfect channel estimation for coherent PSK, and no channel estimation for differential PSK. By conditioning on the timing offsets of the interferers, we derive error performance results that enable us to examine the effect of asynchronous CCI on the performance of the desired signal. Study reveals that the synchronous system is actually the worst case as far as error performance is concerned, while the best case for the detection of the desired signal is that all the interfering signals are half symbol-duration delayed. Therefore, for scientists and engineers who need to design a communication system based on the worst case design, our results provide a quick performance assessment to spare them from having to average the error probability over all the interfering signals' timing offsets.

For a MRT-MRC type diversity system, we develop a practical channel estimation scheme using pilot-symbols-assisted-modulation (PSAM). Based on this particular PSAM scheme, we derive the optimum transmit and receive weighting strategy and study its performance. The optimization of various parameters related to

PSAM is also demonstrated. We then extend the proposed PSAM Tx-Rx diversity system to binary orthogonal signaling, and discuss the feasibility of using the sequence observation to refine the channel estimation from the unmodulated component. We also compare our proposed PSAM Tx-Rx diversity with ideal MRT-MRC diversity where the cause of the performance difference is carefully examined. These results give practical system designers a good reference when considering employing MRT-MRC diversity in reality.

For transmit diversity using space-time codes, we develop an orthogonal FSK modulation-based Alamouti-type code. Channel estimation is done by the unmodulated component of the orthogonal signals. The performance of this ST-FSK system is then analytically examined and compared with that of differential ST codes. It shows that by exploiting the channel measurements from adjacent symbols, FSK signals provide much better performance than their differential counterparts when the channel fading fluctuation is “fast”.

In summary, this work provides a comprehensive performance analysis for digital modulations in diversity systems by considering the effects of various practical issues in wireless mobile communications on error performance, namely, channel fading fluctuation, asynchronous CCI and imperfect channel estimation. Also it discusses the optimization problem for transmit diversity systems with practical channel estimation schemes.

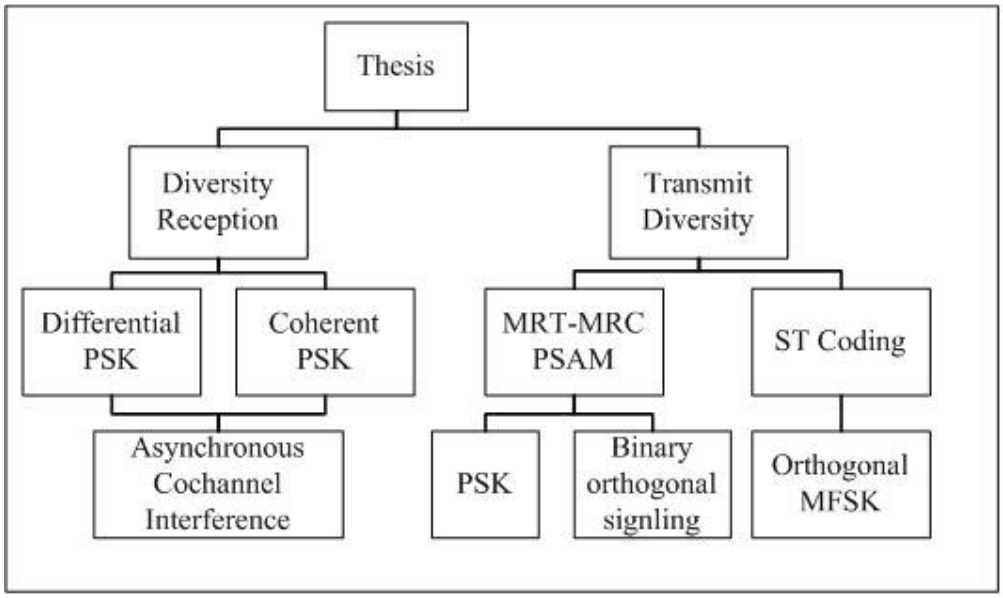

Figure 1.1 Thesis structure

1. 5 Thesis Outline

Chapter 2 presents the performance analysis of CPSK in nonselective Rayleigh fading channels with MRC reception and multiple asynchronous CCI. The effect of the CCI timing offset is also examined. Three Nyquist pulses are considered, namely, the rectangular pulse, conventional RC pulse and the newly proposed BTRC pulse.

Chapter 3 presents the performance analysis of DPSK in nonselective Rayleigh fading channels with MRC reception and multiple asynchronous CCI. Although the approach in Chapter2 is applicable for this case, we adopt a different mathematical method for this case which demonstrates the effect of diversity branch correlation. The effects of the CCI timing offset are also examined. Similar as CPSK case, we also compare the performance of three different Nyquist pulses.

Chapter 4 describes a practical PSAM channel estimation scheme for Tx-Rx diversity system and derives the optimum transmitter/receiver structure for this particular system. Performance analysis is then given based on the optimum design.

Both PSK and binary orthogonal signaling are considered. By applying the ML detection principle, we find that the optimum transceiver structure for PSAM based PSK system remains similar to that derived for ideal coherent PSK system. However, for binary orthogonal signaling, the transceiver utilizes both the estimated CSI from PSAM and that from its own unmodulated component, which is different from what has been obtained by other previous work. An attempt of combing the proposed PSAM scheme with the generalized quadratic receiver (GQR) is given, where only sub-optimal solution is obtainable currently.

Chapter 5 develops another type of transmit diversity using space-time coding with orthogonal signaling. It is shown this new modulation scheme enables channel reference without pilot symbols, thus no transmission rate is sacrificed. And the detection complexity is no more than that of differential ST coding, while the performance of this proposed system does not suffer severely from “fast” fading as a differential system does.

Chapter 6 gives some conclusions for the results obtained and suggests some possible future extension from the current research.

Chapter 2

BEP of Coherent Phase-Shift-Keying in Nonselective Rayleigh Fading Channels with Multiple Asynchronous Cochannel Interference

In this chapter we investigate the error performance of BPSK and QPSK in nonselective Rayleigh fading channels with MRC diversity reception and with multiple asynchronous cochannel interferers. An introduction is given in Section 2.1. The system model is described in Section 2.2 together with the detector structure. In Section 2.3 we carry out the performance analysis. In Section 2.4 we study the effect of the asynchronous interferers' timing offset on the BEP of the desired signal. Numerical results and discussion are given in Section 2.5, and Section 2.6 summarizes this chapter.

2. 1 Introduction

In cellular mobile communications, frequency reuse is necessary to increase spectral efficiency so as to accommodate more subscribers. In such a system, the detection of one user's data is often corrupted by signals from users in other nearby cells using the same frequency. This will result in cochannel interference, which inevitably leads to degradation in the performance of wireless communications. In addition to interference, fading is also a major source of performance impairment in a

mobile wireless environment. The channel fading process introduces both random amplitude and random phase distortion to the transmitted signal. Therefore, channel estimation has to be carried out in order to implement coherent detection for modulation schemes for which accurate phase tracking is crucial, such as PSK.

2. 2 System Model

We consider a system in which the MPSK signal received from the desired user over L independent, identical diversity branches is corrupted by K asynchronous cochannel users' signal and AWGN. The complex baseband transmitted signal of the desired user is

$$\tilde{s}_D(t) = \sqrt{E_{SD}} \sum_{p=-\infty}^{p=\infty} e^{j\phi_D(p)} g_{TD}(t - pT) \tag{2.1}$$

where $1/T$ is the symbol transmission rate and $g_{TD}(t)$ denotes the impulse response of the transmitter pulse shaping filter of the desired user. The average energy per symbol for the desired user is E_{SD}. The phase $\phi_D(k)$ of the transmitted signal contains the kth transmitted symbol information. A reasonable assumption is that all interfering signals have the same modulation format as the desired user's signal. Thus the baseband transmitted signal of the lth interfering user has the similar form

$$\tilde{s}_l(t) = \sqrt{E_{Sl}} \sum_{p=-\infty}^{p=\infty} e^{j\phi_l(p)} g_{Tl}(t - pT) \tag{2.2}$$

where E_{Sl} is the average energy per symbol for the lth interfering user signal. We further assume that all the users use the same transmit pulse shaping filter. Consequently, we have $g_{Tl}(t) = g_T(t)$ for $l = D,1,2,\cdots,K$.

We assume that both the desired user's signal and the interfering users' signal undergo slow nonselective Rayleigh fading. At the receiver, the received signal from the *i*th diversity branch is

$$\tilde{r}_i(t) = \tilde{c}_{D,i}(t)\tilde{s}_D(t) + \sum_{l=1}^{K} \tilde{c}_{l,i}(t+\tau_l)\tilde{s}_l(t+\tau_l) + \tilde{n}_i(t) \tag{2.3}$$

where $\tilde{c}_{D,i}(t)$ and $\tilde{c}_{l,i}(t)$ are the channel fading process of the *i*th diversity channel for the desired user and the *l*th interfering user respectively. The AWGN term $\tilde{n}_i(t)$ has zero mean and a double side PSD of N_0. At the receiver, the received signals are matched filtered and sampled at the symbol time of the desired user signal, assuming perfect symbol synchronization with the desired user's symbol time. As we assume in general an asynchronous system, the *l*th interfering user's signal may come after an arbitrary delay τ_l which is uniformly distributed within $[0,T)$. After matched filtering and sampling, the discrete received signal at the input of the detector over the *i*th diversity channel, *i*=1,…,*L*, for the *k*th symbol interval [*k*T,(*k*+1)*T*] can be represented by a decision statistic $\tilde{r}_i(k)$ as [3, Sec9.2]

$$\begin{aligned}\tilde{r}_i(k) = &\sum_{p=-\infty}^{\infty} \sqrt{E_{SD}}\, e^{j\phi_D(k-p)} \int \tilde{c}_{D,i}(\tau + pT) g_T(\tau) g_R(kT - pT - \tau) d\tau + \tilde{n}_i(k) \\ &+ \sum_{l=1}^{K} \sum_{p=-\infty}^{\infty} \sqrt{E_{Sl}}\, e^{j\phi_l(k-p)} \int \tilde{c}_{l,i}(\tau + pT + \tau_l) g_T(\tau_l) g_R(kT - pT - \tau - \tau_l) d\tau\end{aligned} \tag{2.4}$$

Here $g_R(t)$ is the receive filter matched to the transmit filter such that the overall cascaded impulse response $g(t) = g_R(t) * g_T(t)$ without fading would be a pulse shape that fulfils the Nyquist criterion. Since $g_T(t)$ is a unit-energy pulse, the peak amplitude of $g_T(t)$ is 1. The received signal in a form like (2.4) is generally difficult to manage because of the integral terms. Therefore, we make a commonly adopted assumption that the fading processes affecting the desired and interfering signals

change slowly enough so that they can be considered as constant during the effective length of the impulse response $g_R(t)$ and $g_T(t)$. Thus the fading process inside the integrand of (2.4) could be approximated by its instantaneous value at the sampling time and could be factored out of the integral. The received signal at the detector input can now be written as,

$$\tilde{r}_i(k) = \sqrt{E_{SD}} e^{j\phi_D(k-p)} \tilde{c}_{D,i}(k) + \sum_{l=1}^{K} \sqrt{E_{Sl}} \tilde{c}_{l,i}(k) \sum_{p=-P}^{p=P} e^{j\phi_l(k-p)} g(-pT - \tau_l) + \tilde{n}_i(k) \qquad (2.5)$$

where $\tilde{c}_{D,i}(k)$ and $\tilde{c}_{l,i}(k)$ are the piecewise-constant approximations to the *i*th channel fading process during the *k*th symbol interval [*k*T, (*k*+1)*T*] for the desired user and the *l*th interfering user, respectively. It is obvious that in the presence of a non-zero symbol timing offset τ_l, the effective interfering component comes from a sequence of transmitted symbols in a similar form as ISI. Since in general the Nyquist pulse shaping used in practical communication system has a fast decaying waveform, we could assume that the effective ISI components are composed of the nearest $2P+1$ symbols. For the case of nonselective Rayleigh fading channels with even power density spectrum, $\tilde{c}_{D,i}(k)$ and $\tilde{c}_{l,i}(k)$ are both complex Gaussian random variables whose quadrature components are iid Gaussian RVs, with mean zero, variances $\frac{1}{2}E[|\tilde{c}_{D,i}(k)|^2] = \sigma_{cD}^2$ and $\frac{1}{2}E[|\tilde{c}_{l,i}(k)|^2] = \sigma_{cl}^2$, respectively. The noise term $\tilde{n}_i(k)$ is the sampled output of the AWGN process after matched filtering from the *i*th diversity branch, which is a complex Gaussian random variable with mean zero and variance $\frac{1}{2}E[|\tilde{n}_i(k)|^2] = N_0/2$.

We consider an independent diversity system where the received signals from the same user at different diversity branches have iid channel fading gains, i.e., for arbitrary $i \neq j$, $\tilde{c}_{l,i}(k)$ and $\tilde{c}_{l,j}(k)$ are iid, for $l = D,1,\cdots,K$. Also, the channel fading

gains for different users are assumed to be independent, either at the same diversity branch or different ones, i.e., $\tilde{c}_{il}(k)$ is independent of $\tilde{c}_{jh}(k)$ for arbitrary $l \neq h$. The noise components $\tilde{n}_i(k)$ from different diversity branches are assumed to be independent and identically distributed, and they are independent from channel fading gains of all the users from all diversity branches.

The overall pulse shape $g(t)$ we consider in this work includes the following three types. The first one is the triangular pulse which corresponds to the response of a matched filter to a rectangular pulse [30], [32]. Its corresponding time function and frequency spectrum of the rectangular pulse shaping are given by

$$g_{REC}(\tau) = \begin{cases} 1 - \dfrac{|\tau|}{T} & |\tau| < T \\ 0 & otherwise \end{cases}$$

and

$$G_{REC}(f) = \frac{4\sin^2(Tf/2)}{Tf^2}.$$

With REC, the received signal in (2.5) could be simplified to

$$\tilde{r}_i(k) = \sqrt{E_{SD}}\, e^{j\phi_d(k)} \tilde{c}_{d,i}(k) + \sum_{l=1}^{K} \sqrt{E_{Sl}}\, \tilde{c}_{l,i}(k) \left[e^{j\phi_l(k-1)} \frac{|\tau_l|}{T} + e^{j\phi_l(k)} \left(1 - \frac{|\tau_l|}{T} \right) \right] + \tilde{n}_i(k) \qquad (2.6)$$

where the effective interference comes from the adjacent two symbols only. The second pulse we considered is the popular RC pulse that has been widely used in modern digital communication systems. The RC pulse's time function and the corresponding frequency spectrum are given by

$$g_{RC}(t) = \frac{\sin(\pi t/T)}{\pi t/T} \cdot \frac{\cos(\pi\alpha t/T)}{1 - 4\alpha^2 t^2/T^2}$$

and

$$G_{RC}(f)=\begin{cases} T & 0\le|f|\le\dfrac{1-\alpha}{2T} \\ T/2\left\{1+\cos\left[\pi T/\alpha\left(|f|-\dfrac{1-\alpha}{T}\right)\right]\right\} & \dfrac{1-\alpha}{2T}\le|f|\le\dfrac{1+\alpha}{2T} \\ 0 & |f|\ge\dfrac{1+\alpha}{2T} \end{cases},$$

where $0\le\alpha\le1$ is the roll-off factor and it represents the percentage excess bandwidth. It is worth noting that through out this work, we do not consider a band-limited system, thus the value of the roll-off factor affect the performance through the shape of the pulses when using different value of α, not through the percentage of the lost bandwidth it represents, i.e., the shape of the received signal is not distorted by loss of side-band frequency components.

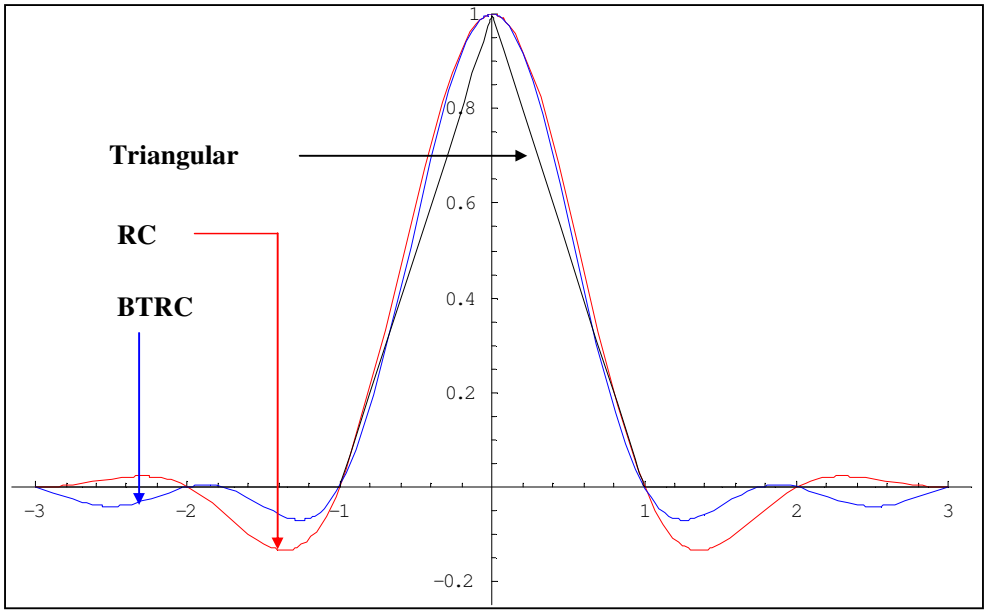

Figure 2.1 A comparison of the time waveform of the three pulses

The third pulse considered in this study is the BTRC pulse that has been proposed recently [55]. Its time function and frequency spectrum are given by,

$$g_{BTRC}(t)=\frac{\sin(\pi t/T)}{\pi t/T}\cdot\frac{4\beta\pi\sin(\pi\alpha t/T)+2\beta^2\cos(\pi\alpha t/T)-\beta^2}{4\pi^2t^2+\beta^2}$$

and

$$G_{BTRC}(f)=\begin{cases} T & 0\le |f|\le \dfrac{1-\alpha}{2T} \\ T\exp\left(\dfrac{2T\ln 2}{\alpha}\left[\dfrac{1-\alpha}{2T}-|f|\right]\right) & \dfrac{1-\alpha}{2T}\le |f|\le \dfrac{1}{2T} \\ T-T\exp\left(\dfrac{2T\ln 2}{\alpha}\left[|f|-\dfrac{1+\alpha}{2T}\right]\right) & \dfrac{1}{2T}\le |f|\le \dfrac{1+\alpha}{2T} \\ 0 & |f|\ge \dfrac{1+\alpha}{2T} \end{cases},$$

where $\beta = 2T\cdot \ln 2/\alpha$ and α is the roll-off factor. This new pulse has been shown to have a better eye diagram and a better error performance than RC pulse in the presence of ISI in a baseband system [55]. A comparison of these three pulses is illustrated in Fig. 2.1, where for the RC and BTRC pulses we use a roll-off factor $\alpha = 0.5$, where for RC pulse and BTRC pulse with the same roll-off factor, we found that BTRC pulse has smaller sidelobes than RC, thus a better performance at the presence of symbol timing error can be anticipated.

In (2.5), the first term represents the desired signal component. The second term represents the CCI components from interfering users and each of these components contains ISI terms due to the imperfect symbol synchronism between the desired user and the interfering users. The third term represents the AWGN noise in each diversity branch.

As mentioned earlier, at the receiver, it is assumed that only the channel fading gains for the desired user is estimated perfectly in each diversity branches. Therefore, a coherent detector is implemented. The received signals from each diversity branch are weighted by the complex conjugate fading gain of the desired user to remove the phase distortion. With equiprobable transmitted symbols, the MRC receiver generates the decision statistics

$$\left\{ q_m(k)=\mathrm{Re}\left[\sum_{i=1}^{L}\tilde{r}_i(k)\tilde{c}_{D,i}{}^{*}(k)\exp(-j2\pi m/M)\right]\right\}_{m=0}^{M-1}$$

based on ML detection principle, and chooses $\phi(k) = 2\pi l/M$ as the detected symbol if $q_l(k) = Max\{q_m(k)\}$. The pre-detection MRC receiver is sketched in Fig. 2.2.

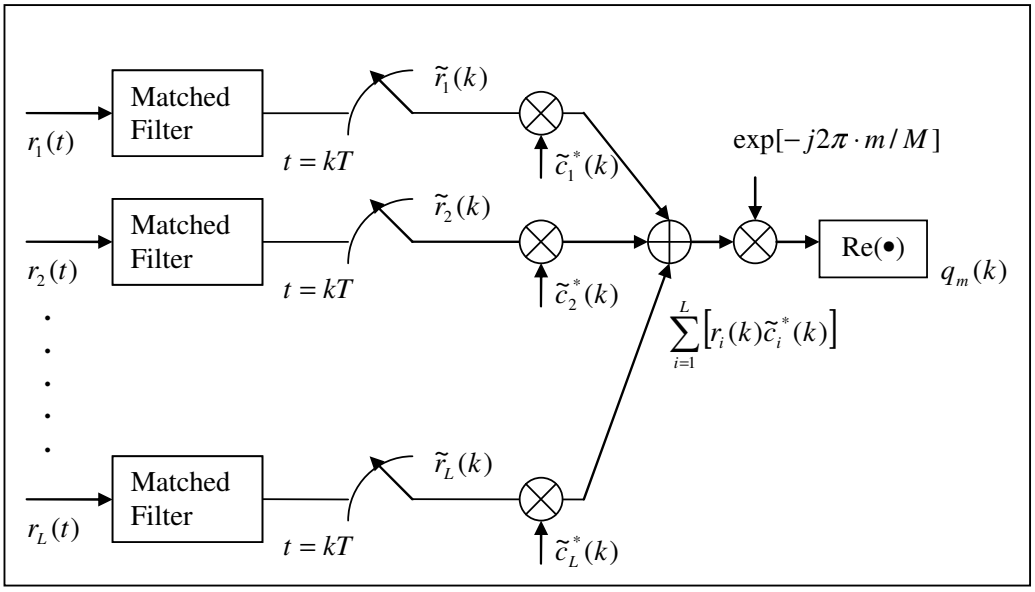

Figure 2.2 Receiver structure for CPSK

2. 3 Performance Analysis

The BEP of BPSK and QPSK, conditioned on the set *I* of known transmitted symbols of all users and known timing offsets of every interfering user can be obtained from the following probability

$$F(\alpha,\phi,\tau) = P\left(\text{Re}\left[\sum_{i=1}^{L}\tilde{r}_i(k)\tilde{c}_{D,i}{}^*(k)e^{j\alpha}\right] < 0 \middle| \{\tau_l, \phi_l(k-p)\}_{l=1,p=-\infty}^{L,\infty} = I\right) \qquad (2.7)$$

where α is one-to-one mapped to the information phase $\phi_D(k)$ in determining the BEP and its specific value will be given later. Note that given the set *I*, the received signal in each diversity branch is a summation of multiple independent complex Gaussian random variables. Therefore, the received signal $\tilde{r}_i(k)|I$ is also a complex Gaussian random variable with conditional mean

$$E[\tilde{r}_i(k)|I] = 0,$$

(2.8a)

conditional variance

$$\sigma_r^2 = \frac{1}{2}E[|\tilde{r}_i(k)|^2] = E_{SD}\sigma_{cD}^2 + \sum_{l=1}^{K} E_{Sl}\sigma_{cl}^2 \left| \sum_{p=-\infty}^{\infty} e^{j\phi_l(k-p)} g(-pT-\tau_l) \right|^2 + N_0, \quad (2.8b)$$

and conditional covariance with $\tilde{c}_{D,i}(k)$

$$\sigma_{rc}^2 = \sigma_r \cdot \sigma_{cD} \cdot \rho = \frac{1}{2}E[\tilde{r}_i(k)\tilde{c}_{D,i}^{\ *}(k)] = \sqrt{E_{Sd}}\, e^{j\phi_D(k)} {\sigma_{cD}}^2, \quad (2.8c)$$

where ρ is the cross correlation coefficient between the channel fading gain of the desired user's signal and the total received signal. As we assume identical diversity branches, this correlation coefficient holds identical for all *i*.

For two jointly distributed complex Gaussian random variables $\tilde{x}$ and $\tilde{y}$, with mean zero, variance $\sigma_x^2 = \frac{1}{2}E[|\tilde{x}|^2]$ and $\sigma_y^2 = \frac{1}{2}E[|\tilde{y}|^2]$, and covariance $\sigma_{xy}^2 = \frac{1}{2}E[\tilde{x}\tilde{y}^*] = \rho\sigma_x\sigma_y$ where ρ denotes the cross-correlation coefficient between $\tilde{x}$ and $\tilde{y}$, we have the relations [56] that when conditioned on $\tilde{y}$, $\tilde{x}$ is a conditional Gaussian random variable with conditional mean $E[\tilde{x}|\tilde{y}] = \rho(\sigma_x/\sigma_y)\tilde{y}$ and conditional variance $\frac{1}{2}E[|\tilde{x}|^2 \,|\tilde{y}] = (1-|\rho|^2)\sigma_x^2$. If we apply these properties to $x_i = \tilde{c}_{D,i}(k)e^{-j\alpha}$ and $\tilde{r}_i(k)$, we obtain the following conditional mean

$$E[\tilde{r}_i(k)|x_i] = \sqrt{E_{SD}}\, e^{j[\phi_D(k)+\alpha]} x_i \quad (2.9a)$$

and variance

$$\frac{1}{2}E[|\tilde{r}_i(k)|^2 \mid x_i] = \left(1 - \left|\frac{\sqrt{E_{SD}}\sigma_{cD}^2}{\sigma_r\sigma_{cD}}\right|^2\right)\sigma_r^2. \quad (2.9b)$$

Therefore we could rewrite the *k*th received signal as:

$$\tilde{r}_i(k) = \sqrt{E_{SD}}\, e^{j[\phi_D(k)+\alpha]} x_i + e_i \quad (2.10)$$

where e_i represents the uncertainty about $\tilde{r}_i(k)$ when conditioned on x_i. It is a complex Gaussian random variable with mean zero and a variance equals to the conditional variance in (2.9b). Substituting this alternative representation of $\tilde{r}_i(k)$ into the decision statistic (2.7), we have

$$\sum_{i=1}^{L} \mathrm{Re}[\tilde{r}_i(k) c_{D,i}^{*}(k) e^{j\alpha}] = \sqrt{E_{SD}} \cos(\phi_D(k) + \alpha) \sum_{i=1}^{L} |x_i|^2 + E \tag{2.11}$$

where $E = \sum_{i=1}^{L} \mathrm{Re}[e_i x_i^{*}]$. As we assume circular symmetry for all the channel fading gains and AWGN components, and independence of the channel fading gains between different diversity branches, it is straightforward to show that E is a real Gaussian random variable with mean zero and variance $(\sigma_r^2 - E_{SD}\sigma_{cD}^2)\sum_{i=1}^{L} |x_i|^2$. Since a Gaussian random variable is completely described by its mean and variance, the probability in (2.7) could now be written as

$$\begin{aligned} F(\alpha,\phi,\tau)|x_i &= P\left(E < -\sqrt{E_{SD}} \cos(\phi_D(k) + \alpha) \sum_{i=1}^{L} |x_i|^2 \,\middle|\, x_i\right) \\ &= \begin{cases} Q\left(\dfrac{|\cos(\phi_D(k) + \alpha)| \sqrt{E_{SD} \sum_{i=1}^{L} |x_i|^2}}{\sqrt{(\sigma_r^2 - E_{SD}\sigma_{cD}^2)}} \right) & \cos(\phi_D(k) + \alpha) \geq 0 \\ 1 - Q\left(\dfrac{|\cos(\phi_D(k) + \alpha)| \sqrt{E_{SD} \sum_{i=1}^{L} |x_i|^2}}{\sqrt{(\sigma_r^2 - E_{SD}\sigma_{cD}^2)}} \right) & \cos(\phi_D(k) + \alpha) < 0 \end{cases} \end{aligned} \tag{2.12}$$

where $Q(x) = \int_x^{\infty} \frac{1}{\sqrt{2\pi}} \exp\left(-\frac{y^2}{2}\right) dy$ is the Gaussian Q-function.

To remove the condition on $\{x_i\}_{i=1}^{L}$, we average the above probability over the distribution of random variable $v = \sum_{i=1}^{L} |x_i|^2$. Since $x_i = \tilde{c}_{D,i}(k) e^{-j\alpha}$ is a complex Gaussian random variable with mean zero and variance σ_{cD}^2, it is easy to show that v has a chi-square distribution [3] with a pdf given by

$$f_v(v) = \frac{1}{\left(2\sigma_{cD}^2\right)^L \Gamma(L)} v^{L-1} \exp[-\frac{v}{2\sigma_{cD}^2}] \tag{2.13}$$

Averaging the conditional probability (2.12) over the p.d.f. of v in (2.13), we get [3, eqn14.4-15]

$$\begin{aligned} F(\alpha,\phi,\tau) &= \int_0^\infty Q\left(\sqrt{\frac{E_{SDd}\cos^2(\phi_D(k)+\alpha)v}{\left(\sigma_r^2 - E_{SD}\sigma_{cD}^2\right)}}\right) \cdot \frac{1}{\left(2\sigma_{cD}^2\right)^L \Gamma(L)} v^{L-1} \exp[-\frac{v}{2\sigma_{cD}^2}] dv \\ &= \left(\frac{1-\mu}{2}\right)^L \sum_{j=0}^{L-1} \frac{(L+j\text{-}1)!}{(L-1)!\,j!}\left(\frac{1+\mu}{2}\right)^j \end{aligned} \tag{2.14a}$$

where

$$\mu = \frac{\cos(\phi_D+\alpha)\sqrt{E_{SD}\sigma_{cD}^2}}{\sqrt{E_{SD}\cos^2(\phi_D+\alpha)\sigma_{cD}^2 + \sigma_r^2 - E_{SD}\sigma_{cD}^2}}. \tag{2.14b}$$

Here we can write Eqn. (2.14) in one expression from the two results in (2.12) by using the relation

$$\left(\frac{1-\mu}{2}\right)^L \sum_{j=0}^{L-1} \frac{(L+j\text{-}1)!}{(L-1)!\,j!}\left(\frac{1+\mu}{2}\right)^j = 1 - \left(\frac{1+\mu}{2}\right)^L \sum_{j=0}^{L-1} \frac{(L+j\text{-}1)!}{(L-1)!\,j!}\left(\frac{1-\mu}{2}\right)^j.$$

To calculate the average bit error probability using the result in (2.14), first we need to average over all the possible interfering users' symbol patterns. As we assume that the dominant cross-term ISI contribution from the lth interfering signal is limited to some $2P$+1 terms, we have

$$F(\alpha,\phi_D(k),\tau) = \frac{1}{M^{(2P+1)K}} \sum_{\forall\phi\,\text{pattern}} F(\alpha,\phi,\tau). \tag{2.15}$$

Finally, averaging the result over the distribution of every interfering user's timing offset gives us

$$F\left(\alpha,\phi_D(k)\right) = \int_0^T \cdots \int_0^T F(\alpha,\phi_D(k),\tau) \cdot f_\tau(\tau_1) \cdot f_\tau(\tau_2) \cdots f_\tau(\tau_K) \cdot d\tau_1 \cdot d\tau_2 \cdots d\tau_K. \tag{2.16}$$

For a system using the rectangular pulse, an alternative approach to derive the

average BEP is possible by directly studying the distribution of the combination of the transmitted symbol and the random timing offset. Substituting (2.6) into (2.8) then (2.14), we have, for REC pulse shaping system,

$$\mu = \frac{\cos\left(\phi_D(k)+\alpha\right)\sqrt{E_{SD}\sigma_{cD}^2}}{\sqrt{E_{SD}\cos^2\left(\phi_D(k)+\alpha\right)\sigma_{cD}^2 + \sum_{i=1}^{K} E_{SI}\sigma_{cI}^2 y_l}} \tag{2.17}$$

where

$$y_l = 2\left[1-\cos\phi_l(k)\right]\left(\frac{\tau_l}{T}-\frac{1}{2}\right)^2 + \frac{1}{2}\left[1+\cos\phi_l(k)\right].$$

To calculate the average BEP, one needs to average (2.14) with (2.17) over the distribution of y_l only. Using the total probability theorem, the cdf of y_l can be calculated from the distribution of the timing offset τ_l together with the assumption of equiprobable symbols as the following

$$\begin{aligned} F_{yl}(Y) &= \Pr\{y_l < Y\} \\ &= \sum_{\phi_l(k)} \Pr\{\phi_l(k)\}\Pr\{y_l < Y \,|\, \phi_l(k)\} \\ &= \begin{cases} \begin{cases} 1 & Y \ge 1 \\ 1/2\sqrt{Y} & 0 < Y < 1 \\ 0 & Y \le 0 \end{cases} & BPSK \\ \begin{cases} 1 & Y \ge 1 \\ 1/4\sqrt{Y} + 1/2\sqrt{2Y-1} & 1/2 < Y < 1 \\ 1/4\sqrt{Y} & 0 < Y \le 1/2 \\ 0 & Y \le 0 \end{cases} & QPSK \end{cases} \end{aligned} \tag{2.18}$$

The corresponding pdf of y_l could then be obtained as

$$p_{yl}(Y)=\frac{\partial F_{yl}(Y)}{\partial Y}$$
$$=\begin{cases}\begin{cases}1/2\delta(Y-1) & Y\geq 1\\ 1/(4\sqrt{Y}) & 0<Y<1\\ 0 & Y\leq 0\end{cases} & BPSK\\ \begin{cases}1/4\delta(Y-1) & Y\geq 1\\ 1/(8\sqrt{Y})+1/(2\sqrt{2Y-1}) & 1/2<Y<1\\ 1/(8\sqrt{Y}) & 0<Y\leq 1/2\\ 0 & Y\leq 0\end{cases} & QPSK\end{cases}. \quad (2.19)$$

where $\delta(Y)$ is the Dirac delta function. As we assume independent CCI, i.e., the transmitted symbols are independent and the delays of the interferers are independent, the distribution of the summation $\sum_{i=1}^{K} E_{Sl}\sigma_{cl}^2 y_l$ can be easily calculated from the CF of each y_l. From (2.19), the CF can be derived as

$$\Phi_{yl}(\omega)=\int_{-\infty}^{\infty} p_{yl}(Y)e^{j\omega Y}dY$$
$$=\begin{cases}\frac{e^{j\omega}}{2}+\frac{\sqrt{\pi}erf[\sqrt{-j\omega}]}{4\sqrt{-j\omega}} & BPSK\\ \frac{e^{j\omega}}{4}+\frac{\sqrt{\pi}erf[\sqrt{-j\omega}]}{8\sqrt{-j\omega}}-\frac{2(1+j)e^{j\omega}\sqrt{\pi}erf[0.5(-1+j)\sqrt{\omega}]}{8\sqrt{\omega}} & QPSK\end{cases} \quad (2.20)$$

where $erf[x]=\int_0^x \frac{2}{\sqrt{\pi}}e^{-t^2}dt$ denotes the error function. The CF of the summation term $S=\sum_{i=1}^{K} E_{Sl}\sigma_{cl}^2 y_l$ in (2.17) can now be calculated as $\Phi_S(\omega)=\prod_{l=1}^{K} E_{Sl}\sigma_{cl}^2\Phi_{yl}(\omega)$. Finally by taking the inverse transform we can get the pdf of *S* which lead to another form for the average probability of (2.7) as

$$F\left(\phi_D(k)+\alpha\right)=\int_0^K F\left(\alpha,\phi_D(k),S\right)dS\int_{-\infty}^{\infty}\Phi_S(\omega)e^{-j\omega S}d\omega. \quad (2.21)$$

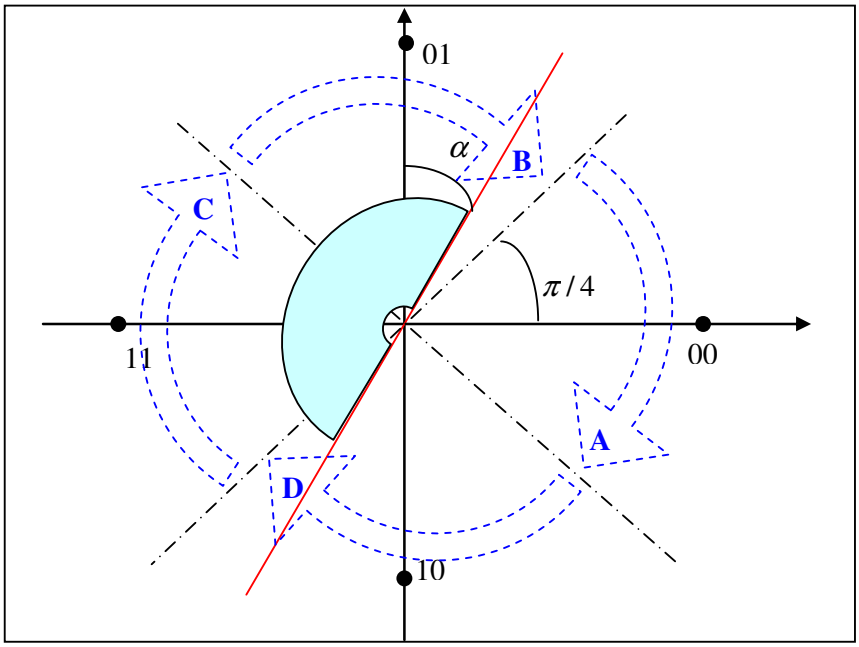

Figure 2.3 Signal constellation and decision region

The signal constellation and decision region are sketched in Fig. 2.3. The probability $F\left(\phi_D(k)+\alpha\right)$ obtained in (2.16) or (2.21) actually denotes the probability that the received signal vector after weighting and combining, $\sum_{i=1}^{L}\tilde{r}_i(k)\tilde{c}_i^*(k)$, falls into the grey zone above which is actually the left half of the complex plane that has been clockwise rotated by an angle α. Using QPSK as an example here, as we assume Gray encoding of the transmitted symbol, when '00' is transmitted, the receiver will make a wrong decision '01' if the vector falls into region B, or '11' if region C, or '10' if region D. The average BEP for this case is then

$$\begin{aligned} P_b\left(\phi_D(k)=0\right) &= \Pr(V\in B)+2\Pr(V\in C)+\Pr(V\in D) \\ &= \left[\Pr(V\in B)+\Pr(V\in C)\right]+\left[\Pr(V\in C)+\Pr(V\in D)\right]. \\ &= F\left(\alpha=\frac{\pi}{4},\phi_D(k)=0\right)+F\left(\alpha=-\frac{\pi}{4},\phi_D(k)=0\right) \end{aligned}$$

Similarly it could be shown that

$$P_b\left(\phi_D(k)=\frac{\pi}{2}\right)=F\left(\alpha=-\frac{\pi}{4},\phi_D(k)=\frac{\pi}{2}\right)+F\left(\alpha=-\frac{3\pi}{4},\phi_D(k)=\frac{\pi}{2}\right),$$

$$P_b\left(\phi_D(k)=\pi\right)=F\left(\alpha=\frac{3\pi}{4},\phi_D(k)=\pi\right)+F\left(\alpha=-\frac{3\pi}{4},\phi_D(k)=\pi\right),$$

$$P_b\left(\phi_D(k)=\frac{3\pi}{2}\right)=F\left(\alpha=\frac{\pi}{4},\phi_D(k)=\frac{3\pi}{2}\right)+F\left(\alpha=\frac{3\pi}{4},\phi_D(k)=\frac{3\pi}{2}\right).$$

Therefore, the average BEP for QPSK is given by

$$\begin{aligned}P_{QPSK}&=\frac{1}{4}\left[P_b\left(\phi_D(k)=0\right)+P_b\left(\phi_D(k)=\frac{\pi}{2}\right)+P_b\left(\phi_D(k)=\pi\right)+P_b\left(\phi_D(k)=\frac{3\pi}{2}\right)\right]\\&=F\left(\alpha+\phi_D(k)=\frac{\pi}{4}\right)\end{aligned}. \tag{2.22}$$

For BPSK system, following a similar derivation, the average BEP is given by

$$\begin{aligned}P_{BPSK}&=\frac{1}{2}\left[F\left(\alpha=0,\phi_D(k)=0\right)+F\left(\alpha=\pi,\phi_D(k)=\pi\right)\right]\\&=F\left(\alpha+\phi_D(k)=0\right)\end{aligned}. \tag{2.23}$$

Equations (2.22), (2.23), together with (2.14), (2.16) and (2.21), summarize the procedure of calculating the average BEP for BPSK and QPSK in nonselective Rayleigh fading channels with multiple asynchronous CCI using MRC diversity reception. It is worth noting that the average BEP is independent of the transmitted symbols of the desired signal. This is due to the symmetry of the signal constellation and the circular symmetry of the fading and the AWGN component we assumed in our system model.

2. 4 Effects of Symbol Timing Offsets

The expression of the average BEP obtained in Section 2.3 involves numerical integrals thus the calculation could be very time consuming for the case of large number of interferers. Similar computational complexity is also encountered in previous research works concerning multiple asynchronous CCI, e.g., [32], [34], [57].

The computational complexity is increased for the asynchronous CCI model mainly because of the fact that with random timing offset, the CCI component becomes non-Gaussian after matched filtered by the pulse shaping waveform synchronized to the desired signal. Another remark on the average BEP is that in a practical communication scenario, the timing offsets between the desired signal and the interfering signals normally remain constant during the transmission of a sequence of symbols. Therefore the average BEP obtained above represents more like the overall performance assessment of the whole communication process during a long period of operation. In many cases, it is actually more important and helpful to investigate the effect of symbol timing offsets between the desired signal and the interfering signals on the error performance. In this section, we consider a system employing REC pulse shaping, and study the behavior on the BEP conditioned on known values of the timing offset. More specifically, we try to find the particular value of the interfering signals' delay that give the best and the worst BEP performance. After that, we also will consider more general case where more practical Nyquist pulses, e.g., the RC and BTRC pulse, are employed.

In order to locate the delay instant of the *l*th interfering user that results in maximum or minimum BEP result, we differentiate the BEP expression with respect to the timing offset τ_l. Since the average BEP expression is the summation of the probability given by (2.14), we perform the differentiation of (2.14) first as

$$\begin{aligned}
&\frac{\partial F(\alpha,\phi,\tau)}{\partial \tau_l} \\
&= \frac{\partial \mu}{\partial \tau_l}\left\{\left(\frac{1-\mu}{2}\right)^L \sum_{p=0}^{L-1}\frac{(L+p-1)!}{(L-1)!\,p!}\left(\frac{1+\mu}{2}\right)^{p-1}\frac{p}{2} - \left(\frac{1-\mu}{2}\right)^{L-1}\sum_{q=0}^{L-1}\frac{(L+q-1)!}{(L-1)!\,q!}\left(\frac{1+\mu}{2}\right)^{q}\frac{L}{2}\right\} \\
&= \frac{\partial \mu}{\partial \tau_l}\left\{\sum_{p=0}^{L-1}\left[\frac{p}{1+\mu}-\frac{L}{1-\mu}\right]\left(\frac{1-\mu}{2}\right)^L \frac{(L+p-1)!}{(L-1)!\,p!}\left(\frac{1+\mu}{2}\right)^{p}\right\}
\end{aligned} \tag{2.24}$$

where μ is a function of τ_l given by (2.17). Its sign is positive as guaranteed by (2.22) and (2.23). Consequently, it is obvious that the sign of the summation term in (2.24) is always negative, and thus the sign of (2.24) is solely determined by the sign of the derivative of μ. Defining the normalized timing offset as $b_l = \tau_l / T$, we rewrite μ as

$$\begin{aligned}\mu &= \frac{\cos\left(\phi_D(k)+\alpha\right)\sqrt{E_{SD}\sigma_{cD}^2}}{\sqrt{E_{SD}\cos^2\left(\phi_D(k)+\alpha\right)\sigma_{cD}^2+\sigma_r^2-E_{SD}\sigma_{cD}^2}} \\ &= \frac{\cos\left(\phi_D(k)+\alpha\right)\sqrt{E_{SD}\sigma_{cD}^2}}{\sqrt{E_{Sd}\cos^2\left(\phi_D(k)+\alpha\right)\sigma_{cD}^2+N_0+\sum_{l=1}^{K}\sigma_l^2}}\end{aligned},$$

where

$$\begin{aligned}\sigma_l^2 &= E_{Sl}{\sigma_{cl}}^2\left[(1-b_l)^2+b_l^2+\left(e^{-j\phi_l(k)}+e^{j\phi_l(k)}\right)(1-b_l)b_l\right] \\ &= E_{Sl}{\sigma_{cl}}^2\left[1-2b_l+b_l^2+b_l^2+2\cos\phi_l(k)(b_l-b_l^2)\right] \\ &= E_{Sl}{\sigma_{cl}}^2\left[2\left(1-\cos\phi_l(k)\right)(b_l-0.5)^2+0.5\left(1+\cos\phi_l(k)\right)\right]\end{aligned}.$$

Carrying out the differentiation of μ with respect to τ_l, we get

$$\begin{aligned}\frac{\partial\mu}{\partial\tau_l} &= \frac{\partial\mu}{T\cdot\partial b_l} \\ &= \frac{-\cos(\phi_D+\alpha)\sqrt{\Gamma_{SNR}}\cdot\Gamma_{INR,l}\,4\left[1-\cos\phi_l(k)\right](b_l-0.5)}{\Gamma_{SNR}\cos^2(\phi_D+\alpha)+\sum_{l=1}^{K}\Gamma_{INR,l}\left[2\left[1-\cos\phi_l(k)\right](b_l-0.5)^2+0.5\left[1+\cos(\phi_l(k)\right]\right]+1}\end{aligned} \tag{2.25}$$

Here we define $\Gamma_{SNR}=\frac{E_{SD}\sigma_{cD}^2}{N_0}$ and $\Gamma_{INR,l}=\frac{E_{Sl}\sigma_{cl}^2}{N_0}$ as the average SNR and INR.

From (2.22) to (2.25) we can see that the sign of the derivative of the conditional BEP with respect to the *l*th interferer's timing offset τ_l is independent of the specific transmitted symbol, and independent of all the rest of the interferers' symbols and timing offsets. When $b_l = 0.5$, i.e. the timing offset is half of the symbol duration, the derivative in (2.25) is zero, and so is that in (2.24), thus we have an

extremum for the BEP when $\tau_l = T/2$. When $0 < \tau_l < T/2$, the right-hand side of (2.25) is always positive, thus the sign of the right-hand side of (2.24) is always negative, which indicates the BEP will decrease as τ_l increases in this range. Similarly, when $T/2 < \tau_l < T$, the BEP will increase as τ_l increases. From this sign change behavior of the BEP, we can conclude that the BEP for BPSK and QPSK have the maximum value when all CCI are synchronous with the desired user's signal, and the minimum value when all CCI are half-symbol-duration delayed with respect to the desired user's signal. Similar observations are given in the numerical results in [35] for the one-interferer case using selection combining. In our analysis we have proven that this result holds for multiple interferers and multiple combining diversity systems.

One direct application of the above finding is the upper and lower bounds of the BEP for BPSK and QPSK in nonselective Rayleigh fading channels with multiple asynchronous CCI using MRC diversity reception. By assigning the timing offsets of all the interfering signals to zero, i.e., assuming a synchronous CCI model, we obtain the upper bound on the BEP in the following simple closed-form

$$P_{e,U} = \left(1 - \frac{\sqrt{a\Gamma_{SNR}}}{\sqrt{a\Gamma_{SNR} + \sum_{l=1}^{K}\Gamma_{INR,l} + 1}}\right)^{L} \cdot \sum_{j=0}^{L-1} \frac{(L+j-1)!}{(L-1)!\,j!}\frac{1}{2^j}\left(1 + \frac{\sqrt{a\Gamma_{SNR}}}{\sqrt{a\Gamma_{SNR} + \sum_{l=1}^{K}\Gamma_{INR,l} + 1}}\right)^{j}. \quad (2.26)$$

where for BPSK $a = 1$ and for QPSK $a = 1/2$. This result has the same form as the result in [3, 14.4.15] for BEP of binary PSK in Rayleigh fading channel with MRC diversity reception, except that in (2.26) the effective noise power is the combination of AWGN and CCI. This can be easily validated because for the synchronous CCI model, the interfering signals with the unknown fading gains can be viewed as a Gaussian noise source and thus combined with the AWGN in the receiver. The lower BEP bound for BPSK and QPSK is obtained when we assign all the interfering

signal's timing offsets to half of the symbol duration, i.e., for one particular data sequence we have the conditional BEP

$$F_L(\alpha,\phi_D)=\frac{1}{2^L}\left(1-\frac{\cos(\phi_D+\alpha)\sqrt{\Gamma_{SNR}}}{\sqrt{\Gamma_{SNR}\cos^2(\phi_D+\alpha)+\sum_{l=1}^{K}\Gamma_{INR,l}\,0.5\left(1+\cos\phi_l(k)\right)+1}}\right)^L$$
$$\cdot\sum_{j=0}^{L-1}\frac{(L+j-1)!}{(L-1)!\,j!}\frac{1}{2^j}\left(1+\frac{\cos(\phi_D+\alpha)\sqrt{\Gamma_{SNR}}}{\sqrt{\Gamma_{SNR}\cos^2(\phi_D+\alpha)+\sum_{l=1}^{K}\Gamma_{INR,l}\,0.5\left(1+\cos\phi_l(k)\right)+1}}\right)^j. \quad (2.27)$$

Using these results in (2.22) and (2.23), we obtain the lower bound on the BEP.

For systems using RC pulse and BTRC pulse, the analysis of the effect of timing offset on the BEP using the above procedure is rather complicated due to the cross-term ISI components involved from adjacent symbols. If we simplify the system model such that only the mainlobe of the pulse is considered as they contain most of the interfering signal's energy, the analysis shown above for REC pulse shaping could be applied and we should expect to see the same results. However, such an assumption is only valid for large roll-off factors scenarios. For small or medium values of the roll-off factors, the first pair of sidelobes, which takes the opposite sign of the mainlobe, could have an opposite effect on the BEP as the timing offsets between the CCI and the desired user varies, i.e., the BEP of the synchronous case could actually be the best while the half-symbol-duration delayed case is the worst. As the number of effective ISI symbols that has to be taken into consideration in a system using RC or BTRC pulse shaping increases, the analytical examination of the relation between the BEP and the timing offsets of the interfering signals becomes even more complicated, if not totally impossible. Therefore we turn to the numerical results calculated from (2.14) to (2.16) and (2.22) to (2.23) to examine this issue.

2. 5 Numerical Results and Discussion

We present here some numerical results. In Fig. 2.4 we plot the BEP as a function of the average SNR for BPSK signal with dual diversity reception using rectangular pulse shaping. One asynchronous interferer with 10 dB of interference-to-noise-ratio (INR) has been assumed in this system and BEP curves associated with different timing offsets between the interferer and the desired signal are compared, where a noticeable difference can be observed. In Fig. 2.5 we plot the BEP as a function of the average SNR for QPSK signal with different INR levels. In both Fig. 2.4 and Fig. 2.5, we present both analytical results and simulated results to verify the correctness of our derivation where good match can be observed.

In Fig. 2.6, we demonstrate the effect of higher order diversity, where substantial performance improvement is obtained. As we use an INR level of 15dB, the performance improvement is quite slim for SNR levels under 15dB as the CCI still has a power level comparable to that of the desired user.

In Fig. 2.7, we compare the BEP of the three pulses we considered in this work. It is obvious that the three pulses have the same BEP when the system is synchronized. This could be anticipated as the mathematical models for the three pulses reduce to the same if we set the relative delays of the interferers to zero in (2.5). However, with non-zero timing offset between the interfering signal and the desired signal, the ISI in RC and BTRC pulse system degrades the performance when compared with REC pulse system. More specifically, RC pulse based system suffers more from ISI than BTRC pulse based system. An interesting phenomenon in this figure is that for higher order diversity systems, the performance of a synchronized system could be better than an asynchronous system for RC and BTRC pulse systems, which is in contrast with the conclusion we obtained for REC pulse based system. This result has also been

observed in the numerical result of [35]. For REC pulse, as our analytical derivation proves, the synchronous case always provides the worst error performance.

In Fig. 2.8 and Fig. 2.9, we plot the BEP as a function of the individual timing offsets for a two-interferer system. As we assume independent interfering signals, the overall minimum BEP is obtained when both interfering signals are half-symbol duration delayed from the desired signal. Again, it shows that the performance of the BTRC pulse is better than that of the RC pulse when the interfering signals are asynchronous with the desired signal.

In Fig. 2.10 and Fig. 2.11, we demonstrate the effect of the number of interferers on error performance for two scenarios – fixed INR level and fixed SIR level. In Fig. 2.10, it is not difficult to understand that when the INR level is fixed, increasing the number of interferers surely degrades the performance as it introduces more interference to the system. However, in Fig. 2.11, we find that when the total power of the interfering signals is fixed, splitting it among more interferers will slightly improve the error performance and this is true, of course only for the asynchronous system, as for synchronous system the CCI components are Gaussian, and thus, only the total CCI energy matters in the error performance.

Finally in Fig. 2.12, we plot the BEP as a function of the normalized timing offset for systems using RC and BTRC pulses with different roll-off factors. The results confirm our discussion at the end of the last section. For smaller roll-off factors, the behavior of the BEP when varying the timing offsets is the same as that of a rectangular pulse system. But for larger roll-off factors, the effect of the timing offsets is the opposite.

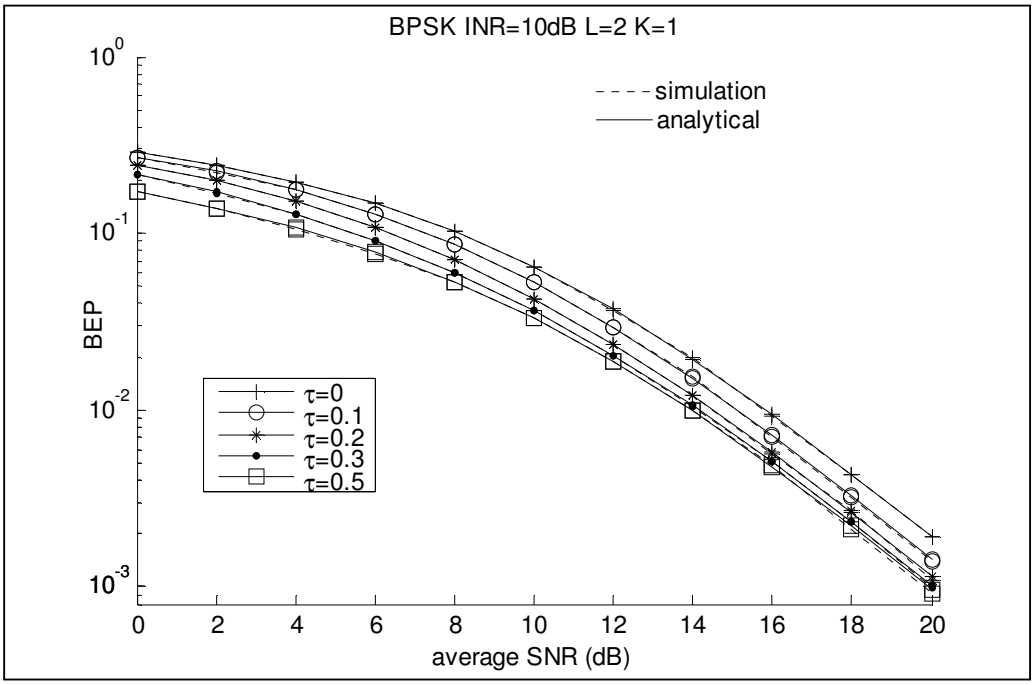

Figure 2.4 BEP vs. average SNR for different timing offset

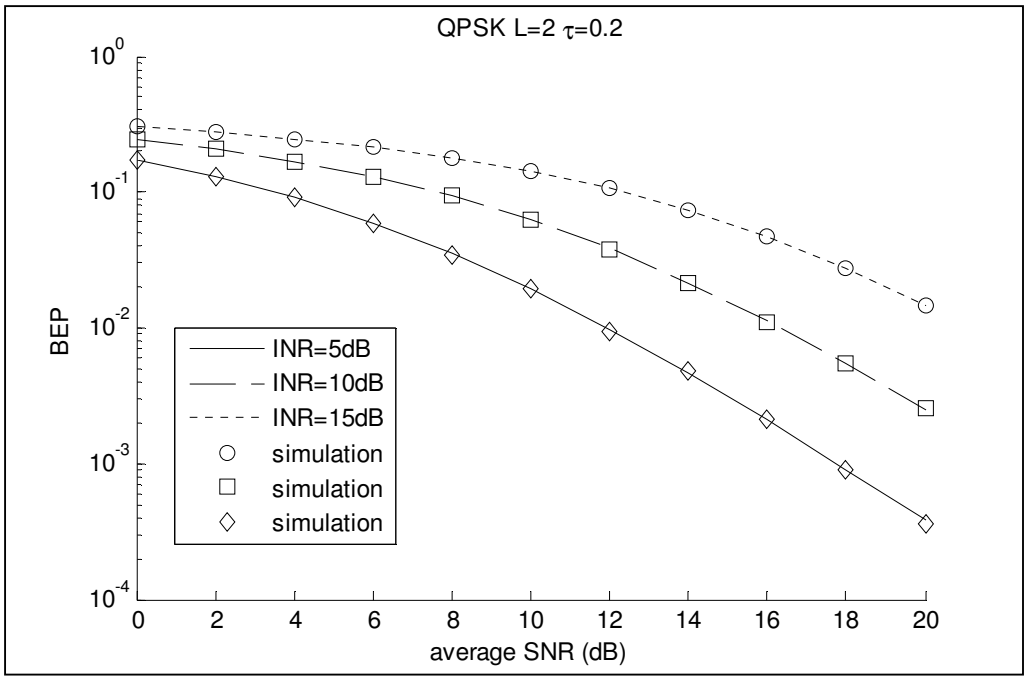

Figure 2.5 BEP vs. average SNR for different INR level

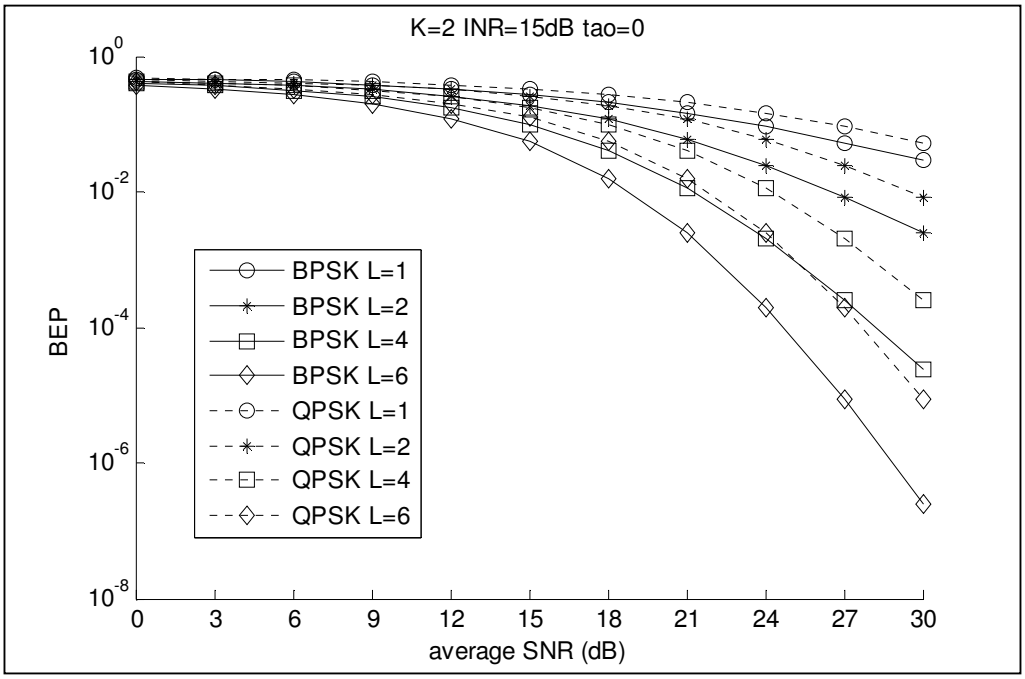

Figure 2.6 BEP vs. average SNR for different diversity orders

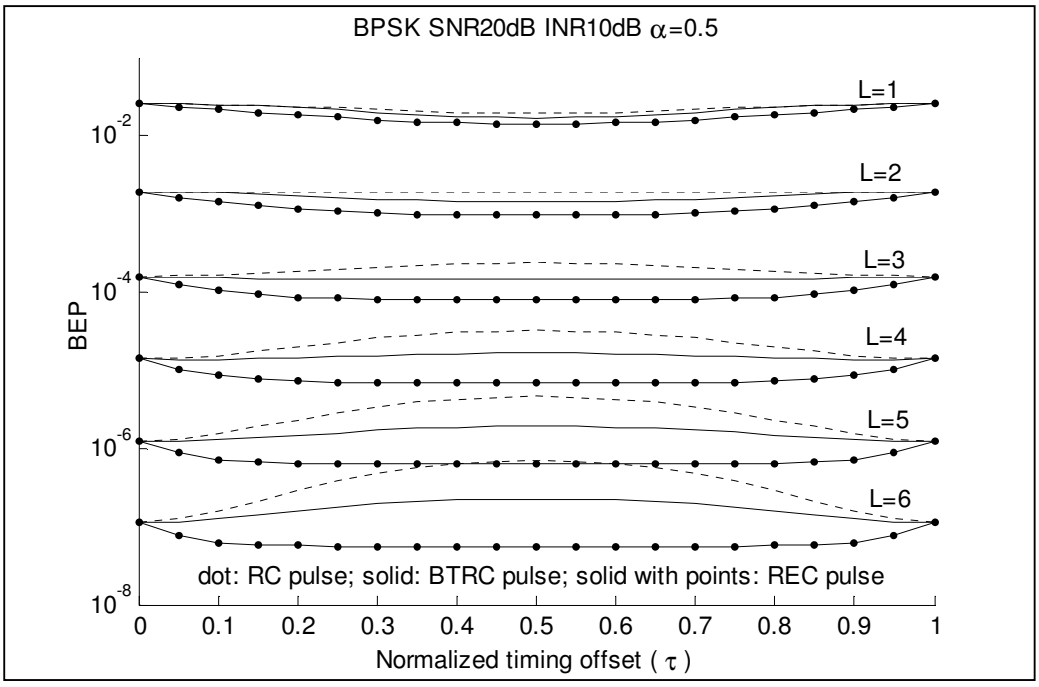

Figure 2.7 BEP vs. normalized timing offset for different pulses with different diversity orders

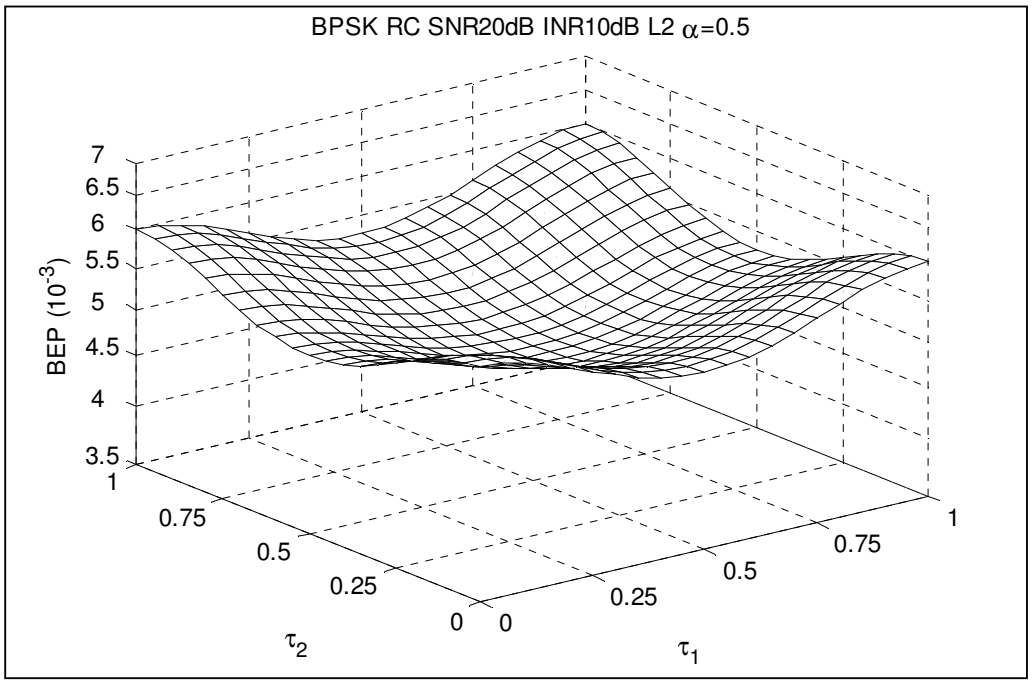

Figure 2.8 BEP vs. normalized timing offsets of a system using RC pulse

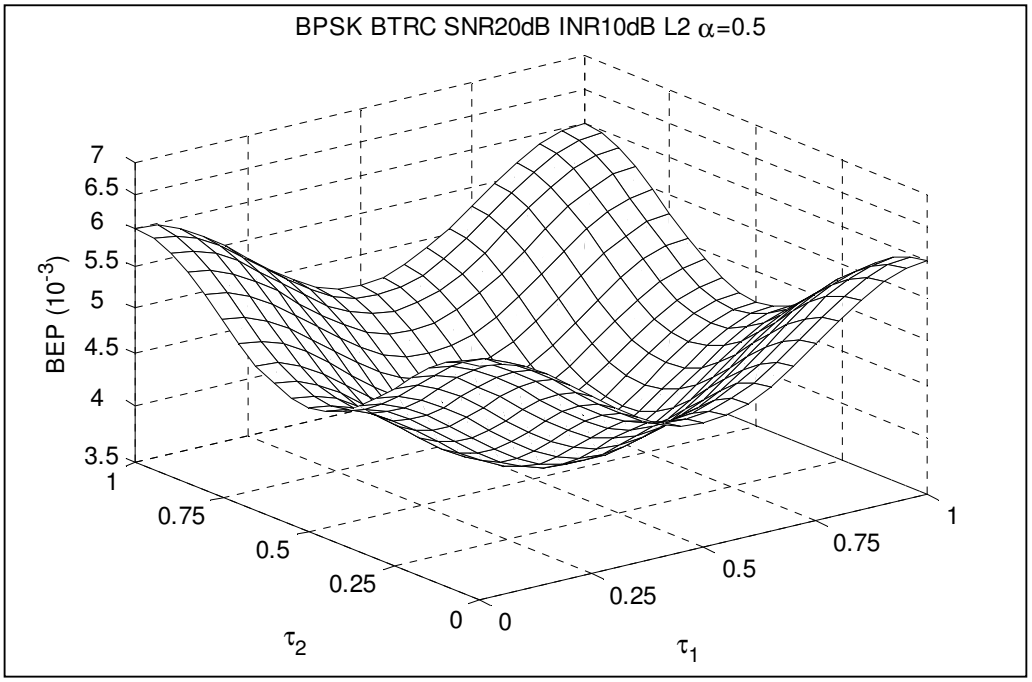

Figure 2.9 BEP vs. normalized timing offsets of a system using BTRC pulse

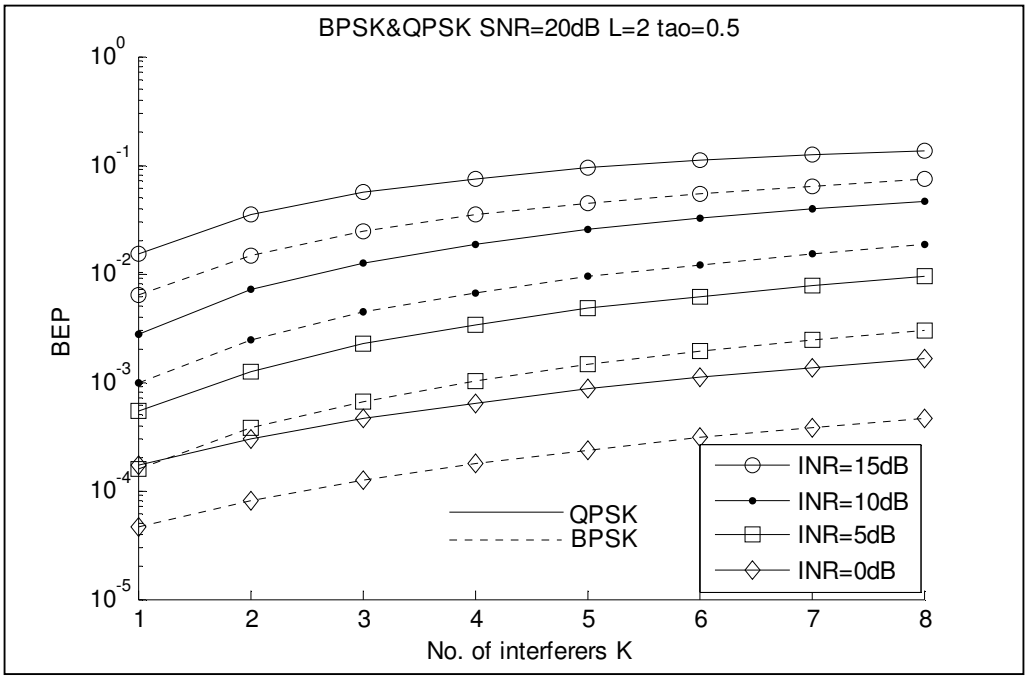

Figure 2.10 BEP vs. number of interferers for different INR levels

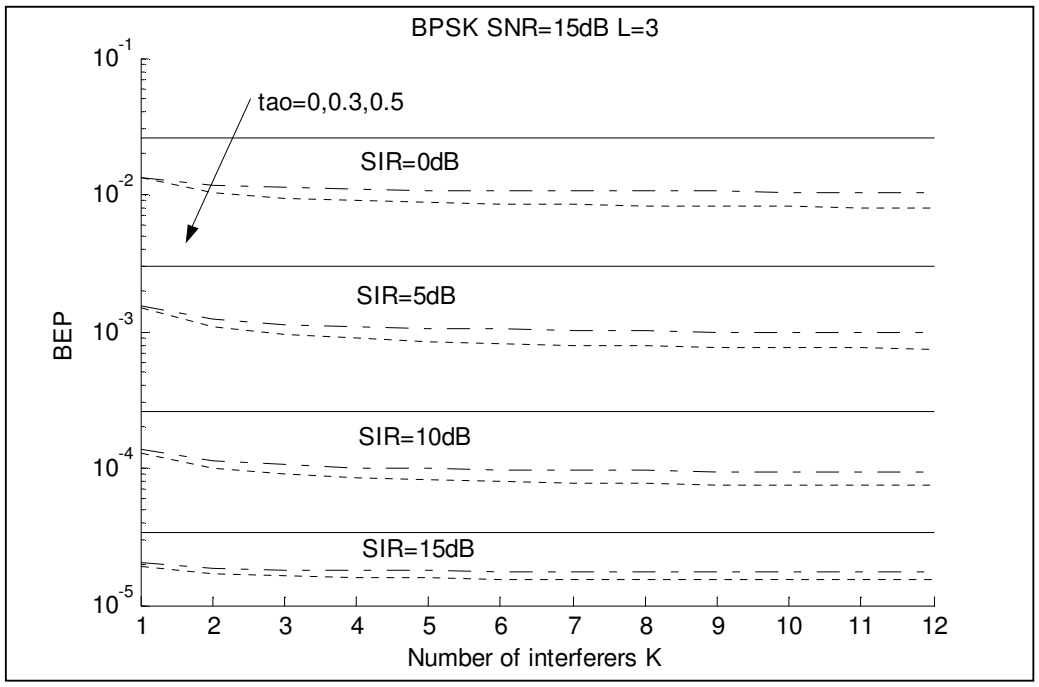

Figure 2.11 BEP vs. number of interferers for different SIR levels

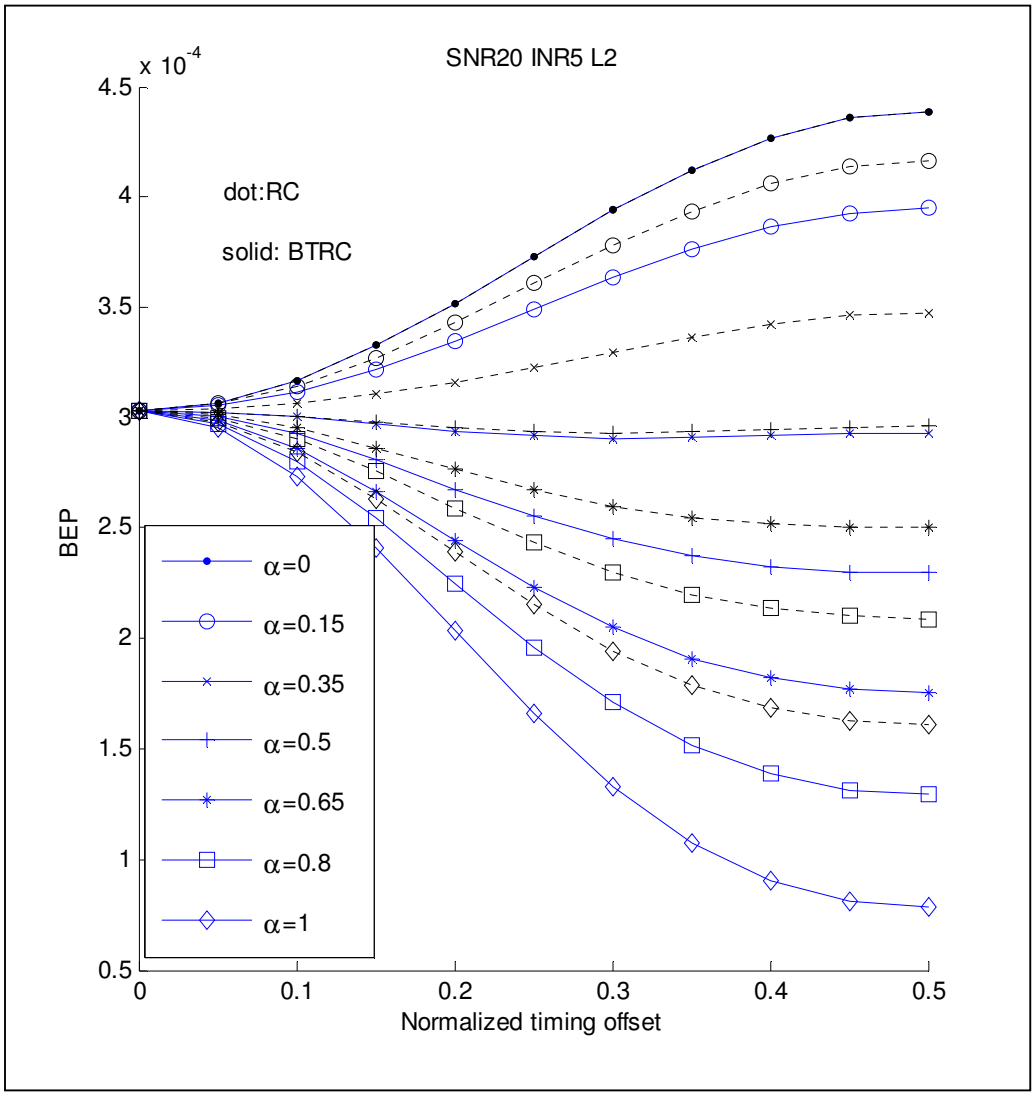

Figure 2.12 BEP vs. normalized timing offset for different roll-off factors

2. 6 Summary

In this chapter, we derived exact results to evaluate the BEP of BPSK and QPSK with multiple asynchronous cochannel interferers in MRC diversity system. By looking into the effect of the CCI timing offsets, we find that for REC pulse based system the synchronous scenario is always the worst case as far as error performance is concerned, while the best performance is obtained when all the interfering signals are half-symbol-duration delayed with respect to the desired user. This enabled us to obtain the upper and lower bounds for the performance of an asynchronous CCI system in exact and explicit closed-form, which are new and easy to evaluate. Our analysis also confirms that with non-zero timing offset between the interfering signals and the desired signal, the performance of the BTRC pulse is better than that of RC pulse.

Chapter 3

BEP of Differentially Detected DPSK in Nonselective Rayleigh Fading Channels with Multiple Asynchronous Cochannel Interferers

In this chapter we investigate the BEP of binary and quaternary DPSK in nonselective Rayleigh fading channels with post-detection MRC diversity reception and with multiple cochannel interferers. After the introduction is given in Section 3.1, the system model is established in Section 3.2 together with the receiver/detector structure. In Section 3.3 we carry out the performance analysis. In Section 3.4 we study the effect of the asynchronous interferers' timing offset on the BEP of the desired user. Numerical results and discussion are given in Section 3.5, and Section 3.6 summarizes this chapter.

3. 1 Introduction

The study in the previous chapter analyzes the performance of coherent PSK modulation in fading channels with cochannel interference. One of the assumptions made in the analysis is the availability of perfect CSI for the desired user's signal. However, this is an impractical assumption because in reality certain channel estimation schemes must be adopted and estimation error is almost inevitable. The performance analysis results based on this assumption could only serve as a lower

bound for a communication system employing certain practical channel estimation schemes. In order to perform coherent detection in a practical system, certain channel estimation schemes must be adopted such as PSAM [58]. This would surely increase the complexity of the system. On the other extreme, the non-coherent detection scheme such as differentially encoded and detected PSK has been known for its simplicity and fair performance, and its performance could be considered as an upper bound where no channel information is needed at the detector. Therefore we are also interested to investigate the performance of DPSK modulation in fading channels with cochannel interference.

3. 2 System Model

As in the previous chapter, we consider a system in which the DPSK signal received from the desired user over L independent, identical diversity branches is corrupted by K asynchronous CCI and AWGN. The complex baseband transmitted signal of the desired user is

$$\tilde{s}_D(t) = \sqrt{E_{SD}} \sum_{p=-\infty}^{p=\infty} e^{j\phi_D(p)} g_{TD}(t - pT)$$

where $1/T$ is the symbol transmission rate and $g_{TD}(t)$ denotes the impulse response of the transmitter pulse shaping filter of the desired user. The average energy per symbol for the desired user is E_{SD}. The information symbol is now embedded in the phase difference between the two adjacent transmitted symbols as $\theta_D(k) = \phi_D(k) - \phi_D(k-1)$. A reasonable assumption is that all interfering signals have the same modulation format as the desired user's signal. Thus the baseband transmitted signal of the *l*th interfering user has the similar form

$$\tilde{s}_l(t) = \sqrt{E_{Sl}} \sum_{p=-\infty}^{p=\infty} e^{j\phi_l(p)} g_{Tl}(t - pT)$$

where E_{Sl} is the average energy per symbol for the *l*th interfering user signal. We further assume that all the users use the same transmit pulse shaping filter. Consequently, we have $g_{Tl}(t) = g_T(t)$ for $l = D,1,2,\cdots,K$.

We assume that both the desired user's signal and the interfering users' signal undergo slow nonselective Rayleigh fading. At the receiver, the received signal from the *i*th diversity branch is

$$\tilde{r}_i(t) = \tilde{c}_{D,i}(t)\tilde{s}_D(t) + \sum_{l=1}^{K} \tilde{c}_{l,i}(t + \tau_l)\tilde{s}_l(t + \tau_l) + \tilde{n}_i(t)$$

where $\tilde{c}_{D,i}(t)$ and $\tilde{c}_{l,i}(t)$ are the channel fading process of the *i*th diversity channel for the desired user and the *l*th interfering user respectively. The AWGN term $\tilde{n}_i(t)$ has zero mean and a double side PSD of N_0. At the receiver, the received signals are matched filtered and sampled at the symbol time of the desired user signal, assuming perfect symbol synchronization with the desired user's symbol time. As we assume in general an asynchronous system, the *l*th interfering user's signal may come after an arbitrary delay τ_l which is uniformly distributed within $[0,T)$. After matched filtering and sampling, the discrete received signal at the input of the detector over the *i*th diversity channel, *i*=1,…,*L*, for the *k*th symbol interval [*k*T,(*k*+1)*T*] can be represented by a decision statistic $\tilde{r}_i(k)$ as [3 Sec9.2]

$$\begin{aligned}\tilde{r}_i(k) = &\sum_{p=-\infty}^{\infty} \sqrt{E_{SD}} e^{j\phi_D(k-p)} \int_{-\infty}^{\infty} \tilde{c}_{D,i}(\tau + pT) g_T(\tau) g_R(kT - pT - \tau) d\tau + \tilde{n}_i(k) \\ &+ \sum_{l=1}^{K} \sum_{p=-\infty}^{p=\infty} \sqrt{E_{Sl}} e^{j\phi_l(k-p)} \int_{-\infty}^{\infty} \tilde{c}_{l,i}(\tau + pT + \tau) g_T(\tau_l) g_R(kT - pT - \tau - \tau_l) d\tau\end{aligned} \quad . \quad (3.1a)$$

Here $g_R(t)$ is the receive filter matched to the transmit filter such that the overall cascaded impulse response $g(t) = g_R(t) * g_T(t)$ without fading would be a pulse shape that fulfils the Nyquist criterion. Since $g_T(t)$ is a unit-energy pulse, the peak amplitude of $g_T(t)$ is 1. The received signal shown in (3.1a) is generally difficult to manage because of the integral terms. Therefore, we make a commonly adopted assumption that the fading processes affecting the desired and interfering signals change slowly enough so that they can be considered as constant during the effective length of the impulse response $g_R(t)$ and $g_T(t)$. Thus the fading process inside the integrand of (3.1a) could be approximated by its instantaneous value at the sampling time and could be factored out of the integral. The received signal at the detector input can now be written as,

$$\tilde{r}_i(k) = \sqrt{E_{SD}}\, e^{j\phi_d(k-p)} \tilde{c}_{D,i}(k) + \sum_{l=1}^{K} \sqrt{E_{Sl}}\, \tilde{c}_{l,i}(k) \sum_{p=-P}^{p=P} e^{j\phi_l(k-p)}\, g(-pT - \tau_l) + \tilde{n}_i(k) \qquad (3.1b)$$

where $\tilde{c}_{D,i}(k)$ and $\tilde{c}_{l,i}(k)$ are the piecewise-constant approximations to the *i*th channel fading process during the *k*th symbol interval [*k*T, (*k*+1)*T*] for the desired user and the *l*th interfering user, respectively. It is obvious that in the presence of a non-zero symbol timing offset τ_l, the effective interfering component comes from a sequence of transmitted symbols in a similar form as ISI. Since in general the Nyquist pulse shaping used in practical communication system has a fast decaying waveform, we could assume that the effective ISI components are composed of the nearest $2P+1$ symbols. For the case of nonselective Rayleigh fading channels with even power density spectrum, $\tilde{c}_{D,i}(k)$ and $\tilde{c}_{l,i}(k)$ are both complex Gaussian random variables whose quadrature components are iid Gaussian RVs, with mean zero, variances $\frac{1}{2}E[|\tilde{c}_{D,i}(k)|^2] = \sigma_{cD}^2$ and $\frac{1}{2}E[|\tilde{c}_{l,i}(k)|^2] = \sigma_{cl}^2$, respectively, and autocorrelation

coefficients $R_D(q) = \frac{1}{2} E[\tilde{c}_{Di}(k)\tilde{c}^*_{Di}(k-q)] / \sigma^2_{cD}$ and $R_l(q) = \frac{1}{2} E[\tilde{c}_{li}(k)\tilde{c}^*_{li}(k-q)] / \sigma^2_{cl}$ respectively. We assume in general different power and different fade rates for different users because the interferers could be located in different distance from the desired user and they could travel at different velocity. The noise term $\tilde{n}_i(k)$ is the sampled output of the AWGN process after matched filtering from the *i*th diversity branch, which is a complex Gaussian random variable with mean zero and variance $\frac{1}{2} E[|\tilde{n}_i(k)|^2] = N_0 / 2$.

We consider an independent diversity system where the received signals from the same user at different diversity branches have iid channel fading gains, i.e., for arbitrary $i \neq j$, $\tilde{c}_{il}(k)$ and $\tilde{c}_{jl}(k)$ are iid, for $l = D, 1, \cdots, K$. Also, the channel fading gains for different users are assumed to be independent, either at the same diversity branch or different ones, i.e., $\tilde{c}_{il}(k)$ is independent of $\tilde{c}_{jh}(k)$ for arbitrary $l \neq h$. The noise components $\tilde{n}_i(k)$ from different diversity branches are assumed to be independent and identically distributed, and they are independent from channel fading gains of all the users from all diversity branches.

The overall pulse shape $g(t)$ we consider in this work are the three types considered in chapter 2, namely, triangular pulse, Raised-Cosine pulse and better-than-Raised-Cosine pulse.

To detect the information symbol, a post-detection MRC receiver is utilized as shown in Figure 3.1. With equiprobable transmitted symbols, the differential detector computes the decision statistics

$$q_m(k) \;=\; \mathrm{Re}[\sum\nolimits_{i=1}^{L} \tilde{r}_i(k)\tilde{r}^*_i(k-1)e^{-j2\pi m/M}],$$

and decides that the kth transmitted symbol is $\theta_D(k) = 2\pi l / M$ if $q_l(k) = \max\{q_m(k)\}_{m=0}^{M-1}$.

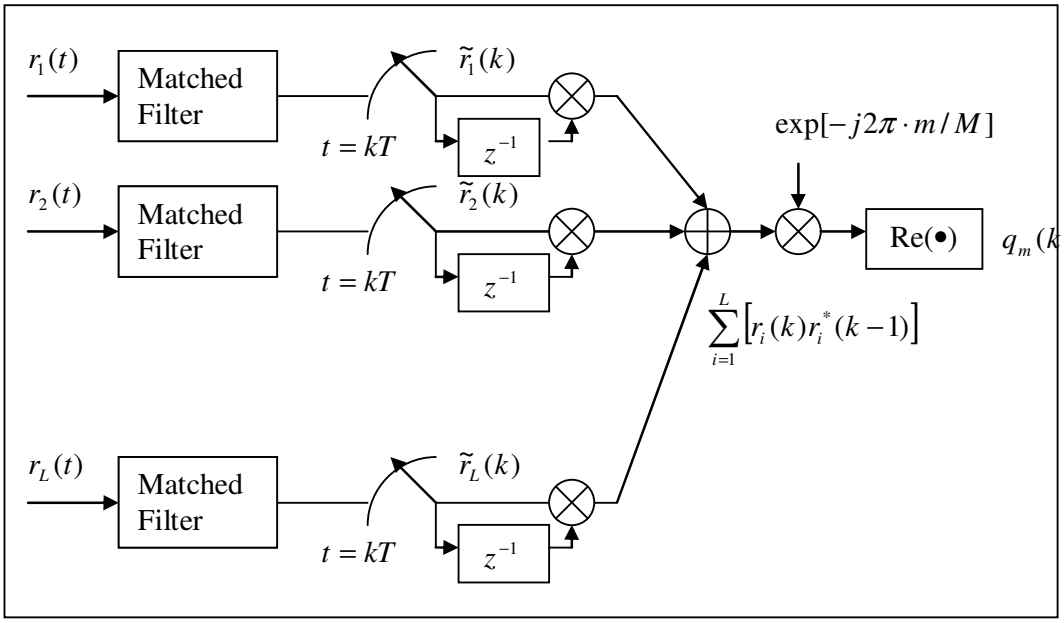

Figure 3.1 Receiver structure for DPSK

3. 3 Performance Analysis

Based on the receiver structure in Figure 3.1, the BEP of binary and quaternary DPSK signal, conditioned on a set I of known transmitted symbols of all users and known timing offsets of all interfering users can be obtained from the probability

$$F(\alpha, \phi, \tau) = P\left(\mathrm{Re}\left[\sum_{i=1}^{L} \tilde{r}_i(k)\tilde{r}_i^*(k-1)e^{j\alpha} \right] < 0 \,\middle|\, \{\tau_l, \phi_l(k-p)\}_{l=1,p=-\infty}^{L,\infty} = I \right) \quad (3.2)$$

where α is related to the information phase $\theta_D(k)$ in determining the BEP and its specific value will be given later. Note that conditioned on the given set I, the received signal in each diversity branch is a summation of multiple independent CGRVs. Therefore, the received signals $\tilde{r}_i(k)|I$ and $\tilde{r}_i(k-1)|I$ are two correlated complex Gaussian random variables, each with conditional mean

$$E[\tilde{r}_i(k) \mid I] = E[\tilde{r}_i(k) \mid I] = 0\,, \tag{3.3a}$$

and conditional variance

$$\sigma_{r,k}^2 = \frac{1}{2}E[|\tilde{r}_i(k)|^2] = E_{SD}\sigma_{cD}^2 + \sum_{l=1}^{K} E_{Sl}\sigma_{cl}^2 \left| \sum_{p=-\infty}^{\infty} e^{j\phi_l(k-p)} g(-pT - \tau_l) \right|^2 + N_0 \tag{3.3b}$$

and

$$\begin{aligned} \sigma_{r,k,k-1}^2 &= \frac{1}{2}E[\tilde{r}_i(k)\tilde{r}_i^*(k-1) \mid I] \\ &= E_{SD}\sigma_{cD}^2 R_D(1) e^{j[\theta_D(k)]} + \sum_{l=1}^{K} \left\{ E_{Sl}\sigma_{cl}^2 R_l(1) \left(\sum_{p=-\infty}^{\infty} e^{j\phi_l(k-p)} g(-pT - \tau_l) \right) \right. \\ &\quad \left. \cdot \left(\sum_{p=-\infty}^{\infty} e^{j\phi_l(k-1-p)} g(-pT - \tau_l) \right) \right\}. \end{aligned} \tag{3.3c}$$

Applying the same property for two correlated Gaussian random variables that leads to (2.9), we find that when conditioned on $x_i = \tilde{r}_i(k-1)e^{-j\alpha}$, $\tilde{r}_i(k)$ is conditionally Gaussian with conditional mean [56]

$$E[\tilde{r}_i(k) | x_i] = R_r(1)\frac{\sigma_{r,k}}{\sigma_{r,k-1}} e^{j\alpha} x_i \tag{3.4a}$$

and conditional variance

$$\frac{1}{2}E[|\tilde{r}_i(k)|^2 \mid x_i] = (1 - |R_r(1)|^2)\sigma_{r,k}^2 \tag{3.4b}$$

where the one-symbol conditional autocorrelation coefficient of the received signal is defined as

$$\begin{aligned} R_r(1) &= \frac{E[\tilde{r}_i(k)\tilde{r}_i^*(k-1) \mid I]}{\sqrt{E[|\tilde{r}_i(k)|^2]E[|\tilde{r}_i(k-1)|^2]}} \\ &= \frac{\sigma_{r,k,k-1}^2}{\sigma_{r,k}\sigma_{r,k-1}} \end{aligned}. \tag{3.5}$$

Therefore we could rewrite the *k*th received signal as:

$$\tilde{r}_i(k) = R_r(1)\frac{\sigma_{r,k}}{\sigma_{r,k-1}} e^{j\alpha} x_i + e_i \tag{3.6}$$

where e_i represents the uncertainty about $\tilde{r}_i(k)$ conditioned on x_i. It is a complex Gaussian random variable with mean zero and variance equal to the conditional variance in (3.4b). Substituting this alternative representation of $\tilde{r}_i(k)$ into the decision statistic (3.2), we have

$$\sum_{i=1}^{L}[\tilde{r}_i(k)\tilde{r}_i^*(k-1)e^{j\alpha}] = \mathrm{Re}\left(R_r(1)\frac{\sigma_{r,k}}{\sigma_{r,k-1}}e^{j\alpha}\right)\sum_{i=1}^{L}|x_i|^2 + E \tag{3.7}$$

where $E = \sum_{i=1}^{L}\mathrm{Re}[e_i x_i^*]$. Following a similar derivation as that in chapter 2, it is straightforward to show that *E* is a real Gaussian random variable with mean zero and variance $(1-|R_r(1)|^2)\sigma_{r,k}^2\sum_{i=1}^{L}|x_i|^2$. Since a Gaussian random variable is completely described by its mean and variance, the probability in (3.2) could now be written as

$$\begin{aligned} F(\alpha,\phi,\tau)\big|x_i &= P\left(E < -\mathrm{Re}\left(R_r(1)\frac{\sigma_{r,k}}{\sigma_{r,k-1}}e^{j\alpha}\right)\sum_{i=1}^{L}|x_i|^2 \,\middle|\, x_i\right) \\ &= \begin{cases} Q\left(\sqrt{\dfrac{|\mathrm{Re}\left(R_r(1)e^{j\alpha}\right)|^2\sum_{i=1}^{L}|x_i|^2}{\left(1-|R_r(1)|^2\right)\sigma_{r,k-1}^2}}\right) & \mathrm{Re}\left(R_r(1)e^{j\alpha}\right)\ge 0 \\ 1-Q\left(\sqrt{\dfrac{|\mathrm{Re}\left(R_r(1)e^{j\alpha}\right)|^2\sum_{i=1}^{L}|x_i|^2}{\left(1-|R_r(1)|^2\right)\sigma_{r,k-1}^2}}\right) & \mathrm{Re}\left(R_r(1)e^{j\alpha}\right)< 0 \end{cases}. \end{aligned} \tag{3.8}$$

Defining $v = \sum_{i=1}^{L}|x_i|^2$, it follows from [3] that *v* has a chi-square distribution with pdf given by

$$f_v(v) = \frac{1}{\left(2\sigma_{r,k-1}^2\right)^L\Gamma(L)}v^{L-1}\exp[-\frac{v}{2\sigma_{r,k-1}^2}]. \tag{3.9}$$

Averaging the conditional probability (3.8) over the p.d.f. of *v* in (3.9), we get [3, eqn14.4-15]

$$
\begin{aligned}
&F(\alpha,\phi,\tau) \\
&= \int_0^{\infty} Q\left(\sqrt{\frac{|\,\mathrm{Re}\left(R_r(1)e^{j\alpha}\right)|^2 \sum_{i=1}^{L}|x_i|^2}{\left(1-|\,R_r(1)\,|^2\right)\sigma_{r,k-1}^2}}\right)\cdot\frac{1}{\left(2\sigma_{r,k-1}^2\right)^L\Gamma(L)}v^{L-1}\exp[-\frac{v}{2\sigma_{r,k-1}^2}]dv \\
&= \left(\frac{1}{2}-\frac{\mathrm{Re}\left(R_r(1)e^{j\alpha}\right)}{2\sqrt{\left[\mathrm{Re}\left(R_r(1)e^{j\alpha}\right)\right]^2+1-|\,R_r(1)\,|^2}}\right)^L \\
&\quad\times\sum_{j=0}^{L-1}\frac{(L+j-1)!}{(L-1)!\,j!}\left(\frac{1}{2}+\frac{\mathrm{Re}\left(R_r(1)e^{j\alpha}\right)}{2\sqrt{\left[\mathrm{Re}\left(R_r(1)e^{j\alpha}\right)\right]^2+1-|\,R_r(1)\,|^2}}\right)^j
\end{aligned}
\tag{3.10}
$$

To calculate the bit error probability conditioned on a certain bit of the desired user's data using the result in (3.10), we first need to average over all the possible patterns of the interfering users' data. In doing this averaging, a reasonable assumption is that the dominant cross-term ISI contributions from the *l*th interfering signals are limited to some 2*P*+1 terms. Thus we have

$$
F\left(\alpha,\theta_D(k),\tau\right)=\frac{1}{M^{(2P+1)K}}\sum_{\forall\phi\ \text{pattern}}F(\alpha,\phi,\tau). \tag{3.11}
$$

Finally, averaging the result over the distribution of every interfering user's timing offset gives us the average BEP conditioned on a certain bit of the desired user's data as

$$
F\left(\alpha,\theta_D(k)\right)=\int_0^T\cdots\int_0^T F(\alpha,\phi_D,\tau)\cdot f_\tau(\tau_1)\cdot f_\tau(\tau_2)\cdots f_\tau(\tau_K)\cdot d\tau_1\cdot d\tau_2\cdots d\tau_K. \tag{3.12}
$$

From (3.10), it is obvious that the calculation of the BEP requires only the calculation of the key quantity $R_r(1)$ which is defined through (3.5). When conditioned on the data sequence and timing offsets of the CCI, and assuming a rectangular pulse system, $R_r(1)$ has the form

$$R_r(1)=\frac{\sigma^2_{r,k,k-1}}{\sigma_{r,k}\sigma_{r,k-1}}=\frac{e^{j\theta_D(k)}\Gamma_S R_D(1)+\sum_{l=1}^{K}A(\tau_l)}{\sqrt{\Gamma_S+\sum_{l=1}^{K}B_1(\tau_l)+1}\sqrt{\Gamma_S+\sum_{l=1}^{K}B_2(\tau_l)+1}} \tag{3.13}$$

where

$$A(\tau_l)=\Gamma_l R_l(1)\left[e^{j\theta_D(k-1)}\left(\frac{\tau_l}{T}\right)^2+e^{j\theta_D(k)}\left(1-\frac{|\tau_l|}{T}\right)^2+\left(1+e^{j\theta_D(k-1)+j\theta_D(k)}\right)\left(1-\frac{|\tau_l|}{T}\right)\left(\frac{\tau_l}{T}\right)\right], \tag{3.14}$$

$$B_1(\tau_l)=\Gamma_S\left[2\left(1-\cos[\theta_l(k-1)]\right)\left(\frac{|\tau_l|}{T}-\frac{1}{2}\right)+\frac{1}{2}\left(1+\cos[\theta_l(k-1)]\right)\right] \tag{3.15}$$

and

$$B_2(\tau_l)=\Gamma_S\left[2\left(1-\cos[\theta_l(k)]\right)\left(\frac{|\tau_l|}{T}-\frac{1}{2}\right)+\frac{1}{2}\left(1+\cos[\theta_l(k)]\right)\right] \tag{3.16}$$

are three different functions of the symbol sequence and the timing offsets, $\Gamma_S=E_{SD}/N_0$, $\Gamma_l=E_{Sl}/N_0$ and $\theta_l(k)=\phi_l(k)-\phi_l(k-1)$ are the average SNR, average INR and the *k*th information symbol of the *l*th interfering signal, respectively. The structure of $R_r(1)$ suggests that in general, for different combinations of α and $\theta_D(k)$, the values of $R_r(1)$ will be the different. With Gray encoding, the average BEP expressions for BDPSK and QDPSK can be obtained from (3.12) in a similar manner as in section 2.3. Thus we have

$$P_{2DPSK}=\frac{1}{2}\left\{F\left(\alpha=\theta_D(k)=0\right)+F\left(\alpha=\theta_D(k)=\pi\right)\right\} \tag{3.17}$$

and

$$
\begin{aligned}
P_{QDPSK} = \frac{1}{8}\Bigg[& F\left(\alpha=\frac{\pi}{4},\theta_D(k)=0\right)+F\left(\alpha=-\frac{\pi}{4},\theta_D(k)=0\right) \\
& +F\left(\alpha=-\frac{\pi}{4},\theta_D(k)=\frac{\pi}{2}\right)+F\left(\alpha=-\frac{3\pi}{4},\theta_D(k)=\frac{\pi}{2}\right) \\
& +F\left(\alpha=\frac{3\pi}{4},\theta_D(k)=\pi\right)+F\left(\alpha=-\frac{3\pi}{4},\theta_D(k)=\pi\right) \\
& +F\left(\alpha=\frac{\pi}{4},\theta_D(k)=\frac{3\pi}{2}\right)+F\left(\alpha=\frac{3\pi}{4},\theta_D(k)=\frac{3\pi}{2}\right)\Bigg]
\end{aligned}
\tag{3.18}
$$

respectively. Comparing (3.17) and (3.18) with the result in [8], we see that the difference is that due to the existence of CCI, the error performance of the desired user becomes dependent on its transmitted symbol.

3. 4 Effects of Symbol Timing Offsets

3. 4. 1 Dependence of BEP on interfering signals' timing offsets

Similar to the coherent PSK case in Chapter 2, we found that the calculation of the average BEP through (3.10)-(3.18) could be a timing consuming process for large numbers of interferers, due to the multiple integral in (3.12). Therefore we here study the effects of the interferers' timing offsets on the BEP of the desired user.

We first consider the binary case and try to investigate how the error performance changes as the timing offsets between the desired and the interfering signals vary. For this purpose, we differentiate, without loss of generality, the conditional BEP $F(\alpha,\phi,\tau)$ in (3.10) with respect to an arbitrary interfering signal's timing offset, say τ_1, while holding the rest of the K interfering signals' timing offsets fixed at arbitrary values, which have no effect on the behavior of τ_1 as we assume that they are all independent. By setting the derivative to zero, we can locate the timing offset that yields the largest/smallest BEP, while the sign of this derivative would indicate how the BEP would change when τ_1 varies within a symbol duration. For

BDPSK signal, the transmitted signal $\theta_D(k)$ is either 0 or π, so (3.10) can be reduced to

$$F(\alpha,\phi,\tau)=\left(\frac{1-R_r(1)\cos(\alpha)}{2}\right)^L\sum_{j=0}^{L-1}\frac{(L+j-1)!}{(L-1)!\,j!}\left(\frac{1+R_r(1)\cos(\alpha)}{2}\right)^j. \tag{3.19}$$

The derivative of (3.19) is then

$$\begin{aligned}&\frac{\partial F(\alpha,\phi,\tau)}{\partial\tau_1}\\&=\frac{\partial R_r(1)}{\partial\tau_1}\cos(\alpha)\left\{-\frac{L}{2}\left(\frac{1-R_r(1)\cos(\alpha)}{2}\right)^{L-1}\sum_{j=0}^{L-1}\frac{(L+j-1)!}{(L-1)!\,j!}\left(\frac{1-R_r(1)\cos(\alpha)}{2}\right)^j\right.\\&\quad\left.+\left(\frac{1-R_r(1)\cos(\alpha)}{2}\right)^L\sum_{j=0}^{L-1}\frac{(L+j-1)!}{(L-1)!\,j!}\left(\frac{1+R_r(1)\cos(\alpha)}{2}\right)^{j-1}\frac{j}{2}\right\}\\&=\frac{\partial R_r(1)}{\partial\tau_1}\cos(\alpha)\left\{\left(\frac{1-R_r(1)\cos(\alpha)}{2}\right)^L\right.\\&\quad\left.+\sum_{j=0}^{L-1}\frac{(L+j-1)!}{(L-1)!\,j!}\left(\frac{1+R_r(1)\cos(\alpha)}{2}\right)^j\left(\frac{j}{1+R_r(1)\cos(\alpha)}-\frac{L}{1-R_r(1)\cos(\alpha)}\right)\right\}\end{aligned} \tag{3.20}$$

In order to simplify the analysis, we assume that the desired signal energy is greater than that of all the interfering signals combined, i.e., $\Gamma_S>\sum_{l=1}^{K}\Gamma_l$, an assumption which is valid for most of the practical systems. This assumption, together with the relationship between α and θ_D in (3.17), ensures that $R_r(1)\cos(\alpha)>0$. Thus in (3.20), the second term multiplying $\partial R_r(1)\cos(\alpha)/\partial\tau_1$ is always negative, independent of the value of τ_1. Consequently, the sign of the derivative in (3.20) is given by the sign of $\left(-\partial R_r(1)\cos(\alpha)/\partial\tau_1\right)$. Using (3.13-3.16), for BDPSK we have

$$
\begin{aligned}
&-\frac{\partial R_r(1)}{\partial \tau_1}\cos(\alpha) \\
&= -\cos(\alpha)\prod_{m=1}^{2}(\Gamma_S + \textstyle\sum_{l=1}^{K} B_m(\tau_l)+1)^{-1} \\
&\quad \cdot\left\{\frac{\partial A(\tau_1)}{\partial \tau_1}\prod_{m=1}^{2}(\Gamma_S + \textstyle\sum_{l=1}^{K} B_m(\tau_l)+1)^{1/2} - \sum_{m=1}^{2}\frac{\partial B_m(\tau_1)}{\partial \tau_1}\frac{\left[\cos(\theta_D)\Gamma_S R_D(1) + \sum_{l=1}^{K} A_1(\tau_l)\right]}{2\sqrt{\Gamma_S + \sum_{l=1}^{K} B_m(\tau_l)+1}}\right\} \\
&= -\cos(\alpha)\prod_{m=1}^{2}(\Gamma_S + \textstyle\sum_{l=1}^{K} B_m(\tau_l)+1)^{-1} \\
&\quad \cdot\left\{\frac{\partial A(\tau_1)}{\partial \tau_1}\prod_{m=1}^{2}(\Gamma_S + \textstyle\sum_{l=1}^{K} B_m(\tau_l)+1)^{1/2} - \sum_{m=1}^{2}\frac{\partial B_m(\tau_1)}{\partial \tau_1}\frac{\sum_{l=1}^{K} A_1(\tau_l)}{2\sqrt{\Gamma_S + \sum_{l=1}^{K} B_m(\tau_l)+1}}\right\} \\
&\quad + \cos(\alpha)\left(\prod_{m=1}^{2}(\Gamma_S + \textstyle\sum_{l=1}^{K} B_m(\tau_l)+1)^{-1}\right)\sum_{m=1}^{2}\frac{\partial B_m(\tau_1)}{\partial \tau_1}\frac{\cos(\theta_D)\Gamma_S R_D(1)}{2\sqrt{\Gamma_S + \sum_{l=1}^{K} B_m(\tau_l)+1}} \\
&= -\cos(\alpha)T_1(\tau_1) + \cos(\alpha)\cos(\theta_D)T_2(\tau_1)
\end{aligned}
\tag{3.21a}
$$

where

$$
\begin{aligned}
T_1(\tau_1) &= \prod_{m=1}^{2}(\Gamma_S + \textstyle\sum_{l=1}^{K} B_m(\tau_l)+1)^{-1} \\
&\quad \cdot\left\{\frac{\partial A(\tau_1)}{\partial \tau_1}\prod_{m=1}^{2}(\Gamma_S + \textstyle\sum_{l=1}^{K} B_m(\tau_l)+1)^{1/2} - \sum_{m=1}^{2}\frac{\partial B_m(\tau_1)}{\partial \tau_1}\frac{\sum_{l=1}^{K} A_1(\tau_l)}{2\sqrt{\Gamma_S + \sum_{l=1}^{K} B_m(\tau_l)+1}}\right\}
\end{aligned}
\tag{3.21b}
$$

and

$$
T_2(\tau_1) = \left(\prod_{m=1}^{2}(\Gamma_S + \textstyle\sum_{l=1}^{K} B_m(\tau_l)+1)^{-1}\right)\sum_{m=1}^{2}\frac{\partial B_m(\tau_1)}{\partial \tau_1}\frac{\Gamma_S R_D(1)}{2\sqrt{\Gamma_S + \sum_{l=1}^{K} B_m(\tau_l)+1}}. \tag{3.21c}
$$

Now from (3.17) we know that in order to calculate the average BEP, we need to combine the case $(\alpha = 0, \theta_D(k) = 0)$ and the case $(\alpha = \pi, \theta_D(k) = \pi)$. Since $T_1(\tau_1)$ and $T_2(\tau_1)$ are independent of α and $\theta_D(k)$, we find that upon substituting $(\alpha = \theta_D(k) = 0)$ and $(\alpha = \theta_D(k) = \pi)$ into (3.21) and combining, $T_1(\tau_1)$ all the related

components will cancel out. Thus, the sign of the derivative (3.21) of the combined average BEP (3.17) is only dependent on the sign of

$$T_2(\tau_1) = \left(\prod_{m=1}^{2} (\Gamma_S + \sum_{l=1}^{K} B_m(\tau_l) + 1)^{-1} \right) \sum_{m=1}^{2} \frac{\partial B_m(\tau_1)}{\partial \tau_1} \frac{\Gamma_S R_D(1)}{2\sqrt{\Gamma_S + \sum_{l=1}^{K} B_m(\tau_l) + 1}} \quad (3.22)$$

which is determined by the sign of $\{\partial B_m(\tau_1)/\partial \tau_1\}_{m=1}^{2}$ as the rest are all positive components. From (3.15) and (3.16), it is easy to show that for $\tau_1 \in \{[0, T/2), T/2, (T/2, T)\}$, the signs of the term $\{\partial B_m(\tau_1)/\partial \tau_1\}_{m=1}^{2}$ are either $\{0,0,0\}$ or $\{-,0,+\}$, for different data symbol sequences of the interfering signals. This allow us to conclude that the average BEP in (3.17) will decrease as τ_1 increases from 0, reach the minimum when $\tau_1 = T/2$, and then increase as τ_1 increases till $\tau_1 = T$ which is equivalent to $\tau_1 = 0$.

For QDPSK, the application of the above derivation is rather complicated because of the complex signal constellation involved. Thus numerical results are used to explore the relationship between the BEP and the timing offsets of the interfering signals, and it will be seen that the same behavior is observed as that of BDPSK.

For systems using RC pulse and BTRC pulse, the discussion follows the one given in Chapter 2 for coherent PSK systems. When the roll-off factor is large, the sidelobes are small and can be neglected, and therefore the above discussion (3.19-3.22) should hold.

Based on the above discussion, the value of the coefficient $R_r(1)$ that gives the maximum BEP for a system using the REC pulse is given by

$$R_r(1) = \frac{e^{j\theta_D}\Gamma_S R_D(1) + \sum_{l=1}^{K} e^{j\theta_l(k)}\Gamma_l R_l(1)}{\Gamma_S + \sum_{l=1}^{K}\Gamma_l + 1} \quad (3.23)$$

and the value of $R_r(1)$ that gives the minimum BEP is given by

$$R_r(1)=\frac{e^{j\theta_D}\Gamma_S R_D(1)+\frac{1}{4}\sum_{l=1}^{K}\Gamma_l R_l(1)\left[e^{j\theta_l(k-1)}+e^{j\theta_l(k)}+e^{j\theta_l(k-1)}\cdot e^{j\theta_l(k)}+1\right]}{\sqrt{\Gamma_S+\frac{1}{2}\sum_{l=1}^{K}\Gamma_l(1+\cos[\theta_l(k)])+1}\sqrt{\Gamma_S+\frac{1}{2}\sum_{l=1}^{K}\Gamma_l(1+\cos[\theta_l(k-1)])+1}}. \tag{3.24}$$

Substituting these two values of the coefficient into (3.10), (3.11), (3.17) and (3.18), simple, explicit closed-form expressions for the upper and lower bounds on the BEP of DPSK signals in Rayleigh fading channels with asynchronous CCI and diversity reception are obtained.

3. 4. 2 Dependence of BEP on transmitted symbols

As pointed out at the end of Section 3.3, due to the existence of CCI, the BEPs for different desired user's transmitted symbols are different in general. This unequal error probability can be seen by comparing the expression of $R_r(1)\cos(\alpha)$ for the synchronous case in (3.23) with the one for the general asynchronous case in (3.13-3.16) or (3.24). Considering the BDPSK case, from (3.10), (3.17) and (3.23), when $\theta_D(k)=\pi$ is transmitted, the corresponding coefficient $R_r(1)\cos(\alpha)$ will be identical to that obtained when $\theta_D(k)=0$ is transmitted if a phase shift of π is added to each of the interfering symbols. Since we assume that the desired signal and CCI use the same modulation scheme with equiprobable transmitted symbols, for an arbitrary sequence of symbols for the interfering signal, there is always another sequence of symbols with π phase difference. As the average BEP is obtained by summing over all possible transmitted symbol sequences, the final BEP results for these two cases will be the same. However, when non-zero symbol timing offset exists, the numerator and denominator in (3.13) will have different values for the two cases of $\theta_D(k)=\pi$ and $\theta_D(k)=0$. Such a phenomenon has only been observed for differentially detected DPSK. The reason is that the differential detector makes decision based on the phase

shift between the two successive symbols. With the presence of asynchronous CCI, each symbol of an interfering signal overlaps partially with two successive received symbols of the desired signal, helping to provide a coherent reference. Thus, the asynchronous CCI is sort of beneficial for the detection of the desired user's symbol that is transmitted with no phase shift, but destructive for the detection of a symbol that has a large phase shift. The same behavior of symbol dependent BEP for DPSK with additive interference has also been observed in [59], [60].

3. 5 Numerical Results and Discussion

In this section we present numerical results to demonstrate the effects of timing offsets between the desired signal and the interfering signals, the SNR, the number of interferers, the number of diversity branches and the temporal fading fluctuation on the system BEP performance. In all the figures, we use the Jakes' Doppler spectrum for the fading process, thus $R(1) = J_0(2\pi f_d T)$, where $J_0(\cdot)$ is the zeroth order Bessel function of the first kind, and $f_d T$ is the normalized Doppler frequency. For simplicity, we assume that all interfering signals have equal powers and the same fade rate unless otherwise specified. For the case when the RC pulse or the BTRC pulse is used, we use a roll-off factor of $\alpha = 0.5$, unless otherwise specified.

In Fig. 3.2 we plot the BEP as a function of average SNR for BDPSK with different timing offsets between the one interfering signal and the desired signal. The normalized Doppler frequency is set to be 0.03 which is equivalent of a fading autocorrelation coefficient of 0.99. This "fast" fading introduces an error floor in the BEP curves for the differential detector. Also demonstrated in this figure is that the interfering signal's delay substantially affects the performance in high SNR scenario when the interference is the major source of detection error.

In Fig. 3.3, we compare the performances of the three pulses with the same system parameters. Similar to the coherent detection case in Chapter 2, the performance of the three pulses are the same when the system is synchronized. When delay is introduced to the interferers, the RC pulse has the highest BEP while REC pulse has the smallest. However, unlike the odd behavior of the RC and BTRC pulses in Fig. 2.7 for coherent PSK, we found that the synchronous system always has the worst performance for all the three pulses through our extensive studies with different parameters. In Fig. 3.4 and Fig. 3.5, we present numerical results for the BEP as a function of timing offsets for a two-interferer system. The concave BEP surface proves that the minimum BEP is achieved when all interfering signals are half-symbol duration delayed. In Fig. 3.4, simulation results are given which agree well with our analytical results. In Fig 3.5, we demonstrate once again that the BTRC pulse has better performance than the RC pulse when the system is asynchronous.

Fig. 3.6 compares the BEP of systems using RC and BTRC pulses with different roll-off factors. Unlike what we observed in Fig 2.12, we found that the synchronous system always has the worst performance.

In Fig. 3.7 we compare two systems with the same total interfering power but different numbers of interferers. The result is similar to what has been observed in Fig. 2.11, i.e., by splitting the same amount of energy into more interferers, the BEP of the desired user will slightly improve. Furthermore, unlike the coherent system, this behavior is also observed even when the system is synchronized.

In Fig. 3.8 and 3.9, we plot the BEP for different transmitted symbols. In Fig. 3.8, where a QDPSK system is studied, we found that the BEP for transmitting symbol ‘00’ which involves a zero phase shift is the smallest, while the BEP for transmitting symbol ‘11’ which involves a π phase shift is the largest. In Fig. 3.9, similar results

are obtained for a two-interferer system. Also in this figure, we assume the two interferers have different energy (INR). It can be seen that the interferer with the larger INR affects the BEP of the desired signal more severely when its delay varies.

In the last two figures, we compare the effect of the fade rate of the desired signal with that of the interfering signal on the BEP of the desired signal. It is well-known that a smaller fade rate, i.e., a larger fading autocorrelation, means a smaller BEP for the desired user, as demonstrated in Fig 3.10. However, Fig. 3.11 shows that when the interfering signals' fading autocorrelation is larger, it actually slightly degrades the performance of the desired signal.

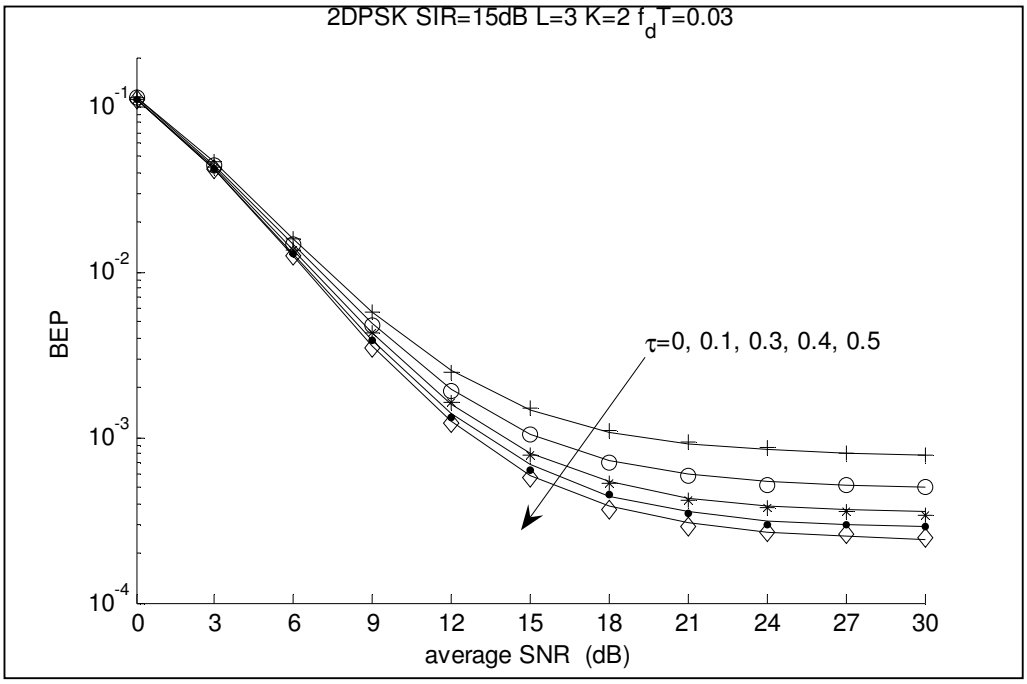

Figure 3.2 BEP vs. average SNR for different timing offset

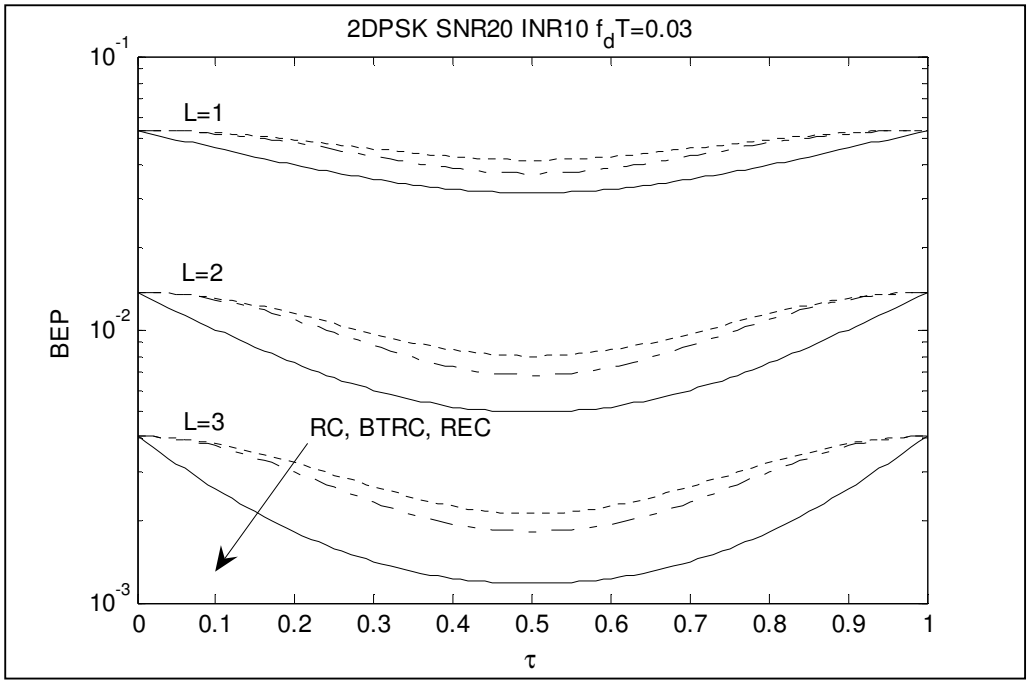

Figure 3.3 BEP vs. normalized timing offset for different pulse shape and different diversity orders

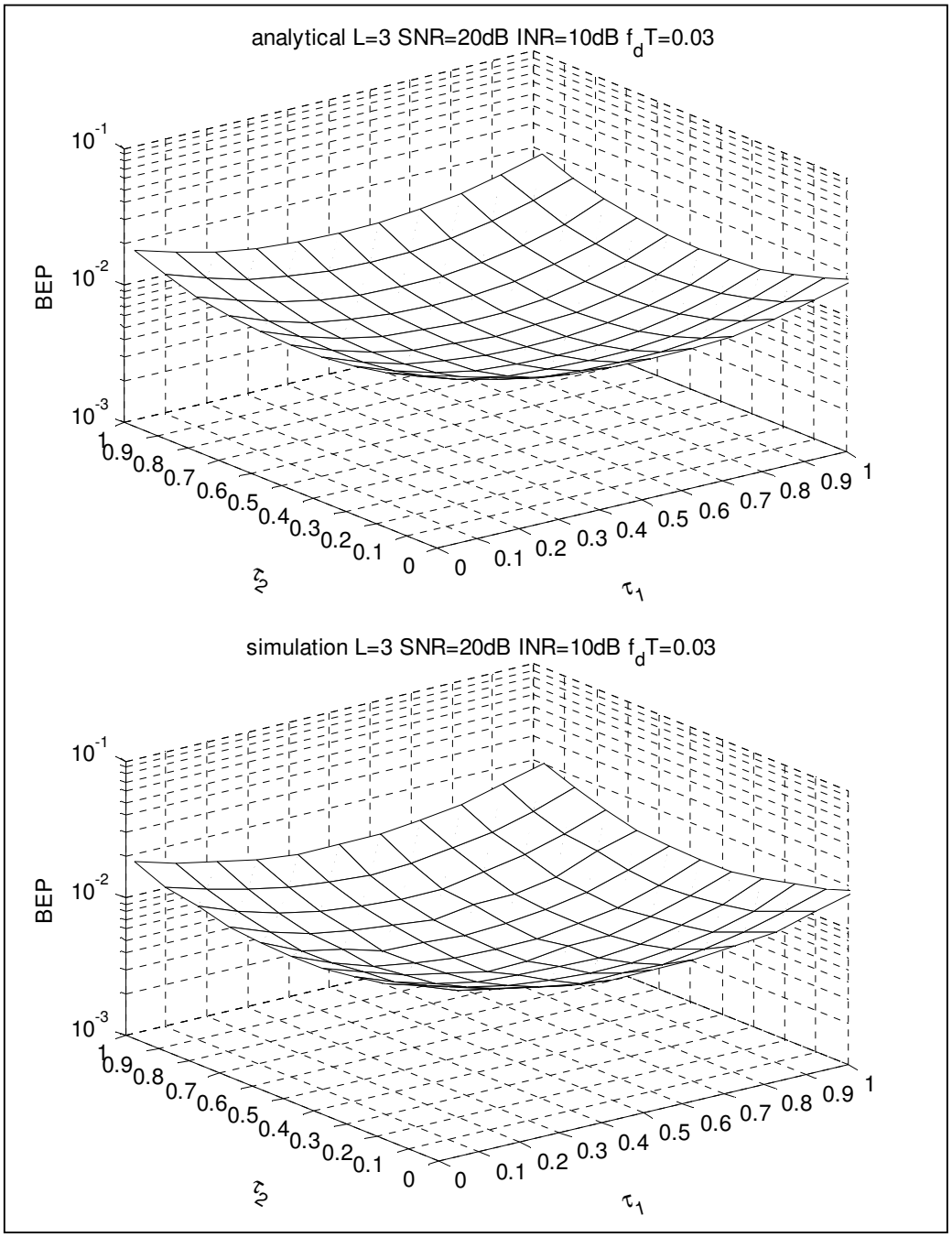

Figure 3.4 BEP vs. normalized timing offset for two-user system with rectangular pulse shaping, both analytical and simulated

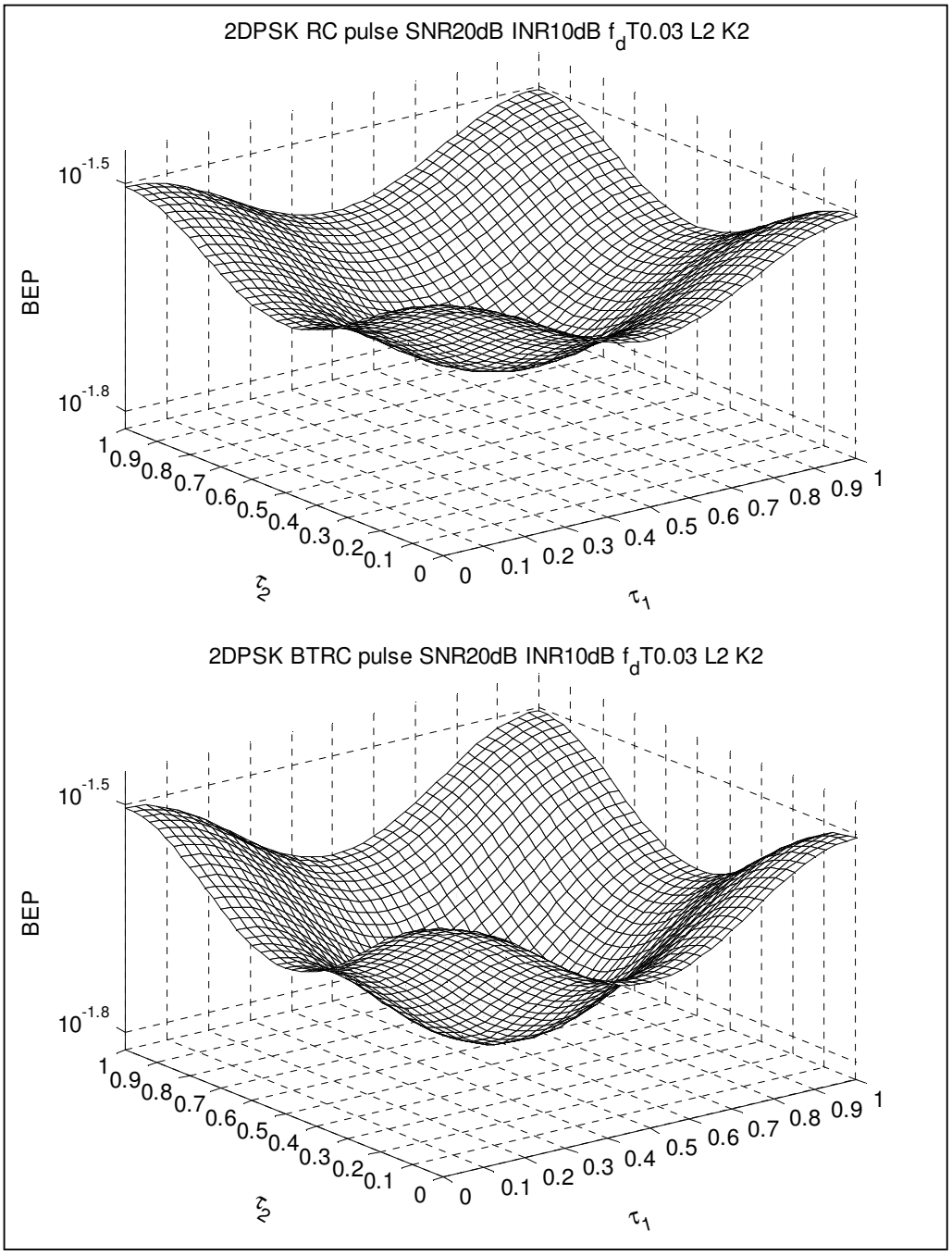

Figure 3.5 BEP vs. normalized timing offset for two-user system with RC pulse and BTRC pulse

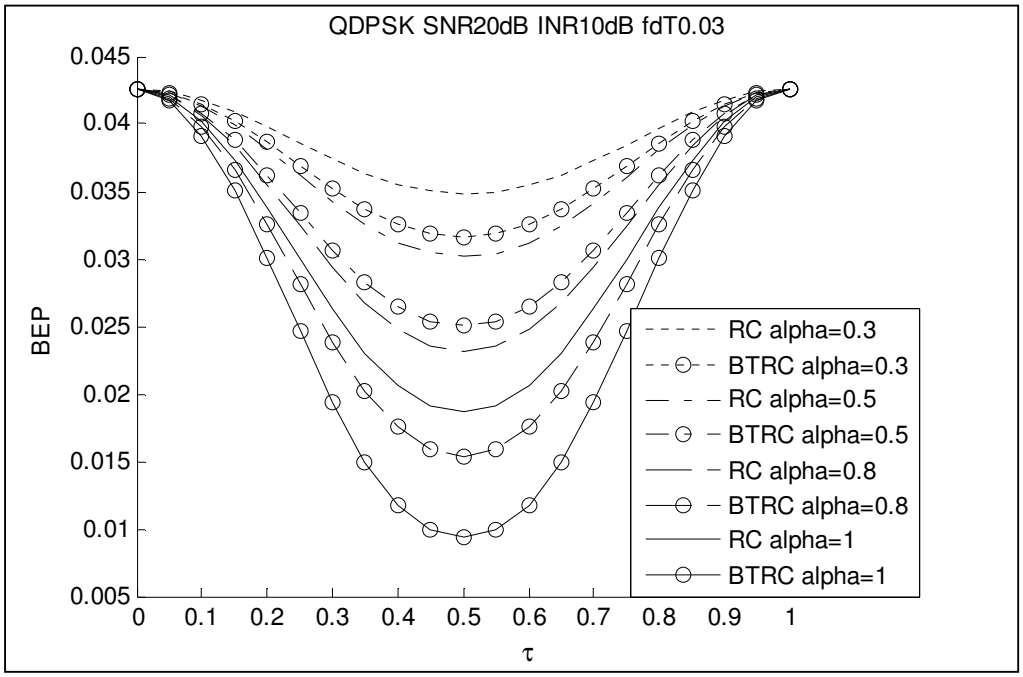

Figure 3.6 BEP vs. normalized timing offset for different roll-off factors

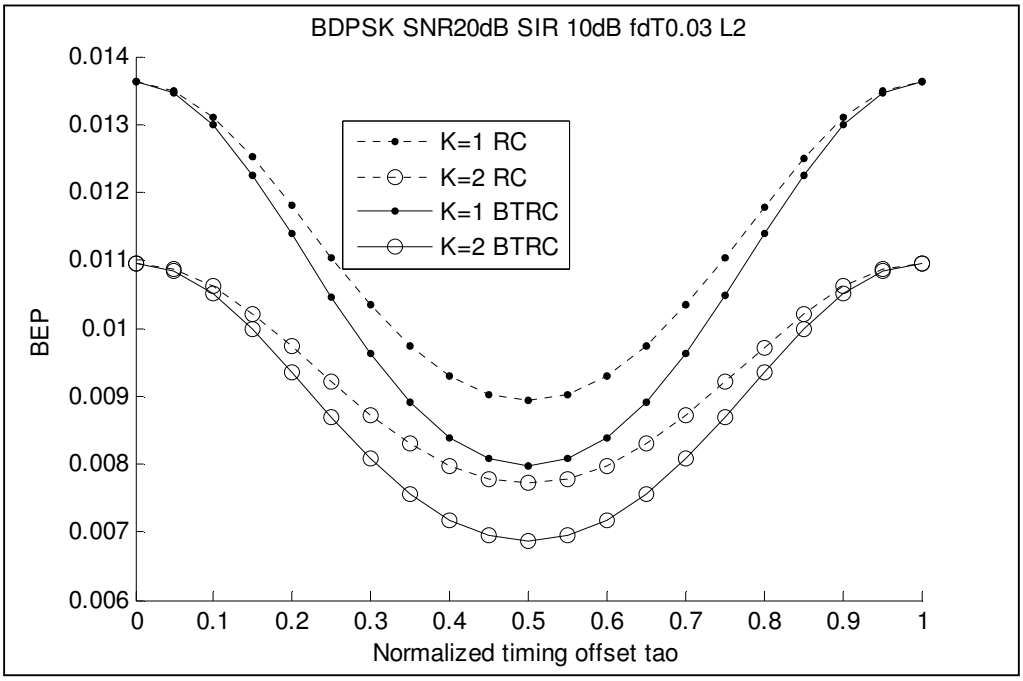

Figure 3.7 BEP vs. normalized timing offset for different pulses with different number of interferers but the same total interfering power

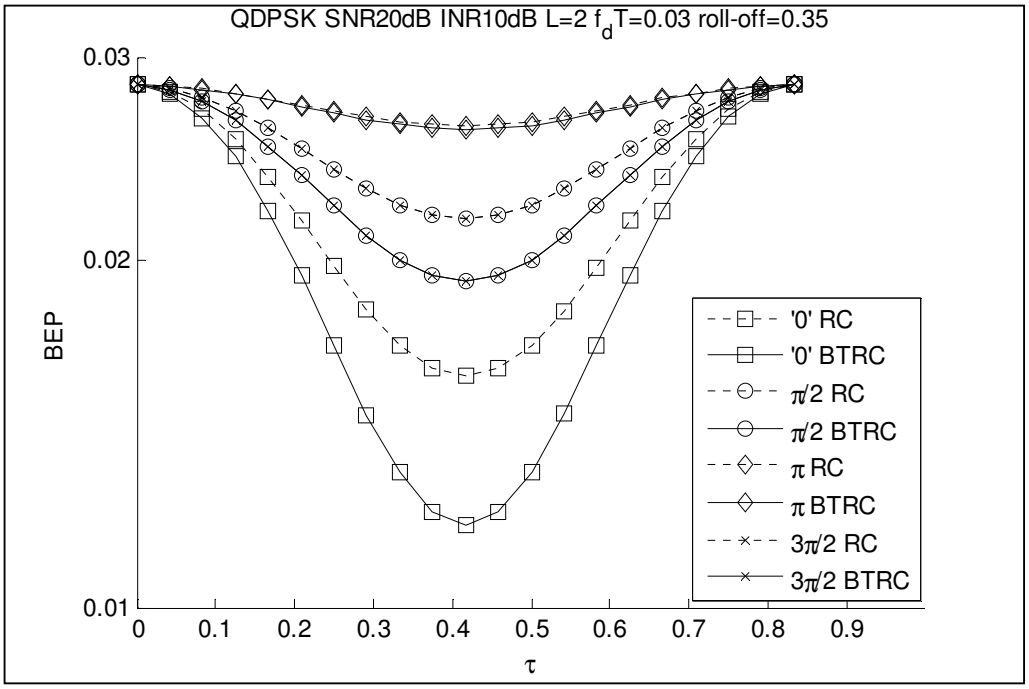

Figure 3.8 BEP vs. normalized timing offset for different pulses with different transmitted data symbols

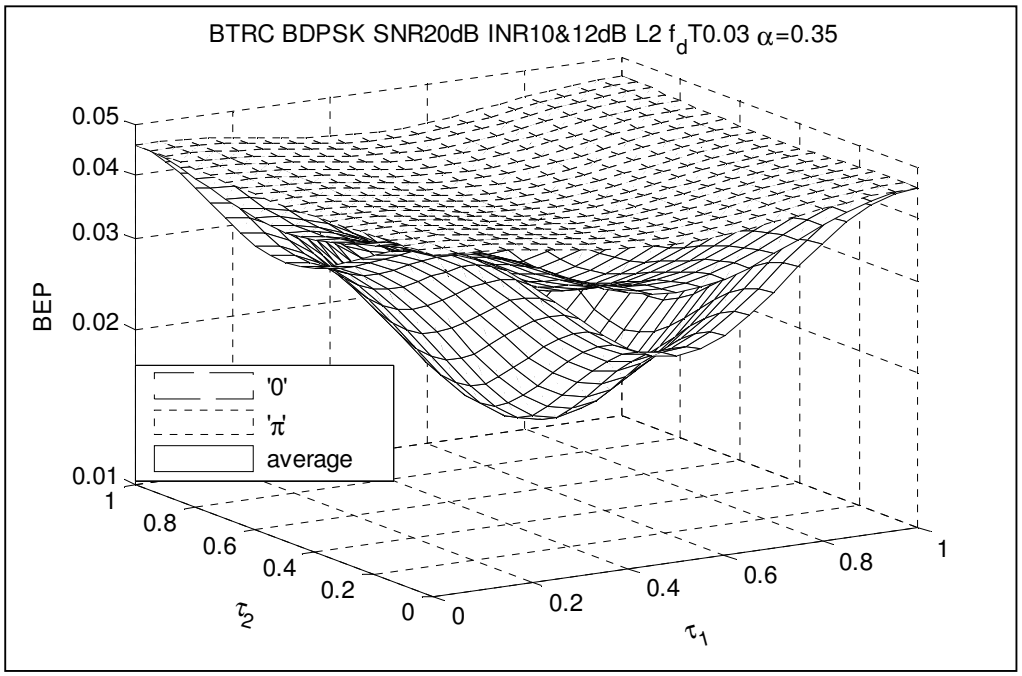

Figure 3.9 BEP vs. normalized timing offset with different transmitted data symbols

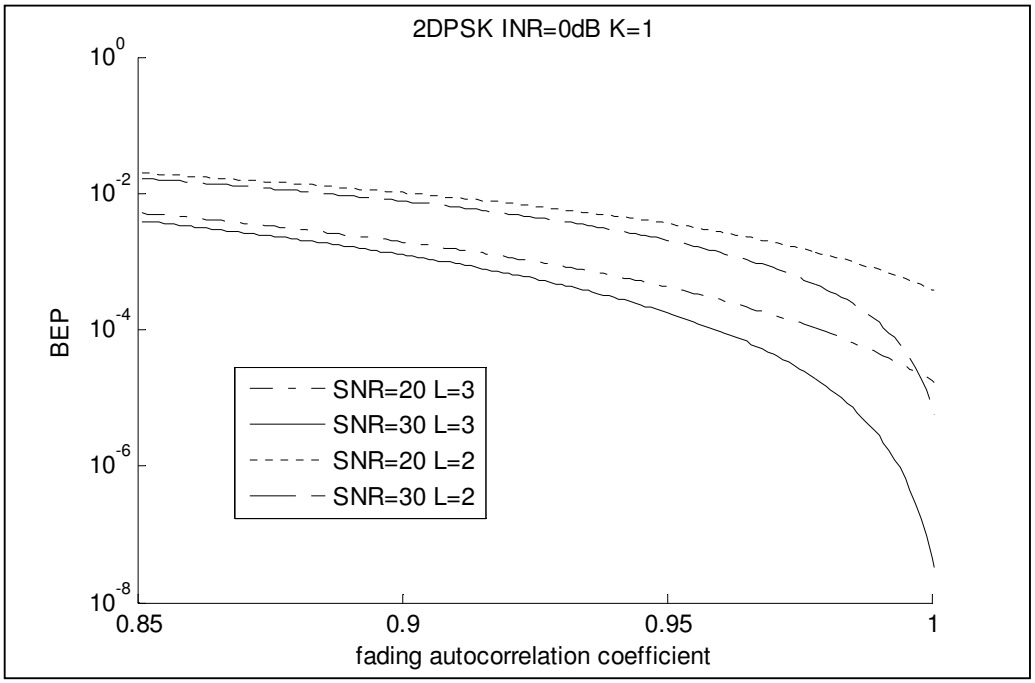

Figure 3.10 BEP vs. fading autocorrelation of the desired signal

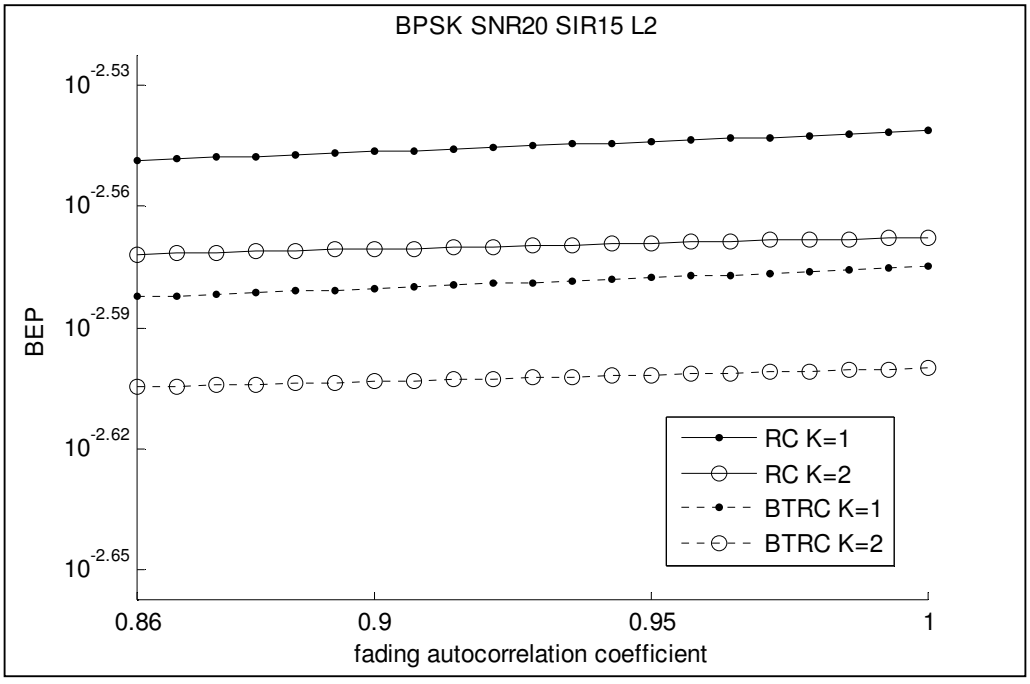

Figure 3.11 BEP vs. fading autocorrelation of the interfering signal

3. 6 Summary

In this chapter, we derived the exact BEP results for BDPSK and QDPSK with multiple asynchronous cochannel interferers in a post-detection MRC diversity system. By examining the effect of CCI synchronism, we find that for the REC pulse based system the synchronous scenario is always the worst case as far as error performance is concerned, while the best performance is obtained when all the interfering signals are half-symbol-duration delayed with respect to the desired user. This enabled us to obtain the upper and the lower bound on the error performance of the asynchronous CCI system in exact and explicit closed-form, which are new and easy to evaluate. Our analysis also confirms that with non-zero timing offset between the interfering signal and the desired signal, the performance of BTRC pulse is better than that of RC pulse. Although not analytically proven, we find from the numerical results that unlike the coherent PSK case, for systems using RC and BTRC pulses, the effect of the interfering signal's timing offset is similar to that of a system using REC pulses.

Chapter 4

Transmit-Receive Diversity System with PSAM

In this chapter we study a Transmit-Receive (Tx-Rx) diversity system for PSK and binary orthogonal signaling with a practical channel estimation strategy, and examine the error performance. An introduction of the current research progress in this area and the motivation of our work are given in Section 4.1. In Section 4.2 we describe the multi-input-multi-output (MIMO) channel model and the pilot-symbol-assisted-modulation (PSAM) scheme for our work. In Section 4.3 we derive the system structure for PSK modulation and analyze its performance. In Section 4.4 we modify the channel estimation strategy for binary orthogonal signaling and analyze its performance. The difference between the two modulation schemes is addressed. The impact of this difference on the design of the transmission and detection strategy for binary orthogonal signal is also discussed. In Section 4.5 numerical results for the performance of the two modulations are presented, and discussions regarding system optimization are given. Section 4.6 summarizes the chapter.

4. 1 Introduction

Recently, it has been recognized that the use of diversity at the transmitter in addition to conventional diversity at the receiver can further reduce the severe effects of fading and improve the system performance. Analogous to Maximum Ratio Combining (MRC) for receive diversity, the concept of Maximum Ratio Transmission

(MRT) for transmit diversity is summarized in [44]. The performance analysis of the Tx-Rx diversity system based on the MRT-MRC structure can be found in [45]-[49]. However, one of the crucial requirements that have been assumed in all these works is the availability of ideal channel state information (CSI) at the receiver for every transmitter-to-receiver link. In a practical system the CSI can only be measured with a certain channel estimation scheme which inevitably will suffer from estimation errors. Therefore, it is important to consider a more realistic system in which the CSI is obtained through a practical channel estimation scheme, and the system should be optimized according to this particular channel estimation scheme, instead of optimizing the structure based on theoretical error-free channel estimation.

In next section we start our development of a practical channel estimation scheme for transmit-receive diversity by considering PSK modulation first.

4. 2 System Model

4. 2. 1 Channel Model

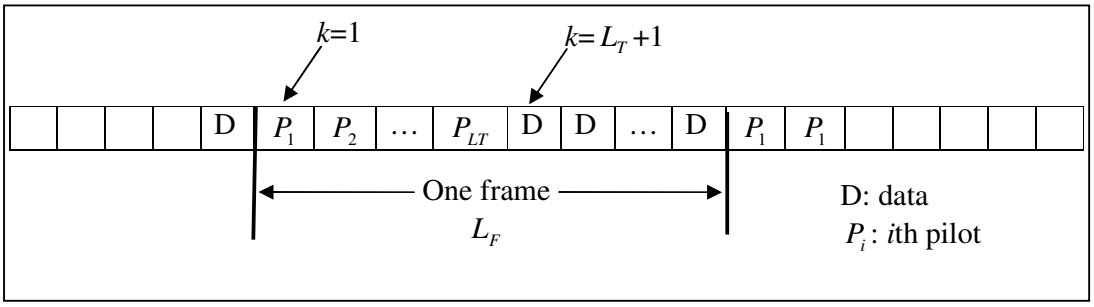

Figure 4.1 Transmitted frame structure

We consider a diversity system with L_T transmit and L_R receive antennas. To estimate the CSI for all the transmitter-to-diversity links, a PSAM scheme is proposed and the corresponding frame structure is shown in Fig. 4.1. Without loss of generality, we consider the frame starting from the first symbol at time k=1. During the pilot

session of each frame, each transmit antenna transmits a pilot symbol at its own designated time slot, e.g., the *j*th transmit antenna will transmit the pilot PSK-type symbol during the *j*th transmission time slot, while the rest of the transmit antennas remain silent until their turns come. At the receiver, based on the known pilot symbol, the *i*th receive antenna will produce, from the received noisy signal, an estimate of the channel gain $\tilde{c}_{i,j}(j)$ which represents the transmission link between the *j*th transmit antenna and the *i*th receive antenna. After the pilot session, the *k*th data symbol $\tilde{s}(k)$ is weighted by a complex weight $\tilde{w}_j(k)$ at the *j*th transmit antenna and sent to the receiver. The objective of this weight is to pre-compensate for channel fading at the transmitter in such a way that the receiver's performance is enhanced. After matched filtering and sampling at the *i*th receive antenna, we obtain the received signal sample for the *k*th symbol transmitted, and this is given by

$$\tilde{r}_i(k) = \sum_{j=1}^{L_T} \tilde{c}_{ij}(k)\tilde{w}_j(k)\tilde{s}(k) + \tilde{n}_i(k)\,. \tag{4.1}$$

The *k*th transmitted data symbol is $\tilde{s}(k) = \sqrt{E_S}\,e^{j\phi(k)}$, where E_S is the average data-symbol energy, and phase $\phi(k) \in \{2m\pi / M; m = 0,1,...,M-1\}$ is the information bearing phase. The AWGN term $\tilde{n}_i(k)$ from the *i*th receive antenna is a complex Gaussian random variable (CGRV) with mean zero and variance N_0. We assume all the channels undergo slow nonselective Rayleigh fading. Therefore the channel fading gains are CGRVs with mean zero and autocorrelation $\frac{1}{2}E[\tilde{c}_{i,j}(k)\tilde{c}^*_{i,j}(k-q)] = \sigma_c^2 R_c(q)$ where $R_c(0) = 1$. In this work we assume a Jake's model where $R_c(q) = J_0(2\pi f_d T q)$ with $J_0(x)$ being the zeroth order Bessel function of the first kind and f_d being the maximum Doppler shift. However, we like to emphasize that the analysis is also applicable to other fading autocorrelation models. The channel fading processes in

different links are assumed iid, i.e., $E[\tilde{c}_{i,j}(k)\tilde{c}^{*}_{s,t}(k)] = 0$ if $i \neq s$ or $j \neq t$, and the AWGN are independent of all the channel fading processes. Such a channel model is also widely used for MIMO system where different transmit antennas transmit different symbols of one user or transmit multiple users' data. It is convenient to express the received signals from all the receive antennas in vector/matrix form as

$$\mathbf{r}(k) = \mathbf{C}(k)\mathbf{w}(k)\tilde{s}(k) + \mathbf{n}(k) \tag{4.2a}$$

where

$$\mathbf{r}(k) = [\tilde{r}_1(k), \tilde{r}_2(k), \cdots, \tilde{r}_{LR}(k)]^T \tag{4.2b}$$

is the received signal vector,

$$\mathbf{w}(k) = [\tilde{w}_1(k), \tilde{w}_2(k), \cdots, \tilde{w}_{LT}(k)]^T \tag{4.2c}$$

is the transmit weight vector,

$$\mathbf{C}(k) = \begin{bmatrix} \tilde{c}_{11}(k) & \tilde{c}_{12}(k) & \cdots & \tilde{c}_{1,LT}(k) \\ \tilde{c}_{21}(k) & & & \vdots \\ \vdots & & \ddots & \\ \tilde{c}_{LR,1}(k) & \cdots & & \tilde{c}_{LR,LT}(k) \end{bmatrix} \tag{4.2d}$$

is the channel fading matrix and

$$\mathbf{n}(k) = [\tilde{n}_1(k), \tilde{n}_2(k), \cdots, \tilde{n}_{LR}(k)]^T \tag{4.2e}$$

is the noise vector.

4. 2. 2 Channel Estimation

With the PSAM channel estimation scheme described earlier in this section, the receiver produces

$$\hat{c}_{i,j}(k) = \sum_{l=1}^{P} \tilde{h}^{*}_{ij}(l,k) \cdot \tilde{r}_i\left((l-P)\cdot L_F + j\right), \tag{4.3}$$

as the estimated version of the channel gain $\tilde{c}_{i,j}(k)$ from the P nearest pilot symbols using the Wiener filter based interpolator

$$\mathbf{h}_{ij}(k) = \left[\tilde{h}_{ij}(1,k), \tilde{h}_{ij}(2,k), \cdots, \tilde{h}_{ij}(P,k) \right]^T \tag{4.4}$$

where $\tilde{h}_{i,j}(l,k)$, $l = 0,1,...,1-P$ are the filter coefficients. Letting

$$\mathbf{r}_{pij} = \left[\tilde{r}_i[L_F(1-P)+j], \tilde{r}_i[L_F(2-P)+j], \cdots, \tilde{r}_i[L_F(P-P)+j] \right]^T, \tag{4.5}$$

be the received pilot samples, then the estimated channel fading gain is

$$\hat{c}_{i,j}(k) = \mathbf{h}_{ij}^H(k)\mathbf{r}_{pij}. \tag{4.6}$$

Based on Wiener filter theory, the optimum filter that minimizes the mean square error (MSE) is [58]

$$\mathbf{h}_{ij}(k) = \mathbf{G}^{-1}\mathbf{v}_{ij}(k) \tag{4.7}$$

where $\mathbf{G} = \frac{1}{2}E\left[\mathbf{r}_{pij} \cdot \mathbf{r}_{pij}^H \right]$ is the $P \times P$ autocorrelation matrix of the pilot vector whose (*s,t*)th entry is

$$g(s,t) = \begin{cases} E_P \sigma_c^2 R_c[|\, s-t \,|\, L_F] & s \neq t \\ E_P \sigma_c^2 + N_0 & s = t \end{cases} \tag{4.8}$$

and $\mathbf{v}_{ij}(k) = \frac{1}{2}E\left[\tilde{c}_{i,j}^*(k) \cdot \mathbf{r}_{pij} \right]$ is the $P \times 1$ covariance vector whose *s*th entry is

$$v_{ij}(k,s) = \sqrt{E_P}\,\sigma_c^2 R_c[k-(s-P)L_F - j]. \tag{4.9}$$

The estimated channel gain in (4.3) can now be rewritten as

$$\hat{c}_{i,j}(k) = \mathbf{v}_{ij}^H(k)(\mathbf{G}^{-1})^H \mathbf{r}_{pij} \tag{4.10}$$

It is a complex Gaussian random variable with mean zero and variance

$$\sigma_{\hat{c}ij}^2(k) = \frac{1}{2}E\left[|\, \hat{c}_{ij}(k) \,|^2 \right] = \mathbf{v}_{ij}^H(k)\mathbf{G}^{-1}\mathbf{v}_{ij}(k).$$

The resultant estimation error, $\tilde{e}_{i,j}(k) = \tilde{c}_{i,j}(k) - \hat{c}_{i,j}(k)$, is also a zero mean complex Gaussian random variable, and it has the smallest possible variance of

$$\begin{aligned}\sigma_{eij}^2(k) &= \frac{1}{2}E\left[|\tilde{c}_{i,j}(k) - \hat{c}_{i,j}(k)|^2\right] \\ &= \sigma_c^2 - \mathbf{v}_{ij}^H(k)(\mathbf{G}^{-1})^H \mathbf{v}_{ij}(k)\end{aligned} \tag{4.11}$$

It is important to point out that in our proposed PSAM scheme, only pilot symbols received before the data session of the current frame are utilized to estimate the channel, or more precisely, to predict the channel; see (4.5). This is because the receiver needs to feed back either the estimated channel gains or the optimized transmit weights so that the transmitter can pre-compensate for the fading effects during the data transmission phase in each frame. For this reason, "future" pilot symbols cannot be utilized in our system for CSI feedback. However, during the data detection phase, the receiver can utilize future pilot symbols to further suppress the residual fading effect in the pre-compensated signal, just like in a conventional PSAM receiver.

It is also worth noting that although we index the variance of the estimated channel gain and that of the corresponding estimation error with both *i* and *j*, their values for different indices *i* and *j* are determined by the value of $\mathbf{v}_{ij}(k)$ which only depends on the *j* index. Therefore both $\sigma_{\hat{c}ij}^2(k)$ and $\sigma_{eij}^2(k)$ shown above also depend on the index *j* only. More specifically, the variance of the estimation error varies across the transmit array direction with $\sigma_{eij}^2(k) > \sigma_{eil}^2(k)$ if $l > j$, but remains the same across the receive array, i.e., $\sigma_{eij}^2(k) = \sigma_{elj}^2(k)$. This is because in our proposed PSAM system the pilot from different transmit antennas are transmitted at different time during the pilot session while the observation of pilot symbols at the receiver is simultaneously made at all receive antennas.

4. 3 PSK System

Having described the MIMO channel model and the channel estimation strategy, in the following, we derive the optimum receiver structure which exploits the characteristics of the PSAM scheme proposed in last section. Unlike those previous works on Tx-Rx diversity system design where a MRC receiver structure is presumed and the transmitter structure is obtained in order to maximize the instantaneous signal-to-noise ratio (SNR), we derive the optimum receiver structure based on the ML detection principle, and derive the optimum transmit strategy that minimizes the instantaneous error probability. In this way, our approach may lead to different transmit and receive weighting schemes other than the standard results obtained earlier in related works.

4. 3. 1 Receiver Design

Based on the estimated channel matrix $\hat{\mathbf{C}}(k) = \left[\hat{c}_{ij}(k)\right]_{i=1,j=1}^{L_R,L_T}$, and assuming that the transmit weighting vector is known for the moment, the received signal during the kth symbol interval could be written as

$$\begin{aligned}\mathbf{r}(k) &= \mathbf{C}(k)\mathbf{w}(k)\tilde{s}(k) + \mathbf{n}(k) \\ &= \underbrace{\hat{\mathbf{C}}(k)\mathbf{w}(k)\tilde{s}(k)}_{\text{effective signal}} + \underbrace{\hat{\mathbf{E}}(k)\mathbf{w}(k)\tilde{s}(k) + \mathbf{n}(k)}_{\text{effective noise}}\end{aligned} \tag{4.12}$$

where $\hat{\mathbf{E}}(k) = \left[\tilde{e}_{ij}(k)\right]_{i=1,j=1}^{L_R,L_T}$ is the channel estimation error matrix. The optimum combiner first calculates the likelihood of the received signal, conditioned on the estimated channel matrix and the transmit weight vector, for all possible value of the transmitted symbol $\tilde{s}_l(k) = \sqrt{E_S}\, e^{j2l\pi/M}$, $l = 0,1,\cdots,M-1$, according to

$$
\begin{aligned}
&P\left(\mathbf{r}(k)\middle|\tilde{s}(k)=\tilde{s}_l(k),\hat{\mathbf{C}}(k),\mathbf{w}(k)\right)\\
&=\prod_{i=1}^{L_R}\frac{1}{\pi N_{0i}(k)}\exp\left[-\frac{\left|\tilde{r}_i(k)-\tilde{H}_i(k)\tilde{s}_l(k)\right|^2}{N_{0i}(k)}\right]\\
&=\left(\prod_{i=1}^{L_R}\frac{1}{\pi N_{0i}(k)}\exp\left[-\frac{\left|\tilde{r}_i(k)\right|^2+\left|\tilde{H}_i(k)\tilde{s}_l(k)\right|^2}{N_{0i}(k)}\right]\right)\exp\left[\frac{2\mathrm{Re}\left[\sum_{i=1}^{L_R}\tilde{r}_i(k)\tilde{H}_i^*(k)\tilde{s}_l^*(k)\right]}{N_{0i}(k)}\right]\\
&=\left(\prod_{i=1}^{L_R}\frac{1}{\pi N_{0i}(k)}\exp\left[-\frac{\left|\tilde{r}_i(k)\right|^2+\left|\tilde{H}_i(k)\tilde{s}_l(k)\right|^2}{N_{0i}(k)}\right]\right)\exp\left[\frac{2\mathrm{Re}\left[\mathbf{w}(k)^H\hat{\mathbf{C}}(k)^H\mathbf{r}(k)\tilde{s}_l^*(k)\right]}{N_{0i}(k)}\right]
\end{aligned}
\tag{4.13}
$$

where $\tilde{H}_i(k)=\sum_{j=1}^{L_T}\hat{c}_{i,j}(k)\tilde{w}_j(k)$ is the effective channel fading gain seen by the *i*th receive antenna, and

$$
\begin{aligned}
N_{0i}(k)&=\frac{1}{2}E[\left|\tilde{n}_i(k)+\tilde{s}(k)\sum_{j=1}^{L_T}\tilde{e}_{i,j}(k)\tilde{w}_j(k)\right|^2]\\
&=N_0+E_S\sum_{j=1}^{L_T}\sigma_{eij}^2\left|\tilde{w}_j(k)\right|^2
\end{aligned}
\tag{4.14}
$$

is the variance of the effective noise in the *i*th receive antenna which is identical for different indices *i*. The ML detector chooses $\tilde{s}_q(k)$ as the detected symbol if it has the largest likelihood. Since the first factor in (4.13) is irrelevant to the hypothesis $\tilde{s}_q(k)$, the maximization of (4.13) is equivalent to the maximization of the term $\mathrm{Re}\left[\mathbf{w}(k)^H\hat{\mathbf{C}}(k)^H\mathbf{r}(k)\tilde{s}_l^*(k)\right]$. At this point, it becomes obvious that the optimum receive weight vector is

$$
\mathbf{f}(k)=\mathbf{w}(k)^H\hat{\mathbf{C}}(k)^H \tag{4.15}
$$

In other word, our receiver is identical to a conventional MRC receiver except that the channel fading matrix is replaced by the estimated channel matrix.

With the optimum receiver structure determined above, our next step is to study the error performance for a given transmit weight vector $\mathbf{w}(k)$, and derive the optimum transmit weighting strategy.

4. 3. 2 Performance Analysis

Conditioned on the channel estimation matrix $\hat{\mathbf{C}}(k)$ and the transmit weight vector $\mathbf{w}(k)$, we can derive the BEP expression of the optimum receiver derived in the last section with BPSK and QPSK signaling. Using an approach similar to that in Chapter 2 for coherent PSK, we found that the conditional BEP is related to the conditional probability

$$\begin{aligned} F(\alpha,k)\Big|_{\hat{\mathbf{C}}(k),\mathbf{w}(k)} &= \Pr\left(\mathrm{Re}\left[\mathbf{w}(k)^H\hat{\mathbf{C}}(k)^H\mathbf{r}(k)e^{j\alpha}\right]<0\Big|\hat{\mathbf{C}}(k),\mathbf{w}(k)\right) \\ &= \Pr\Big(\mathrm{Re}\Big[\mathbf{w}(k)^H\hat{\mathbf{C}}(k)^H\mathbf{n}(k)e^{j\alpha}+\mathbf{w}(k)^H\hat{\mathbf{C}}(k)^H\hat{\mathbf{E}}(k)\mathbf{w}(k)\tilde{s}(k)e^{j\alpha}\Big] \\ &\qquad <-\mathbf{w}(k)^H\hat{\mathbf{C}}(k)^H\hat{\mathbf{C}}(k)\mathbf{w}(k)\tilde{s}(k)\cos(\alpha)\Big|\hat{\mathbf{C}}(k),\mathbf{w}(k)\Big) \\ &= \Pr\left(\mathrm{Re}(\eta_1+\eta_2)<-D\Big|\hat{\mathbf{C}}(k),\mathbf{w}(k)\right) \end{aligned} \tag{4.16}$$

where $D=\mathbf{w}(k)^H\hat{\mathbf{C}}(k)^H\hat{\mathbf{C}}(k)w(k)\tilde{s}(k)\cos(\alpha)$ is a constant when conditioned on $\hat{\mathbf{C}}(k)$ and $\mathbf{w}(k)$. The effective noise due to AWGN and the channel estimation error are defined as $\eta_1(k)=\mathbf{w}(k)^H\hat{\mathbf{C}}(k)^H n(k)e^{j\alpha}$ and $\eta_2=\mathbf{w}(k)^H\hat{\mathbf{C}}(k)^H\hat{\mathbf{E}}(k)\mathbf{w}(k)\tilde{s}(k)e^{j\alpha}$, which are two independent circular symmetric complex Gaussian random variables with mean zero and variances

$$\begin{aligned} \sigma_{\eta 1}^2(k) &= \frac{1}{2}E[\eta_1(k)\eta_1^*(k)] \\ &= \frac{1}{2}E[\mathbf{w}(k)^H\hat{\mathbf{C}}(k)^H\mathbf{n}(k)e^{j\alpha}e^{-j\alpha}\mathbf{n}^H(k)\hat{\mathbf{C}}(k)\mathbf{w}(k)] \\ &= N_0\mathbf{w}(k)^H\hat{\mathbf{C}}(k)^H\hat{\mathbf{C}}(k)\mathbf{w}(k) \end{aligned}$$

and

$$\begin{aligned}\sigma_{\eta 2}^2(k) &= \frac{1}{2}E[\eta_2(k)\eta_2^*(k)] \\ &= \frac{1}{2}E[\mathbf{w}(k)^H\hat{\mathbf{C}}(k)^H\hat{\mathbf{E}}(k)\mathbf{w}(k)\tilde{s}(k)e^{j\alpha}e^{-j\alpha}\tilde{s}^*(k)\mathbf{w}(k)^H\hat{\mathbf{E}}(k)^H\hat{\mathbf{C}}(k)\mathbf{w}(k)] \\ &= E_S\mathbf{w}(k)^H\hat{\mathbf{C}}(k)^H\left(\mathbf{I}_{L_R}\sum_{j=1}^{L_T}|w_j(k)|^2\ \sigma_{eij}^2\right)\hat{\mathbf{C}}(k)\mathbf{w}(k) \\ &= E_S\left(\sum_{j=1}^{L_T}|w_j(k)|^2\ \sigma_{eij}^2\right)\mathbf{w}(k)^H\hat{\mathbf{C}}(k)^H\hat{\mathbf{C}}(k)\mathbf{w}(k)\end{aligned}$$

Based on these statistics, (4.16) can be calculated as

$$\begin{aligned}F(\alpha,k)\Big|_{\hat{\mathbf{C}}(k),\mathbf{w}(k)} &= \int_{-\infty}^{-D}\frac{1}{\sqrt{2\pi(\sigma_{\eta 1}^2+\sigma_{\eta 2}^2)}}\exp\left[-\frac{x^2}{2(\sigma_{\eta 1}^2+\sigma_{\eta 2}^2)}\right]dx \\ &= Q\left(\sqrt{\frac{E_S\mathbf{w}(k)^H\hat{\mathbf{C}}(k)^H\hat{\mathbf{C}}(k)\mathbf{w}(k)\cos^2(\alpha)}{N_0+E_S\sum_{j=1}^{L_T}|w_j(k)|^2\ \sigma_{eij}^2}}\right) \\ &= Q\left(\sqrt{\frac{E_S\mathbf{w}(k)^H\mathbf{A}(k)\mathbf{w}(k)\cos^2(\alpha)}{\mathbf{w}(k)^H\mathbf{B}(k)\mathbf{w}(k)}}\right)\end{aligned} \tag{4.17}$$

where $\mathbf{A}(k)=\hat{\mathbf{C}}(k)^H\hat{\mathbf{C}}(k)$ is a Hermitian matrix, and $\mathbf{B}(k)=diag\left\{E_S\sigma_{eij}^2(k)+N_0\right\}$, $j=1,2,\cdots,L_T$ is a real diagonal matrix. In arriving at (4.17), we make use of the constraint $\sum_i^{L_T}|\tilde{w}_i(k)|^2=1$ on the total transmitted power.

From (4.17), it is obvious that in the presence of channel estimation errors, which have non-identical variances along the transmit array, the optimum transmit weight vector that minimizes the BEP is the one that maximizes the argument of the *Q*-function, which is the ratio of two quadratic forms. According to [61, Theorem 2.4.7], this ratio is bounded by the largest and the smallest eigenvalues of $\mathbf{B}^{-1}(k)\mathbf{A}(k)$ and **the maximum value is attained when $\mathbf{w}(k)$ is chosen to point in the same direction as the principal eigenvector[1] of $\mathbf{B}^{-1}(k)\mathbf{A}(k)$. This result gives us the optimum transmit weighting strategy that minimizes the error probability of the**

[1] The principal eigenvector is the eigenvector corresponds to the largest eigenvalue of the matrix.

system. It is worth noting that in order to allow the transmitter to transmit the data symbols using the optimum transmit weights, either the channel estimates or the weights themselves have to be fed back to the transmitter instantaneously and correctly, which is quite an idealistic assumption. In general, the quality and frequency of the feedback information will definitely affect the overall performance of the Tx-Rx diversity system. However, this issue is not the focus of this investigation. For references on the impact of imperfect feedback, one can refer to, for instance, [62]. Another note is that as indicated at the end of Section 4.2, the data detector should utilize pilot symbols before and after the data symbol under detection to "remove" the residual fading effects in the pre-compensated signal. In such a system, the optimum transmit weights derived above is, strictly speaking, no longer optimal. We will demonstrate later that using "future" pilot symbols during the data detection phase can substantially improve the performance of the proposed system. Next, we examine the performance of our proposed PSAM Tx-Rx diversity system.

From matrix theory, we know that the eigenvalues of the product of two matrices $\mathbf{X}$ and $\mathbf{Y}$ are actually the roots of the determinantal equation

$$| \mathbf{XY} - \lambda \mathbf{I} | = 0,$$

or equivalently the roots of

$$| \mathbf{X}^{-\frac{1}{2}} | \cdot | \mathbf{XY} - \lambda \mathbf{I} | \cdot | \mathbf{X}^{\frac{1}{2}} | = | \mathbf{X}^{-\frac{1}{2}} \mathbf{Y} \mathbf{X}^{\frac{1}{2}} - \lambda \mathbf{I} | = 0,$$

if $| \mathbf{X}^{-\frac{1}{2}} | \neq 0$ and $| \mathbf{X}^{\frac{1}{2}} | \neq 0$. Applying this relation to our case, it follows that the eigenvalues of $\mathbf{B}^{-1}(k)\mathbf{A}(k)$ will coincide with the eigenvalues of

$$\mathbf{B}(k)^{-\frac{1}{2}} \mathbf{A}(k) \mathbf{B}(k)^{-\frac{1}{2}} = \mathbf{B}(k)^{-\frac{1}{2}} \hat{\mathbf{C}}(k)^{H} \hat{\mathbf{C}}(k) \mathbf{B}(k)^{-\frac{1}{2}}$$

for every realization of $\hat{\mathbf{C}}(k)$. Since $\mathbf{B}(k)$ is deterministic, we can conclude that the statistical distributions of the eigenvalues of $\mathbf{B}(k)^{-\frac{1}{2}} \hat{\mathbf{C}}(k)^{H} \hat{\mathbf{C}}(k) \mathbf{B}(k)^{-\frac{1}{2}}$ and $\mathbf{B}^{-1}(k)\mathbf{A}(k)$

are identical. Here, we assume all these eigenvalues are nonzero which is valid when the square matrix $\mathbf{B}(k)^{-\frac{1}{2}}\hat{\mathbf{C}}(k)^H\hat{\mathbf{C}}(k)\mathbf{B}(k)^{-\frac{1}{2}}$ has full rank. Thus our following analysis is valid for the case when $L_T \le L_R$. However, this assumption is made only for the purpose of performance analysis. The optimum transmit weighting strategy discussed above is valid for arbitrary values of L_T and L_R. We will have more to say about this later after we have finished the performance analysis. Since $\mathbf{B}(k)$ is a real diagonal matrix, we can rewrite the matrix of interest as

$$\mathbf{B}(k)^{-\frac{1}{2}}\hat{\mathbf{C}}(k)^H\hat{\mathbf{C}}(k)\mathbf{B}(k)^{-\frac{1}{2}} = \mathbf{Z}(k)^H\mathbf{Z}(k) = \mathbf{W}(k)$$

where $\mathbf{Z}(k) = \hat{\mathbf{C}}(k)\mathbf{B}(k)^{-\frac{1}{2}}$ is the weighted version of the channel estimation matrix. Thus, $\tilde{z}_{i,j}(k)$, the (i, j) th entry of $\mathbf{Z}(k)$, is a complex Gaussian random variable with zero mean and a variance

$$\sigma^2_{zi,j}(k) = \frac{\hat{\sigma}^2_{cij}(k)}{\left(E_S\sigma^2_{eij}(k) + N_0\right)}. \tag{4.18}$$

For our proposed PSAM scheme, both $\sigma^2_{\hat{c}ij}(k)$ and $\sigma^2_{eij}(k)$ vary along the transmit array index, but remain identical along the receive array index. Thus $\mathbf{Z}(k)^H$ satisfies the description of eqn.78 of [63] whose columns can be viewed as samples of correlated complex Gaussian random variables with covariance matrix $\mathbf{\Sigma} = \mathbf{\Sigma}_i = diag\left\{(\sigma^2_{zi,j})_{j=1,\cdots,L_T}\right\}$. Consequently, the joint pdf of the ordered eigenvalues $\mathbf{\Lambda} = [\lambda_1, \cdots, \lambda_{L_T}]$ of $\mathbf{W}(k)$ with $\lambda_1 \ge \lambda_2 \ge \cdots \ge \lambda_{L_T}$ is given by

$$p_{\mathbf{\Lambda}}(x_1,\cdots,x_{L_T},k)=\frac{|\mathbf{\Sigma}|^{-L_R}\,{}_0\tilde{F}_0(-\mathbf{\Sigma}^{-1},\mathbf{W})\,|\mathbf{W}|^{L_R-L_T}}{\prod_{p=1}^{L_T}(L_T-p)!(L_R-p)!}\prod_{i<j}(x_i-x_j)^2$$
$$=\frac{{}_0\tilde{F}_0(-\mathbf{\Sigma}^{-1},\mathbf{W})\prod_{p=1}^{L_T}x_p^{L_R-L_T}\,|\mathbf{V}_1(\mathbf{x})|^2}{\prod_{p=1}^{L_T}(L_T-p)!(L_R-p)!\sigma_{zi,p}^{2L_R}(k)}$$

where $\mathbf{x}=[x_1,\cdots,x_{L_T}]$ is a dummy variable vector, ${}_0\tilde{F}_0(a,b)$ is the hypergeometric function with matrix arguments, and $\mathbf{V}_1(x)$ is the Vandermonde matrix [64, p.29].

As mentioned earlier, we only concentrate on the case where the diversity order at the receiver side is equal to or greater than that at the transmitter side $L_T \le L_R$. This is because only for this case the square matrix $\mathbf{W}(k)$ has full rank and consequently its eigenvalues will all be non-zero. In another case when $L_T > L_R$, the square matrix $\mathbf{W}(k)$ is not full-ranked and contains $L_T - L_R$ zeros eigenvalues. Unfortunately, the distribution of the eigenvalues of $\mathbf{W}(k)$ is unknown for this case. Thus our performance can only be done for the first case at the moment.

Using the alternative form of the hypergeometric function with matrix arguments as in [65], we have

$$p_{\mathbf{\Lambda}}(x_1,\cdots,x_{L_T},k)=\frac{\left[\prod_{i=1}^{L_T}(i-1)!\right]|\mathbf{D}(\mathbf{x},\boldsymbol{\sigma}_z)|\cdot|\mathbf{V}_1(\mathbf{x})|\prod_{p=1}^{L_T}x_p^{L_R-L_T}}{|\mathbf{V}_2(\boldsymbol{\sigma}_z)|\prod_{p=1}^{L_T}(L_T-p)!(L_R-p)!\sigma_{zi,p}^{2L_R}} \tag{4.19}$$
$$=T(k)\cdot|\mathbf{D}(\mathbf{x},\boldsymbol{\sigma}_z)|\cdot|\mathbf{V}_1(\mathbf{x})|\prod_{p=1}^{L_T}x_p^{L_R-L_T},$$

where

$$\boldsymbol{\sigma}_z(k)=[\sigma_{zi,L_T}^2(k),\cdots,\sigma_{zi,2}^2(k),\sigma_{zi,1}^2(k)],$$

$$\mathbf{V}_2\left(\boldsymbol{\sigma}_z(k)\right)\equiv\mathbf{V}_1(-[\sigma_{zi,L_T}^{-2}(k),\cdots,\sigma_{zi,2}^{-2}(k),\sigma_{zi,1}^{-2}(k)]),$$

$T(k)$ is the part that does not depend on $\mathbf{x}$, and

$$\mathbf{D}(\mathbf{x},\boldsymbol{\sigma}_z(k)) = \begin{bmatrix} \exp\left[-\dfrac{x_1}{\sigma^2_{zi,L_T}(k)}\right] & \exp\left[-\dfrac{x_2}{\sigma^2_{zi,L_T}(k)}\right] & \cdots & \exp\left[-\dfrac{x_{L_T}}{\sigma^2_{zi,L_T}(k)}\right] \\ \exp\left[-\dfrac{x_1}{\sigma^2_{zi,L_T-1}(k)}\right] & \ddots & & \vdots \\ \vdots & & \ddots & \\ \exp\left[-\dfrac{x_1}{\sigma^2_{zi,1}(k)}\right] & \cdots & & \exp\left[-\dfrac{x_{L_T}}{\sigma^2_{zi,1}(k)}\right] \end{bmatrix}$$
$$= \left[D\left(x_t, \sigma_{zi,L_T-s+1}(k)\right)\right]_{s,t=1}^{L_T,L_T},$$

with $D(x_t,\sigma_{zi,L_T-s+1}(k)) = \exp\left[-\dfrac{x_t}{\sigma^2_{zi,L_T-s+1}(k)}\right]$. Consequently we can calculate the pdf of the largest eigenvalue by averaging (4.19) over all the other eigenvalues as

$$p_{\lambda_1}(x_1,k) = \int\cdots\int_{\Xi} p_{\Lambda}(x_1,\cdots,x_{L_T},k)d\mathbf{x}$$
$$= T(k)\int\cdots\int_{\Xi} |\mathbf{D}(\mathbf{x},\boldsymbol{\sigma}_z)|\cdot|\mathbf{V}_1(\mathbf{x})|\prod_{p=1}^{L_T} x_p^{L_R-L_T}\,d\mathbf{x}$$

where the integration range is $\Xi = \{\lambda = x_1 \geq x_2 \geq \ldots \geq x_{L_T} \geq 0 = x_{L_T+1}\}$. Using the definition of matrix determinants in [65, eqn.37] and following a similar procedure that leads to Corollary 2 of [65], we find the integral above can be calculated as

$$\int\cdots\int_{\Xi} |\mathbf{D}(\mathbf{x},\boldsymbol{\sigma}_z)|\cdot|\mathbf{V}_1(\mathbf{x})|\prod_{p=1}^{L_T} x_p^{L_R-L_T}\,d\mathbf{x}$$
$$= \sum_{\mu}\mathrm{sgn}(\mu)\sum_{\xi}\mathrm{sgn}(\xi)\int\cdots\int_{\Xi}\prod_{p=1}^{L_T} D(x_p,\sigma_{z,\mu_p}(k))\cdot V_{\xi_p}(x_p)x_p^{L_R-L_T}\,d\mathbf{x}$$
$$= \sum_{\mu}\mathrm{sgn}(\mu)\sum_{\xi}\mathrm{sgn}(\xi)\left(\exp\left[-\frac{\lambda}{\sigma_{z,\mu_1}(k)}\right]\cdot\lambda^{\xi_1-1}\lambda^{L_R-L_T}\cdot\prod_{p=2}^{L_T}\int_{x_{p+1}}^{x_{p-1}}\exp\left[-\frac{\lambda}{\sigma_{z,\mu_p}(k)}\right]\cdot x_p^{\xi_p-1}x_p^{L_p-L_T}\,dx_p\right)$$
$$= \sum_{q=1}^{L_T}|\mathbf{G}_q(k,\lambda)|$$

which gives us

$$p_{\lambda_1}(\lambda,k) = T(k)\cdot\sum_{q=1}^{L_T}|\mathbf{G}_q(k,\lambda)| \tag{4.20a}$$

where $\mathbf{G}_q(k,\lambda)$ is a matrix with its (*s*, *t*)th element given by

$$g_q(s,t,\lambda)=\begin{cases}\sigma_{zi,L_T-s+1}^{2\cdot(L_R-L_T+t)}(L_R-L_T+t-1)! & \\ \quad\cdot\left(1-\exp\left[-\dfrac{\lambda}{\sigma_{zi,L_T-s+1}^2}\right]\sum\limits_{m=0}^{L_R-L_T+t-1}\dfrac{\lambda^m}{m!\sigma_{zi,L_T-s+1}^{2m}}\right) & t\neq q \\ \lambda^{L_R-L_T+t-1}\exp\left[-\dfrac{\lambda}{\sigma_{zi,L_T-s+1}^2}\right] & t=q\end{cases}. \qquad (4.20b)$$

From (4.17), we see that with the optimum transmit weight vector, the conditional BEP attains the minimum value of $F(\alpha,k)\big|_{\lambda}=Q\left(\sqrt{E_S\lambda\cos^2(\alpha)}\right)$. The average BEP could now be calculated by averaging $F(\alpha,k)\big|_{\lambda}=Q\left(\sqrt{E_S\lambda\cos^2(\alpha)}\right)$ over the pdf of λ in (4.20) as

$$F(\alpha,k)=\int_0^{\infty}Q\left(\sqrt{E_S\lambda\cos^2(\alpha)}\right)p_{\lambda_{\max}}(\lambda)d\lambda. \qquad (4.21)$$

In principle, we can use (4.20) and (4.21) to express the average BEP in closed form for an arbitrary number of the transmit antennas. However, the determinants of the matrices in (4.20) are difficult to manipulate in general, except for the case where the square matrix $\mathbf{G}_q(k,\lambda)$ has a dimension of 2×2, which corresponds to the case when $L_T=2$. Therefore, we will use symbolic mathematical tools to calculate the BEP for higher order transmit diversity systems. For the simple case of a dual-transmit ($L_T=2$) and L_R-receive diversity system ($L_R\geq 2$), the derivation of the closed form BEP result is summarized below, starting with the distribution of the largest eigenvalue in (4.20):

$$
\begin{aligned}
p_{\lambda_1}(\lambda,k) = T(k) & \\
&\cdot\Bigg\{(L_R-1)!\sigma_{zi,1}^{2L_R}\lambda^{L_R-2}\exp\left[-\frac{\lambda}{\sigma_{zi,2}^2}\right]+(L_R-2)!\sigma_{zi,2}^{2(L_R-1)}\lambda^{L_R-1}\exp\left[-\frac{\lambda}{\sigma_{zi,1}^2}\right] \\
&-(L_R-2)!\sigma_{zi,1}^{2(L_R-1)}\lambda^{L_R-1}\exp\left[-\frac{\lambda}{\sigma_{zi,2}^2}\right]-(L_R-1)!\sigma_{zi,2}^{2L_R}\lambda^{L_R-2}\exp\left[-\frac{\lambda}{\sigma_{zi,1}^2}\right]. \\
&-(L_R-1)!\exp\left[-\frac{\lambda}{\sigma_{zi,2}^2}-\frac{\lambda}{\sigma_{zi,1}^2}\right]\sum_{m=0}^{L_R-1}\frac{\lambda^{L_R-2+m}}{m!}\left(\sigma_{zi,1}^{2(L_R-m)}-\sigma_{zi,2}^{2(L_R-m)}\right) \\
&-(L_R-2)!\exp\left[-\frac{\lambda}{\sigma_{zi,2}^2}-\frac{\lambda}{\sigma_{zi,1}^2}\right]\sum_{m=0}^{L_R-2}\frac{\lambda^{L_R-1+m}}{m!}\left(\sigma_{zi,2}^{2(L_R-1-m)}-\sigma_{zi,1}^{2(L_R-1-m)}\right)\Bigg\}
\end{aligned}
\tag{4.22}
$$

Substituting this distribution into (4.21) and using the result in (2.14), we have

$$
\begin{aligned}
F(\alpha,k) = T(k) & \\
&\cdot\left\{\begin{array}{l}
(L_R-1)!\sigma_{zi,1}^{2L_R}U(L_R-2,\sigma_{zi,2}^2)+(L_R-2)!\sigma_{zi,2}^{2(L_R-1)}U(L_R-1,\sigma_{zi,1}^2) \\
-(L_R-2)!\sigma_{zi,1}^{2(L_R-1)}U(L_R-1,\sigma_{zi,2}^2)-(L_R-1)!\sigma_{zi,2}^{2L_R}U(L_R-2,\sigma_{zi,1}^2) \\
-(L_R-1)!\displaystyle\sum_{m=0}^{L_R-1}\frac{\left(\sigma_{zi,1}^{2(L_R-m)}-\sigma_{zi,2}^{2(L_R-m)}\right)}{m!}U\left(L_R-2+m,\frac{\sigma_{zi,1}^2\sigma_{zi,2}^2}{\sigma_{zi,1}^2+\sigma_{zi,2}^2}\right) \\
-(L_R-2)!\displaystyle\sum_{m=0}^{L_R-2}\frac{\left(\sigma_{zi,2}^{2(L_R-1-m)}-\sigma_{zi,1}^{2(L_R-1-m)}\right)}{m!}U\left(L_R-1+m,\frac{\sigma_{zi,1}^2\sigma_{zi,2}^2}{\sigma_{zi,1}^2+\sigma_{zi,2}^2}\right)
\end{array}\right\}
\end{aligned}
\tag{4.23a}
$$

where for notation simplicity we have defined

$$
\begin{aligned}
U(b,c) &= \int_0^\infty Q(\sqrt{a\gamma})\cdot\gamma^b\cdot e^{-\frac{\gamma}{c}}d\gamma \\
&= b!c^{b+1}\left(\frac{1}{2}\left[1-\sqrt{\frac{ac}{2+ac}}\right]\right)^{b+1}\sum_{j=0}^{b}\binom{b+j}{j}\left(\frac{1}{2}\left[1+\sqrt{\frac{ac}{2+ac}}\right]\right)^j
\end{aligned}
\tag{4.23b}
$$

where $a \equiv E_S\cos^2(\alpha)$. Similar to the case of Coherent PSK and Differential PSK, the average BEP can be calculated from (4.23) as $P_{2DPSK}(k) = F(\alpha=0,k)$ and $P_{4DPSK}(k) = F\left(\alpha=\frac{\pi}{4},k\right)$. As it is well-known that the quality of the estimated channel gain for a given data symbol using pilot-symbol based channel estimation scheme is dependent on the time distance between the concerned data symbol and the

pilot symbols, the average BEP should be obtained by averaging the above BEP over the whole data session in one frame as

$$p_e(\alpha) = \frac{1}{L_F - L_T} \sum_{k=L_T+1}^{L_F} p_e(\alpha, k). \tag{4.24}$$

4. 4 Binary Orthogonal Signaling

Throughout the limited available results on performance analysis for Tx-Rx diversity system, PSK seems to be the only modulation scheme considered so far. When perfect channel estimation is available, orthogonal signaling is known to have inferior performance compared with PSK. However, in a practical communication system, a certain channel estimation strategy such as PSAM must be adopted in order to coherently detect PSK signals, which would reduce the data rate and the SNR and also introduce some performance loss in "fast" fading environment. On the other hand for orthogonal signals, the detection could be done "non-coherently" without any additional channel estimation strategy, so no data rate reduction would be incurred. In this section we apply the proposed PSAM channel estimation scheme to binary orthogonal signaling, and discuss its feasibility and performance.

4. 4. 1 Implicit PSAM Scheme

For a system using binary orthogonal signaling, the transmitted signal in $s_0 s_1$-space is given in vector notation as

$$\mathbf{s}(k) = \begin{cases} \sqrt{E_S}\mathbf{s}_0 = \sqrt{E_S}\begin{bmatrix} 1 \\ 0 \end{bmatrix} & \text{'0' is transmitted} \\ \sqrt{E_S}\mathbf{s}_1 = \sqrt{E_S}\begin{bmatrix} 0 \\ 1 \end{bmatrix} & \text{'1' is transmitted} \end{cases} \tag{4.25}$$

where E_S is the energy per bit, and $\mathbf{s}_0$ and $\mathbf{s}_1$ are the orthonormal basis vectors. An alternative interpretation of the orthogonal signal constellation in a rotated coordinates is demonstrated in [4, Fig.1] which we include in Fig. 4.2 for completeness. In the rotated coordinates, the orthogonal signal can be seen as an antipodal signal plus an unmodulated component that exists in both basis signals. This unmodulated component actually provides channel reference in a conventional quadratic receiver which leads to a coherent detection interpretation for conventional "non-coherent detection". Therefore, no additional pilot symbols are needed for orthogonal signals to provide channel estimation. With this feature of orthogonal signals, we set up the following PSAM scheme for a Tx-Rx diversity system.

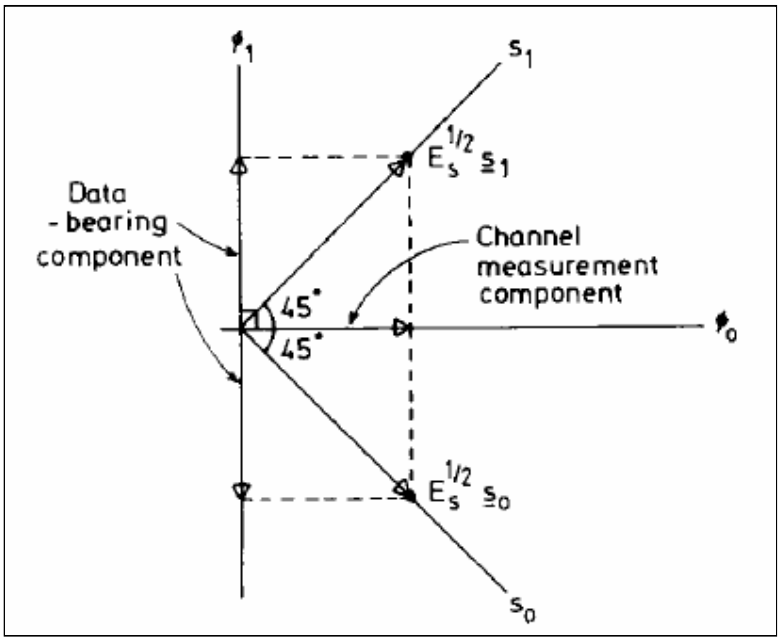

Figure 4.2 Binary orthogonal signals in rotated coordinates

The implicit PSAM (IPSAM) frame structure is similar as for PSK which is shown in Fig. 4.1. The major difference here is that the "pilot" session is composed of data symbols instead of known training symbols. The channel estimation is achieved by the unmodulated component of orthogonal signals, therefore the pilot-symbols we are referring here is not actually pilot symbols and we denote this scheme "implicit"

PSAM scheme to distinguish it from the conventional PSAM (CPSAM) scheme. These estimated channel state information are then used to predict the channel gain for the data session, which is then used to optimize the transmit weights to pre-compensate for the fading. Here one should be reminded that although this IPSAM scheme provides full transmission rate, its estimated channel gain is less accurate than that of PSAM-PSK with the same SNR level, because the unmodulated component has only half of the symbol energy.

Now consider a system employing L_T transmit and L_R receive antennas. Without loss of generality, we consider the frame starting from time instance $k = 1$. During the pilot session of each frame, each transmit antenna transmits a pilot symbol, which is also an information bearing data symbol, at its own designated time slot, e.g., the *j*th transmit antenna will transmit symbol $\mathbf{s}_p(j) = \sqrt{E_{SP}}\mathbf{s}_l$, $l = 0$ or 1, during the *j*th transmission time slot, while all the rest of the transmit antennas remain silent. At the receiver, based on the received symbols and using the interpretation from [4], the *i*th receive antenna will produce an estimate of the channel gain $\tilde{c}_{i,j}(j)$ from the unmodulated component, for the transmission link between the *j*th transmit antenna and the *i*th receive antenna. After the pilot session, the *k*th data symbols are weighted by complex weights $\tilde{w}_j(k)$ at the *j*th transmit antenna and sent to the receiver where the weights should be optimized, as will be shown later, to minimize the error probability. After correlating with the basis signal, the received signal from the *i*th receive antenna during the *k*th symbol duration can be written as

$$\tilde{\mathbf{r}}_i(k) = \begin{bmatrix} \tilde{r}_{i0}(k) \\ \tilde{r}_{i1}(k) \end{bmatrix} = \begin{cases} \sqrt{E_{SP}}\mathbf{s}_l(k)\tilde{c}_{ik}(k) + \tilde{\mathbf{n}}_i(k) & k = j\ ;\ k \le L_T \\ & \text{(pilot session)} \\ \sqrt{E_{SD}}\mathbf{s}_l(k)\sum_{j=1}^{L_T}\tilde{c}_{ij}(k)\tilde{w}_j(k) + \tilde{\mathbf{n}}_i(k) & k > L_T \\ & \text{(data session)} \end{cases} \tag{4.26}$$

where E_{SP} and E_{SD} denote, respectively, the energy of the transmitted symbol during the pilot session and the data session, and $\tilde{\mathbf{n}}_i(k) = [\tilde{n}_{i0}(k), \tilde{n}_{i1}(k)]^T$ is the AWGN vector with mean zero and covariance matrix $\frac{1}{2}E[\tilde{\mathbf{n}}_i(k)\tilde{\mathbf{n}}_i^H(k)] = N_0\mathbf{I}$. As we assume independent and identically distributed nonselective Rayleigh fading channels for all the transmission links, the channel fading gains are therefore, iid CGRVs with mean zero and autocorrelation $\frac{1}{2}E[\tilde{c}_{ij}(k)\tilde{c}_{st}^*(k-q)] = \sigma_c^2 R_c(q)\delta_{is}\delta_{jt}$ where σ_c^2 is the power of the channel fading process, δ_{ab} denotes the Kronecker delta function and $R_c(q)$ is the channel autocorrelation coefficient.

The channel estimation process for the data session is based on the CSI extracted from pilot symbols using a Wiener filter as in Section 4.2. From the interpretation demonstrated in Fig. 4.2, we form the pilot symbol vector as

$$\mathbf{r}_{pij} = \left[\left\{ \tilde{r}_{i0}(L_F(s-P)+j) + \tilde{r}_{i1}(L_F(s-P)+j) \right\}_{s=1}^{P} \right].$$

The channel estimate $\hat{c}_{ij}(k)$ is then generated as

$$\hat{c}_{ij}(k) = \mathbf{h}_{ij}^H(k) \cdot \mathbf{r}_{pij}$$

where the optimum filter coefficient vector that minimizes the MSE is given by

$$\mathbf{h}_{ij} = \mathbf{R}^{-1} \cdot \mathbf{v}_{ij}(k). \tag{4.27}$$

The pilot sequence covariance matrix $\mathbf{R}$ and the cross correlation vector $\mathbf{v}_{ij}(k)$ are defined in a similar manner as in the case of PSAM-PSK scheme. Thus the (*s*, *t*)th entry of $\mathbf{R}$ is given by

$$\begin{aligned}\mathbf{R}(s,t) &= \frac{1}{2}E\Big(\big[\tilde{r}_{i0}(L_F(s-P)+j)+\tilde{r}_{i1}(L_F(s-P)+j)\big] \\ &\qquad \cdot\big[\tilde{r}_{i0}(L_F(t-P)+j)+\tilde{r}_{i1}(L_F(t-P)+j)\big]^*\Big) \\ &= \begin{cases} R_c[(s-t)L_F]\sigma_c^2 E_{SP} & s \neq t \\ E_{SP}\sigma_c^2 + 2N_0 & s = t \end{cases}\end{aligned} \tag{4.28}$$

and the sth entry of $\mathbf{v}_{ij}(k)$ is

$$\begin{aligned}\mathbf{v}_{ij}(k,s) &= \frac{1}{2}E[\tilde{c}_{ij}^*(k)\cdot\{\tilde{r}_{i0}(L_F(s-P)+j)+\tilde{r}_{i1}(L_F(s-P)+j)\}] \\ &= R_c[k-L_F(s-P)-j]\sqrt{E_{SP}}\end{aligned}. \tag{4.29}$$

Comparing (4.28) with (4.8), we find that the channel estimate provided by binary orthogonal signals has twice the amount of noise compared to that of PSK pilot symbols. Therefore, the estimation quality of using the unmodulated component of orthogonal signal is worse than using a known pilot symbol. The channel estimation error from the above scheme is

$$\tilde{e}_{ij}(k) = \tilde{c}_{ij}(k) - \hat{c}_{ij}(k) \tag{4.30}$$

which is a complex Gaussian random variable with mean zero and variance

$$\sigma_{eij}^2(k) = \frac{1}{2}E[|\,\tilde{e}_{ij}(k)\,|^2] = \sigma_c^2 - \mathbf{v}_{ij}^H(k)\mathbf{R}^{-1}\mathbf{v}_{ij}(k)\,. \tag{4.31}$$

Now we can rewrite the received signal during the data session as

$$\tilde{\mathbf{r}}_i(k) = \underbrace{\sqrt{E_{SD}}\,\mathbf{s}_l(k)\sum_{j=1}^{L_T}\hat{c}_{ij}(k)\tilde{w}_j(k)}_{\text{Effective Signal}} + \underbrace{\sqrt{E_{SD}}\,\mathbf{s}_l(k)\sum_{j=1}^{L_T}\tilde{e}_{ij}(k)\tilde{w}_j(k)+\tilde{\mathbf{n}}_i(k)}_{\text{Effective Noise}}\,. \tag{4.32}$$

The effective noise vector is a complex Gaussian vector with independent but non-identical components. It is trivial to show that for all *i*, the effective noise vector conditioned on hypothesis *l* has zero mean, and a covariance matrix given by

$$\begin{aligned}\mathbf{\Phi}_{Nl}(k) &= E_{SD}\sum_{j=1}^{L_T}|\,\tilde{w}_j(k)\,|^2\;\sigma_{eij}^2(k)\cdot\mathbf{s}_l\mathbf{s}_l^T + N_0\mathbf{I} \\ &= \begin{bmatrix}\phi_{Nl0}(k) & 0\\ 0 & \phi_{Nl1}(k)\end{bmatrix},\end{aligned} \tag{4.33a}$$

where

$$\phi_{N00}(k) = \phi_{N11}(k) = E_{SD}\sum_{j=1}^{L_T}|\,\tilde{w}_j(k)\,|^2\;\sigma_{eij}^2(k) + N_0 \tag{4.33b}$$

and

$$\phi_{N01}(k) = \phi_{N10}(k) = N_0\,. \tag{4.33c}$$

Having specified the IPSAM scheme in detail and obtained all the necessary parameters, next we discuss the receiver structure.

4. 4. 2 Feasibility of Generalized Quadratic Receiver

In the previous part of our proposed Tx-Rx diversity system with PSAM for PSK, the detection is based on channel estimation from the pilot symbols. For orthogonal signaling, as we have discussed earlier, the received signal itself contains a hidden unmodulated component that could be considered as a “virtual pilot”. Inspired by this idea, in [66], it has been shown that the implementable version of the optimum symbol-by-symbol detector for orthogonal signaling in fading channel is actually a generalized quadratic receiver (GQR) that utilizes the unmodulated components of the adjacent received symbols as well for channel estimation. By exploiting the fact that the fading process is temporally correlated while the noise is temporally white, this GQR can refine the channel estimation from the unmodulated component in the same way a conventional PSAM channel estimator does. The performance of the GQR is then very close to that of a coherent detector with ideal channel estimation. Therefore, it is interesting to examine the feasibility of GQR to our proposed PSAM Tx-Rx diversity system.

With the received signal given in (4.26), in order to detect the *k*th transmitted symbol, first the receiver need to form a virtual pilot sequence for the *i*th diversity branch using the unmodulated components of the $2L+1$ nearest received symbols, with the *k*th symbol in the middle. This virtual pilot sequence is given by

$$\mathbf{r}_{pi}(k) = \left[\left\{ \tilde{r}_{i0}(k+q) + \tilde{r}_{i1}(k+q) \right\}_{q=-L}^{L} \right].$$

Then similar to (4.3-4.10), channel estimation filters that exploit the channel fading autocorrelation property are utilized to estimate the channel gain for the *k*th symbol duration. In a conventional receive diversity system, the channel fading autocorrelation function could be assumed time invariant and known to the receiver, for example, a Jakes' fading power spectrum is assumed in Section 4.3 for PSK signal. Now in a Tx-Rx diversity system, the effective channel fading observed by each receive antenna is sum of the weighted version of the true channel fading from all the transmit antenna. Thus when the GQR exploits the received signal's fading autocorrelation property to jointly produce optimum channel estimation, it also needs to take the weights $\left\{ \mathbf{w}(k+q) \right\}_{q=-L}^{L}$ into consideration. Supposing now we need to estimate the *0*th symbol's channel gain seen by the *i*th receive branch $H_i(0) = \sum_{j=1}^{L_T} c_{ij}(0) w_j(0)$, the optimum wiener filter is then given by

$$\mathbf{h}(0) = \mathbf{R}^{-1}(0) \cdot \mathbf{v}(0) \tag{4.34}$$

where $\mathbf{R}(0)$ is the covariance matrix of $\mathbf{r}_{pi}(0)$ with its (*s*, *t*) th element given by

$$\begin{aligned} \mathbf{R}(s,t,0) &= \frac{1}{2} E\left[H_i(-L+s-1) H_i(-L+t-1)^* \right] \\ &= \frac{1}{2} E\left[\left(\sum_{j=1}^{L_T} c_{ij}(-L+s-1) w_j(-L+s-1) + \sum_{k=0}^{1} n_{ik}(-L+s-1) \right) \right. \\ &\qquad \left. \left(\sum_{j=1}^{L_T} c_{ij}^*(-L+t-1) w_j^*(-L+t-1) + \sum_{k=0}^{1} n_{ik}^*(-L+t-1) \right) \right] \end{aligned} \tag{4.35}$$

and $\mathbf{v}(0)$ is the covariance vector between $H_i(0)$ and $\mathbf{r}_{pi}(0)$ with its sth element given by

$$\begin{aligned}\mathbf{v}(s,0) &= \frac{1}{2}E\left[H_i^*(0)H_i(-L+s-1)\right] \\ &= \frac{1}{2}E\left[\left(\sum_{j=1}^{L_T} c_{ij}^*(0)w_j^*(0) + \sum_{k=0}^{1} n_{ik}^*(0)\right)\right. \\ &\qquad \left.\left(\sum_{j=1}^{L_T} c_{ij}(-L+s-1)w_j(-L+s-1) + \sum_{k=0}^{1} n_{ik}(-L+s-1)\right)\right].\end{aligned} \tag{4.36}$$

In general, the transmit weights $\{\mathbf{w}(k+q)\}_{q=-L}^{L}$ are optimized according to the instantaneous value of the channel fading gains or their estimates. Therefore, the calculation of (4.35) and (4.36) should include the statistics of $\{\mathbf{w}(k+q)\}_{q=-L}^{L}$ as well. Unfortunately, these weights are normally related to the fading gains through the eigenvector of the instantaneous channel matrix. Thus their distribution is currently unknown. Consequently the GQR is difficult to implement for Tx-Rx diversity system.

4. 4. 3 PSAM channel estimation based ML detector

In this sub-section we consider a detector that utilizes the channel estimation from pilot symbols and that from the unmodulated component of the current data symbols. Using the received signal model in (4.32), the likelihood of the received signal on hypothesis l when conditioned on channel fading estimates $\hat{\mathbf{C}}(k) = \left[\hat{c}_{ij}(k)\right]_{i=1,j=1}^{L_R,L_T}$, and known transmit weights $\tilde{\mathbf{w}}(k) = \left[\tilde{w}_j(k)\right]_{j=1}^{L_T}$, can be calculated as

$$\begin{aligned}&p\left(\tilde{\mathbf{r}}_i(k)\,|_{i=1}^{L_R}\,\mathbf{s}_l, \hat{\mathbf{C}}(k), \tilde{\mathbf{w}}(k)\right) \\ &= \prod_{i=1}^{L_R} \frac{\exp\left\{-\frac{1}{2}[\tilde{\mathbf{r}}_i(k) - \sqrt{E_{SD}}\mathbf{s}_l\tilde{H}_i(k)]^H \mathbf{\Phi}_{Nl}^{-1}(k)[\tilde{\mathbf{r}}_i(k) - \sqrt{E_{SD}}\mathbf{s}_l\tilde{H}_i(k)]\right\}}{(2\pi)^2 \,|\, \mathbf{\Phi}_{Nl}(k) \,|}.\end{aligned} \tag{4.37}$$

Substituting the symbol value into the above conditional pdf, and using the fact that the determinant of the effective noise covariance matrix for the two hypothesises are the same, we have the following LRT (likelihood ratio test)

$$\Lambda = \frac{\prod_{i=1}^{L_R} \exp\left\{-\frac{1}{2}[\tilde{\mathbf{r}}_i(k) - \sqrt{E_{SD}}\mathbf{s}_0\tilde{H}_i(k)]^H \boldsymbol{\Phi}_{N0}^{-1}(k)[\tilde{\mathbf{r}}_i(k) - \sqrt{E_{SD}}\mathbf{s}_0\tilde{H}_i(k)]\right\} \underset{\mathbf{s}_1}{\overset{\mathbf{s}_0}{>}} 1,}{\prod_{i=1}^{L_R} \exp\left\{-\frac{1}{2}[\tilde{\mathbf{r}}_i(k) - \sqrt{E_{SD}}\mathbf{s}_1\tilde{H}_i(k)]^H \boldsymbol{\Phi}_{N1}^{-1}(k)[\tilde{\mathbf{r}}_i(k) - \sqrt{E_{SD}}\mathbf{s}_1\tilde{H}_i(k)]\right\}}$$

which, after using (4.33) and some manipulation, is equivalent to

$$\sum_{i=1}^{L_R}\left(\left[|\tilde{r}_{i0}(k)|^2 - |\tilde{r}_{i1}(k)|^2\right]\frac{\phi_{N00}(k) - \phi_{N01}(k)}{\phi_{N00}(k)\phi_{N01}(k)} + 2\,\mathrm{Re}\left[\frac{[\tilde{r}_{i0}(k) - \tilde{r}_{i1}(k)]\sqrt{E_{SD}}\tilde{H}_i^*(k)}{\phi_{N00}(k)}\right]\right) \underset{\mathbf{s}_1}{\overset{\mathbf{s}_0}{>}} 0$$

Applying the equality $|\tilde{x}|^2 - |\tilde{y}|^2 = \mathrm{Re}\left[(\tilde{x} - \tilde{y})(\tilde{x} + \tilde{y})^*\right]$, the above LRT gives

$$\sum_{i=1}^{L_R}\mathrm{Re}\left\{[\tilde{r}_{i0}(k) - \tilde{r}_{i1}(k)]\cdot\left[\left(\tilde{r}_{i0}^*(k) + \tilde{r}_{i1}^*(k)\right)\cdot\left(\phi_{N00}(k) - \phi_{N01}(k)\right) + 2\sqrt{E_{SD}}\tilde{H}_i^*(k)\phi_{N01}(k)\right]\right\} \underset{\mathbf{s}_0}{\overset{\mathbf{s}_0}{>}} 0.$$

Substituting (4.33) into the above equation gives us the final LRT as

$$\sum_{i=1}^{L_R}\mathrm{Re}\left\{[\tilde{r}_{i0}(k) - \tilde{r}_{i1}(k)]\cdot\left[\left(\tilde{r}_{i0}^*(k) + \tilde{r}_{i1}^*(k)\right)\cdot E_{SD}\sum_{j=1}^{L_T}|\tilde{w}_j(k)|^2\ \sigma_{eij}^2(k) + 2\sqrt{E_{SD}}\tilde{H}_i^*(k)N_0\right]\right\} \underset{\mathbf{s}_0}{\overset{\mathbf{s}_0}{>}} 0. \tag{4.38}$$

Now (4.38) shows that the PSAM channel estimation based ML detector actually utilizes the channel estimation from pilot symbols and also that from the unmodulated component of the current received signal. For the ideal case when the channel estimation from pilot symbols is perfect, the estimation error vanishes, thus the detector reduces to an ideal coherent detector. In the other extreme, when no pilot

symbols are used to provide the predicted channel estimates, the receiver reduces to a conventional QR.

Next, we analyze the BEP of this PSAM channel estimation based ML detector conditioned on known transmit weights and channel estimates. Then we try to derive the optimal weighting strategy that provides the minimum error probability for this case. Without loss of generality, we assume $\mathbf{s}_0$ is transmitted. The conditional BEP in this case can be calculated as

$$\begin{aligned} & P_e(k)\Big|\{\hat{c}_{ij}(k),\tilde{w}_j(k)\}_{i=1,j=1}^{L_R,L_T} \\ & = \Pr\Big\{\sum_{i=1}^{L_R}\mathrm{Re}\Big[\big(\tilde{x}_i(k)+\tilde{\eta}_i(k)+\tilde{n}_{i0}(k)-\tilde{n}_{i1}(k)\big) \\ & \qquad \cdot\left([\tilde{x}_i(k)+\tilde{\eta}_i(k)+\tilde{n}_{i0}(k)+\tilde{n}_{i1}(k)]^* + \frac{2N_0}{N_E}\tilde{x}_i^*(k)\right)\Big] < 0\Big\} \\ & = \Pr\Big\{\sum_{i=1}^{L_R}\mathrm{Re}\Big[\big(\tilde{x}_i(k)+\tilde{\eta}_i(k)+\tilde{n}_{i0}(k)-\tilde{n}_{i1}(k)\big) \\ & \qquad \cdot\left(\tilde{x}_i(k)+\frac{N_E\left[\tilde{\eta}_i(k)+\tilde{n}_{i0}(k)+\tilde{n}_{i1}(k)\right]}{2N_0+N_E}\right)^*\Big] < 0\Big\} \end{aligned} \tag{4.39a}$$

where

$$\tilde{x}_i(k) = \sqrt{E_{SD}}\,\tilde{H}_i(k) = \sqrt{E_{SD}}\sum_{j=1}^{L_T}\hat{c}_{ij}(k)\tilde{w}_j(k), \tag{4.39b}$$

$$\tilde{\eta}_i(k) = \sqrt{E_{SD}}\sum_{j=1}^{L_T}\tilde{e}_{ij}(k)\tilde{w}_j(k) \tag{4.39c}$$

and

$$\begin{aligned} N_E &= E_{SD}\sum_{j=1}^{L_T}|\,\tilde{w}_j(k)\,|^2\;\sigma_{eij}^2(k) \\ &= E_{SD}\,\mathbf{w}(k)^H\,diag\{\sigma_{eij}^2(k)_{j=1}^{L_T}\}\mathbf{w}(k) \end{aligned}. \tag{4.39d}$$

Now further define

$$\tilde{a}_i(k) = \tilde{\eta}_i(k)+\tilde{n}_{i0}(k)-\tilde{n}_{i1}(k) \tag{4.40}$$

and

$$\tilde{b}_i(k) = \frac{N_E\left[\tilde{\eta}_i(k) + \tilde{n}_{i0}(k) + \tilde{n}_{i1}(k)\right]}{2N_0 + N_E}. \tag{4.41}$$

It is trivial to show that they both are complex Gaussian random variables with means zero, variances $N_E + 2N_0$ and $N_E^2/(N_E + 2N_0)$, respectively, and a cross correlation $\frac{1}{2}E[\tilde{a}_i(k)\tilde{b}_i^*(k)] = N_E^2/(N_E + 2N_0)$. Therefore, conditioning on $\tilde{b}_i(k)$ and following the same approach which leads to (2.9)-(2.12), we could write

$$\tilde{a}_i(k) = \frac{\tilde{b}_i(k)(N_E + 2N_0)}{N_E} + \tilde{\xi}_i(k) \tag{4.42}$$

where $\tilde{\xi}_i(k)$ represents the uncertain component of $\tilde{a}_i(k)$ when conditioned on $\tilde{b}_i(k)$, which is a complex Gaussian random variable with mean zero and a variance $(4N_0^2 + 4N_E N_0)/(N_E + 2N_0)$. With these changes of variables, the conditional BEP conditioned on both $\{\tilde{x}_i(k)\}_{i=1}^{L_R}$ and $\{\tilde{b}_i(k)\}_{i=1}^{L_R}$ is now

$$\begin{aligned}
&P_e\left(k \middle| \{\hat{c}_{ij}(k), \tilde{w}_j(k), \tilde{b}_i(k)\}_{i=1,j=1}^{L_R,L_T}\right) \\
&= \Pr\left\{\sum_{i=1}^{L_R} \mathrm{Re}\left[\left(\tilde{x}_i(k) + \tilde{b}_i(k)\frac{N_E + 2N_0}{N_E} + \tilde{\xi}_i(k)\right)\right.\right. \\
&\qquad \left.\left. \cdot\left(\tilde{x}_i(k) + \tilde{b}_i(k)\frac{N_E + 2N_0}{N_E}\right)^*\right] < 0 \middle| \{\hat{c}_{ij}(k), \tilde{w}_j(k), \tilde{b}_i(k)\}_{i=1,j=1}^{L_R,L_T}\right\} \\
&= Q\left(\sqrt{\frac{\left[\mathbf{x}(k) + \mathbf{b}(k)\frac{N_E + 2N_0}{N_E}\right]^H\left[\mathbf{x}(k) + \mathbf{b}(k)\frac{N_E + 2N_0}{N_E}\right]}{(4N_0^2 + 4N_E N_0)/(N_E + 2N_0)}}\right) \\
&= Q\left(\sqrt{\frac{\gamma(N_E + 2N_0)}{(4N_0^2 + 4N_E N_0)}}\right)
\end{aligned} \tag{4.43}$$

where $\mathbf{x}(k)$ and $\mathbf{b}(k)$ are vector forms of $\{\tilde{x}_i(k)\}_{i=1}^{L_R}$ and $\{\tilde{b}_i(k)\}_{i=1}^{L_R}$. The conditional error probability shown above suggests a similar form as that for an MRC receiver in

Rician channels with known specular component, where γ is noncentral chi-square distributed as

$$p_\gamma(\gamma) = \frac{1}{2\sigma_\gamma^2}\left(\frac{\gamma}{m^2}\right)^{\frac{[L_R-1]}{2}} \exp\left[-\frac{m^2+\gamma}{2\sigma_\gamma^2}\right] I_{L_R-1}\left(\sqrt{\gamma}\frac{m}{\sigma_\gamma^2}\right) \tag{4.44a}$$

with

$$\sigma_\gamma^2 = N_E + 2N_0 \tag{4.44b}$$

and

$$m^2 = \mathbf{x}(k)^H \mathbf{x}(k) = \mathbf{w}(k)^H \hat{\mathbf{C}}(k)^H \hat{\mathbf{C}}(k)\mathbf{w}(k)\,. \tag{4.44c}$$

Here $I_N(\cdot)$ is the *N*-order modified Bessel function of the first kind. Averaging (4.43) over (4.44) gives us the conditional BEP as

$$\begin{aligned} &P_e\left(k\left|\{\hat{c}_{ij}(k), \tilde{w}_j(k)\}_{i=1,j=1}^{L_R,L_T}\right.\right) \\ &= \int_0^\infty Q\left(\sqrt{\frac{\gamma(N_E+2N_0)}{(4N_0^2+4N_EN_0)}}\right) p_\gamma(\gamma)d\gamma \\ &= \int_0^\infty Q\left(\sqrt{\frac{\gamma(N_E+2N_0)}{(4N_0^2+4N_EN_0)}}\right) \frac{1}{2\sigma_\gamma^2}\left(\frac{\gamma}{m^2}\right)^{\frac{[L_R-1]}{2}} \exp\left[-\frac{m^2+\gamma}{2\sigma_\gamma^2}\right] I_{L_R-1}\left(\sqrt{\gamma}\frac{m}{\sigma_\gamma^2}\right) d\gamma. \end{aligned}$$

Using the alternative formula for Gaussian *Q*-function [16]

$$Q(t) = \frac{1}{\pi}\int_0^{\pi/2} \exp\left(-\frac{t^2}{2\sin^2\theta}\right) d\theta$$

together with the integral relation

$$\int_0^\infty x^\nu e^{-\alpha x} I_{2\nu}(2\beta\sqrt{x})dx = \alpha^{-(2\nu+1)}\beta^{2\nu}\exp\left[\frac{\beta^2}{\alpha}\right],$$

we arrive at the following results after some manipulation

$$
\begin{aligned}
&P_e(k)\Big|\{\hat{c}_{ij}(k),\tilde{w}_j(k)\}_{i=1,j=1}^{L_R,L_T} \\
&= \int_0^{\infty}\frac{1}{\pi}\int_0^{\pi/2}\exp\left[-\frac{\gamma(N_E+2N_0)}{2\sin^2\theta(4N_EN_0+4N_0^2)}\right]\frac{1}{2\sigma_\gamma^2}\left(\frac{\gamma}{m^2}\right)^{\frac{[L_R-1]}{2}}\exp\left[-\frac{m^2+\gamma}{2\sigma_\gamma^2}\right]I_{L_R-1}\left(\sqrt{\gamma}\frac{m}{\sigma_\gamma^2}\right)d\theta d\gamma \\
&= \int_0^{\pi 2}\frac{1}{\pi}\left(1+\frac{(N_E+2N_0)^2}{\sin^2\theta(4N_EN_0+4N_0^2)}\right)^{-L_R}\exp\left[\frac{-\mathbf{w}(k)^H\hat{\mathbf{C}}(k)^H\hat{\mathbf{C}}(k)\mathbf{w}(k)(N_E+2N_0)}{2\left[(N_E+2N_0)^2+\sin^2\theta(4N_EN_0+4N_0^2)\right]}\right]d\theta.
\end{aligned}
\tag{4.45}
$$

Unfortunately, this conditional error probability cannot be further simplified at the moment. As the transmit weights $\mathbf{w}(k)$ affect the conditional BEP through N_E (4.39d), which exists in both the binomial term and the exponential term, the optimization of $\mathbf{w}(k)$ to minimize the BEP seems unattainable at the moment. Therefore, as a sub-optimal solution, we will use the optimum transmit weights that maximize only the term $\mathbf{w}(k)^H\hat{\mathbf{C}}(k)^H\hat{\mathbf{C}}(k)\mathbf{w}(k)\big/(N_E+2N_0)$ instead, which is the optimum weights when the receiver uses only the channel estimation generated from the pilot symbols, similar to the result for PSK signals in Section 4.3. With this choice of the transmit weights, for a detector using the channel estimation generated by our proposed IPSAM scheme, the error performance follows the same derivation as for PSK signals., except the AWGN component is doubled, and thus at least 3dB more SNR to achieve the same BEP level is expected. For the detector shown in (4.38), the error probability is given by (4.45) where we now have $\lambda=\mathbf{w}(k)^H\hat{\mathbf{C}}(k)^H\hat{\mathbf{C}}(k)\mathbf{w}(k)\big/(N_E+2N_0)$ with a pdf in the same form as (4.20) or (4.22) for dual-transmit system. However, in this case N_E is also a random variable as it depends on the transmit weights, and its distribution is currently impossible to calculate. Therefore, the BEP result can only be obtained by simulation.

4. 5 Numerical Results and Discussion

Fig. 4.3 to Fig. 4.5 demonstrate the BEP of BPSK and QPSK signal in a Tx-Rx diversity system with our proposed PSAM scheme at different fade rates. It is clear that our analytical results agree well with the simulation results. Fig 4.3 and Fig 4.4 show substantial performance loss with increasing fade rates. However, this does not mean the proposed PSAM scheme is inefficient, as the frame length in this figure is fixed and is not optimized for individual fading rates. It is obvious that when the fading process is less correlated in time due to a higher fade rate, a smaller frame length should be used to keep up with the fading fluctuations. In Fig 4.5, we optimize the frame length for different fade rates and the improvement is quite substantial even with smaller receive diversity order. Comparing the result in Fig 4.5 with that of a conventional diversity receiver with PSAM [58], our result seems inferior even with optimized frame length. This is anticipated as our PSAM scheme uses only the pilot before the current frame. However, this restriction is only required for channel estimation for the purpose of optimizing the transmit weight. For data detection, a conventional PSAM scheme can be implemented that uses both the pilot symbols before and after the current frame. In Fig 4.6 we compare the performance of our PSAM scheme with conventional PSAM (CPSAM). It shows that for faster fading channels, exploiting the information from future pilot symbols could improve the system performance substantially, though this improvement is not so significant for slower fading rates.

In Fig 4.7, we present the average BEP as a function of the frame length for different fade rates. In a fast fading environment where the channel fading is not strongly correlated temporally, pilot symbols needed to be inserted more frequently in order to estimate the changing channel gain accurately at the receiver. With fixed total

transmitted energy, too many pilot symbols will decrease the transmitted energy allocated to the data symbols, resulting in a drop in the effective SNR available for data detection. These two contradicting phenomena result in an optimum frame length as far as the BEP is concerned. Fig 4.7 clearly demonstrates this conjecture and it shows that the optimum frame length is shorter for faster fade rates, e.g., 5 for $f_d T = 0.03$ but 12 for $f_d T = 0.001$, at an SNR level of 20dB. However, to achieve these minimum error probabilities, it also means that the data rate has to be reduced tremendously for the fast fading scenario.

In Fig 4.7 we have assumed that the pilot symbols and the data symbols have same energy, thus the pilot to data energy ratio (PDR) can simply be expressed in terms of the frame length, or, the frequency of pilot symbol insertion. Another way to adjust this ratio is to assign different amounts of energies to pilot symbols and data symbols. In Fig 4.8 we plot the BEP as a function of PDR. When the average symbol energy is fixed, increasing the pilot symbol's leads to more accurate channel estimates while decreasing the energy of the data symbol at the same time. Thus again, there exists an optimum PDR that balances these two effects, providing a minimum error probability. From Fig 4.8, we found that this optimum PDR is larger in a faster fading environment than in a slower fading environment. Fig 4.7 and Fig 4.8 jointly imply that as far as the error probability is concerned, a faster fading channel requires larger pilot symbol energy, either through more frequent pilot symbol insertion, or by assigning a higher power level to the pilot symbols.

It is well-known that the accuracy of the channel estimates depends on the length of the Wiener filter used. Theoretically speaking, a longer filter provides a higher accuracy and hence better performance. However, the detector complexity also increases with a longer filter, not to mention the increased detection delay (if the

detection is based on a conventional PSAM scheme). Therefore, a practical system must compromise between these two conflicting requirements. Fig 4.9 shows that for most of the fade rates considered, the improvement in the error probability is very insignificant after the filter length is increased beyond 10 symbols.

Up to here, the results we present are all based on a Wiener estimation filter, i.e., the system knows exactly the channel fading autocorrelation function and fade rate. In a practical wireless mobile communication system, the fade rate could change from time to time when the mobile terminal travels at different speeds or in different directions. Thus there could be situations when the estimation filter is not optimized to the true fade rate. The result of using a mismatched channel estimation filter is shown in Fig 4.10 and Fig 4.11, where we found that a receiver operating in a slower fading channel with a mismatched filter actually performs worse than a receiver in a faster fading channel but with a perfectly matched estimation filter. This suggests that in practice, an adaptive filter that tracks the channel's fade rate should be employed to continuously adjust the estimation filter to the changing channel condition.

In Fig 4.12, we compare the BEP for different transmit diversity orders. Unlike conventional receive diversity where higher order diversity always provides better performance, we found that for transmit diversity, a higher diversity order provides diminishing performance improvement. For instance, when increasing the diversity order from 4 to 6 at the transmitter, the improvement is rather limited when compared to that achieved when increasing the diversity order from 2 to 4. The reason could be that for higher diversity orders at the transmitter side, more pilot symbols need to be inserted into each frame to estimate the individual fading channel.

In Fig 4.13, we compare the performance of systems with different combinations of transmit and receive antennas when the total number of antennas is

fixed at 6. As mentioned in the introduction, splitting the total number of antennas equally between the transmitter and the receiver maximizes the total number of transmission links, and therefore should provide the best performance. However we found with the PSAM scheme we proposed, such results may not hold. When comparing the 4-transmit-2-receive antennal system, 3-transmit-3-receive case with the 2-transmit-4-receive case, we found the best performance is actually achieved by the last configuration. The reason is that with more transmit antennas, our PSAM scheme requires more pilot symbols in a frame, thus reducing the energy that can be allocated to the data symbol, which in turn reduces the effective SNR during data detection.

In Fig. 4.14, we present the BEP for binary orthogonal signaling with our proposed PSAM Tx-Rx diversity scheme. In the figure we compare the performance of the detector given by (4.38) and that of a conventional PSAM based detector that uses both the past and future pilot symbols. It shows that for small fade rates, utilizing the future pilot symbols during detection can only slightly improve the performance while for moderate fade rates, the improvement is more noticeable. However, comparing with the case of ideal coherent detection, the performance of both these two detectors seems not satisfactory at all. In order to examine the cause of this substantial performance loss, we present in Fig. 4.15 the performance of a hypothetical system in which we assume the transmit weighting strategy is based on the channel estimation from our proposed PSAM scheme, while during the data detection the detector has ideal channel information. Thus the performance difference between this hypothetical system and an ideal coherent system is solely due to imperfect transmit weighting. From Fig 4.15, we found that imperfect transmit weighting is obviously the main cause of the performance loss between our proposed PSAM Tx-Rx diversity system and an

ideal coherent system, especially for small fade rates. These results also indicate that the performance of MRT-MRC type transmit diversity is very sensitive to the weights at the transmitter. To further demonstrate the effect of imperfect transmit weighting on the error performance, we compare in Fig. 4.16 the performance of BPSK signal in a dual-transmit-dual-receive diversity system with and without optimum transmit weights. It is obvious that substantial performance improvement can be obtained by optimizing the transmit weights, even with channel estimation error.

Finally in Fig. 4.17, we plot the BEP of binary orthogonal signaling as a function of the frame length for our proposed PSAM Tx-Rx diversity system. Two effects come along when the frame length is reduced – improved quality of channel estimation and less transmit-weight optimized data symbols in a whole frame. Therefore, the system should choose the right frame length to compromise between these two effects and produce the minimum BEP. From Fig. 4.17, we find that for large a fade rate of 0.03, the optimum frame length is 5, while for a moderate fade rate of 0.01, the optimum frame length is 8.

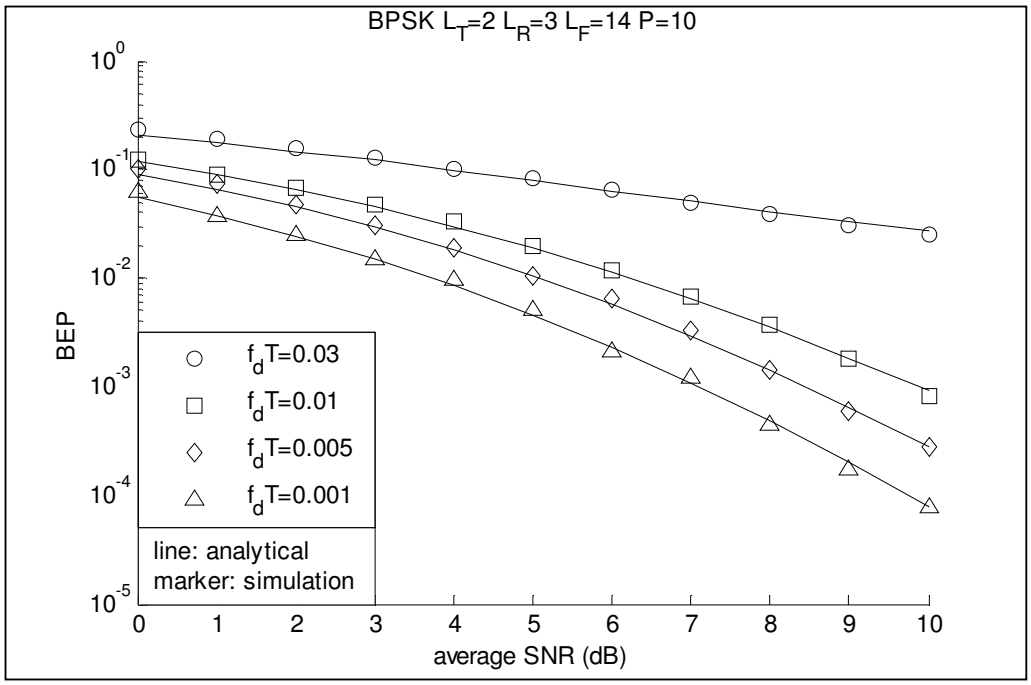

Figure 4.3 BEP vs. average SNR for different fade rate

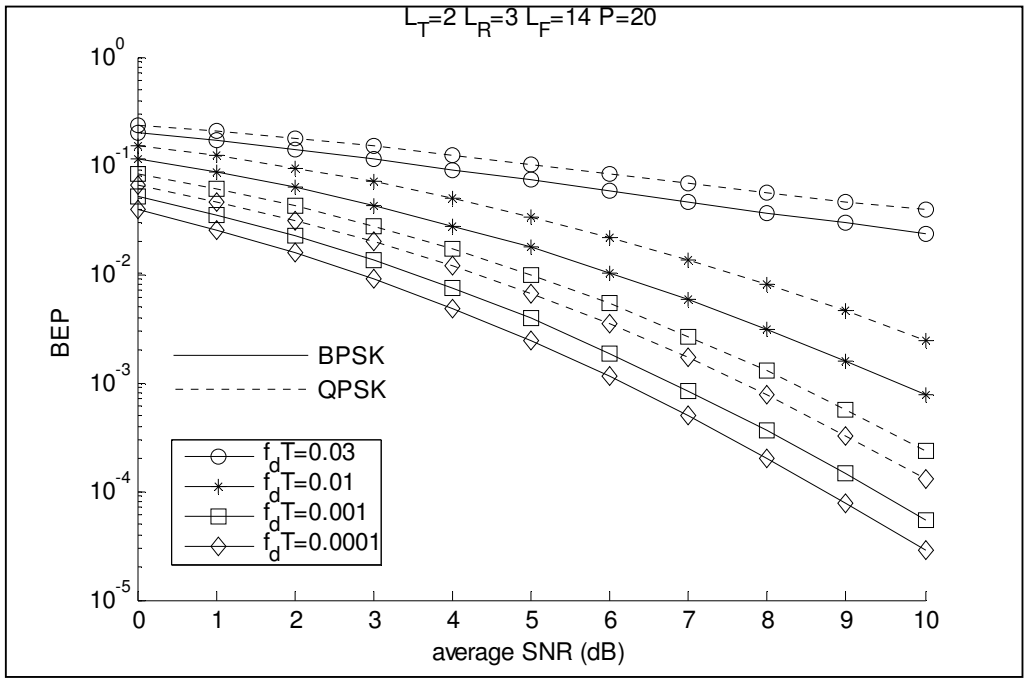

Figure 4.4 BEP vs. average SNR for different fade rate

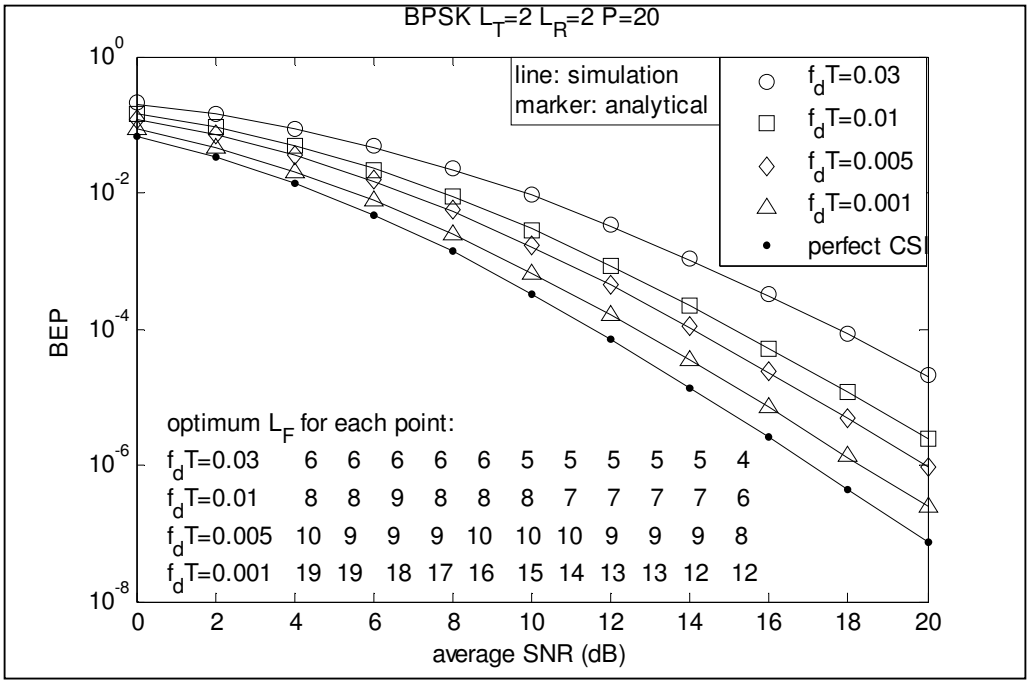

Figure 4.5 BEP vs. average SNR for different fade rate with optimized frame length

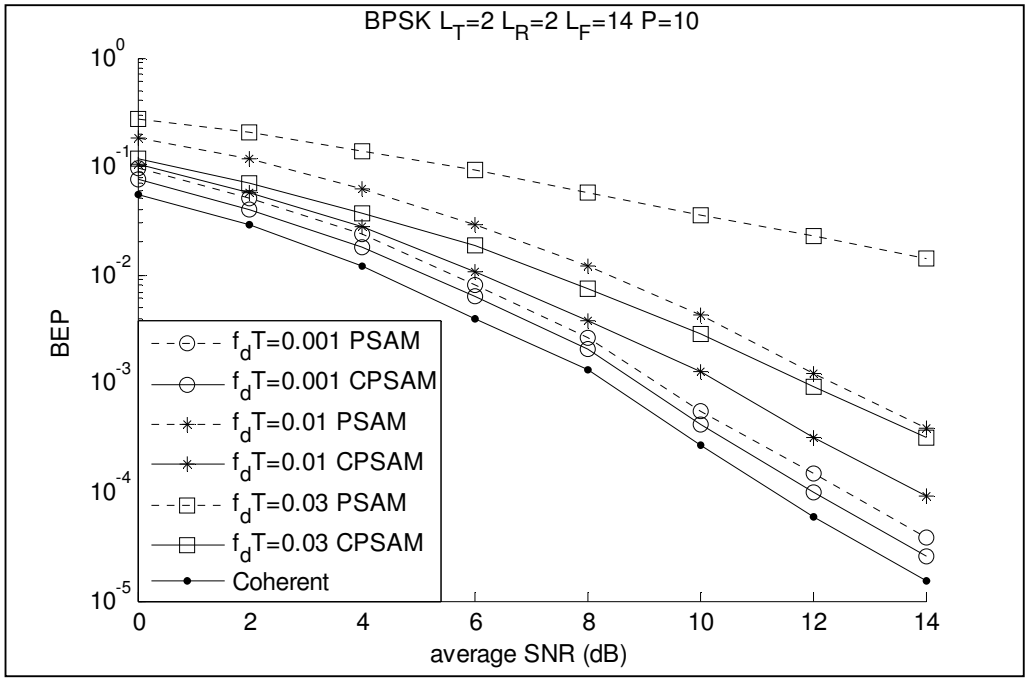

Figure 4.6 BEP vs. average SNR for different fade rate with our PSAM compare to that with conventional PSAM (detection only)

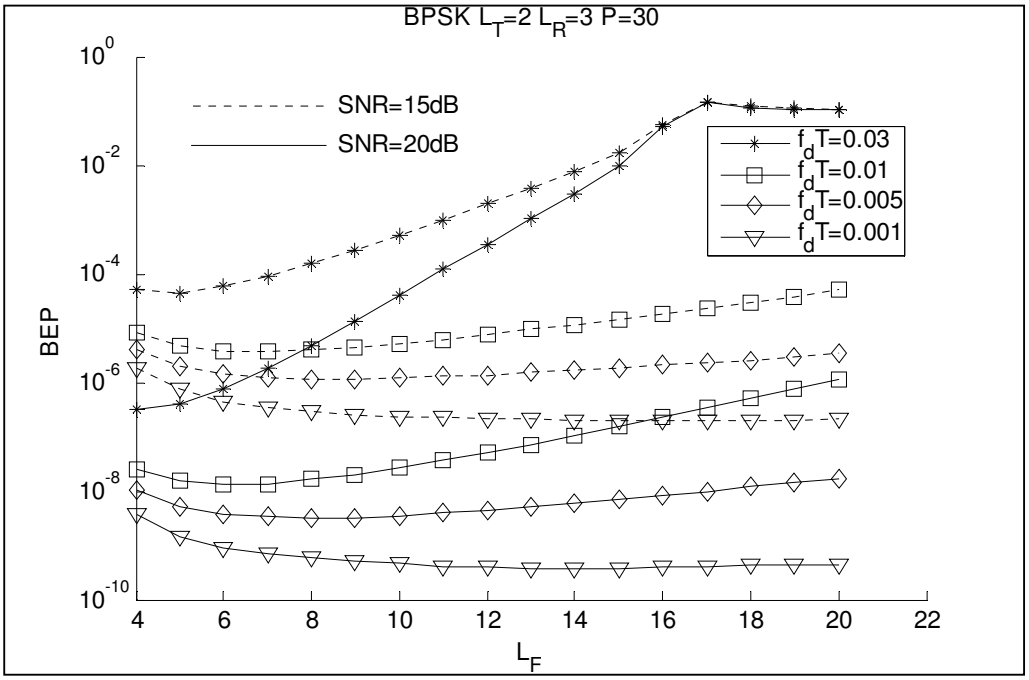

Figure 4.7 BEP vs. frame length for different fade rate

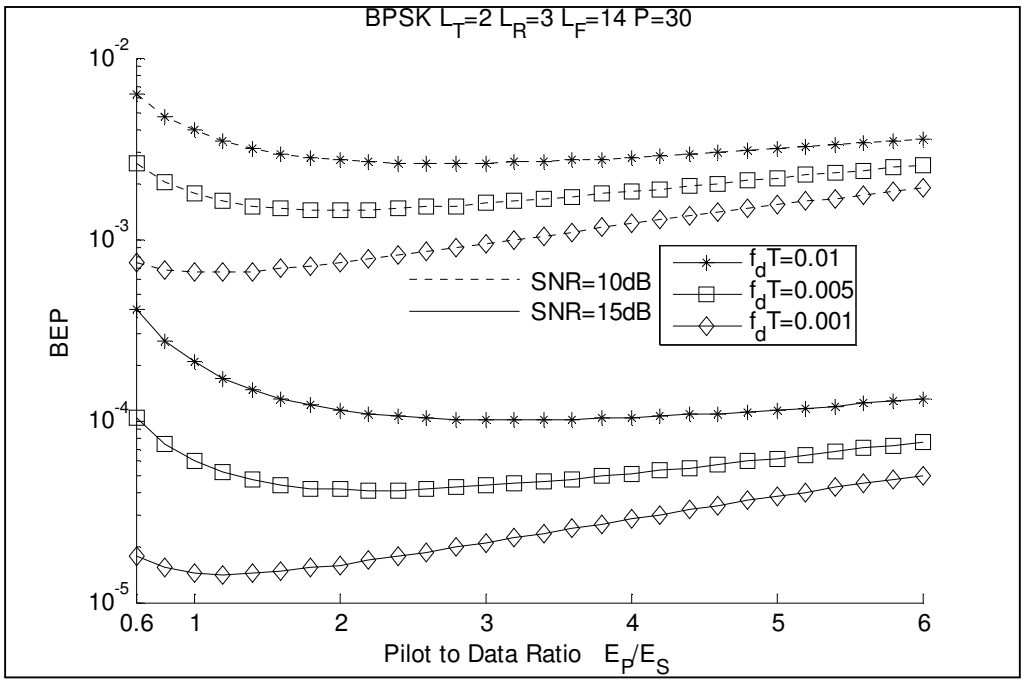

Figure 4.8 BEP vs. PDR for different fade rate

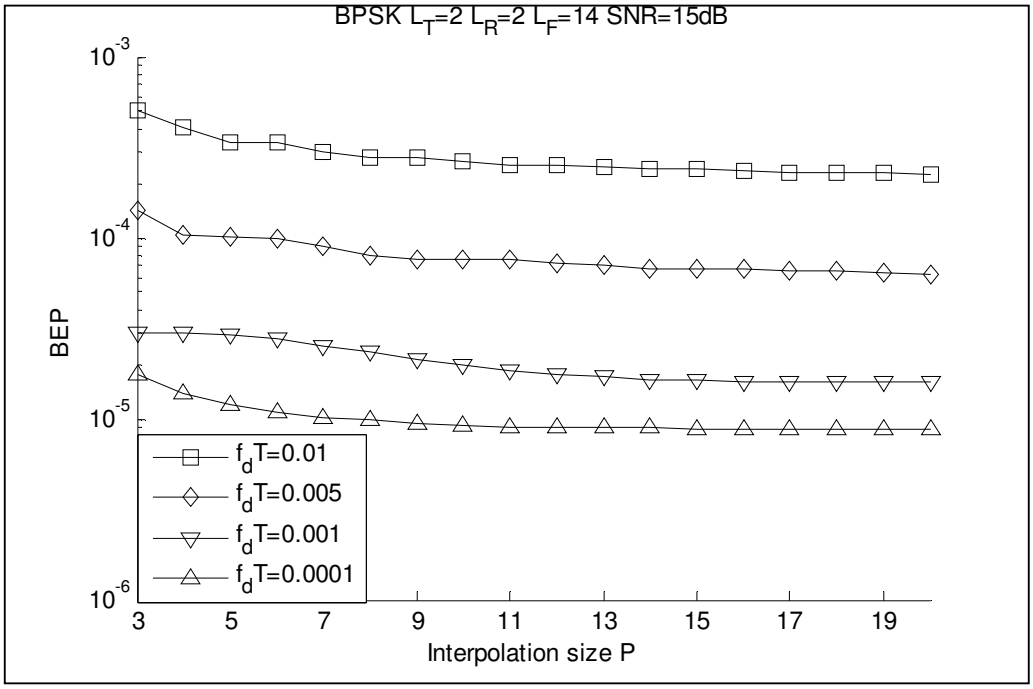

Figure 4.9 BEP vs. channel estimation filter length for different fade rate

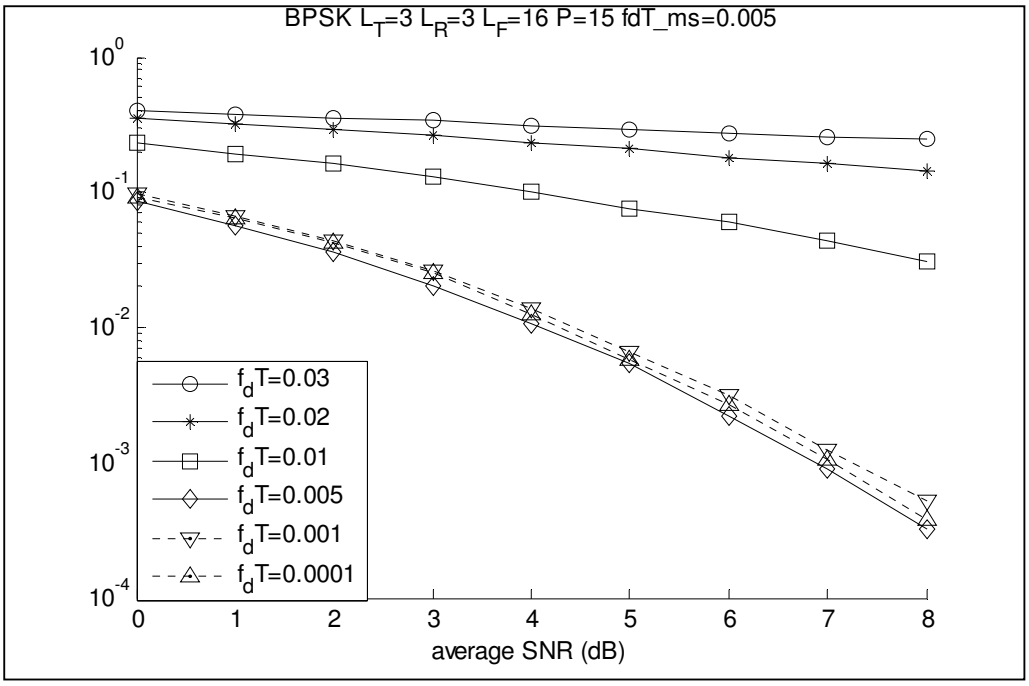

Figure 4.10 BEP vs. average SNR for different mismatched fade rate

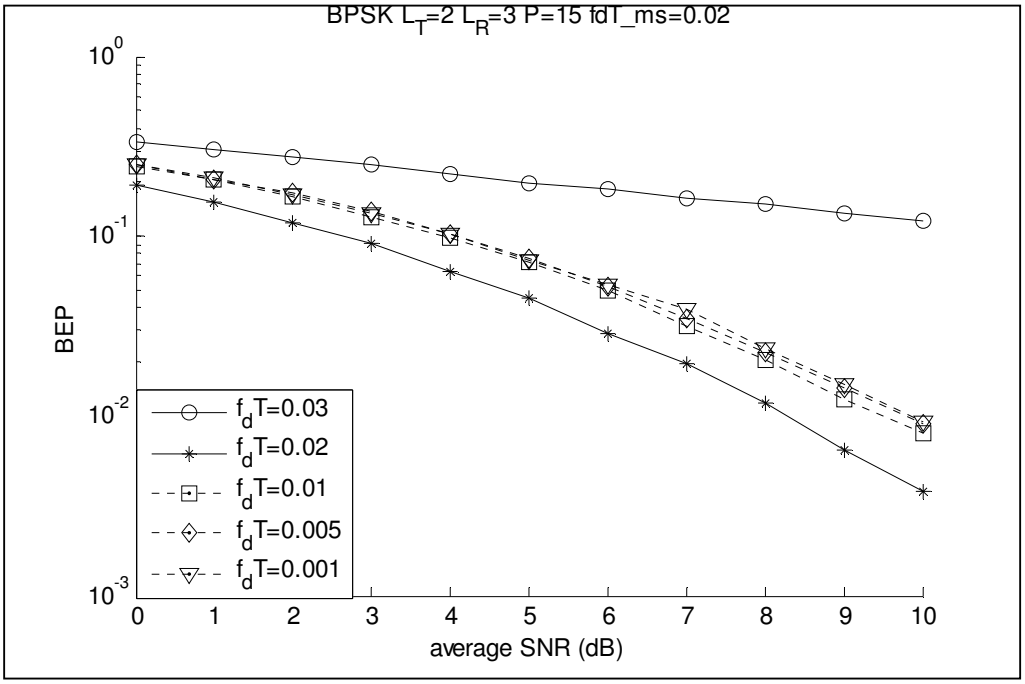

Figure 4.11 BEP vs. average SNR for different mismatched fade rate

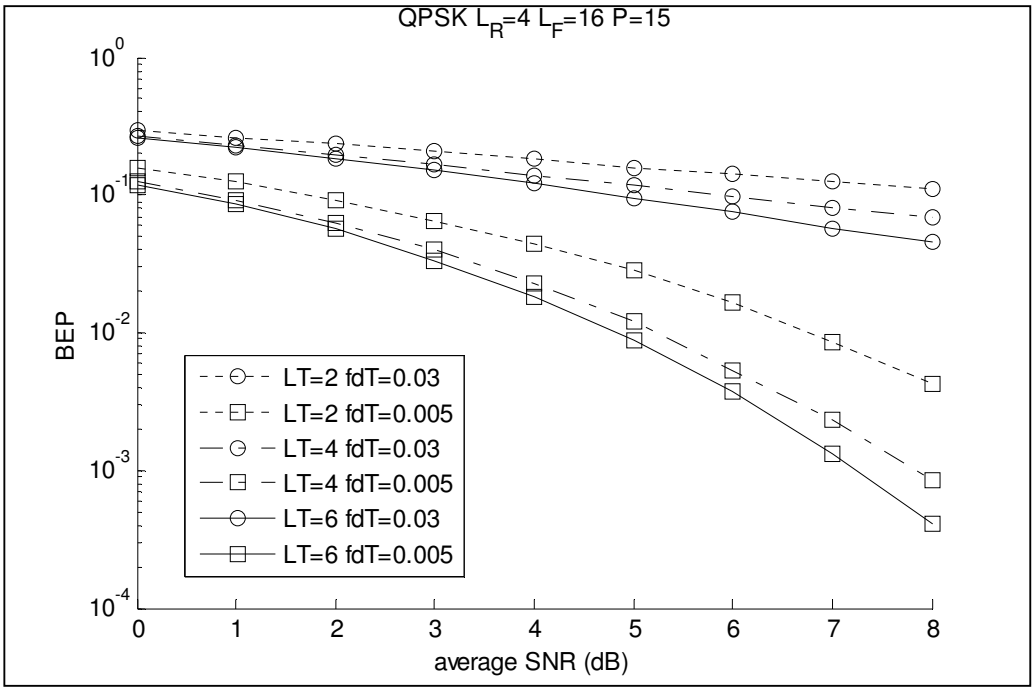

Figure 4.12 BEP vs. average SNR for different number of transmit antennas

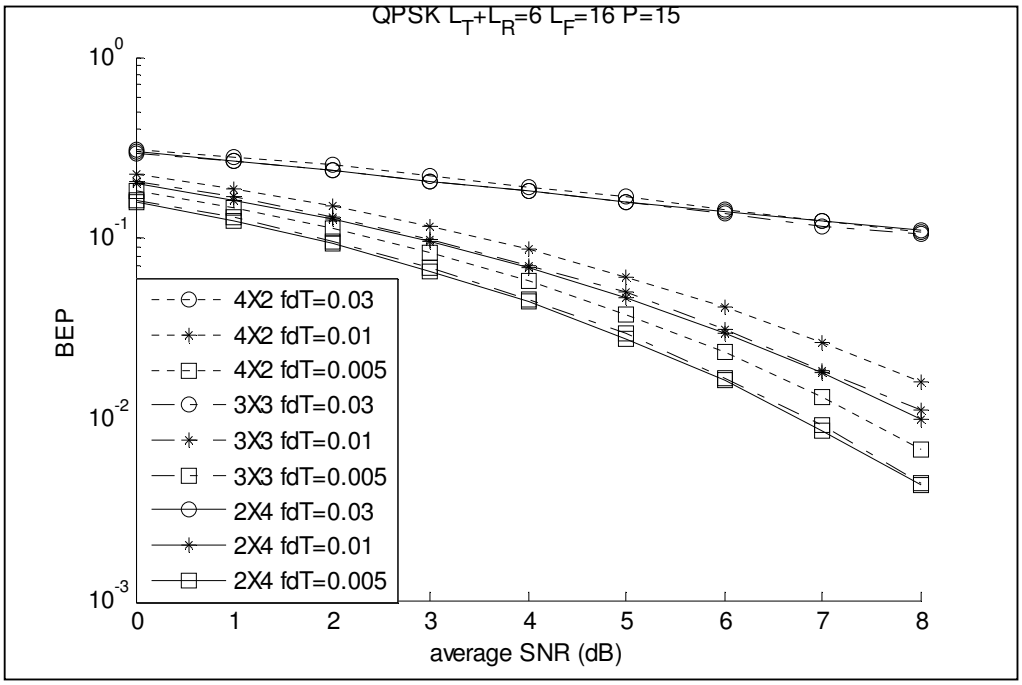

Figure 4.13 BEP vs. average SNR for different Tx-Rx antenna numbers with the total number of antennas fixed

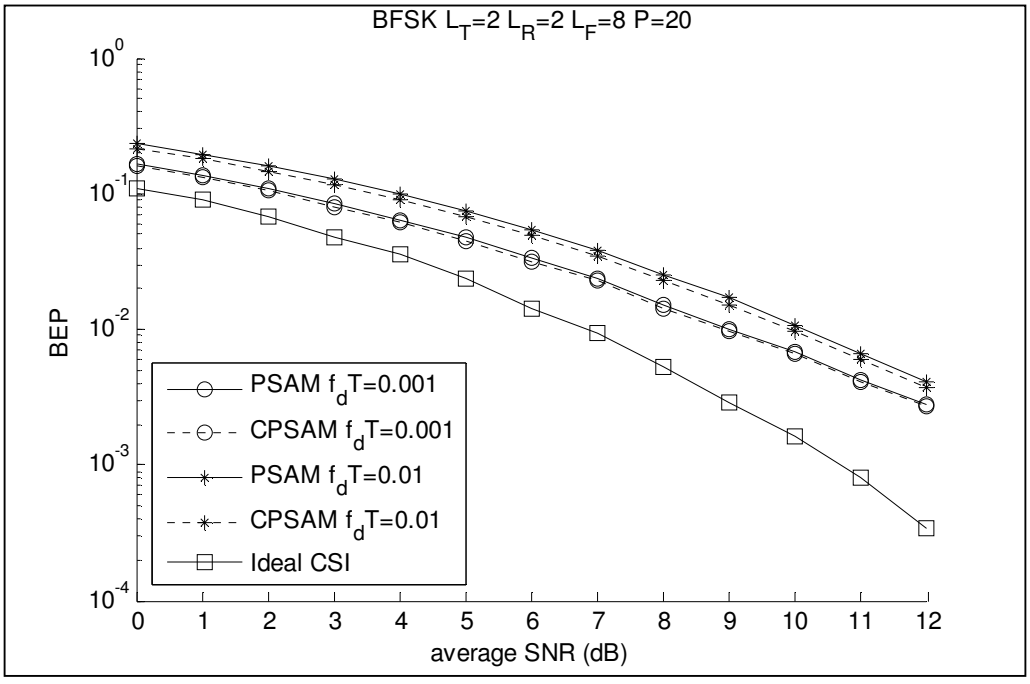

Figure 4.14 BEP vs. average SNR for different fade rate with our PSAM compare to that with conventional PSAM (detection only), binary orthogonal signaling

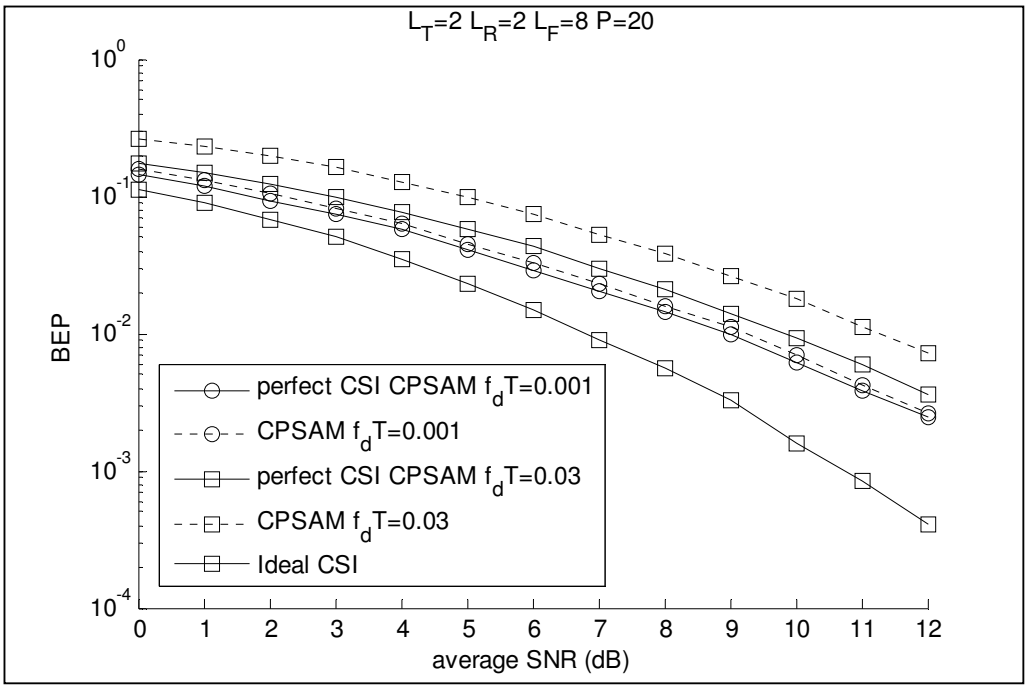

Figure 4.15 BEP vs. average SNR, cause of performance loss

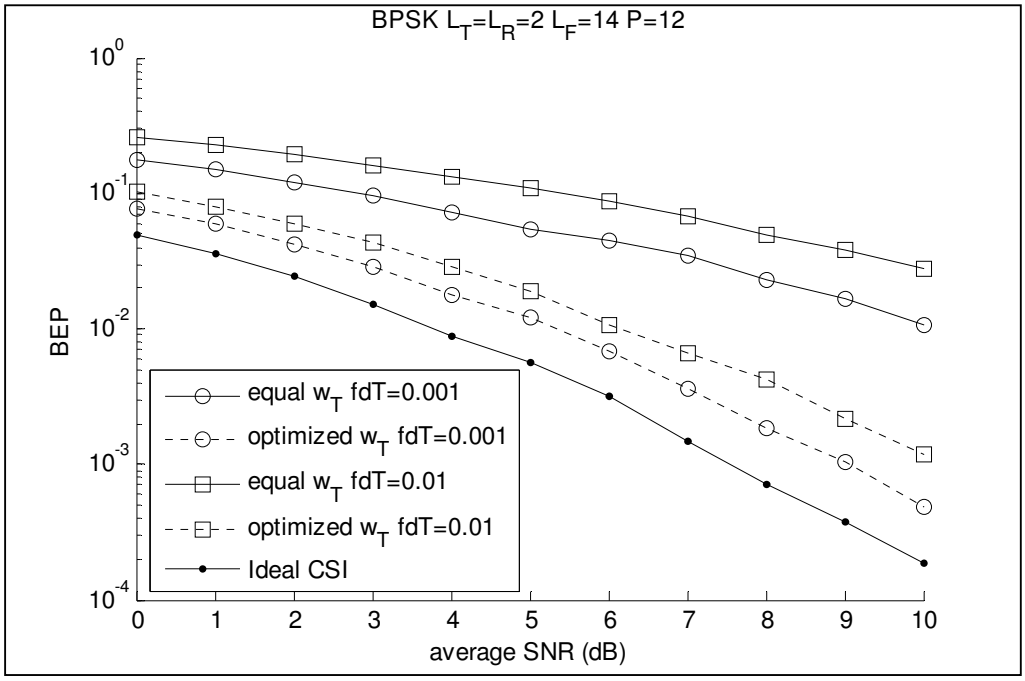

Figure 4.16 BEP vs. average SNR, with and without transmit weighting

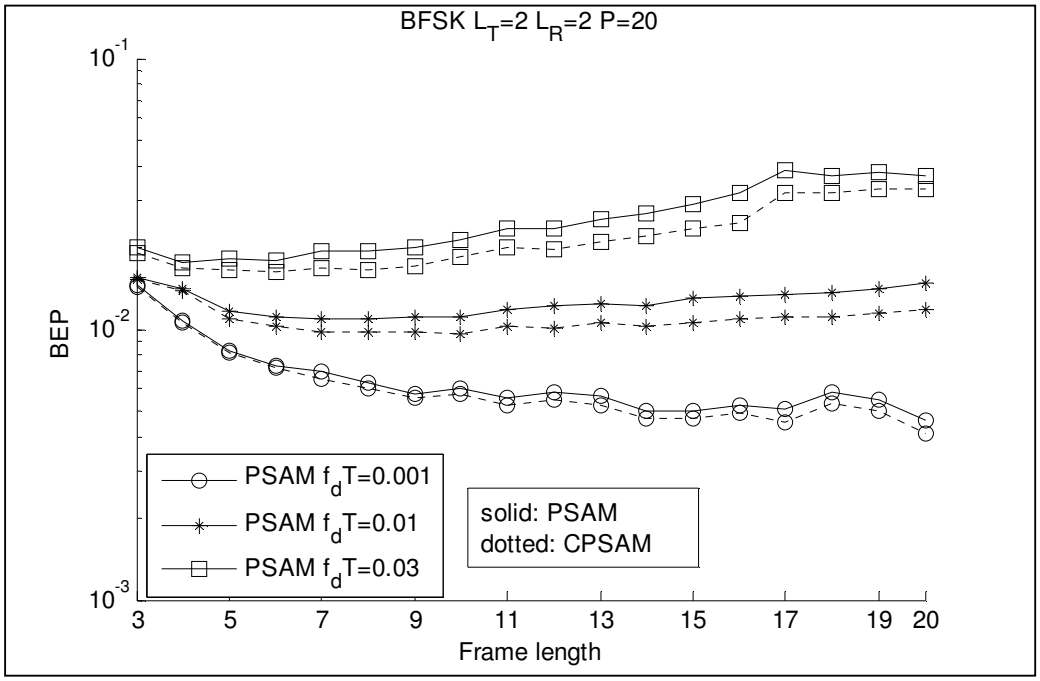

Figure 4.17 BEP vs. Frame Length for BFSK

4. 6 Summary

In this chapter we developed a PSAM channel estimation scheme for MRT-MRC type diversity system. For systems using PSK modulation, we derived the optimum receiver structure based on ML detection principle, and the optimum transmit weighting scheme that minimizes the BEP conditioned on available channel information. The performance of the resultant system is then studied, and its optimization with respect to the various parameters of PSAM system is discussed through numerical results. For a system using binary orthogonal signaling, we develop a PSAM channel estimation scheme based on the alternative interpretation of the signal constellation. By exploiting the channel measurement component embedded in orthogonal signals, our proposed PSAM scheme for orthogonal signaling does not suffer from data rate loss, but this is at the expense of less accurate channel estimation when compared to PSK modulation based system. We also examined the cause of the performance loss of a practical Tx-Rx diversity system compared to an ideal MRT-MRC diversity system, and found that imperfect transmit weights substantially degrade the performance from the ideal case.

Chapter 5

Space-time block codes with Orthogonal MFSK

In this chapter we develop an Alamouti-type Space-Time block code with orthogonal MFSK. The idea of using orthogonal FSK in Space-Time codes originates from the alternative interpretation of orthogonal signaling in [66]. A brief introduction of this work will be given in Section 5.1. In Section 5.2, we study the case where binary orthogonal FSK is used. The system model, detection procedure and resultant error performance will be given. In Section 5.3, we extend the analysis to *M*-ary orthogonal FSK. Diversity reception of the proposed ST-MFSK block codes is discussed in Section 5.4. Numerical results and discussion are given in Section 5.5. Section 5.6 summarizes the chapter.

5.1 Introduction

Space-Time (ST) block codes, as a means of transmit diversity that requires no prior-transmission channel information, is known for its good performance and high capacity. In order to coherently detect the transmitted symbol from channel fading in a practical Space-Time coded system, certain channel estimation scheme must be used to provide channel reference. Just as in a single channel system, differential encoding and detection can also be performed on a Space-Time coded signal, as demonstrated in [54]. In light of the idea discussed in chapter 4 that orthogonal signaling contains an implicit channel sounding component, we found it could be another choice of

modulation scheme for Space-Time codes. The advantage of using orthogonal signaling is that the channel memory can be used to refine the channel estimation, thus making it less vulnerable to fast fading than a differentially detected system. To the best of the author's knowledge, the idea of using orthogonal signaling, specifically orthogonal binary and *M*-ary frequency shift keying, has not been considered in the literature. In the following, we will first establish the basic transmitter and receiver structure for the binary FSK case, and then generalizes it to MFSK. Performance comparison with differential ST codes with the same alphabet sizes will be made.

5.2 Binary Orthogonal FSK

5. 2. 1 System Model

Assuming binary orthogonal FSK signal transmission through a two-transmit-antenna system and a space-time coded interval of $T_S = 2T$, the basic FSK waveforms are:

$$w_1(t) = \frac{1}{\sqrt{T}} \exp(-\frac{j\pi t}{T}), \tag{5.1}$$

and

$$w_2(t) = \frac{1}{\sqrt{T}} \exp(+\frac{j\pi t}{T}). \tag{5.2}$$

An implicit property of the waveforms in (1)-(2) is that they are phase-synchronized. An alternative view is that (1) and (2) constitutes a continuous phase FSK (CPFSK) scheme with a modulation index of unity [3].

With Alamouti-type [52] ST coding of dual-transmission-single-reception, the received signal waveform in the first sub-interval of the *k*-th interval, i.e., when $2kT < t < (2k+1)T$, is

$$r(t) = c_1[k]s_1(t) + c_2[k]s_2(t) + n(t), \tag{5.3}$$

and in the second subinterval, i.e., when $(2k+1)T < t < (2k+2)T$, is

$$r(t) = -c_1[k]s_2^*(t) + c_2[k]s_1^*(t) + n(t), \tag{5.4}$$

where $s_1(t)$ and $s_2(t)$ are data waveforms chosen randomly and independently from the set $\{w_1(t), w_2(t)\}$ to represent information bit '0' or '1', $c_1[k]$ and $c_2[k]$ are the piece-wise constant approximation of the fading gains in the two transmission links. These fading gains are independent and identically distributed (iid) complex Gaussian random variables (CGRV) with mean zero, variance $\sigma_c^2 = \frac{1}{2}E[|c_i(k)|^2]$, and autocorrelation function

$$\phi_c[n] = \tfrac{1}{2}E\left[c_i^*[k]c_i[k+n]\right] = \sigma_c^2 J_0\left(2\pi n f_d[2T]\right) \tag{5.5}$$

where f_d is the maximum Doppler frequency, and $J_0(\cdot)$ is the zeroth order Bessel function of the first kind. The AWGN component $n(t)$ has a power spectral density of N_0 and thus the average signal-to-noise ratio (SNR) per bit is

$$\gamma_b = \frac{\frac{1}{2}E\left[\int_{kT}^{kT+T}\left|c_i[k]s(t)\right|^2 dt\right]}{N_0} = \frac{\sigma_c^2}{N_0} \qquad \text{(BFSK)} \tag{5.6}$$

We will plot the bit-error probability (BEP) of the proposed signaling and detection scheme against this parameter.

5. 2. 2 Channel Estimation

Now, inspired by the alternative interpretation of orthogonal signaling in [4], we found that the sum of the orthonormal basis $w_1(t) + w_2(t)$ and the difference of the orthonormal basis $w_1(t) - w_2(t)$ are orthogonal. Therefore, if we correlate $r(t)$ in the first subinterval with the sum waveform

$$u(t) = w_1^*(t) + w_2^*(t) = \frac{2}{\sqrt{T}}\cos\left(\frac{\pi t}{T}\right) \tag{5.7}$$

the result will always be

$$\begin{aligned} a[2k] &= \int_{2kT}^{(2k+1)T} r(t)u(t)dt \\ &= (c_1[k] + c_2[k]) + n_1[2k] + n_2[2k] \end{aligned}, \tag{5.8}$$

independent of what $s_1(t)$ and $s_2(t)$ are. Similarly, if we correlate $r(t)$ in the second subinterval with the summed waveform $u(t)$, we get

$$\begin{aligned} a[2k+1] &= \int_{(2k+1)T}^{(2k+2)T} r(t)u(t)dt \\ &= (c_2[k] - c_1[k]) + n_1[2k+1] + n_2[2k+1] \end{aligned}. \tag{5.9}$$

Note that $\left\{ n_m[2k+i] = \int_{(2k+i)T}^{(2k+i+1)T} n(t)w_m^*(t)dt \right\}$, $m = 1,2;\ i = 0,1$ are the filtered AWGN terms with a variance of $\sigma_n^2 = N_0$ and are independent of each other. At this point, it becomes clear that

$$\begin{aligned} x_1[k] &= \frac{1}{2}\big(a[2k] - a[2k+1]\big) \\ &= c_1[k] + \frac{1}{2}\big(n_0[2k] + n_1[2k] - n_0[2k+1] - n_1[2k+1]\big) \\ &= c_1[k] + v_1[k] \end{aligned} \tag{5.10}$$

provides a noisy observation of $c_1[k]$, and

$$\begin{aligned} x_2[k] &= \frac{1}{2}\big(a[2k] + a[2k+1]\big) \\ &= c_2[k] + \frac{1}{2}\big(n_0[2k] + n_1[2k] + n_0[2k+1] + n_1[2k+1]\big) \\ &= c_2[k] + v_2[k] \end{aligned} \tag{5.11}$$

provides a noisy observation of $c_2[k]$. The noise components $v_1[k]$ and $v_2[k]$ are both complex Gaussian random variables with mean zero and variance $\sigma_v^2 = \frac{1}{2}E[|v_i[k]|^2] = N_0$, and they are independent of one another. Equations (5.10) and (5.11) suggest that, just like in the case of a single-input-single-output (SISO) system [4], a ST-BFSK receiver is also capable of deriving channel estimates from the received signal without explicit pilot symbols. Put simply, every transmitted ST-BFSK

symbol has an implicit pilot component, and the existence of these implicit pilot component agrees with the observation that the power spectrum of the proposed BFSK scheme has discrete spectral lines at $f = \pm 1/(2T)$. These spectral lines can be considered as pilot-tones and the sum filter in (5.7) attempts to extract these faded tones from the received composite signal and use them as local references.

The noisy observation of the channel fading in (5.10) and (5.11) can be refined by passing them to two identical Wiener filters in the same manner as what we would do in a PSAM system. Without loss of generality, assume that we want to estimate the fading gains at time zero, i.e. $c_j[0]$, $j \in \{0,1\}$, from the observations

$$\mathbf{X}_j[0] = \begin{bmatrix} x_j[-P] \\ x_j[-P+1] \\ \vdots \\ x_j[P] \end{bmatrix} = \begin{bmatrix} c_j[-P] \\ c_j[-P+1] \\ \vdots \\ c_j[P] \end{bmatrix} + \begin{bmatrix} v_j[-P] \\ v_j[-P+1] \\ \vdots \\ v_j[P] \end{bmatrix} \tag{5.12}$$

in the neighboring $2P+1$ code intervals. The optimal filter weight vector is [58]

$$\mathbf{f} = \boldsymbol{\varphi}_{c\mathbf{X}} \boldsymbol{\Phi}_{\mathbf{XX}}^{-1}, \tag{5.13}$$

where

$$\boldsymbol{\varphi}_{c\mathbf{X}} = \frac{1}{2} E\left[c_j[0] \mathbf{X}_j^H[0] \right] = \begin{bmatrix} \phi_c[-P] & \phi_c[-P+1] & \cdots & \phi_c[P-1] & \phi_c[P] \end{bmatrix} \tag{5.14}$$

is the correlation between $c_i[0]$ and $\mathbf{X}_i[0]$,

$$\boldsymbol{\Phi}_{\mathbf{XX}} = \frac{1}{2} E\left[\mathbf{X}_j[0] \mathbf{X}_j^H[0] \right] = \left[\phi_c[n-m] \right]_{n,m=-P}^{P} + N_0 \mathbf{I}_{2P+1} \tag{5.15}$$

is the covariance matrix of $\mathbf{X}_j[0]$, $\phi_c[n]$ is the autocorrelation function of the fading process in (5.5), and $\mathbf{I}_{2P+1}$ is an identity matrix of size $2P+1$. Note that $\mathbf{f}$ is independent of the time index.

Based on the Wiener filter design we have adopted above, the MMSE estimate of $c_j[0]$ is $\hat{c}_j[0] = \mathbf{f}\mathbf{X}_j[0]$, or in general, the estimate of $c_j[k]$ is

$$\hat{c}_j[k] = \mathbf{f}\mathbf{X}_j[k] \tag{5.16}$$

where $\mathbf{X}_j[k] = \left[x_j[k-P], x_j[k-P+1], ..., x_j[k+P] \right]^T$. The corresponding mean-square estimation error $e_j[k] = c_j[k] - \hat{c}_j[k]$ is therefore a complex Gaussian random variable with mean zero and variance

$$\sigma_e^2 = \frac{1}{2} E\left[\left| c_j[k] - \hat{c}_j[k] \right|^2 \right] = \sigma_c^2 - \boldsymbol{\varphi}_{c\mathbf{X}} \boldsymbol{\Phi}_{\mathbf{XX}}^{-1} \boldsymbol{\varphi}_{c\mathbf{X}}^H . \tag{5.17}$$

We will later express the BEP in terms of σ_e^2. Note that the correlation between $c_j[k]$ and $\hat{c}_j[k]$ is

$$\rho_{c\hat{c}} = \frac{1}{2} E\left[\left| c_j[k] \hat{c}_j^*[k] \right|^2 \right] = \boldsymbol{\varphi}_{c\mathbf{X}} \boldsymbol{\Phi}_{\mathbf{XX}}^{-1} \boldsymbol{\varphi}_{c\mathbf{X}}^H \tag{5.18a}$$

and the variance of $\hat{c}_j[k]$ is

$$\sigma_{\hat{c}}^2 = \frac{1}{2} E\left[\left| \hat{c}_j[k] \right|^2 \right] = \boldsymbol{\varphi}_{c\mathbf{X}} \boldsymbol{\Phi}_{\mathbf{XX}}^{-1} \boldsymbol{\varphi}_{c\mathbf{X}}^H = \sigma_c^2 - \sigma_e^2 \tag{5.18b}$$

Following the orthogonality principle of wiener filter design, the estimation error and the channel estimate are statistically independent.

5. 2. 3 Data Detection

Let the received signal in (5.3) and (5.4) be denoted by $r_{2k}(t)$ and $r_{2k+1}(t)$, respectively. Similarly, let the channel's AWGN $n(t)$ in these intervals be denoted by $n_{2k}(t)$ and $n_{2k+1}(t)$. The column concatenation of $r_{2k}(t)$ and $r_{2k+1}^*(t)$ is the vector

$$\mathbf{R}_k(t) = \begin{bmatrix} r_{2k}(t) \\ r_{2k+1}^*(t) \end{bmatrix} = \begin{bmatrix} c_1[k] & c_2[k] \\ c_2^*[k] & -c_1^*[k] \end{bmatrix} \begin{bmatrix} s_1(t) \\ s_2(t) \end{bmatrix} + \begin{bmatrix} n_{2k}(t) \\ n_{2k+1}^*(t) \end{bmatrix} \tag{5.19}$$

If we correlate $\mathbf{R}_k(t)$ with the difference waveform

$$d(t) = w_1^*(t) - w_2^*(t) = j \frac{2}{\sqrt{T}} \sin(\frac{\pi t}{T}), \tag{5.20}$$

the result is

$$\mathbf{r}[k] = \mathbf{C}[k]\mathbf{s}[k] + \mathbf{z}[k], \tag{5.21}$$

where

$$\mathbf{C}[k] = \begin{bmatrix} c_1[k] & c_2[k] \\ c_2^*[k] & -c_1^*[k] \end{bmatrix} \tag{5.22}$$

is the channel gain matrix,

$$\mathbf{s}[k] = \begin{bmatrix} s_1[k] \\ s_2[k] \end{bmatrix} \in \left\{ \begin{bmatrix} -1 \\ -1 \end{bmatrix}, \begin{bmatrix} -1 \\ +1 \end{bmatrix}, \begin{bmatrix} +1 \\ -1 \end{bmatrix}, \begin{bmatrix} +1 \\ +1 \end{bmatrix} \right\} \tag{5.23}$$

is the effective data vector, where $s_i[k]$ equals +1 and −1 if $s_i(t)$ equals $w_1(t)$ and $w_2(t)$ respectively, and

$$\begin{aligned} \mathbf{z}[k] &= \begin{bmatrix} z_1[k] \\ z_2[k] \end{bmatrix} \\ &= \begin{bmatrix} \int_{2kT}^{2kT+T} n(t)d(t)dt \\ \int_{2kT+T}^{2(k+1)T} n^*(t)d(t)dt \end{bmatrix} \\ &= \begin{bmatrix} n_1[2k] - n_2[2k] \\ n_1^*[2k+1] - n_2^*[2k+1] \end{bmatrix} \end{aligned} \tag{5.24}$$

is the noise vector due to AWGN. Note that $z_1[k]$ and $z_2[k]$ are independent zero mean complex Gaussian random variables with a variance of $\sigma_z^2 = 2N_0$. Furthermore, it is important to realize that

$$\frac{1}{2} E\left[z_i[k] v_j^*[k] \right] = 0, \; i = 1,2; \; j = 1,2, \tag{5.25}$$

which follows directly from the fact that the sum of the orthonormal basis $w_1(t) + w_2(t)$ and the difference of the orthonormal basis $w_1(t) - w_2(t)$ are orthogonal.

Conditioned on the channel estimates $\hat{c}_1[k]$ and $\hat{c}_2[k]$, the gains $c_1[k]$ and $c_2[k]$ complex Gaussian random variables with conditional means $\hat{c}_1[k]$ and $\hat{c}_2[k]$,

and identical conditional variance of σ_e^2 (5.17). In other word, we can express $c_1[k]$ and $c_2[k]$ as

$$\begin{aligned} c_1[k] &= \hat{c}_1[k] + e_1[k] \\ c_2[k] &= \hat{c}_2[k] + e_2[k] \end{aligned}, \tag{5.26}$$

where $e_1[k]$ and $e_2[k]$ are the estimation errors. This means (5.21) becomes

$$\mathbf{r}[k] = \hat{\mathbf{C}}[k]\mathbf{s}[k] + \mathbf{E}[k]\mathbf{s}[k] + \mathbf{z}[k] \tag{5.27}$$

where

$$\hat{\mathbf{C}}[k] = \begin{bmatrix} \hat{c}_1[k] & \hat{c}_2[k] \\ \hat{c}_2^*[k] & -\hat{c}_1^*[k] \end{bmatrix}, \tag{5.28}$$

and

$$\mathbf{E}[k] = \begin{bmatrix} e_1[k] & e_2[k] \\ e_2^*[k] & -e_1^*[k] \end{bmatrix}. \tag{5.29}$$

It should be clear that **E**[k]**s**[k] is a zero-mean complex Gaussian vector. Moreover, it can be shown that $\frac{1}{2}E\left[\mathbf{E}[k]\mathbf{s}[k]\mathbf{s}^H[k]\mathbf{E}^H[k]\right] = 2\sigma_e^2\mathbf{I}_2$, independent of the value of the data vector **s**[k]. This means **E**[k]**s**[k] and **z**[k] can be lumped together to form the effective noise term

$$\boldsymbol{\alpha}[k] = \mathbf{E}[k]\mathbf{s}[k] + \mathbf{z}[k] = \begin{bmatrix} \alpha_1[k] \\ \alpha_2[k] \end{bmatrix}, \tag{5.30}$$

where $\alpha_1[k]$ and $\alpha_2[k]$ are independent CGRVs with zero mean and variance $\sigma_\alpha^2 = 2\left(N_0 + \sigma_e^2\right)$.

Now from the detector structure in Alamouti's original work, it is intuitive to extend it such that the data detector first obtains the decision statistic $\mathbf{y}(k)$ from the received signal $\mathbf{r}(k)$ as

$$\begin{aligned}\mathbf{y}[k] &= \begin{bmatrix} y_1[k] & y_2[k] \end{bmatrix}^T \\ &= \hat{\mathbf{C}}^H[k]\mathbf{r}[k] \\ &= \begin{bmatrix} \hat{c}_1^*[k] & \hat{c}_2[k] \\ \hat{c}_2^*[k] & -\hat{c}_1[k] \end{bmatrix}\begin{bmatrix} \hat{c}_1[k] & \hat{c}_2[k] \\ \hat{c}_2^*[k] & -\hat{c}_1^*[k] \end{bmatrix}\begin{bmatrix} s_1[k] \\ s_2[k] \end{bmatrix} + \begin{bmatrix} \hat{c}_1^*[k] & \hat{c}_2[k] \\ \hat{c}_2^*[k] & -\hat{c}_1[k] \end{bmatrix}\begin{bmatrix} \alpha_1[k] \\ \alpha_2[k] \end{bmatrix} \\ &= \left(\left|\hat{c}_1[k]\right|^2 + \left|\hat{c}_2[k]\right|^2\right)\begin{bmatrix} s_1[k] \\ s_2[k] \end{bmatrix} + \begin{bmatrix} \beta_1[k] \\ \beta_2[k] \end{bmatrix}\end{aligned} \tag{5.31}$$

where $\beta_1[k] = \hat{c}_1^*[k]\alpha_1[k] + \hat{c}_2[k]\alpha_2[k]$ and $\beta_2[k] = \hat{c}_2^*[k]\alpha_1[k] - \hat{c}_1[k]\alpha_2[k]$ are independent CGRVs with mean zero and variance $\sigma_\beta^2 = 2\left(N_0 + \sigma_e^2\right)\left(\left|\hat{c}_1[k]\right|^2 + \left|\hat{c}_2[k]\right|^2\right)$.

The corresponding decision rule is

$$\hat{\mathbf{s}}[k] = \operatorname{sgn}\left\{\operatorname{Re}\left(\mathbf{y}[k]\right)\right\}. \tag{5.32}$$

where $\operatorname{sgn}(\cdot)$ is the sign function.

5. 2. 4 Error Performance Analysis

We define the instantaneous signal to noise ratio as

$$\gamma = \frac{\left(\left|\hat{c}_1[k]\right|^2 + \left|\hat{c}_2[k]\right|^2\right)^2}{2\sigma_\beta^2} = \frac{\left|\hat{c}_1[k]\right|^2 + \left|\hat{c}_2[k]\right|^2}{4\left(N_0 + \sigma_e^2\right)}. \tag{5.33}$$

Then the BEP conditioned on γ of (each of) the antipodal signal in (5.32) is

$$P_b(\gamma) = Q\left(\sqrt{2\gamma}\right), \tag{5.34}$$

where $Q(\cdot)$ is the Gaussian Q-function. Since γ is a sum of two independent exponential random variables with an identical mean value of

$$\lambda = E\left[\frac{\left|\hat{c}_i[k]\right|^2}{4\left(N_0 + \sigma_e^2\right)}\right] = \frac{\sigma_{\hat{c}}^2}{2\left(N_0 + \sigma_e^2\right)} = \frac{\sigma_c^2 - \sigma_e^2}{2\left(N_0 + \sigma_e^2\right)}, \tag{5.35}$$

so the probability density function (pdf) of γ is

$$p_\gamma(\gamma) = \frac{\gamma}{\lambda^2} e^{-\gamma/\lambda} U(\gamma), \tag{5.36}$$

where $U(\gamma)$ is the unit step function. Consequently, the average error probability is [3]

$$P_b = \int_0^\infty Q\left(\sqrt{2\gamma}\right) p_\gamma(\gamma) d\gamma$$
$$= \left[\frac{1}{2}\left(1 - \sqrt{\frac{1}{1+\lambda^{-1}}}\right)\right]^2 \left[2 + \sqrt{\frac{1}{1+\lambda^{-1}}}\right]. \quad (5.37a)$$

In contrast, the BEP of ST-BPSK (as well as ST-QPSK) with perfect channel state information (CSI) is

$$P_b = \left[\frac{1}{2}\left(1 - \sqrt{\frac{1}{1+\gamma_b^{-1}}}\right)\right]^2 \left[2 + \sqrt{\frac{1}{1+\gamma_b^{-1}}}\right]. \quad \text{(ideal BPSK/QPSK)} \quad (5.37b)$$

where γ_b is the bit SNR defined in (5.6).

When there is no estimation error, i.e. when $\sigma_e^2 = 0$, then the BEP of the proposed coherent ST-BFSK scheme has an asymptotic value of $3(2\gamma_b)^{-2}$, Compared to $3(4\gamma_b)^{-2}$, the asymptotic BEP of the ideal coherent ST-BPSK detector, we can see that BFSK experiences a 3 dB degradation in power efficiency, as expected. When compared to differential ST-BPSK[2] [54], [67], [68], which is also 3 dB less power efficient than coherent ST-BPSK, one is tempted to conclude that ST-BFSK performs at the same level as differential ST-BPSK, at best. While this is true when fading is slow, we shall see in Section 5.5 that ST-FSK can actually perform much better than differential ST-BPSK in a fast fading channel. Further more, in order to estimate the channel for coherent ST-BPSK detection, normally decision-directed channel estimation and / or pilot symbol aided channel estimation is needed to provide the channel estimates. However, for our proposed ST-BFSK system, the channel estimation is carried out using the implicit PSAM scheme, which is very stable even in fast fading environment and does not suffer from data rate loss.

[2] For the completeness of presentation, we include in appendix C an introduction on differential ST-PSK with some code examples.

Another interesting comparison between ST-FSK and differential ST-PSK is the receiver complexity. On the surface, the proposed ST-FSK receiver appears to be more complex than a differential ST detector, as it requires channel estimation. The channel estimator comprises an integrate-and-dump (I/D) filter (5.8)-(5.9) followed by an estimation filter (5.16). However the I/D filter is no different from the sampler required in a differential ST-PSK receiver. In addition, the computational complexity and delay of the estimation filter are similar to those of the digital matched filter required in the differential ST-PSK receiver, as both filters span only a few consecutive symbol intervals. In short, the proposed coherent ST-BFSK provides robustness against fast fading with a complexity and delay similar to that of differential ST-BPSK. Furthermore, if we are willing to sacrifice bandwidth efficiency for power efficiency by increasing M (the size of the modulation alphabet), then the error performance of ST-MFSK can actually surpass that of its differential ST-MPSK counterpart even in a static fading channel. In the following section, we generalize the proposed ST-BFSK scheme to MFSK.

5.3 *M*-ary Orthogonal FSK

5. 3. 1 System Model

Again, we assume here Alamouti-type ST block code with a code interval of $T_S = 2T$. However, the waveforms we use now to transport the information are drawn from the M-ary orthogonal FSK signal set; $M = 2^K$, $K = 1, 2, \cdots$. The basic FSK waveforms are

$$w_m(t) = \frac{1}{\sqrt{T}} \exp\left(\frac{j\pi t}{T} (2m - M - 1) \right) \quad m = 1, \cdots, M \,. \tag{5.38}$$

The received waveforms during the two sub intervals of a code interval have the same form as (5.3) and (5.4), except that $s_1(t)$ and $s_2(t)$ are data waveforms chosen randomly and independently from the set $\{w_m(t)\}_{m=0}^{M-1}$. Now if we correlate (5.3) and (5.4) with the sum waveform

$$u(t) = \sum_{m=1}^{M} w_m^*(t) = \sum_{m=1}^{\frac{M}{2}} \frac{2}{\sqrt{T}} \cos\left((2m-1)\frac{\pi t}{T}\right), \tag{5.39}$$

we have

$$\begin{aligned} a[2k] &= \int_{2kT}^{(2k+1)T} r(t)u(t)dt \\ &= (c_1[k] + c_2[k]) + \sum_{m=1}^{M} n_m[2k] \end{aligned}, \tag{5.40a}$$

and

$$\begin{aligned} a[2k+1] &= \int_{(2k+1)T}^{(2k+2)T} r(t)u(t)dt \\ &= (c_2[k] - c_1[k]) + \sum_{m=1}^{M} n_m[2k+1] \end{aligned}, \tag{5.40b}$$

where $n_m[2k+i] = \int_{(2k+i)T}^{(2k+i+1)T} n(t)w_m^*(t)dt$ as in (5.8) and (5.9). The channel estimation process is then the same as that for BFSK described in (5.10-5.18), except that $\left\{v_i[k] = \sum_{m=1}^{M} n_m[2k] + (-1)^i \sum_{m=1}^{M} n_m[2k+1]\right\}$ $i = 1, 2$ now has a variance of $\sigma_n^2 = \frac{M}{2} N_0$ and therefore (5.15) is now given by

$$\mathbf{\Phi}_{\mathbf{xx}} = \frac{1}{2} E\left[\mathbf{X}_j[0]\mathbf{X}_j^H[0]\right] = \left[\phi_c[n-m]\right]_{n,m=-P}^{P} + \frac{M}{2} N_0 \mathbf{I}_{2P+1}.$$

This change in noise variance will in general degrade the estimator's accuracy. Fortunately though, the effect of increasing noise variance is partially or wholly compensated for by an increase in the symbol energy (which directly affects the $\phi_c[n]$s in (5.15)). Specifically for MFSK, the mean received SNR per bit is given by

$$\gamma_b = \frac{1}{\log_2 M}\left(\frac{\sigma_c^2}{N_0}\right) \qquad \text{(MFSK)} \qquad (5.40c)$$

This means the effective SNR in the $x_i[k]$s in (5.10) and (5.11) is γ_b for 4FSK and $3\gamma_b/4$ for 8FSK. Compared to the effective SNR of γ_b for BFSK, we can conclude that there is no loss in channel estimation accuracy when we go from *M*=2 to *M*=4 but there is a degradation of 1.25 dB in going from *M*=2 to *M*=8.

5. 3. 2 Data Detection

Write the received signal as in (5.19), now if we correlate the received signal with the basis waveform vector

$$\mathbf{w}(t) = \left[w_m^*(t) \right]_{m=1}^{M}, \qquad (5.41)$$

the result will be

$$\mathbf{R}[k] = \mathbf{C}[k]\mathbf{S}[k] + \mathbf{Z}[k] \qquad (5.42)$$

where $\mathbf{C}[k]$ is given by (5.22),

$$\mathbf{S}[k] = \begin{bmatrix} s_{1,1}[k] & \cdots & s_{1,m}[k] & \cdots & s_{1,M}[k] \\ s_{2,1}[k] & \cdots & s_{2,m}[k] & \cdots & s_{2,M}[k] \end{bmatrix} \qquad (5.43a)$$

is the effective data matrix, with $s_{i,m}[k]$ equals +1 if $s_i(t)$ equals $w_m(t)$ and zero otherwise. In other word, there is one and only one non-zero element in each row of $\mathbf{S}[k]$. The AWGN matrix is

$$\mathbf{Z}[k] = \begin{bmatrix} z_{1,1}[k] & \cdots & z_{1,m}[k] & \cdots & z_{1,M}[k] \\ z_{2,1}[k] & \cdots & z_{2,m}[k] & \cdots & z_{2,M}[k] \end{bmatrix} \qquad (5.43b)$$

with

$$\begin{aligned} z_{1,m}[k] &= \int_{2kT}^{(2k+1)T} n(t) w_m^*(t) dt \\ &= n_m[2k] \end{aligned} \qquad (5.43c)$$

and

$$\begin{aligned} z_{2,m}[k] &= \int_{(2k+1)T}^{(2k+2)T} n^*(t) w_m^*(t) dt \\ &= n_m^*[2k+1] \end{aligned} \tag{5.43d}$$

be independent zero mean complex Gaussian random variable with a variance of $\sigma_z^2 = N_0$. Rewriting (5.41) in the same way as (5.27), we have

$$\mathbf{R}[k] = \hat{\mathbf{C}}[k]\mathbf{S}[k] + \mathbf{E}[k]\mathbf{S}[k] + \mathbf{Z}[k] \tag{5.44}$$

where $\hat{\mathbf{C}}[k]$ and $\mathbf{E}[k]$ are given by (5.28) and (5.29).

Now it is intuitive from Alamouti's detector that the data detector in our proposed ST-MFSK system first compensates for fading by multiplying the received vector in (5.44) by the conjugate of the estimated channel gain matrix according to

$$\begin{aligned} \mathbf{Y}[k] &= \begin{bmatrix} y_{1,1}[k] & \cdots & y_{1,m}[k] & \cdots & y_{1,M}[k] \\ y_{2,1}[k] & \cdots & y_{2,m}[k] & \cdots & y_{2,M}[k] \end{bmatrix} \\ &= \hat{\mathbf{C}}[k]^H \mathbf{R}[k] \\ &= \left(|\hat{c}_1[k]|^2 + |\hat{c}_2[k]|^2 \right) \mathbf{S}[k] + \begin{bmatrix} \beta_{1,1}[k] & \cdots & \beta_{1,m}[k] & \cdots & \beta_{1,M}[k] \\ \beta_{2,1}[k] & \cdots & \beta_{2,m}[k] & \cdots & \beta_{2,M}[k] \end{bmatrix} \end{aligned} \tag{5.45a}$$

where

$$\begin{bmatrix} \beta_{1,l}[k] \\ \beta_{2,l}[k] \end{bmatrix} = \hat{\mathbf{C}}[k]^H \mathbf{E}[k] \begin{bmatrix} s_{1,l}[k] \\ s_{2,l}[k] \end{bmatrix} + \hat{\mathbf{C}}[k]^H \begin{bmatrix} z_{1,l}[k] \\ z_{2,l}[k] \end{bmatrix} \tag{5.45b}$$

is the effective noise comprising of channel estimation error and AWGN. In order to detect the transmitted signal $s_i(t)$, the detector simply chooses $y_{i,h}[k]$ among $\{y_{i,m}[k]\}_{m=1}^{M}$, if $\mathrm{Re}\left(y_{i,h}[k]\right) = \max\left(\left\{\mathrm{Re}\left(y_{i,m}[k]\right)\right\}_{m=1}^{M}\right)$, and decides that $w_h(t)$ is the transmitted signal. It's worth noting that when *M*=2, this Max-Real detector in (5.45b) reduces to the sign detector in (5.32)

It is worth pointing out that the optimum detector should be the one that directly follows the maximum likelihood principle. In appendix A we will discuss this

issue in detail. In the mean time, the detector in (5.45) is actually an easy-to-implement suboptimum detector that performs very close to the optimum detector.

5. 3. 3 Error Performance Analysis

Since the signal waveforms are orthogonal, without loss of generality, we could assume $s_1(t) = w_1(t)$ and $s_2(t) = w_q(t)$ in error performance analysis. When $q = 1$, we have the scenario of transmitting identical tones in the two transmit antennas in the first subinterval of a code-interval.

Conditioned on $\hat{\mathbf{C}}[k]$, we have

$$y_{1,1}[k] = \left(|\hat{c}_1[k]|^2 + |\hat{c}_2[k]|^2 \right) + \beta_{1,1}[k] \tag{5.46}$$

where $\beta_{1,1}[k] = \beta_{1,1,c}[k] + j\beta_{1,1,s}[k]$ is a complex Gaussian random variable with mean zero and a variance that will be determined later for easy of presentation here, and

$$y_{1,m}[k] = \beta_{1,m}[k] \ , \qquad m = 2, \cdots, M \tag{5.47}$$

where $\beta_{1,m}[k] = \beta_{1,m,c}[k] + j\beta_{1,m,s}[k]$ is another zero mean complex Gaussian random variable having a variance different from that of $\beta_{1,1}[k]$. Note that

$$s_{2,m}[k] = \begin{cases} 1 & m = q \\ 0 & \text{otherwise} \end{cases}. \tag{5.48}$$

Unfortunately, unlike the case for BFSK detection, the noise samples $z_{i,m}[k]$ (5.43b) in the data detector are correlated with the noise samples in the channel estimator. Consequently it is also correlated with the estimated channel gain $\hat{\mathbf{C}}[k]$ and the estimation error $\mathbf{E}[k]$. In appendix B, we show that conditioned on $\hat{c}_1[k]$, $\hat{c}_2[k]$, $e_1[k]$ and $e_2[k]$, the pair $z_{1,m}[k]$ and $z_{2,m}[k]$ are conditional complex Gaussian random variables and could be written as

$$z_{1,m}[k] = \left(\frac{\hat{c}_1[k] + \hat{c}_2[k]}{\sigma_{\hat{c}}^2} - \frac{e_1[k] + e_2[k]}{\sigma_e^2} \right) \frac{f_0 N_0}{2} + z'_{1,m}[k] \tag{5.49a}$$

and

$$z_{2,m}[k]=\left(\frac{\hat{c}_2^*[k]-\hat{c}_1^*[k]}{\sigma_{\hat{c}}^2}+\frac{e_1^*[k]-e_2^*[k]}{\sigma_e^2}\right)\frac{f_0N_0}{2}+z'_{2,m}[k] \tag{5.49b}$$

where f_0 is the middle coefficient of the channel estimation filter given in (5.13), $z'_{1,m}[k]$ and $z'_{2,m}[k]$ are both conditional complex Gaussian random variables with mean zero and variance

$$\sigma_{z'}^2=N_0-\frac{\left(f_0N_0\right)^2}{2\sigma_{\hat{c}}^2}-\frac{\left(f_0N_0\right)^2}{2\sigma_e^2}. \tag{5.49c}$$

The pair $z'_{1,m}[k]$ and $z'_{2,m}[k]$ are uncorrelated with $\hat{c}_1[k]$, $\hat{c}_2[k]$, $e_1[k]$ and $e_2[k]$. Furthermore,

$$\frac{1}{2}E\left[z'_{1,l}[k]z'^*_{2,l}[k]\right]=0, \tag{5.49d}$$

that is, $z'_{1,m}[k]$ and $z'_{2,m}[k]$ are uncorrelated. This stems from the fact that

$$\begin{aligned}
&\frac{1}{2}E\left[z_{1,m}[k]z^*_{2,m}[k]\right]\\
&=\left(\frac{f_0N_0}{2\sigma_{\hat{c}}^2}\right)^2\frac{1}{2}E\left[\left(\hat{c}_1[k]+\hat{c}_2[k]\right)\left(\hat{c}_2[k]-\hat{c}_1[k]\right)\right]\\
&\quad+\left(\frac{f_0N_0}{2\sigma_e^2}\right)^2\frac{1}{2}E\left[\left(e_1[k]+e_2[k]\right)\left(e_2[k]-e_1[k]\right)\right]+\frac{1}{2}E\left[z'_{1,m}[k]z'^*_{2,m}[k]\right]\\
&=0+0+\frac{1}{2}E\left[z'_{1,m}[k]z'^*_{2,m}[k]\right]=0.
\end{aligned},$$

On the other hand,

$$\frac{1}{2}E\left[z'_{i,m}[k]z'^*_{i,q}[k]\right]=-\frac{\left(f_0N_0\right)^2}{2\sigma_{\hat{c}}^2}-\frac{\left(f_0N_0\right)^2}{2\sigma_e^2}=R_{z'},m\neq q, \tag{5.50}$$

i.e., when conditioned on $\hat{c}_1[k]$, $\hat{c}_2[k]$, $e_1[k]$ and $e_2[k]$, the noise samples in different filter outputs are correlated with a correlation coefficient $\rho_{z'}=R_{z'}/\sigma_{z'}^2$. We arrive at this conclusion from the analysis

$$\frac{1}{2}E\left[z_{i,m}[k]z_{i,q}^{*}[k]\right]_{l\neq q}$$
$$=\left(\frac{f_0N_0}{2\sigma_{\hat{c}}^2}\right)^2\frac{1}{2}E\left[|\hat{c}_1[k]\pm\hat{c}_2[k]|^2\right]+\left(\frac{f_0N_0}{2\sigma_e^2}\right)^2\frac{1}{2}E\left[|e_1[k]\pm e_2[k]|^2\right]$$
$$+\frac{1}{2}E\left[z'_{i,m}[k]z'^{*}_{i,q}[k]\right]$$
$$=\frac{(f_0N_0)^2}{2\sigma_{\hat{c}}^2}+\frac{(f_0N_0)^2}{2\sigma_e^2}+\frac{1}{2}E\left[z'_{i,m}[k]z'^{*}_{i,q}[k]\right]=0.$$

$$\Downarrow$$

$$\frac{1}{2}E\left[z'_{i,m}[k]z'^{*}_{i,q}[k]\right]=-\frac{(f_0N_0)^2}{2\sigma_{\hat{c}}^2}-\frac{(f_0N_0)^2}{2\sigma_e^2}$$

Now consider the case $q=1$, i.e. transmitting identical tones in the two transmit antennas, both equal to $w_1(t)$. The data matrix $\mathbf{S}[k]$ now possesses the properties $s_{1,1}[k]=s_{2,1}[k]=1$ and $s_{1,m}[k]=s_{2,m}[k]=0$ for $m=2,\cdots,M$. From (5.45b) we have

$$\begin{bmatrix}\beta_{1,1}[k]\\ \beta_{2,1}[k]\end{bmatrix}=\hat{\mathbf{C}}[k]^H\mathbf{E}[k]\begin{bmatrix}1\\1\end{bmatrix}+\hat{\mathbf{C}}[k]^H\begin{bmatrix}z_{1,1}[k]\\ z_{2,1}[k]\end{bmatrix}$$
$$=\begin{bmatrix}\hat{c}_1^*[k]e_1[k]+\hat{c}_2[k]e_2^*[k]+\hat{c}_1^*[k]e_2[k]-\hat{c}_2[k]e_1^*[k]+\hat{c}_1^*[k]z_{1,1}[k]+\hat{c}_2[k]z_{2,1}[k]\\ \hat{c}_2^*[k]e_1[k]-\hat{c}_1[k]e_2^*[k]+\hat{c}_2^*[k]e_2[k]+\hat{c}_1[k]e_1^*[k]+\hat{c}_2^*[k]z_{1,1}[k]-\hat{c}_1[k]z_{2,1}[k]\end{bmatrix} \quad (5.51a)$$

and

$$\begin{bmatrix}\beta_{1,m}[k]\\ \beta_{2,m}[k]\end{bmatrix}=\hat{\mathbf{C}}[k]^H\begin{bmatrix}z_{1,m}[k]\\ z_{2,m}[k]\end{bmatrix}=\begin{bmatrix}\hat{c}_1^*[k]z_{1,m}[k]+\hat{c}_2[k]z_{2,m}[k]\\ \hat{c}_2^*[k]z_{1,m}[k]-\hat{c}_1[k]z_{2,m}[k]\end{bmatrix},\quad m=2,\cdots,M. \quad (5.51b)$$

To correctly detect $s_1(t)$, the real part of (5.46) has to be greater than the real part of (5.47) for all indices m from 2 to M. Define

$$\begin{aligned}\mu_{1,1}[k] &= \mathrm{Re}\left(|\hat{c}_1[k]|^2 + |\hat{c}_2[k]|^2 + \beta_{1,1}[k]\right) \\ &= \left(1+\frac{f_0 N_0}{2\sigma_{\hat{c}}^2}\right)\left(|\hat{c}_1[k]|^2 + |\hat{c}_2[k]|^2\right) + \eta_{1,1a} + \eta_{1,1b} \\ &= \left(1+\frac{f_0 N_0}{2\sigma_{\hat{c}}^2}\right)\lambda + \eta_{1,1}\end{aligned} \tag{5.52a}$$

and

$$\begin{aligned}\mu_{1,m}[k] &= \mathrm{Re}\left(\beta_{1,m}[k]\right) \\ &= \frac{f_0 N_0}{2\sigma_{\hat{c}}^2}\left(|\hat{c}_1[k]|^2 + |\hat{c}_2[k]|^2\right) + \eta_{1,ma} + \eta_{1,mb} \\ &= \frac{f_0 N_0}{2\sigma_{\hat{c}}^2}\lambda + \eta_{1,m},\ m = 2,\cdots,M\end{aligned} \tag{5.52b}$$

where $\gamma = \left(|\hat{c}_1[k]|^2 + |\hat{c}_2[k]|^2\right)$,

$$\eta_{1,1a} = \mathrm{Re}\left[\hat{c}_1^*[k]z'_{1,1}[k] + \hat{c}_2[k]z'_{2,1}[k]\right], \tag{5.52c}$$

$$\eta_{1,1b} = \left(1-\frac{f_0 N_0}{2\sigma_e^2}\right)\mathrm{Re}\left[\hat{c}_1^*[k](e_1[k]+e_2[k]) + \hat{c}_2[k](e_2^*[k]-e_1^*[k])\right], \tag{5.52d}$$

$$\eta_{1,ma} = \mathrm{Re}\left[\hat{c}_1^*[k]z'_{1,m}[k] + \hat{c}_2[k]z'_{2,m}[k]\right], \tag{5.52e}$$

and

$$\begin{aligned}\eta_{1,mb} &= \frac{f_0 N_0}{2\sigma_e^2}\mathrm{Re}\left[-\hat{c}_1^*[k](e_1[k]+e_2[k]) + \hat{c}_2[k](e_1^*[k]-e_2^*[k])\right] \\ &= \eta_{1,b}\end{aligned} \tag{5.52f}$$

are four real Gaussian RVs. It is trivial to show that $\eta_{1,1a}$ and $\eta_{1,ma}$ have means zero, variances

$$\sigma_{\eta 1,1a}^2 = \sigma_{\eta 1,ma}^2 = \gamma\sigma_{z'}^2 = \sigma_{\eta 1,a}^2 \tag{5.52g}$$

and covariance

$$R_{\eta 1,a} = E[\eta_{1,ma}\eta_{1,pa}] = \gamma\left(-\frac{\left(f_0 N_0\right)^2}{2\sigma_{\hat{c}}^2} - \frac{\left(f_0 N_0\right)^2}{2\sigma_e^2}\right),\quad m \neq p\,. \tag{5.52h}$$

Similarly it is easy to show that $\eta_{1,1b}$ and $\eta_{1,lb}$ have means zero, variances

$$\sigma^2_{\eta 1,1b} = \left(1 - \frac{f_0 N_0}{2\sigma_e^2}\right)^2 \gamma 2\sigma_e^2 \tag{5.52i}$$

and

$$\sigma^2_{\eta 1,mb} = \left(\frac{f_0 N_0}{2\sigma_e^2}\right)^2 \gamma 2\sigma_e^2,\ m = 2,\cdots,M \tag{5.52j}$$

respectively, and covariance

$$R_{\eta 1,b1m} = E[\eta_{1,1b}\eta_{1,mb}] = \left(1 - \frac{f_0 N_0}{2\sigma_e^2}\right)\left(-\frac{f_0 N_0}{2\sigma_e^2}\right)\gamma 2\sigma_e^2,\quad m = 2,\cdots,M\ . \tag{5.52k}$$

Consequently, $\eta_{1,1}$ and $\eta_{1,m}$ are correlated real Gaussian random variables with mean zero, variance $\sigma^2_{\eta 11} = \sigma^2_{\eta 1,a} + \sigma^2_{\eta 1,1b}$ and $\sigma^2_{\eta 1m} = \sigma^2_{\eta 1,a} + \sigma^2_{\eta 1,mb}$ respectively, and covariance

$$R_{\eta,1m} = E[\eta_{1,1}\eta_{1,m}] = R_{\eta 1,a} + R_{\eta 1,b1m} \tag{5.52l}$$

and

$$R_{\eta,mp} = E[\eta_{1,m}\eta_{1,p}] = R_{\eta 1,a} + \sigma^2_{\eta 1,mb},\ m \neq p\,. \tag{5.52m}$$

Based on discussion in (5.52a-m), the probability of a correct detection for the scenario $s_1(t) = s_2(t) = w_1(t)$ (equal tones), when conditioned on $\gamma = \left(|\hat{c}_1[k]|^2 + |\hat{c}_2[k]|^2\right)$, can be calculated as

$$\begin{aligned} P_{c,1}(\gamma) &= \Pr\left\{\bigcup_{m=2}^{M} \mu_{1,m}[k] < \mu_{1,1}[k]\right\} \\ &= \Pr\left\{\bigcup_{m=2}^{M} \eta_{1,m}[k] < \eta_{1,1}[k] + \gamma\right\} \\ &= \int_{-\infty}^{\infty} d\eta_{1,1} \int_{-\infty}^{\eta_{1,1}[k]+\gamma} d\eta_{1,2} \cdots \int_{-\infty}^{\eta_{1,1}[k]+\gamma} d\eta_{1,M}\, f_{\boldsymbol{\eta}}(\boldsymbol{\eta}) \end{aligned} \tag{5.53a}$$

where

$$f_{\boldsymbol{\eta}}(\boldsymbol{\eta}) = \frac{1}{(2\pi)^{N/2}\left|\boldsymbol{\Phi}_{\boldsymbol{\eta}}\right|^{1/2}} \exp\left(-\tfrac{1}{2}\boldsymbol{\eta}^T \boldsymbol{\Phi}_{\boldsymbol{\eta}}^{-1}\boldsymbol{\eta}\right) \tag{5.53b}$$

is the joint pdf of the M real Gaussian random variables $\boldsymbol{\eta} = [\eta_{1,1}, \eta_{1,2}, \cdots, \eta_{1,M}]^T$, and

$$\boldsymbol{\Phi}_{\boldsymbol{\eta}} = E\left[\boldsymbol{\eta}\boldsymbol{\eta}^T\right] \begin{bmatrix} \sigma_{\eta 11}^2 & R_{\eta,1l} & \cdots & R_{\eta,1l} & R_{\eta,1l} \\ R_{\eta,1l} & \sigma_{\eta 1l}^2 & R_{\eta,lq} & \cdots & R_{\eta,lq} \\ \vdots & R_{\eta,lq} & \sigma_{\eta 1l}^2 & \ddots & \vdots \\ R_{\eta,1l} & \vdots & \ddots & \ddots & R_{\eta,lq} \\ R_{\eta,1l} & R_{\eta,lq} & \cdots & R_{\eta,lq} & \sigma_{\eta 1l}^2 \end{bmatrix} \tag{5.53c}$$

is the corresponding covariance matrix. The average correct decision probability can now be obtained by averaging (5.53) over the pdf of γ as follows

$$\begin{aligned} P_{c,1} &= \int_0^\infty P_{c,1}(\gamma)\, p_\gamma(\gamma) d\gamma \\ &= \int_0^\infty P_{c,1}(\gamma) \frac{\lambda}{(2\sigma_{\hat{c}}^2)^2} \exp\left[-\frac{\lambda}{2\sigma_{\hat{c}}^2}\right] d\gamma. \end{aligned} \tag{5.54}$$

Using the same approach, we can calculate the average probability of a correct decision, $P_{c,2}$, for the scenario $s_1(t) = w_1(t)$ and $s_2(t) = w_q(t)$, $q \neq 1$. The average symbol error probability (SEP) is thus $P_s = 1 - \left(\frac{1}{M} P_{c,1} + \frac{M-1}{M} P_{c,2}\right)$. From (5.53) it is clear that the determination of the conditional correct decision probability requires the calculation of a multi-dimension joint Gaussian probability integral. Unfortunately there is no simple form for this pdf except for the case of two jointly Gaussian random variables [17]. Therefore for $M = 2^K$, $K \geq 2$, the M-fold integral (5.53) and (5.54) can only be evaluated numerically, and the final average SEP requires another integral over the pdf of γ which makes the total numerical integral increases to M+1 fold, all with infinite integral range.

Since the exact error performance for the proposed ST-MFSK scheme described above requires multiple-dimensional integration, we choose to evaluate its performance by deriving simple and yet tight upper bounds for the BEP of its receiver.

5. 3. 4 Predictor Upper Bound

From (5.49), we realize that the correlation between the noise samples $z_{i,l}[k]$ (5.43b) in the data detector and the noise samples in the channel estimator is introduced through the middle entry of the channel estimation filter f_0. One intuitive idea to make this correlation vanish is to set $f_0 = 0$, in which case the channel estimation quality would degrade, but when the channel estimation filter is sufficiently long, the performance loss would be minimal, especially for slow or moderate fade rate. Thus by constructing a channel estimation filter that does not make use of $x_j[k]$ in estimating $c_j[k]$, we obtain a sub-optimum receiver whose BEP gives us a tight upper bound on the BEP of the optimum receiver. We call this bound the Predictor Bound, as nulling f_0 is equivalent to using a forward linear predictor and a backward predictor simultaneously. In the following, we show how to optimize the two predictors jointly.

With simultaneous forward-backward prediction, the channel estimation filter is

$$\mathbf{f}' = \boldsymbol{\varphi}'_{c\mathbf{X}}\, \boldsymbol{\Phi}'^{-1}_{\mathbf{XX}}, \tag{5.55}$$

where

$$\begin{aligned} \boldsymbol{\Phi}'_{\mathbf{XX}} &= \frac{1}{2} E\left[\mathbf{X}'_j[0]\mathbf{X}'^{H}_j[0]\right] \\ &= \left[\phi_c[n-m]\right] + N_0\left(\tfrac{M}{2}\right)\mathbf{I}_{2P}, \qquad n,m = -P,\cdots,-1,1,\cdots,P \end{aligned} \tag{5.56}$$

is the covariance matrix of the observation vector

$$\mathbf{X}'_j[k] = \left[x_j[k-P], \cdots, x_j[k-1], x_j[k+1], ..., x_j[k+P] \right]^T, \quad j = 1,2 \tag{5.57}$$

$$\boldsymbol{\varphi}'_{c\mathbf{X}} = \frac{1}{2} E\left[c_j[k] \mathbf{X}'^H_j[k] \right] = \left[\phi_c[-P], \cdots, \phi_c[-1], \phi_c[1], , \phi_c[P] \right] \tag{5.58}$$

is the correlation between $c_j[k]$ and $\mathbf{X}'_j[k]$, and

$$\hat{c}'_j[k] = \mathbf{f}' \mathbf{X}'_j[k], \tag{5.59}$$

is the estimate of $c_j[k]$. The channel estimate $\hat{c}'_i[k]$ and the estimation error $e'_i[k] = c_i[k] - \hat{c}'_i[k]$ are independent CGRV with mean zero and variance

$$\sigma^2_{\hat{c}'} = \frac{1}{2} E\left[\left| \hat{c}'_j[k] \right|^2 \right] = \boldsymbol{\varphi}'_{c\mathbf{X}} \boldsymbol{\Phi}'^{-1}_{\mathbf{XX}} \boldsymbol{\varphi}'^H_{c\mathbf{X}} \tag{5.60a}$$

and

$$\sigma^2_{e'} = \frac{1}{2} E\left[\left| c_j[k] - \hat{c}'_j[k] \right|^2 \right] = \sigma^2_c - \boldsymbol{\varphi}'_{c\mathbf{X}} \boldsymbol{\Phi}'^{-1}_{\mathbf{XX}} \boldsymbol{\varphi}'^H_{c\mathbf{X}} \tag{5.60b}$$

respectively. The detection procedure is the same as optimum receiver.

To assess the error performance of this linear predictive ST-MFSK receiver, we first consider the case of identical transmitted tones, i.e. $s_1(t) = s_2(t) = w_1(t)$. Following the approach outlined in (5.41-5.46), we define

$$\mu = \mathrm{Re}\left(y_{1,1}[k] \right) = \left(|\hat{c}_1[k]|^2 + |\hat{c}_2[k]|^2 \right) + \beta_{1,1,c}[k]$$

and

$$\mu_m = \mathrm{Re}\left(y_{1,m}[k] \right) = \beta_{1,m,c}[k], \qquad m = 2, \cdots, M$$

where $\beta_{1,1,c}[k]$ and $\beta_{1,l,c}[k]$ are independent real Gaussian RVs with mean zeros and variances

$$E\left[\beta^2_{1,1,c}[k] \right] = \left[2\sigma^2_{e'} + 2N_0 \right] \gamma = \sigma^2_{\beta 1} \qquad \text{(when } s_1(t) = s_2(t) \text{)}, \tag{5.61a}$$

and

$$E\left[\beta^2_{1,m,c}[k] \right] = 2N_0 \gamma = \sigma^2_{\beta m1}, \quad m > 1 \qquad \text{(when } s_1(t) = s_2(t) \text{)} \tag{5.61b}$$

respectively, where $\gamma = |\hat{c}'_1[k]|^2 + |\hat{c}'_2[k]|^2$. Given μ, the probability that the detector makes a correct decision is then

$$\begin{aligned} P_{c,1}(\mu) &= \prod_{m=2}^{M} \Pr(\mu_m < \mu) \\ &= \left[\int_{-\infty}^{\mu} \frac{1}{\sqrt{2\pi\sigma_{\beta m1}^2}} \exp\left(\frac{-t^2}{2\sigma_{\beta m1}^2} \right) dt \right]^{M-1}. \end{aligned} \tag{5.62}$$

Now averaging this conditional correct decision probability over the distribution of $\beta_{1,1,c}[k]$ we get the correct decision probability conditioned on γ as

$$\begin{aligned} P_{c,1}(\gamma) &= \int_{-\infty}^{\infty} P_{c,1}(\mu) p_{\beta 11c}(\mu - \gamma) d\gamma \\ &= \int_{-\infty}^{\infty} \left[\int_{-\infty}^{\gamma+x} \frac{1}{\sqrt{2\pi\sigma_{\beta m1}^2}} \exp\left(\frac{-t^2}{2\sigma_{\beta m1}^2} \right) dt \right]^{M-1} p_{\beta 11c}(x) dx \\ &= \int_{-\infty}^{-\gamma} Q\left(\frac{-\gamma - x}{\sigma_{\beta m1}} \right)^{M-1} \cdot \frac{1}{\sqrt{2\pi\sigma_{\beta 1}^2}} \exp\left(-\frac{x^2}{2\sigma_{\beta 1}^2} \right) dx \\ &\quad + \int_{-\gamma}^{\infty} \left[1 - Q\left(\frac{\gamma + x}{\sigma_{\beta m1}} \right) \right]^{M-1} \cdot \frac{1}{\sqrt{2\pi\sigma_{\beta 1}^2}} \exp\left(-\frac{x^2}{2\sigma_{\beta 1}^2} \right) dx \end{aligned} \tag{5.63}$$

Similarly, for the case of different tones in the two transmit antennas, i.e. $s_1(t) = w_1(t)$ and $s_2(t) = w_q(t)$, where $q \neq 1$, we have the following counterparts of (5.56) :

$$E\left[\beta_{1,1,c}^2[k] \right] = \left[\sigma_{e'}^2 + 2N_0 \right] \gamma = \sigma_{\beta 2}^2, \qquad \text{(when } s_1(t) \neq s_2(t) \text{)} \tag{5.64a}$$

and

$$E\left[\beta_{1,m,c}^2[k] \right] = \begin{cases} \sigma_{\beta 2}^2, & m = q, \\ \sigma_{\beta m2}^2, & m > 1 \text{ and } l \neq q, \end{cases} \qquad \text{(when } s_1(t) \neq s_2(t) \text{)} \tag{5.64b}$$

where

$$\begin{aligned} \sigma_{\beta 2}^2 &= \left[\sigma_{e'}^2 + 2N_0 \right] \gamma \\ \sigma_{\beta m2}^2 &= \sigma_{\beta m1}^2 = 2N_0 \gamma \end{aligned} \tag{5.65}$$

Now the counterpart of (5.63) becomes

$$P_{c,2}(\mu)=\prod_{l=2}^{M}\Pr\left(\mu_l<\mu\right)$$
$$=\left[\int_{-\infty}^{\mu}\frac{1}{2\sigma_{\beta 2}^2}\exp\left(\frac{-t}{2\sigma_{\beta 2}^2}\right)dt\right]\left[\int_{-\infty}^{\mu}\frac{1}{\sqrt{2\pi\sigma_{\beta m2}^2}}\exp\left(\frac{-t^2}{2\sigma_{\beta m2}^2}\right)dt\right]^{M-2} \tag{5.66}$$

and the counterpart of (5.58) becomes

$$P_{c,2}(\gamma)=\int_{-\infty}^{\infty}P_{c,2}(\mu)\,p_{\beta 11c}(\mu-\gamma)\,d\mu$$
$$=\int_{-\infty}^{\infty}\left[\int_{-\infty}^{\gamma+x}\frac{1}{2\sigma_{\beta 2}^2}\exp\left(\frac{-t^2}{2\sigma_{\beta 2}^2}\right)dt\right]\left[\int_{-\infty}^{\gamma+x}\frac{1}{\sqrt{2\pi\sigma_{\beta m2}^2}}\exp\left(\frac{-t^2}{2\sigma_{\beta m2}^2}\right)dt\right]^{M-2}p_{\beta 11c}(x)dx$$
$$=\int_{-\varpi}^{-\gamma}Q\left(\frac{-\gamma-x}{\sigma_{\beta 2}}\right)Q\left(\frac{-\gamma-x}{\sigma_{\beta m2}}\right)^{M-2}\cdot\frac{1}{\sqrt{2\pi\sigma_{\beta 2}^2}}\exp\left(-\frac{x^2}{2\sigma_{\beta 2}^2}\right)dx$$
$$+\int_{-\gamma}^{\varpi}\left[1-Q\left(\frac{\gamma+x}{\sigma_{\beta 2}}\right)\right]\left[1-Q\left(\frac{\gamma+x}{\sigma_{\beta m2}}\right)\right]^{M-2}\cdot\frac{1}{\sqrt{2\pi\sigma_{\beta 2}^2}}\exp\left(-\frac{x^2}{2\sigma_{\beta 2}^2}\right)dx \tag{5.67}$$

Finally, the average SEP can be calculated from (5.63) and (5.67) as

$$P_s=\frac{1}{M}\int_0^{\infty}\left[1-P_{c,1}(\gamma)\right]p_\gamma(\gamma)d\gamma+\frac{M-1}{M}\int_0^{\infty}\left[1-P_{c,2}(\gamma)\right]p_\gamma(\gamma)d\gamma \tag{5.68a}$$

where γ has a pdf as

$$p_\gamma(\gamma)=\frac{\gamma}{(2\sigma_{\hat{c}'}^2)^2}\exp\left[-\frac{\gamma}{2\sigma_{\hat{c}'}^2}\right]U(\gamma). \tag{5.68b}$$

Since for orthogonal MFSK, the Euclidian distances between any two symbols are independent of the alphabet size *M*, the BEP can be easily obtained from the SEP as [3, 5-4.48]

$$P_b=\frac{M}{2(M-1)}P_s. \tag{5.69}$$

Equations (5.58) and (5.61) show that the evaluation of the average SEP of *M*-ary orthogonal FSK involves calculation of the integer powers of the *Q*-function. This translates into the evaluation of a multiple integral in (5.62).

To perform the averaging in (5.62), we first consider a system using 4FSK signaling. Substituting M=4 into (5.62) we have

$$\begin{aligned} P_s &= \frac{1}{4}\int_0^{\infty}\left[1-P_{c,1}(\gamma)\right]p_\gamma(\gamma)d\gamma+\frac{3}{4}\int_0^{\infty}\left[1-P_{c,2}(\gamma)\right]p_\gamma(\gamma)d\gamma \\ &= 1-\int_0^{\infty}\left[\frac{1}{4}P_{c,1}(\gamma)+\frac{3}{4}P_{c,2}(\gamma)\right]p_\gamma(\gamma)d\gamma \end{aligned} \quad . \tag{5.70}$$

By using the single finite integral representation of the integer powers of the Q-function [69],

$$Q(t)=\frac{1}{\pi}\int_0^{\pi/2}\exp(-\frac{t^2}{2\sin^2\theta})d\theta,$$

$$Q^2(t)=\frac{1}{\pi}\int_0^{\pi/4}\exp(-\frac{t^2}{2\sin^2\theta})d\theta,$$

and

$$\begin{aligned} Q^3(t) &= \frac{1}{\pi^2}\int_0^{\pi/6}D(\theta)\exp(-\frac{t^2}{2\sin^2\theta})d\theta \\ &\quad+\frac{1}{2\pi^2}\int_0^{\kappa}\left[\pi-D(\theta)\right]\exp(-\frac{t^2}{2\sin^2\theta})d\theta, \end{aligned}$$

where $\kappa=\sin^{-1}(1/\sqrt{3})$ and $D(\theta)=\cos^{-1}\left(\frac{3\cos 2\theta}{2\cos^3 2\theta}-1\right)$, we could calculate (5.63) as

$$\begin{aligned} P_{c,1}(\gamma) &= \int_{-\infty}^{-\gamma}Q^3\left(\frac{-\gamma-x}{\sigma_{\beta m1}}\right)\cdot\frac{1}{\sqrt{2\pi\sigma_{\beta1}^2}}\exp\left(-\frac{x^2}{2\sigma_{\beta1}^2}\right)dx \\ &\quad+\int_{-\gamma}^{\infty}\left[1-Q\left(\frac{\gamma+x}{\sigma_{\beta m1}}\right)\right]^3\cdot\frac{1}{\sqrt{2\pi\sigma_{\beta1}^2}}\exp\left(-\frac{x^2}{2\sigma_{\beta1}^2}\right)dx \\ &= \int_0^{\frac{\pi}{6}}\frac{D(\theta)}{\pi^2}\sqrt{\frac{\sigma_{\beta m1}^2\sin^2\theta}{\sigma_{\beta1}^2+\sigma_{\beta m1}^2\sin^2\theta}}\exp\left[\frac{-\gamma^2}{2(\sigma_{\beta1}^2+\sigma_{\beta m1}^2\sin^2\theta)}\right] \\ &\quad\cdot\left\{\frac{2}{\pi}\int_0^{\frac{\pi}{2}}\exp\left[\frac{-\gamma^2\sigma_{\beta m1}^2\sin^2\theta}{2\sigma_{\beta1}^2(\sigma_{\beta1}^2+\sigma_{\beta m1}^2\sin^2\theta)\sin^2\vartheta}\right]d\vartheta-1\right\}d\theta \end{aligned}$$

$$+\int_0^{\kappa}\frac{\pi-D(\theta)}{2\pi^2}\sqrt{\frac{\sigma_{\beta m1}^2\sin^2\theta}{\sigma_{\beta1}^2+\sigma_{\beta m1}^2\sin^2\theta}}\exp\left[\frac{-\gamma^2}{2(\sigma_{\beta1}^2+\sigma_{\beta m1}^2\sin^2\theta)}\right]$$
$$\cdot\left\{\frac{2}{\pi}\int_0^{\frac{\pi}{2}}\exp\left[\frac{-\gamma^2\sigma_{\beta m1}^2\sin^2\theta}{2\sigma_{\beta1}^2(\sigma_{\beta1}^2+\sigma_{\beta m1}^2\sin^2\theta)\sin^2\vartheta}\right]d\vartheta-1\right\}d\theta$$
$$-\frac{3}{\pi}\int_{\frac{\pi}{4}}^{\frac{\pi}{2}}\sqrt{\frac{\sigma_{\beta m1}^2\sin^2\theta}{\sigma_{\beta1}^2+\sigma_{\beta m1}^2\sin^2\theta}}\exp\left[\frac{-\gamma^2}{2(\sigma_{\beta1}^2+\sigma_{\beta m1}^2\sin^2\theta)}\right]$$
$$\cdot\left\{1-\frac{1}{\pi}\int_0^{\frac{\pi}{2}}\exp\left[\frac{-\gamma^2\sigma_{\beta m1}^2\sin^2\theta}{2\sigma_{\beta1}^2(\sigma_{\beta1}^2+\sigma_{\beta m1}^2\sin^2\theta)\sin^2\vartheta}\right]d\vartheta\right\}d\theta$$
$$+1-\frac{1}{\pi}\int_0^{\frac{\pi}{2}}\exp\left[\frac{-\gamma^2}{2\sigma_{\beta1}^2\sin^2\theta}\right]d\theta. \tag{5.71}$$

Similarly we can calculate (5.67) as

$$P_{c,2}(\gamma)=\int_{-\infty}^{-\gamma}Q\left(\frac{-\gamma-x}{\sigma_{\beta2}}\right)Q\left(\frac{-\gamma-x}{\sigma_{\beta m2}}\right)^{M-2}\frac{1}{\sqrt{2\pi\sigma_{\beta2}^2}}\exp\left(-\frac{x^2}{2\sigma_{\beta2}^2}\right)dx$$
$$+\int_{-\gamma}^{\infty}\left[1-Q\left(\frac{\gamma+x}{\sigma_{\beta2}}\right)\right]\left[1-Q\left(\frac{\gamma+x}{\sigma_{\beta m2}}\right)\right]^{M-2}\frac{1}{\sqrt{2\pi\sigma_{\beta2}^2}}\exp\left(-\frac{x^2}{2\sigma_{\beta2}^2}\right)dx \tag{5.72a}$$
$$=A(\gamma)+B(\gamma)$$

where

$$A(\gamma)=\frac{1}{\pi^3}\int_0^{\frac{\pi}{2}}d\theta\int_0^{\frac{\pi}{4}}d\vartheta\int_0^{\frac{\pi}{2}}d\psi\frac{\sqrt{\sigma_{\beta m2}^2\sin^2\theta\sin^2\vartheta}\exp\left[-\frac{\gamma^2}{2}F_A(\theta,\vartheta,\psi)\right]}{\sqrt{\sigma_{\beta2}^2\sin^2\theta+\sigma_{\beta m2}^2\sin^2\vartheta+\sigma_{\beta m2}^2\sin^2\theta\sin^2\vartheta}} \tag{5.72b}$$

with

$$F_A(\theta,\vartheta,\psi)=\frac{\sigma_{\beta m2}^2\sin^2\theta\sin^2\vartheta+\left(\sigma_{\beta2}^2\sin^2\theta+\sigma_{\beta m2}^2\sin^2\vartheta\right)\sin^2\psi}{\sigma_{\beta2}^2\left(\sigma_{\beta2}^2\sin^2\theta+\sigma_{\beta m2}^2\sin^2\vartheta+\sigma_{\beta m2}^2\sin^2\theta\sin^2\vartheta\right)\sin^2\psi}, \tag{5.72c}$$

and

$$
\begin{aligned}
B(\gamma) = 1 &- \frac{1}{\pi}\int_0^{\frac{\pi}{2}} \exp\left[\frac{-\gamma^2}{2\sigma_{\beta 2}^2 \sin^2\theta}\right] d\theta \\
&- \frac{2}{\pi}\int_0^{\frac{\pi}{2}} d\vartheta \sqrt{\frac{\sigma_{\beta m2}^2 \sin^2\vartheta}{\sigma_{\beta 2}^2 + \sigma_{\beta m2}^2 \sin^2\vartheta}} \exp\left[\frac{-\gamma^2}{2(\sigma_{\beta 2}^2 + \sigma_{\beta m2}^2 \sin^2\vartheta)}\right] \\
&\quad \cdot \left\{1 - \frac{1}{\pi}\int_0^{\frac{\pi}{2}} \exp\left[\frac{-\gamma^2 \sigma_{\beta m2}^2 \sin^2\vartheta}{2\sigma_{\beta 2}^2(\sigma_{\beta 2}^2 + \sigma_{\beta m2}^2 \sin^2\vartheta)\sin^2\psi}\right] d\psi\right\} \\
&+ \frac{1}{\pi}\int_0^{\frac{\pi}{4}} d\vartheta \sqrt{\frac{\sigma_{\beta m2}^2 \sin^2\vartheta}{\sigma_{\beta 2}^2 + \sigma_{\beta m2}^2 \sin^2\vartheta}} \exp\left[\frac{-\gamma^2}{2(\sigma_{\beta 2}^2 + \sigma_{\beta m2}^2 \sin^2\vartheta)}\right] \\
&\quad \cdot \left\{1 - \frac{1}{\pi}\int_0^{\frac{\pi}{2}} \exp\left[\frac{-\gamma^2 \sigma_{\beta m2}^2 \sin^2\vartheta}{2\sigma_{\beta 2}^2(\sigma_{\beta 2}^2 + \sigma_{\beta m2}^2 \sin^2\vartheta)\sin^2\psi}\right] d\psi\right\} \\
&- \frac{1}{\pi}\int_0^{\frac{\pi}{4}} d\theta \sqrt{\frac{\sin^2\theta}{1+\sin^2\theta}} \exp\left[\frac{-\gamma^2}{2\sigma_{\beta 2}^2(1+\sin^2\theta)}\right] \\
&\quad \cdot \left\{1 - \frac{1}{\pi}\int_0^{\frac{\pi}{2}} \exp\left[\frac{-\gamma^2 \sin^2\theta}{2\sigma_{\beta 2}^2(1+\sin^2\theta)\sin^2\psi}\right] d\psi\right\} \\
&+ \frac{2}{\pi^2}\int_0^{\frac{\pi}{2}} d\theta \int_0^{\frac{\pi}{2}} d\vartheta F_{B1}(\theta,\vartheta) - \frac{1}{\pi^2}\int_0^{\frac{\pi}{2}} d\theta \int_0^{\frac{\pi}{4}} d\vartheta F_{B1}(\theta,\vartheta)
\end{aligned}
\tag{5.72d}
$$

with

$$
\begin{aligned}
&F_{B1}(\theta,\vartheta) \\
&= \sqrt{\frac{\sigma_{\beta m2}^2 \sin^2\theta \sin^2\vartheta}{\sigma_{\beta 2}^2 \sin^2\theta + \sigma_{\beta m2}^2 \sin^2\vartheta + \sigma_{\beta m2}^2 \sin^2\theta \sin^2\vartheta}} \\
&\cdot \exp\left[\frac{-\gamma^2(\sigma_{\beta 2}^2 \sin^2\theta + \sigma_{\beta m2}^2 \sin^2\vartheta)}{2\sigma_{\beta 2}^2(\sigma_{\beta 2}^2 \sin^2\theta + \sigma_{\beta m2}^2 \sin^2\vartheta + \sigma_{\beta m2}^2 \sin^2\theta \sin^2\vartheta)}\right] \\
&\cdot \left\{1 - \frac{1}{\pi}\int_0^{\frac{\pi}{2}} \exp\left[\frac{-\gamma^2 \sigma_{\beta m2}^2 \sin^2\theta \sin^2\vartheta)}{2\sigma_{\beta 2}^2(\sigma_{\beta 2}^2 \sin^2\theta + \sigma_{\beta m2}^2 \sin^2\vartheta + \sigma_{\beta m2}^2 \sin^2\theta \sin^2\vartheta)\sin^2\psi}\right] d\psi\right\}.
\end{aligned}
\tag{5.72e}
$$

Since $\sigma_{\beta 1,}^2 \sigma_{\beta 2}^2, \sigma_{\beta m1}^2, \sigma_{\beta m2}^2$ all contain γ, the integrand in (5.65) and (5.66) are actually functions of the form $\exp[-b\gamma]$. The average SEP is then calculated by substituting (5.65), (5.66) and (5.62b) into (5.64). After applying the identity $\int_0^\infty \gamma e^{-a\gamma} d\gamma = a^{-2}$, the final average SEP for 4FSK can be obtained by performing a triple-fold numerical integration with finite range.

Since simple form for power of the *Q*-function exists only up to $Q^4(x)$ [69], the SEP calculation for *M*>4 FSK will involve numerical (double) integration over infinite range. This is quite computational intensive.

5. 3. 5 Union Bound

The simplest bound we can derive for the proposed coherent ST-MFSK receiver is the union bound:

$$P_b \le \frac{1}{\log_2 M} \sum_{m=2}^{M} I_{1,m} P_{1,m} \tag{5.73}$$

where

$$P_{1,m} = \Pr\left[\mathrm{Re}\left(y_{1,1}[k] \right) - \mathrm{Re}\left(y_{1,m}[k] \right) < 0 \right] \tag{5.74}$$

is the pairwise error probability (PEP) between $w_1(t)$ and $w_m(t)$, $I_{1,m}$ is the corresponding bit error count, and $\log_2 M$ is the number of information bits per MFSK symbol. Because of mutual orthogonality in the $w_m(t)$ s, the PEP $P_{1,m}$ is actually independent of the index *m*. Consequently, both the union bound and the PEP can be rewritten as

$$P_b \le \left(\frac{1}{\log_2 M} \sum_{m=2}^{M} I_{1,m} \right) P_2 = \frac{M}{2} P_2, \tag{5.75}$$

where

$$P_2 = \Pr\left[\mathrm{Re}\left(y_{1,1}[k] - y_{1,2}[k] \right) < 0 \right] \tag{5.76}$$

is the PEP between $w_1(t)$ and $w_2(t)$. Compared to the exact BEP calculation in Section 5.3.3 and the Predictor Bound in Section 5.3.4, the determination of this PEP is relatively straight forward because the noise term in $y_{1,1}[k]-y_{1,2}[k]$ is independent of the estimation error and that there is no need to distinguish between identical or non-identical tones. As a matter of fact, the determination of the PEP P_2 is similar to the exact BEP analysis for ST-BFSK in Section 5.2.

To determine the PEP in (5.75), we first subtract the second column of $\mathbf{Y}[k]$ from the first column. This generates the vector

$$\mathbf{d}[k]=\left(|\hat{c}_1[k]|^2+|\hat{c}_2[k]|^2\right)\mathbf{1}_2+\hat{\mathbf{C}}[k]\left(\mathbf{E}[k]\cdot\mathbf{1}_2+\mathbf{q}[k]\right), \tag{5.77a}$$

where $\mathbf{1}_2$ is an all-one column vector of size 2,

$$\mathbf{q}[k]=\begin{bmatrix}q_1[k]\\ q_2[k]\end{bmatrix}=\begin{bmatrix}z_{1,1}-z_{1,2}\\ z_{2,1}-z_{2,2}\end{bmatrix}=\begin{bmatrix}\int_{2kT}^{2kT+T} n(t)d(t)dt\\ \int_{2kT+T}^{2(k+1)T} n^*(t)d(t)dt\end{bmatrix} \tag{5.77b}$$

and

$$d(t)=w_1^*(t)-w_2^*(t) \tag{5.77c}$$

is a difference waveform that is analogous to the one in (5.20). As in the binary FSK case in (5.24), $q_1[k]$ and $q_2[k]$ are independent zero mean CGRVs with a variance of $\sigma_z^2=2N_0$. Furthermore, (5.25) continues to hold. So once again, the channel estimation errors are independent of the difference noise terms $q_1[k]$ and $q_2[k]$. At this point, it becomes evident that the analytical model in (5.27)-(5.37) applies to MFSK too. The only changes to these equations are the relationships between σ_c^2 and γ_b which is

$$\gamma_b=\frac{1}{\log_2 M}\left(\frac{\sigma_c^2}{N_0}\right).$$

5. 4 Diversity Reception

Now we consider a ST-FSK system with L receive antennas. Assuming non-selective Rayleigh fading in the $2L$ links, the received waveform at the ith receive antenna during the first and second sub-intervals of the k-th code interval are

$$r_i(t) = c_{i1}[k]s_1(t) + c_{i2}[k]s_2(t) + n_i(t),\ 2kT < t < (2k+1)T, \tag{5.78}$$

and

$$r_i(t) = -c_{i1}[k]s_2^*(t) + c_{i2}[k]s_1^*(t) + n_i(t),\ (2k+1)T < t < (2k+2)T, \tag{5.79}$$

where the $c_{ij}[k]$ s, $i = 1,2,\cdots,L$, $j = 1,2$, are iid zero mean CGRVs with variance σ_c^2. Since there are now L receivers, the channel estimation has to be performed at each receiver using the same procedure outlined in (5.5-5.18). The channel estimate obtained at a receiver will then be used to compensate for the fading effect in that receiver according to (5.45). The L resultant observations $\mathbf{Y}_1[k], \mathbf{Y}_2[k], ..., \mathbf{Y}_L[k]$ are combined (added) together to form the final observation. At this point, data detection can be carried out in exactly the same manner as in a single receiver system.

Due to the complexity we encountered during the performance analysis of M-FSK, we only use the binary case for demonstration purpose. With BFSK, the decision rule is

$$\hat{\mathbf{s}}[k] = \text{sgn}\left\{\sum_{i=1}^{L} \text{Re}\left(\mathbf{y}_i[k]\right)\right\} \tag{5.80a}$$

where

$$\mathbf{y}_i[k] = \begin{bmatrix} \left(|\hat{c}_{i1}[k]|^2 + |\hat{c}_{i2}[k]|^2\right)s_1[k] + \beta_{i1}[k] \\ \left(|\hat{c}_{i1}[k]|^2 + |\hat{c}_{i2}[k]|^2\right)s_2[k] + \beta_{i2}[k] \end{bmatrix} \tag{5.80b}$$

and $\{\beta_{ij}[k]\}$ for $i=1,\cdots,L$, $j=1,2$ are independent CGRVs with mean zero and variance $\sigma_{\beta i}^2 = 2\left(N_0+\sigma_e^2\right)\left(\left|\hat{c}_{i1}[k]\right|^2+\left|\hat{c}_{i2}[k]\right|^2\right)$. The BEP conditioned on $\gamma_i = \left(|\hat{c}_{i1}[k]|^2+|\hat{c}_{i2}[k]|^2\right)$ is then given by

$$P_e(\gamma) = Q\left(\sqrt{2\gamma}\right) \tag{5.81}$$

where $\gamma = \dfrac{\sum_{i=1}^{L}\gamma_i}{4(\sigma_e^2+N_0)}$ is the sum of $2L$ independent exponential random variables with an identical mean value as (5.35). The probability density function (pdf) of γ is therefore

$$p(\gamma) = \frac{\gamma^{2L-1}}{(L-1)!\lambda^{2L}} e^{-\gamma/\lambda} U(\gamma). \tag{5.82}$$

The average BEP then follows [3, 14.4-15]

$$\begin{aligned} P_b &= \int_0^{\infty} Q\left(\sqrt{2\gamma}\right) p_\gamma(\gamma) d\gamma \\ &= \left[\frac{1}{2}\left(1-\sqrt{\frac{\sigma_c^2-\sigma_e^2}{\sigma_c^2+\sigma_e^2+2N_0}}\right)\right]^{2L} \sum_{p=0}^{2L-1} \frac{(2L+p-1)!}{(2L-1)!\,j!}\left[\frac{1}{2}\left(1-\sqrt{\frac{\sigma_c^2-\sigma_e^2}{\sigma_c^2+\sigma_e^2+2N_0}}\right)\right]^{p}. \end{aligned} \tag{5.83}$$

5. 5 Numerical Results and Discussion

In Fig. 5.1 and 5.2, we compare the performance of our proposed ST-BFSK receiver with different interpolator size, and also with that of an ideal coherent detector. It is well-known that the detection of orthogonal FSK based on one symbol interval observation has 3dB loss in SNR when compared with ideal coherent detection. Here we demonstrate by jointly estimate the channel using adjacent received symbols can gain back most of the 3dB SNR loss, even in the case of “fast fading”. On the other

hand, for differential ST codes, as the fade rate becomes faster and faster, the error performance will degrade substantially.

In Fig. 5.3, we compare the performance of ST-BFSK and differential ST-BPSK with a small fade rate of $f_d T = 0.01$, where the error probability is at the same level. In Fig. 5.4, as we increase the fade rate to a relatively higher level of $f_d T = 0.05$ we find that the performance of differential ST-BPSK is much worse than that of ST-BFSK at higher SNR levels, where channel estimation error due to channel fluctuation becomes the major source of detection error. In Fig. 5.5, we compare the performance of ST-4FSK and that of differential ST-QPSK at different fade rates. It is evident that as the fading becomes faster and faster, the performance of differential ST codes becomes worse and worse, while for ST-MFSK, the performance is quite stable with only slightly degradation.

In Fig. 5.6, the symbol-error-probability (SEP) for different alphabet sizes are compared. As the noise power in the channel estimator is proportional to the alphabet size *M*, the larger the alphabet size has higher SEP. While this is true when we measure the error performance against the symbol SNR, the picture is changed when we use the bit SNR (i.e. $\sigma_c^2 / N_0 / \log_2 M$) instead. This is because when the bit SNR is fixed, then the symbol SNR increases at a rate of $\log_2 M$, meaning a better detector SNR (partially offset by a drop in estimator accuracy as M increases). In Fig. 5.7, we present the BEPs for different alphabet sizes as functions of the average SNR per bit. As *M* increases, the BEP is actually decreasing. However, as just mentioned, due to the drop in estimator accuracy as *M* increases, such improvement in a practical system is not as prominent as in an ideal coherent system.

In Fig. 5.8 – Fig. 5.10, we compare the exact BEP performance from simulation with the upper bound we derived in Section 5.4 for *M*-FSK with *M*>2. It

shows that the union bound becomes looser and looser as the alphabet size increases. However, given its extremely simple form, it still can be used as a good reference for performance assessment.

In Fig. 5.11 and 5.12, we examine the performance improvement by increasing the interpolator size for ST-MFSK. It is easy to understand that for ideal coherent detection of MFSK signals, when the average SNR per bit is fixed, the larger the modulation alphabet M means lower BEP. However, with the channel estimation scheme we adopted in our analysis, the amount of noise entering the channel estimator is proportional to the modulation alphabet M. Consequently, when the channel estimation is not accurate enough, the BEP of a larger modulation alphabet may be worse than that of a smaller modulation alphabet. This is demonstrated in Fig. 5.11 where in a relatively slow fading environment with $f_d T = 0.001$, only when the channel interpolator size P is greater than 5, the BEP of 16FSK is smaller than that of 4FSK. In Fig. 5.12, it shows that for a system with a relatively fast fade rate of $f_d T = 0.03$, the channel interpolator need to be as large as 16 for 16FSK to give better BEP than 4FSK.

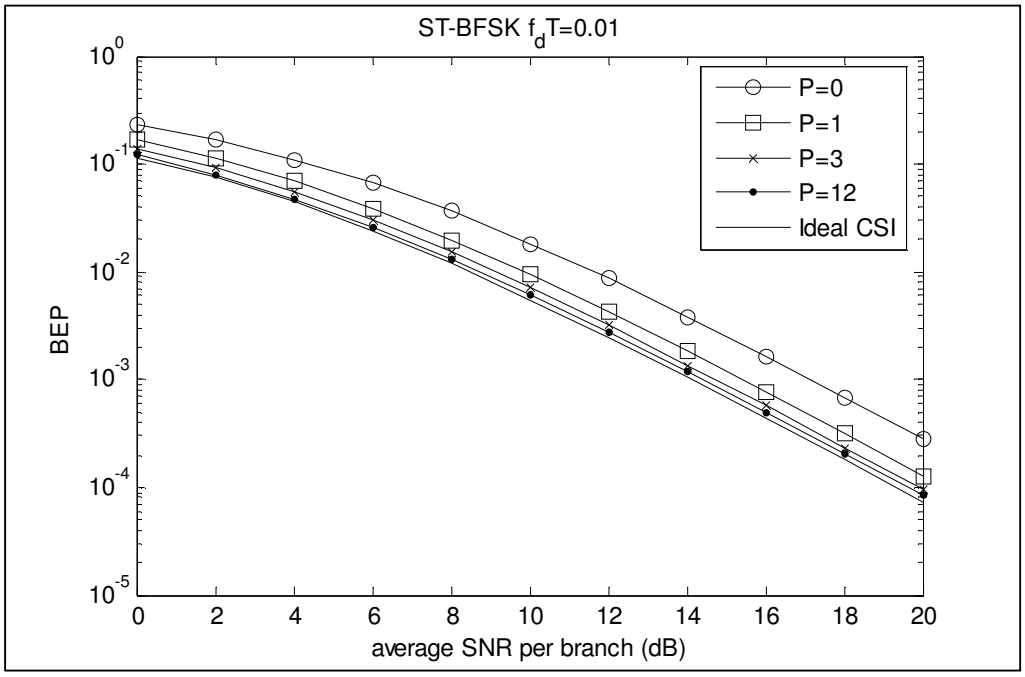

Figure 5.1 BEP vs. average SNR of BFSK with different interpolator size at moderate fade rate

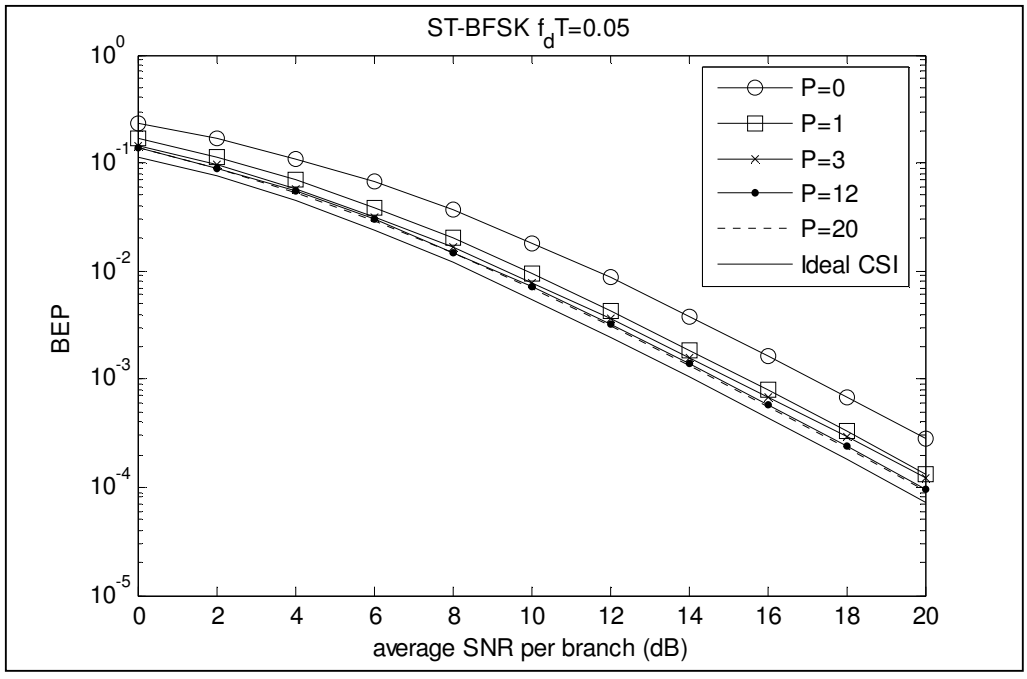

Figure 5.2 BEP vs. average SNR of BFSK with different interpolator size at large fade rate

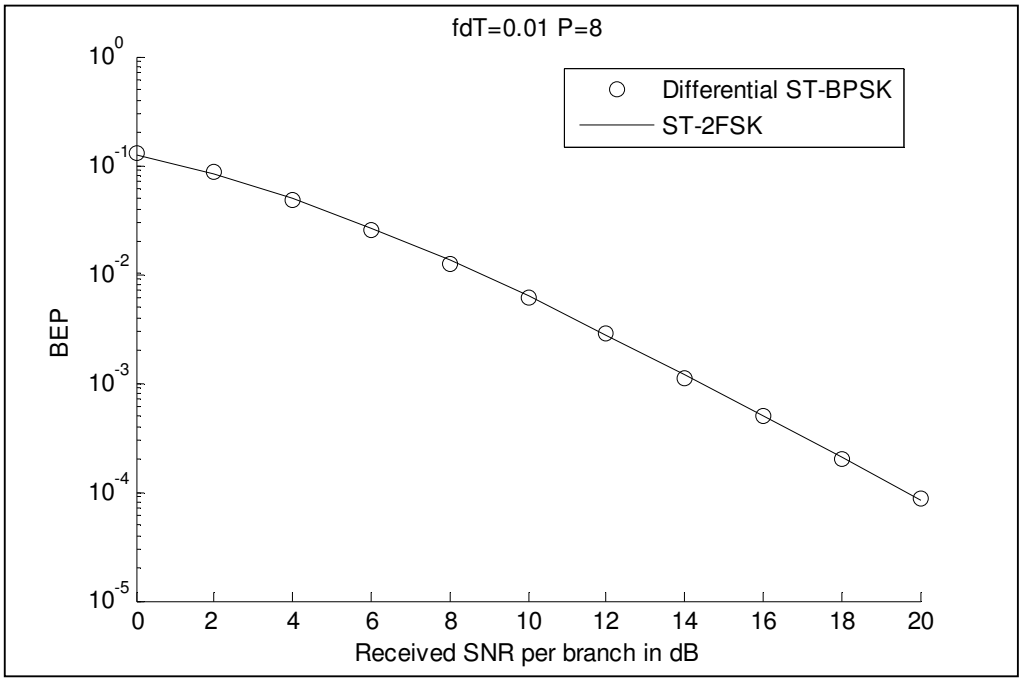

Figure 5.3 BEP vs. average SNR for BFSK and BDPSK at small fade rate

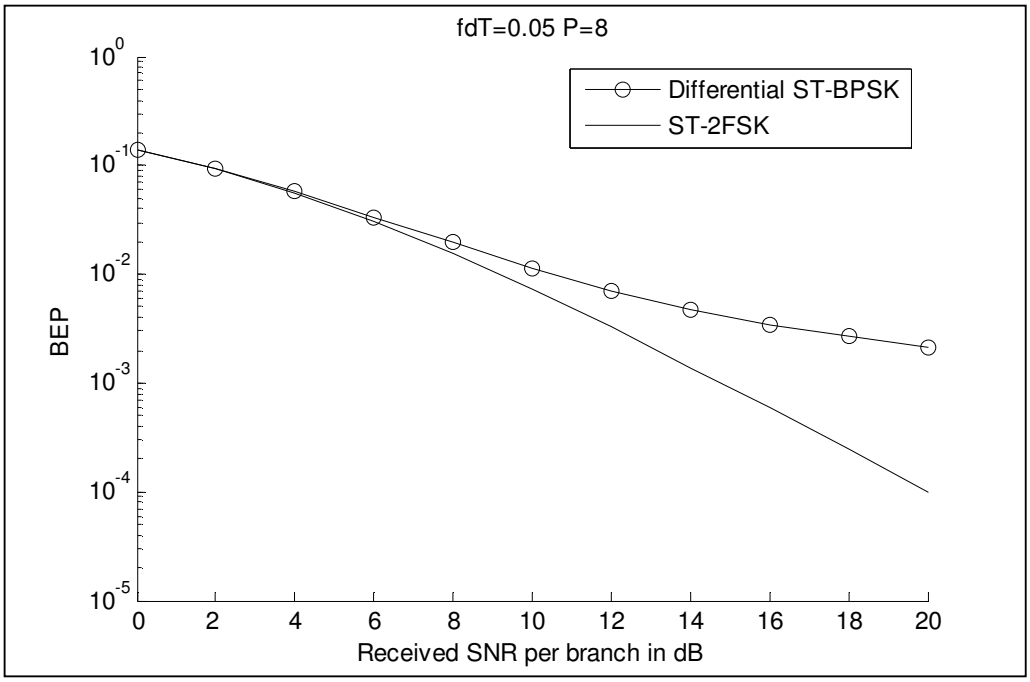

Figure 5.4 BEP vs. average SNR for BFSK and BDPSK at large fade rate

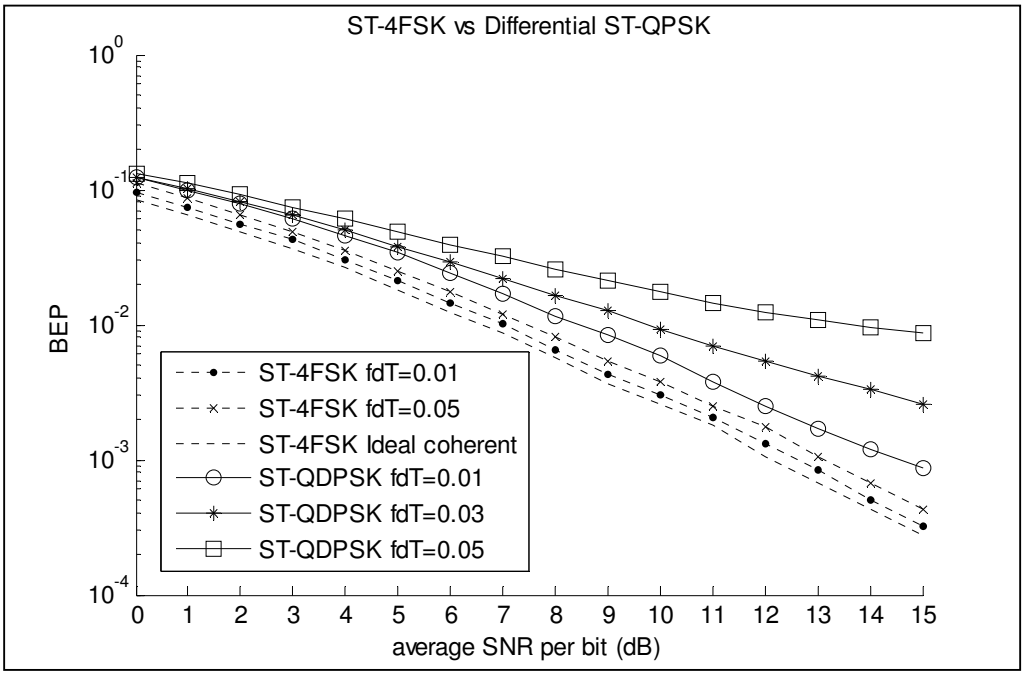

Figure 5.5 BEP vs. average SNR for 4FSK and QDPSK at various fade rates

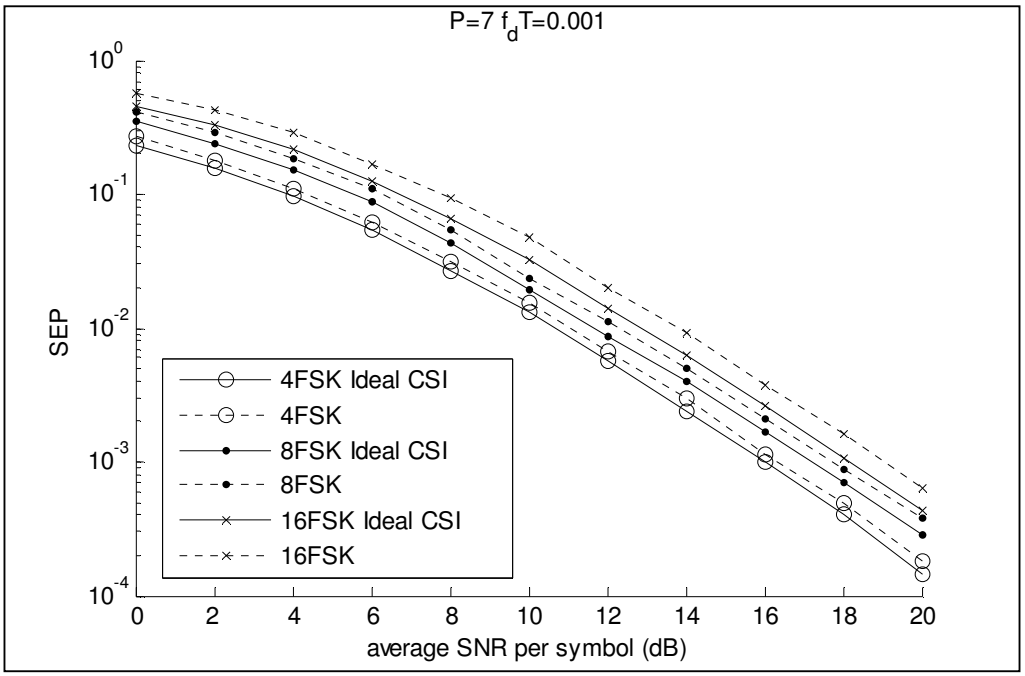

Figure 5.6 SEP vs. average SNR of MFSK

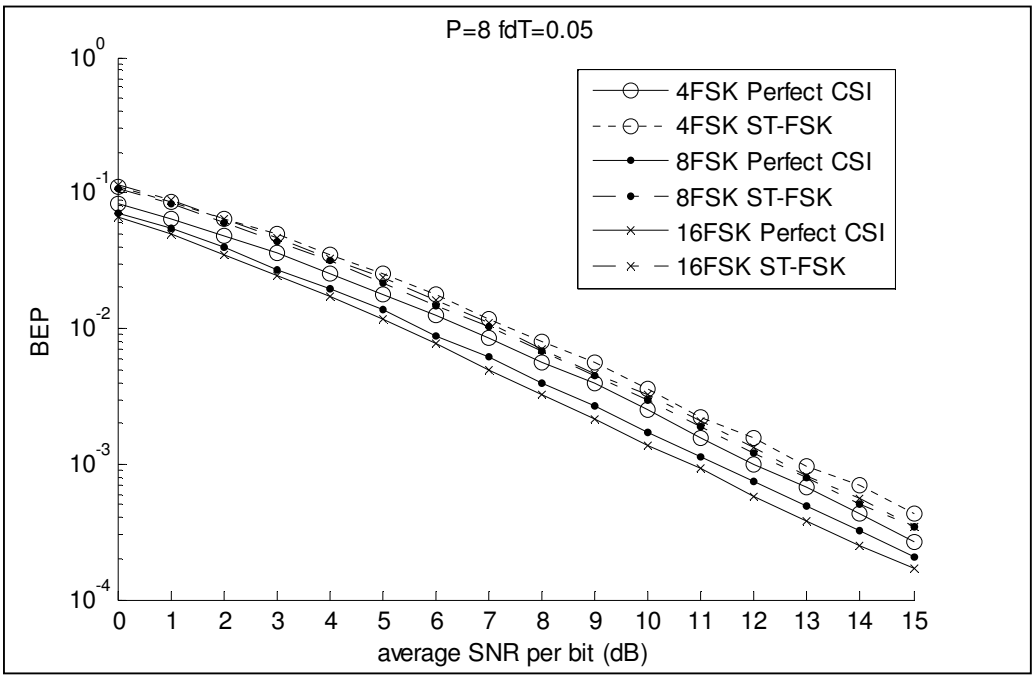

Figure 5.7 BEP vs. average SNR of MFSK

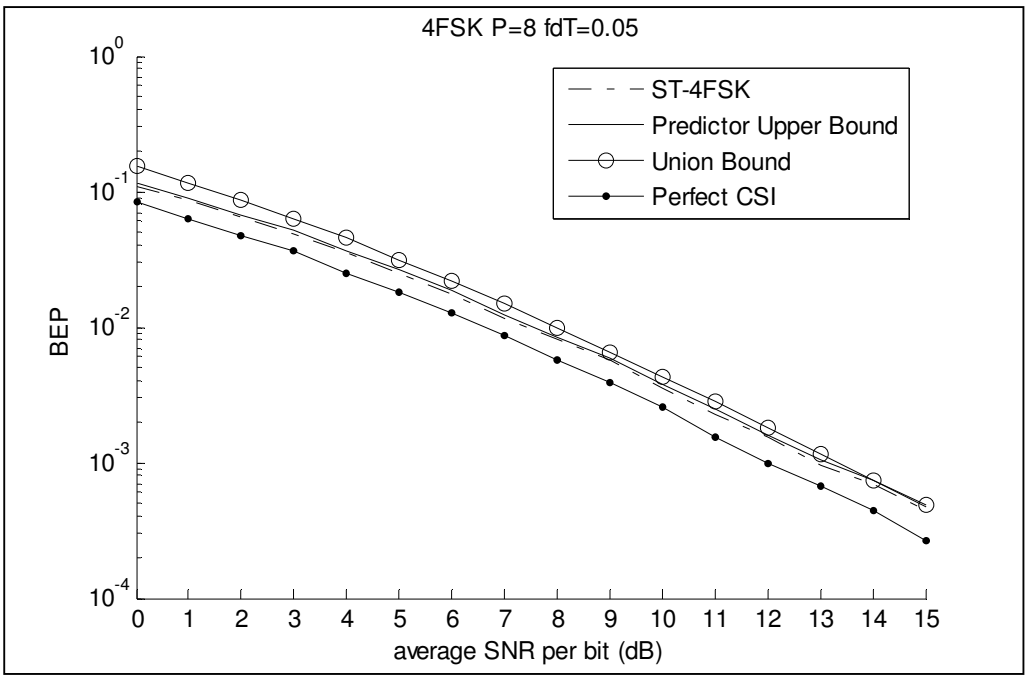

Figure 5.8 BEP vs. average SNR of 4FSK

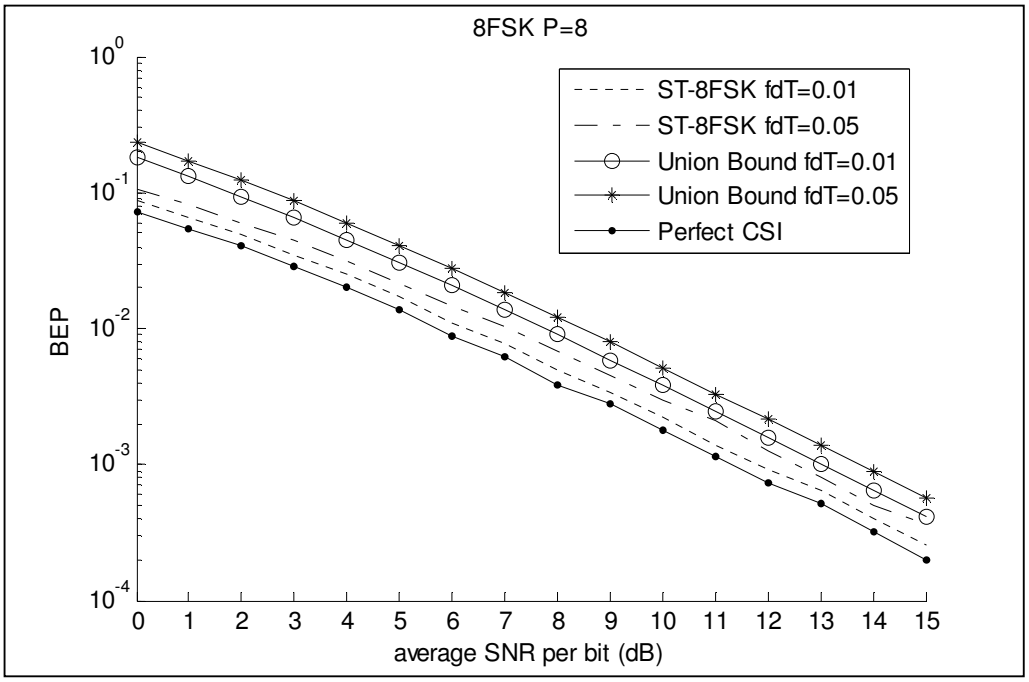

Figure 5.9 BEP vs. average SNR of 8FSK

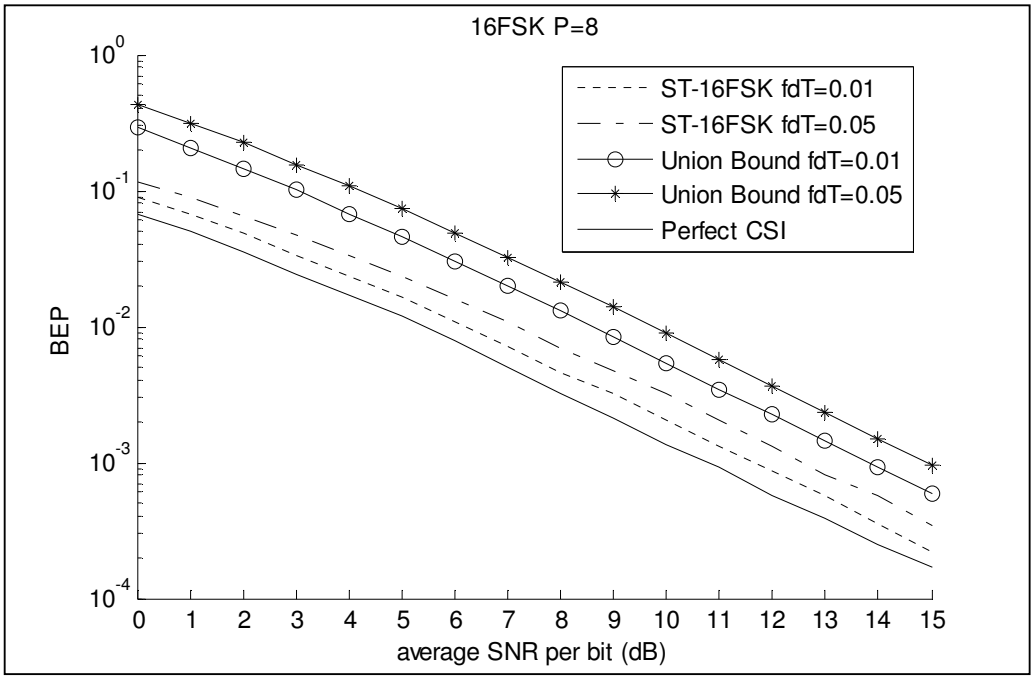

Figure 5.10 BEP vs. average SNR of 16FSK

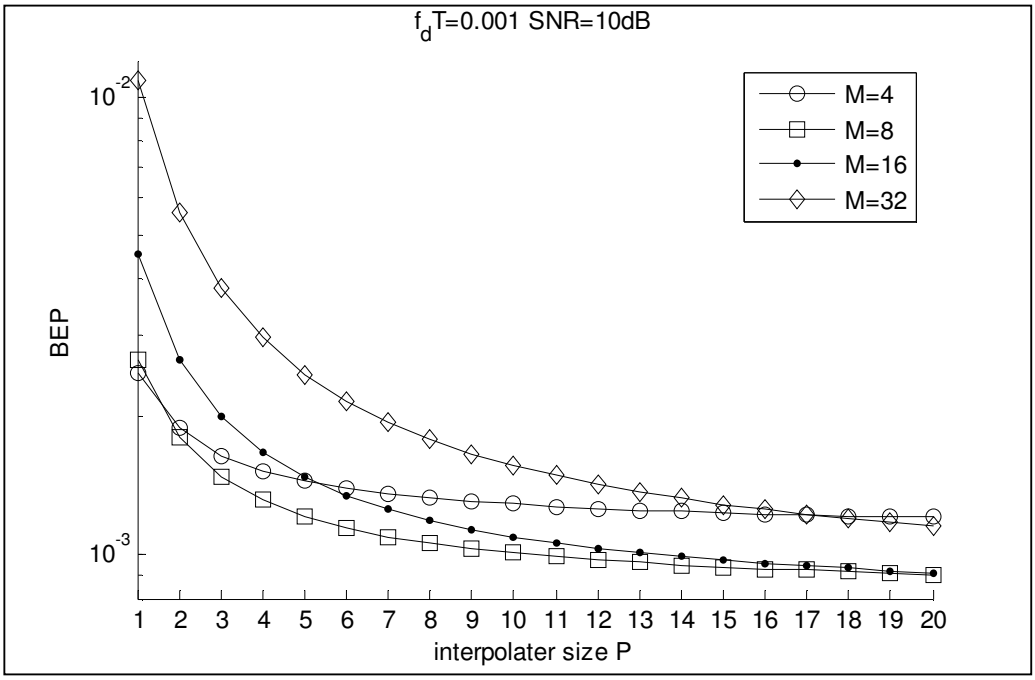

Figure 5.11 BEP vs. Interpolator size for small fade rate

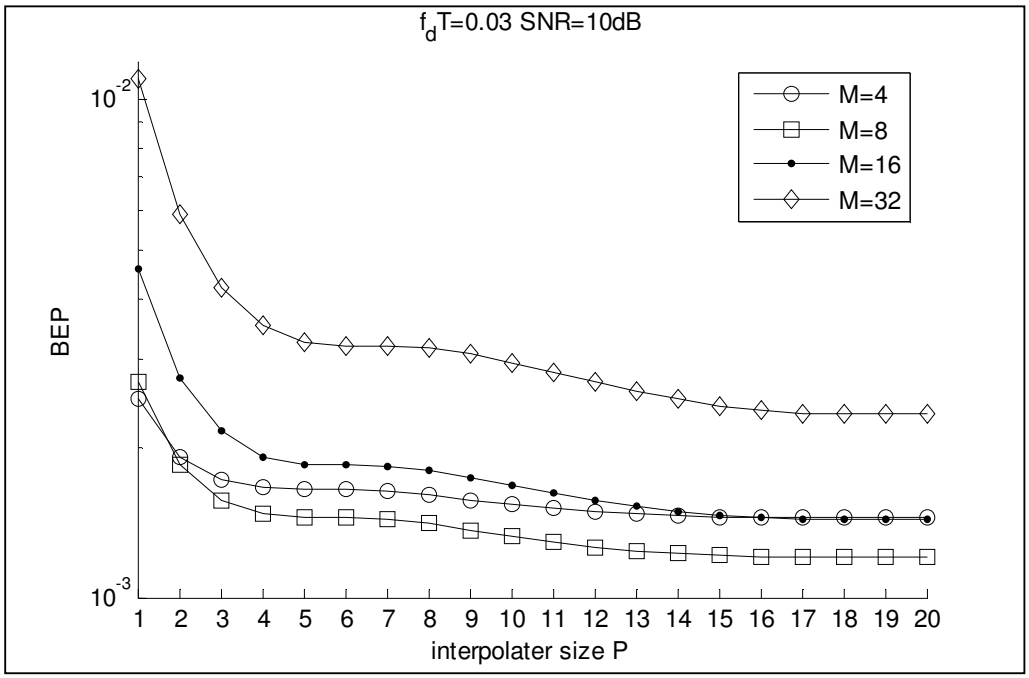

Figure 5.12 BEP vs. Interpolator size for large fade rate

5. 6 Summary

In this chapter, we extend the Alamouti type space-time codes to orthogonal FSK modulation. By making use of the unmodulated component of the orthogonal signal, we can actually form a "virtual pilot" sequence that jointly produces channel estimation with quite good quality. We've shown that this channel estimation scheme leads to a detector that is capable of gain back most of the 3dB loss of conventional quadratic receiver over ideal coherent detector. Exact error performance for binary orthogonal FSK is derived in very simple form, while for MFSK with $M>2$, two upper bounds are derived. The extension of this ST-MFSK system to diversity reception is also addressed.

Chapter 6

Conclusion and Suggestion for Future Work

6. 1 Conclusion

In this thesis, we designed and analyzed wireless diversity systems. More specifically, we examined the performance of diversity systems with practical channel estimation schemes.

For conventional single-transmit-multiple-receiver diversity receiver, we examined the performance of ideal coherent PSK and differentially encoded and detected PSK in nonselective Rayleigh fading channels with maximum ratio combining and multiple asynchronous cochannel interferers. Exact average error probability expressions were derived in terms of numerical integrals with finite integration range. By studying the effects of the timing offsets between the interferers' signal and the desired user's signal, we found that a symbol-synchronized system actually has the worst error performance, while the best performance for detection of the desired user's signal is achieved when all the interferers' signals are half-symbol-duration delayed with respect to the desired users' signal. This result holds true for systems using the rectangular pulse shaping at the transmitter and receiver. For systems using the raised-cosine pulse and the better-than-raised-cosine pulse as the overall pulse, the same conclusions are expected when the roll-off factor is large. We also compared the performances of systems using these two pulses. It was found that when the system is unsynchronized, the system using better-than-raised-cosine pulse

outperforms the system using raised-cosine pulse. Nevertheless they both perform worse than the system using rectangular pulse. For synchronized system, the three pulses have the same performance as far as error performance is concerned.

For transmit-receive diversity using PSK modulation, we developed a practical channel estimation scheme using pilot-symbol-assisted-modulation. An optimum receive weighting scheme was derived based on maximum-likelihood detection principle, and an optimum transmit weighting scheme was derived in order to minimize the instantaneous error probability. We also studied the error performance of this optimized transmit-receive diversity system. By examining the numerical results, we found that in order to achieve the best performance, for system undergoing faster fading, more energy should be distributed to the pilot symbols, either by increasing the power of the pilot symbols, or by increasing the frequency of pilot symbol insertion. In recognition of the fact that pilot-symbol based channel estimation scheme actually reduces the data rate, we then considered using binary orthogonal signaling, which had been shown to contain a hidden channel measurement component with each symbol. However, we found that due to the complex transmit weights involved, a generalized quadratic receiver is not implementable at the moment for our proposed transmit-receive diversity system. A transmitter-receiver structure that is similar to the one we used for the PSK case was then employed. The performance of this orthogonal signaling based system was then examined through simulation. We found that for this system, the main cause of the performance loss when compared to the ideal coherent case is the imperfect transmit weighting scheme, or, in other words, the performance of the proposed system is rather sensitive to the transmit weighting strategy.

Lastly, we developed an Alamouti-type space-time block code using orthogonal MFSK. The channel estimation was done by the unmodulated components

of the orthogonal signals. The performance of the proposed ST-MFSK system was then compared with that of a differential ST-PSK system. It was found that the performance of the latter degrades faster as the fade rate increases, while the performance of our proposed ST-MFSK is quite stable in both fast and slow fading environments. On the other hand, when the alphabet size M is increased, the error probability of ST-MFSK would not change much because the Euclidean distance between any two symbols remain unchanged in this case, while for linear modulation scheme such as PSK or QAM, the Euclidean distance would decrease if we increase the constellation size M. Therefore, the performance would degrade unless the symbol energy is increased as well. Of course, this advantage of ST-MFSK is achieved at the expense of consuming more bandwidth.

6. 2 Suggestion for Future Work

In this thesis, the average error probability of diversity receiver with multiple asynchronous cochannel interferers is obtained through multiple numerical integrals in this thesis. The computational complexity increases as the number of interferers increases. This surely brings inconvenience to system designers when they want to assess the performance of a system with asynchronous cochannel interferers. Therefore, further research could be carried out with the aim of at deriving more concise error probability expression or simple closed form approximations.

Another possible research area related to the asynchronous cochannel interference issue is to develop optimum combining schemes or detection schemes to suppress the interference, as has been done for synchronous cochannel interference. For example, joint detection of both the desired user's signal and the interferers' signals from a multiuser detection perspective has been shown to be a promising

method to suppress the destructive effect of cochannel interference, which offers even better performance than optimum combining. However, both of these two techniques are currently developed for synchronous cochannel interferers only [19] [39]. From our results it shows that synchronous case actually provides the worst error performance. Therefore, it would be interesting to consider extending the interference suppression techniques in [19] and [39] above to the asynchronous cochannel interference case.

In the design and analysis of our proposed PSAM transmit-receive diversity system, we have assumed an error-free and instantaneous feedback link between the receiver and the transmitter so that the optimized transmit weights can be sent to the transmitter to improve the performance of data symbol detection. This is certainly not an easy task in reality. Therefore, more practical means of feedback link should be developed, and the transmit weights and receive weights should be optimized based on both a practical channel estimation scheme and a practical feedback strategy. For example, instead of feeding back all the exact optimum transmit weights from the receiver to the transmitter, one can consider first a simple on-off control strategy, where among the total L_T transmit antennas, only a subset of it with the largest weights amplitude are selected and all the rest of the transmit antennas with smaller weights amplitude are turned off. Although inferior in performance when compared to optimum weighting scheme, this strategy only need to send binary information back to the receiver and it could reduce the complexity of the feedback link design substantially.

In our proposed orthogonal MFSK based space-time block code, we only considered Alamouti-type transmission scheme with two transmit antennas. After Alamouti's initial work, space-time block codes from generalized orthogonal design

have been developed to use more transmit antennas. Therefore, it will be useful to extend out ST-MFSK codes to larger code sizes as well.

Another interesting observation we found in our proposed ST-MFSK codes is that for the symbols to be transmitted during the first half and the second half of a code interval, no specific symbol constraint is needed as in ST-PSK codes or differential ST-PSK codes, while at the same time the channel estimation strategy still works. If we transmit different data symbols during the first and second half of a code interval, the detection of each pair of data symbols in each symbol interval actually becomes a multiuser detection problem. The advantage would be the increased data rate while the disadvantage is that no diversity gain is obtained. In other words, technically, our ST-MFSK code can support flexible transmission rate at the expense of diversity gains.

Although our proposed ST-MFSK code has been shown to provide better performance in fast fading environment than differential ST codes, its performance is still not comparable with that of a coherent ST code such as ST-PSK. On the other hand, it is known that minimum-shift-keying (MSK) offers performance that is close to ideal coherent PSK by using sequence detection. Therefore, it is interesting to develop space-time codes using MSK, and compare its performance with that of ST-PSK.

Appendix A

Maximum Likelihood Detection of ST-MFSK

In this appendix we discuss the optimum detection procedure for our proposed ST-MFSK block code.

First we cascade the two rows of the received signal in (5.42) to form a $2M \times 1$ column vector as

$$\begin{aligned}\mathbf{r}[k] &= \begin{bmatrix} \vdots \\ c_1[k]s_{1m}[k] + c_2[k]s_{2m}[k] + n_{1m}[k] \\ \vdots \\ c_2[k]s_{1m}[k] - c_1[k]s_{2m}[k] + n_{2m}[k] \\ \vdots \end{bmatrix} \\ &= \begin{bmatrix} c_1[k]\mathbf{I}_2 & c_2[k]\mathbf{I}_2 \\ c_2[k]\mathbf{I}_2 & -c_1[k]\mathbf{I}_2 \end{bmatrix} \begin{bmatrix} \mathbf{s}_1[k] \\ \mathbf{s}_2[k] \end{bmatrix} + \begin{bmatrix} \mathbf{n}_1[k] \\ \mathbf{n}_2[k] \end{bmatrix}\end{aligned} \tag{A.1}$$

where $\mathbf{s}_i[k] = [s_{i1}[k], ..., s_{iM}[k]]^T$ is the signal vector and $\mathbf{n}_i[k] = [n_{i1}[k], ..., n_{iM}[k]]^T$ represents the AWGN vector. Now conditioned on the channel estimates produced by the adjacent $2P$ received signal blocks, which is given by (5.59) as

$$\hat{c}'_j[k] = \mathbf{f}'\mathbf{X}'_j[k], \quad j = 1, 2, \tag{A.2}$$

(A.1) can be written as

$$\begin{aligned}\mathbf{r}[k] &= \begin{bmatrix} \hat{c}'_1[k]\mathbf{I}_2 & \hat{c}'_2[k]\mathbf{I}_2 \\ \hat{c}'_2[k]\mathbf{I}_2 & -\hat{c}'_1[k]\mathbf{I}_2 \end{bmatrix} \begin{bmatrix} \mathbf{s}_1[k] \\ \mathbf{s}_2[k] \end{bmatrix} + \begin{bmatrix} e'_1[k]\mathbf{I}_2 & e'_2[k]\mathbf{I}_2 \\ e'_2[k]\mathbf{I}_2 & -e'_1[k]\mathbf{I}_2 \end{bmatrix} \begin{bmatrix} \mathbf{s}_1[k] \\ \mathbf{s}_2[k] \end{bmatrix} + \begin{bmatrix} \mathbf{n}_1[k] \\ \mathbf{n}_2[k] \end{bmatrix} \\ &= \underbrace{\hat{\mathbf{C}}'[k] \begin{bmatrix} \mathbf{s}_1[k] \\ \mathbf{s}_2[k] \end{bmatrix}}_{\text{effective signal}} + \underbrace{\mathbf{E}'[k] \begin{bmatrix} \mathbf{s}_1[k] \\ \mathbf{s}_2[k] \end{bmatrix} + \begin{bmatrix} \mathbf{n}_1[k] \\ \mathbf{n}_2[k] \end{bmatrix}}_{\text{effective noise}}\end{aligned} . \tag{A.3}$$

The likelihood of the received signal $\mathbf{r}[k]$ on hypothesis $\mathbf{s}_1[k]=\mathbf{h}_m[k], \mathbf{s}_2[k]=\mathbf{h}_q[k]$ and conditioned on (A.2) is given by

$$\begin{aligned} & P(\mathbf{r}[k]\left|\hat{c}'_j[k], \mathbf{s}_1[k]=\mathbf{h}_m[k], \mathbf{s}_2[k]=\mathbf{h}_q[k]\right.) \\ & = \frac{\exp\left\{-\frac{1}{2}\left(\mathbf{r}[k]-\hat{\mathbf{C}}'[k]\begin{bmatrix}\mathbf{h}_m[k]\\ \mathbf{h}_q[k]\end{bmatrix}\right)^H \boldsymbol{\Phi}_{mq}^{-1}[k]\left(\mathbf{r}[k]-\hat{\mathbf{C}}'[k]\begin{bmatrix}\mathbf{h}_m[k]\\ \mathbf{h}_q[k]\end{bmatrix}\right)\right\}}{2\pi\left|\boldsymbol{\Phi}_{mq}[k]\right|} \end{aligned} \tag{A.4}$$

where $\boldsymbol{\Phi}_{mq}[k]$ is the covariance matrix of the effective noise component in (A.3) defined by

$$\begin{aligned} & \boldsymbol{\Phi}_{mq}[k] \\ & = \begin{bmatrix} \phi_{m,m}=\sigma_{e'}^2 & & & \phi_{m,M+q}=-\sigma_{e'}^2 \\ & \phi_{q,q}=\sigma_{e'}^2 & \phi_{q,M+m}=\sigma_{e'}^2 & \\ & \phi_{M+m,q}=\sigma_{e'}^2 & \phi_{M+m,M+m}=\sigma_{e'}^2 & \\ \phi_{M+q,m}=-\sigma_{e'}^2 & & & \phi_{M+q,M+q}=\sigma_{e'}^2 \end{bmatrix} + N_0\mathbf{I}_{2M} \end{aligned} \tag{A.5}$$

for the case when $m \neq q$. For notational simplicity, in (A.5) we use $\phi_{s,t}$ to represent the (*s, t*)-th element of a matrix. All the elements in (A.5) are zero except those being specified. For the case when $m = q$, (A.5) reduces to

$$\begin{aligned} & \boldsymbol{\Phi}_{mq}[k] \\ & = \begin{bmatrix} \phi_{m,m}=2\sigma_{e'}^2 & \\ & \phi_{M+m,M+m}=2\sigma_{e'}^2 \end{bmatrix} + N_0\mathbf{I}_{2M} \end{aligned} . \tag{A.6}$$

Now the optimum detection strategy based on maximizing the likelihood function in (A.4) suggests a multiuser detection problem for two users. Unfortunately, since the effective noise vector's covariance matrix shown in (A.5) and (A.6) takes different forms on different hypothesis, simplifying this ML detector seems difficult at the moment, although not totally impossible. Also exact error probability solutions for the error performance analysis of multiuser detection remain rare in literature, even for the simplest case of binary signals [41] – [43], [70]. On the other hand, if we consider the

ideal case where the channel estimation is perfect, then this ML detector coincides with the one we used in section 5.3.2. From the numerical result in section 5.5, we find that the detection scheme we used in section 5.3.2 actually provides near ideal error performance, given that the channel interpolator is sufficiently long. Therefore, the detector we use is in fact a sub-optimum solution at the presence of channel estimation error which offers near optimum performance.

Appendix B

Derivation for the conditional representation of (5.49)

Here we derive the representation of a complex Gaussian random variables conditioned on correlated multiple complex Gaussian random variables that lead to (5.49).

Assume $\tilde{x}$ is a circular symmetric complex Gaussian random variable with mean zero and variance $\sigma_x^2 = \frac{1}{2}E[|\tilde{x}|^2]$, and $\{\tilde{y}_i\}_{i=1}^{L}$ are L circular symmetric independent complex Gaussian random variables with mean zero and variance $\sigma_{yi}^2 = \frac{1}{2}E[|\tilde{y}_i|^2]$ respectively. We assume $\tilde{x}$ is correlated with $\{\tilde{y}_i\}_{i=1}^{L}$ with covariance $\sigma_{xyi}^2 = \frac{1}{2}E[\tilde{x}\tilde{y}_i^*] = \rho_{xyi}\sigma_x\sigma_{yi}$ where ρ_{xyi} is the correlation coefficient between $\tilde{x}$ and $\tilde{y}_i$. Now conditioned on $\tilde{y}_1$, similar as (2.8)-(2.10), $\tilde{x}$ can be rewritten as

$$\tilde{x} = \rho_{xy1}\frac{\sigma_x}{\sigma_{y1}}\tilde{y}_1 + e_1 = \frac{\sigma_{xy1}^2}{\sigma_{y1}^2}\tilde{y}_1 + e_1 \tag{B.1}$$

where e_1 represents the uncertainty of $\tilde{x}$ when given $\tilde{y}_1$, which is a circular symmetric complex Gaussian random variable with mean zero and variance

$$\sigma_{e1}^2 = \left(1 - \left|\rho_{xy1}\right|^2\right)\sigma_x^2. \tag{B.2}$$

As we assume $\{\tilde{y}_i\}_{i=1}^{L}$ are independent with each other, we have

$$\begin{aligned}\sigma_{xy2}^2 &= \frac{1}{2}E\left[\tilde{x}\tilde{y}_2^*\right] = \rho_{xy2}\sigma_x\sigma_{y2} \\ &= \frac{1}{2}E\left[\left(\frac{\sigma_{xy1}^2}{\sigma_{y1}^2}\tilde{y}_1 + e_1\right)\tilde{y}_2^*\right] = \frac{1}{2}E\left[e_1\tilde{y}_2^*\right] = \rho_{e1y2}\sigma_{e1}\sigma_{y2}\ .\end{aligned} \tag{B.3}$$

Therefore, we could rewrite e_1 in terms of $\tilde{y}_2$ as

$$e_1 = \rho_{e1y2}\frac{\sigma_{e1}}{\sigma_{y2}}\tilde{y}_2 + e_2 = \rho_{xy2}\frac{\sigma_x}{\sigma_{y2}}\tilde{y}_2 + e_2 = \frac{\sigma_{xy2}^2}{\sigma_{y2}^2}\tilde{y}_2 + e_2 \tag{B.4}$$

where e_2 represents the uncertainty of e_1 when given $\tilde{y}_2$, which is a circular symmetric complex Gaussian random variable with mean zero and variance

$$\begin{aligned}\sigma_{e2}^2 &= \left(1-\left|\rho_{e1y2}\right|^2\right)\sigma_{e1}^2 \\ &= \left(1-\left|\frac{\rho_{xy2}\sigma_x}{\sigma_{e1}}\right|^2\right)\sigma_{e1}^2 \\ &= \sigma_{e1}^2 - \left|\rho_{xy2}\sigma_x\right|^2 \\ &= \left(1-\left|\rho_{xy1}\right|^2 - \left|\rho_{xy2}\right|^2\right)\sigma_x^2\ .\end{aligned} \tag{B.5}$$

Since e_1 is independent of $\tilde{y}_1$, and $\{\tilde{y}_i\}_{i=1}^L$ are independent with each other, from (B.4) it is obvious that e_2 is independent of $\tilde{y}_1$ as well. Now cascade (B.1) and (B.4), we have

$$\tilde{x} = \frac{\sigma_{xy1}^2}{\sigma_{y1}^2}\tilde{y}_1 + \frac{\sigma_{xy2}^2}{\sigma_{y2}^2}\tilde{y}_2 + e_2\,. \tag{B.6}$$

Repeat the process in (B.4) – (B.6), it is simple to generalize the above derivation to all $\{\tilde{y}_i\}_{i=1}^L$, and finally we can rewrite $\tilde{x}$ as

$$\tilde{x} = \sum_{i=1}^{L}\frac{\sigma_{xyi}^2}{\sigma_{yi}^2}\tilde{y}_i + e_L \tag{B.7}$$

with e_L be a circular symmetric complex Gaussian random variable uncorrelated with $\{\tilde{y}_i\}_{i=1}^L$, with mean zero and variance

$$\sigma_{eL}^2 = \left(1 - \sum_{i=1}^{L} \left|\rho_{xyi}\right|^2\right)\sigma_x^2 \ . \tag{B.8}$$

From (5.43) we have $z_{1,m}[k] = n_m[2k]$ and $z_{2,m}[k] = n_m^*[2k+1]$. They are related to the channel estimation $\hat{c}_1[k]$ and $\hat{c}_2[k]$ through $\left\{\hat{c}_j[k] = \mathbf{f}\mathbf{X}_j[k]\right\}_{j=1}^{2}$ where

$$\mathbf{X}_j[k] = \left[x_j[k-P], x_j[k-P+1], ..., x_j[k+P]\right]^T$$

with

$$x_1[k] = c_1[k] + \frac{1}{2}\left(\sum_{m=1}^{M} n_m[2k] - \sum_{m=1}^{M} n_m[2k+1]\right)$$

and

$$x_2[k] = c_2[k] + \frac{1}{2}\left(\sum_{m=1}^{M} n_m[2k] + \sum_{m=1}^{M} n_m[2k+1]\right).$$

Now it is easy to show that

$$\frac{1}{2}E\left[z_{1,m}[k]\hat{c}_i^*[k]\right] = \frac{f_0 N_0}{2} \ , \ i = 1,2 \tag{B.9}$$

and

$$\frac{1}{2}E\left[z_{2,m}[k]\hat{c}_i\,[k]\right] = (-1)^i \frac{f_0 N_0}{2} \ , \ i = 1,2\,. \tag{B.10}$$

Similarly, $\left\{z_{i,m}[k]\right\}_{i=1}^{2}$ is correlated with $\left\{e_i[k] = \tilde{c}_i[k] - \hat{c}_i[k]\right\}_{i=1}^{2}$ as

$$\frac{1}{2}E\left[z_{1,m}[k]e_i^*[k]\right] = -\frac{f_0 N_0}{2} \ , \ i = 1,2 \tag{B.11}$$

and

$$\frac{1}{2}E\left[z_{2,m}[k]e_i\,[k]\right] = (-1)^{i-1} \frac{f_0 N_0}{2} \ , \ i = 1,2\,. \tag{B.12}$$

Substituting (B.9) - (B.12) into (B.7) and (B.8), we obtain the relation in (5.49). (Note that for circular symmetric Rayleigh fading channels, the coefficients of the channel estimation filter are all real, thus we have f_0 instead of f_0^* in (B.10) and (B.12).)

Appendix C

Differential Space Time Block Code[3]

Here we describe the system model of an Alamouti-type differential space-time modulation with code examples. This differential ST code is used to compare with our proposed ST-MFSK.

C.1 Signal Model

We assume Alamouti-type space-time modulation with a code-symbol period of $T_s = 2T$. The *k*-th coded-interval is divided into the subintervals $[2kT, 2kT+T]$ and $[2kT+T, 2(k+1)T]$. The transmitted signals at the two antennas are

$$s_i(t) = \sum_{n=-\infty}^{\infty} s_i[n]\, p(t-nT); \qquad i = 1, 2, \tag{C.1}$$

where $s_i[n]$ denotes the *n*-th symbol transmitted by the *i*-th antenna, and $p(t)$ is a unit-energy square root raised cosine (SQRC) pulse. The transmitted symbols have the constraints

$$\begin{aligned} s_1[2k+1] &= -s_2^*[2k] = -a_2^*[k] \\ s_2[2k+1] &= +s_1^*[2k] = +a_1^*[k] \end{aligned}, \tag{C.2}$$

where $a_i[k] = s_i[2k]$. The received signal is

$$r(t) = c_1(t)s_1(t) + c_2(t)s_2(t) + n(t), \tag{C.3}$$

[3] The material in this appendix is part of the content of [71], quoted here in agreement with the original authors.

where $n(t)$, $c_1(t)$ and $c_2(t)$ are all zero-mean complex Gaussian processes and they represent receiver noise and fading in the two links respectively. The fading processes $c_1(t)$ and $c_2(t)$ are independent and identically distributed (iid) with an autocorrelation function

$$\phi_c(\tau) = \frac{1}{2} E\left[c_i(t+\tau) c_i^*(t) \right] = \sigma_c^2 J_0(2\pi f_d \tau), \tag{C.4}$$

where f_d is the maximum Doppler frequency and σ_c^2 is the variance. The noise term $n(t)$ is white and has a power spectral density of N_0.

The received signal in (C.3) is passed to a matched filter and sampled periodically at a rate of $1/T$, with the sample at $t = nT$ denoted by $r[n]$. Assuming quasi-static fading within one coded-interval, then the received samples $r[2k]$ and $r[2k+1]$ can be written as

$$\mathbf{r}[k] = \begin{bmatrix} r[2k] \\ r[2k+1] \end{bmatrix} = \mathbf{a}[k]\mathbf{c}[k] + \mathbf{n}[k], \tag{C.5}$$

where

$$\mathbf{a}[k] = \begin{bmatrix} a_1[k] & a_2[k] \\ -a_2^*[k] & a_1^*[k] \end{bmatrix} \tag{C.6}$$

is the *k*-th transmitted space-time (ST) symbol,

$$\mathbf{g}[k] = \begin{bmatrix} g_1[k] \\ g_2[k] \end{bmatrix} \tag{C.7}$$

is the channel's gain vector, with $g_i[k] = c_i(2kT)$, and

$$\mathbf{n}[k] = \begin{bmatrix} n_1[k] \\ n_2[k] \end{bmatrix} \tag{C.8}$$

is the filtered noise vector. We impose the (energy) constraint $|a_1[k]|^2 + |a_2[k]|^2 = 2$. Consequently

$$\mathbf{a}[k]\mathbf{a}^H[k] = 2\mathbf{I}_2, \tag{C.9}$$

where $\mathbf{I}_n$ denotes an identity matrix of size *n*. From (C.4), we can deduced that the discrete-time fading processes $g_1[k]$ and $g_2[k]$ have identical autocorrelation function of

$$\phi_g[n] = \frac{1}{2}E\left[g_i[k+n]g_i^*[k]\right] = \phi_c\left(2nT\right). \tag{C.10}$$

The noise terms $n_1[k]$ and $n_2[k]$, on the other hand, are independent and white. Both have a variance of $\sigma_n^2 = N_0$. The bit signal-to-noise ratio (SNR) is defined as

$$\Gamma_b = \frac{1}{n_b}\left(\frac{\sigma_c^2}{N_0}\right), \tag{C.11}$$

where n_b is the number of information bits per *T* second. The bit-error probability (BEP) will be plot against this parameter in the paper.

C. 2 Differential Space-Time Encoding and Detection

C. 2. 1 Differential Encoding Rule

For differential space-time MPSK modulation, the ST data symbol, **b**[*k*], is chosen randomly from a set of matrix symbols

$$S_b = \{\mathbf{B}_1, \mathbf{B}_2, ..., \mathbf{B}_J\}, \tag{C.12}$$

where

$$J = 2^{2n_b} \tag{C.13}$$

and every $\mathbf{B}_i$ has the structure

$$\mathbf{B}_i = \begin{bmatrix} b_{i,1} & b_{i,2} \\ -b_{i,2}^* & b_{i,1}^* \end{bmatrix}, \tag{C.14}$$

with

$$\left|b_{i,1}\right|^2+\left|b_{i,2}\right|^2=1 \tag{C.15}$$

and $b_{i,k}$, $i=1,2,...,J$, $k=1,2$, is either zero or from a MPSK constellation. From (C.14) and (C.15), it is easy to show that

$$\mathbf{B}_i\mathbf{B}_i^H=\mathbf{I}_2, \tag{C.16}$$

and

$$\mathbf{B}_i+\mathbf{B}_i^H=2\,\mathrm{Re}\{b_{i,1}\}\mathbf{I}_2 \tag{C.17}$$

Furthermore, if $\mathbf{A}$ is a matrix that satisfies $\mathbf{A}\mathbf{A}^H=C\mathbf{I}_2$, then the product $(\mathbf{B}_i\mathbf{A})(\mathbf{B}_i\mathbf{A})^H$ also equals $C\mathbf{I}_2$. In other word, the symbol energy remains unchanged when we multiply a unitary symbol by any of the $\mathbf{B}_i$s, as in the case of differential ST encoding. In such a system, the data symbol **a**[k] is obtained from the data symbol **b**[k] according to

$$\mathbf{a}[k]=\mathbf{b}[k]\mathbf{a}[k-1]. \tag{C.18}$$

The symbol set for **a**[k] is denoted by

$$S_a=\{\mathbf{A}_1,\mathbf{A}_2,...,\mathbf{A}_K\}, \tag{C.19}$$

where K is at least as large as J, and $\mathbf{A}_i\mathbf{A}_i^H=2\mathbf{I}_2$ (as defined in (C.9)). If the individual entries in the $\mathbf{A}_i$s are not restricted to a MPSK constellation, it means there is a constellation expansion. Such an expansion usually occurs when we attempt to send $n_b=\log_2 M$ bits per T second.

C. 2. 2 Differential Detection

With differential ST encoding, the received vectors for the (k-1)-th and the k-th coded intervals are

$$\begin{aligned}\mathbf{r}[k]&=\mathbf{b}[k]\mathbf{a}[k-1]\mathbf{c}[k]+\mathbf{n}[k]\\ \mathbf{r}[k-1]&=\mathbf{a}[k-1]\mathbf{c}[k-1]+\mathbf{n}[k-1]\end{aligned} \tag{C.20}$$

The optimal detector computes the metrics

$$\delta_i = 2\,\mathrm{Re}\left\{\mathbf{r}^H[k]\mathbf{B}_i\mathbf{r}[k-1]\right\} = \mathbf{R}^H\mathbf{Q}_i\mathbf{R}, \qquad i = 1,2,...,J, \tag{C.21}$$

where

$$\mathbf{R} = \begin{bmatrix} \mathbf{r}[k] \\ \mathbf{r}[k-1] \end{bmatrix} = \begin{bmatrix} \mathbf{b}[k]\mathbf{a}[k-1] & \mathbf{0}_2 \\ \mathbf{0}_2 & \mathbf{a}[k-1] \end{bmatrix} \begin{bmatrix} \mathbf{c}[k] \\ \mathbf{c}[k-1] \end{bmatrix} + \begin{bmatrix} \mathbf{n}[k] \\ \mathbf{n}[k-1] \end{bmatrix}, \tag{C.22}$$

$$\mathbf{Q}_i = \begin{bmatrix} \mathbf{0}_2 & \mathbf{B}_i \\ \mathbf{B}_i^H & \mathbf{0}_2 \end{bmatrix}, \tag{C.23}$$

and $\mathbf{0}_n$ denotes an all-zero square matrix of size *n*. If δ_j is the largest, then the differential ST detector decision on the data symbol $\mathbf{b}[k]$ is $\hat{\mathbf{b}}[k] = \mathbf{B}_j$.

C. 2. 3 BEP Analysis

When $\mathbf{b}[k] = \mathbf{B}_i$, then a symbol error occurs when $D_{ij} = \delta_i - \delta_j$ is less than zero. The probability that $D_{ij} < 0$ is called is a pair-wise error probability (PEP) and is denoted by P_{ij}. The union bound on the bit-error probability (BEP) is

$$P_b < \frac{1}{2n_b} \times \frac{1}{J} \sum_{i=1}^{J} \sum_{\substack{j=1 \\ j \neq i}}^{J} n_{ij} P_{ij} \tag{C.24}$$

where n_{ij} is the bit error count when $\mathbf{B}_j$ is chosen by the detector instead of the correct symbol $\mathbf{B}_i$, $2n_b$ is the number of information bits per coded interval, and 1/*J* is the probability that $\mathbf{b}[k] = \mathbf{B}_i$. We show in the following how to compute the P_{ij} s.

The random variable $D_{ij} = \delta_i - \delta_j$ is a quadratic form of complex Gaussian vector $\mathbf{R}$ and it can be written as

$$D_{ij} = \mathbf{R}^H\mathbf{F}_{ij}\mathbf{R} \tag{C.25}$$

where

$$\mathbf{F}_{ij} = \mathbf{Q}_i - \mathbf{Q}_j = \begin{bmatrix} \mathbf{0}_2 & \mathbf{\Delta}_{ij} \\ \mathbf{\Delta}_{ij}^H & \mathbf{0}_2 \end{bmatrix}, \tag{C.26}$$

and

$$\mathbf{\Delta}_{ij} = \mathbf{B}_i - \mathbf{B}_j \tag{C.27}$$

It can be easily shown that $\mathbf{\Delta}_{ij}$ has the properties

$$\mathbf{\Delta}_{ij}\mathbf{\Delta}_{ij}^H = d_{ij}^2\mathbf{I}_2 \tag{C.28}$$

and

$$\mathbf{\Delta}_{ij}\mathbf{B}_i^H + \mathbf{B}_i\mathbf{\Delta}_{ij}^H = d_{ij}^2\mathbf{I}_2, \tag{C.29}$$

where $d_{ij}^2 > 0$ is the square distance between ST code symbols $\mathbf{B}_j$ and $\mathbf{B}_i$. This diagonal nature of $\mathbf{\Delta}_{ij}\mathbf{\Delta}_{ij}^H$ and $\mathbf{\Delta}_{ij}\mathbf{B}_i^H + \mathbf{B}_i\mathbf{\Delta}_{ij}^H$ is used in the Appendix to simplify the error analysis substantially.

The characteristic function of the random variable D_{ij} is

$$\Phi_{ij}(s) = \frac{1}{\left|\mathbf{I}_4 + 2s\mathbf{\Phi}_{RR}\mathbf{F}_{ij}\right|} \tag{C.30}$$

where

$$\mathbf{\Phi}_{RR} = \begin{bmatrix} \alpha\mathbf{I}_2 & \beta\mathbf{B}_i \\ \beta\mathbf{B}_i^H & \alpha\mathbf{I}_2 \end{bmatrix}, \tag{C.31}$$

is the covariance matrix of the vector $\mathbf{R}$ in (C.22) conditioned on $\mathbf{b}[k] = \mathbf{B}_i$, and

$$\begin{aligned} \alpha &= 2\sigma_c^2 + N_0 \\ \beta &= 2\sigma_c^2\rho \\ \rho &= J_0\left(4\pi f_d T\right) \end{aligned} \tag{C.32}$$

As shown in the Appendix C-1,

$$\Phi_{ij}(s) = \left[\frac{p_{1,ij}p_{2,ij}}{\left(s - p_{1,ij}\right)\left(s - p_{2,ij}\right)}\right]^2 \tag{C.33}$$

where

$$\begin{bmatrix} p_{1,ij} \\ p_{2,ij} \end{bmatrix} = \frac{\beta \mp \sqrt{\beta^2 + \frac{4}{d_{ij}^2}\left(\alpha^2 - \beta^2\right)}}{4\left(\alpha^2 - \beta^2\right)} \tag{C.34}$$

are the left-plane and right-plane poles. The PEP can be expressed in terms of these poles as

$$P_{ij} = \left[\frac{p_{1,ij}}{p_{1,ij} - p_{2,ij}}\right]^2 \left[1 + 2\frac{p_{2,ij}}{p_{2,ij} - p_{1,ij}}\right] = \left[\frac{1}{2}\left(1 - \frac{1}{\sqrt{1 + \Lambda_{ij}^{-1}}}\right)\right]^2 \left[2 + \frac{1}{\sqrt{1 + \Lambda_{ij}^{-1}}}\right], \tag{C.31}$$

where

$$\begin{aligned} \Lambda_{ij} &= \frac{\beta^2}{4\left(\alpha^2 - \beta^2\right)} d_{ij}^2 \\ &= \frac{\left(n_b \Gamma_b J_0(4\pi f_d T)\right)^2}{\left[2n_b\Gamma_b\left(1 + J_0(4\pi f_d T)\right) + 1\right]\left[2n_b\Gamma_b\left(1 - J_0(4\pi f_d T)\right) + 1\right]} d_{ij}^2 \end{aligned} \tag{C.32}$$

is the effective SNR and Γ_b is the bit SNR defined in (11). The form of this equation is appealing as it separates the effect of the channel from that of the modulation. It indicates that the larger the square distance d_{ij}^2, the larger the effective SNR and hence the smaller the PEP.

When $\Gamma_b \gg 1$ and $f_d = 0$, Λ_{ij} can be approximated as

$$\Lambda_{ij} \approx \left(\frac{n_b d_{ij}^2}{4}\right)\Gamma_b \qquad (\Gamma_b \gg 1, f_d = 0) \tag{C.33}$$

and the PEP as

$$P_{ij} \approx \frac{3}{\left(n_b d_{ij}^2 \Gamma_b\right)^2}. \qquad (\Gamma_b \gg 1, f_d = 0) \tag{C.34}$$

On the other hand, when $\Gamma_b \gg 1$ and $f_d \neq 0$, then

$$\Lambda_{ij} \approx \frac{J_0^2(4\pi f_d T)}{1-J_0^2(4\pi f_d T)}\left(\frac{d_{ij}^2}{4}\right) \qquad (\Gamma_b \gg 1, f_d \neq 0) \tag{C.35}$$

and the irreducible error probability can be calculated accordingly.

Because of the property in (16), the set of square distances is independent of the transmitted pattern $\mathbf{B}_i$. With proper bit assignment, we may be able to make the pairing (n_{ij}, P_{ij}) independent of $\mathbf{B}_i$ too. In this case, the union bound of the BEP can be obtained by considering any transmitted pattern.

C. 3 Code Examples

C. 3. 1 BPSK, $n_b = 1/2$

The transmitted symbol set and the data symbol set of this code are

$$S_a = \left\{ \mathbf{A}_1 = \begin{bmatrix} +1 & +1 \\ -1 & +1 \end{bmatrix}, \mathbf{A}_2 = \begin{bmatrix} -1 & -1 \\ +1 & -1 \end{bmatrix} \right\} \tag{C.36}$$

and

$$S_b = \left\{ \mathbf{B}_1 = \begin{bmatrix} +1 & 0 \\ 0 & +1 \end{bmatrix}, \mathbf{B}_2 = \begin{bmatrix} -1 & 0 \\ 0 & -1 \end{bmatrix} \right\} \tag{C.37}$$

respectively. It is obvious that $\mathbf{B}_i\mathbf{B}_j \in S_b$ and $\mathbf{B}_i\mathbf{A}_j \in S_a$. Furthermore, $d_{12}^2 = 4$ and $n_{12} = 1$. Consequently the BEP of this simple code is

$$P_b = P_{12},$$

(BPSK, $n_b = 1/2$)

$$\Lambda_{12} = \frac{\left(\Gamma_b J_0(4\pi f_d T)\right)^2}{\left[\Gamma_b\left(1+J_0(4\pi f_d T)\right)+1\right]\left[\Gamma_b\left(1-J_0(4\pi f_d T)\right)+1\right]}, \tag{C.38}$$

where Λ_{12} is the effective SNR that appears in P_{12}. With static fading and a large channel SNR , Λ_{12} is approximately $\Gamma_b/2$, which is half that seen in a ST-BPSK system with perfect channel state information (CSI). The BEP of this ideal system is

$$P_b = \left[\frac{1}{2}\left(1-\sqrt{\frac{1}{1+\Gamma_b^{-1}}}\right)\right]^2\left[2+\sqrt{\frac{1}{1+\Gamma_b^{-1}}}\right], \qquad \text{(BPSK, perfect CSI)} \tag{C.39}$$

C. 3. 2 BPSK $n_b = 1$

The data symbols of this code is chosen from the set

$$S_b = \left\{\mathbf{B}_1 = \begin{bmatrix}+1 & 0\\ 0 & +1\end{bmatrix}, \mathbf{B}_2 = \begin{bmatrix}-1 & 0\\ 0 & -1\end{bmatrix}, \mathbf{B}_3 = \begin{bmatrix}0 & -1\\ +1 & 0\end{bmatrix}, \mathbf{B}_4 = \begin{bmatrix}0 & +1\\ -1 & 0\end{bmatrix}\right\} \tag{C.40}$$

while the transmitted symbols are from the set

$$S_a = \left\{\mathbf{A}_1 = \begin{bmatrix}+1 & +1\\ -1 & +1\end{bmatrix}, \mathbf{A}_2 = \begin{bmatrix}-1 & -1\\ +1 & -1\end{bmatrix}, \mathbf{A}_3 = \begin{bmatrix}+1 & -1\\ +1 & +1\end{bmatrix}, \mathbf{A}_4 = \begin{bmatrix}-1 & +1\\ -1 & -1\end{bmatrix}\right\}. \tag{C.41}$$

The detail encoding rule, with bit-assignment, is given in the table below

Input (bit assignment)	Previous Output / Current Output			
	$\mathbf{A}_1$	$\mathbf{A}_2$	$\mathbf{A}_3$	$\mathbf{A}_4$
$\mathbf{B}_1$ (0,0)	$\mathbf{A}_1$	$\mathbf{A}_2$	$\mathbf{A}_3$	$\mathbf{A}_4$
$\mathbf{B}_2$ (1,1)	$\mathbf{A}_2$	$\mathbf{A}_1$	$\mathbf{A}_4$	$\mathbf{A}_3$
$\mathbf{B}_3$ (1,0)	$\mathbf{A}_3$	$\mathbf{A}_4$	$\mathbf{A}_2$	$\mathbf{A}_1$
$\mathbf{B}_4$ (0,1)	$\mathbf{A}_4$	$\mathbf{A}_3$	$\mathbf{A}_1$	$\mathbf{A}_2$

Table C.1: Differential encoding rule for ST-BPSK, $n_b = 1$.

As in the case of the $n_b = 1/2$ BPSK code, the $\mathbf{B}_i$s forms a group under multiplication. Furthermore, the sizes of S_a and S_b are identical.

It can be verified that for any given data symbol, there is always 1 error event of square distance $d_{12}^2 = 4$ with $n_{12} = 2$ erroneous bits, and 2 events of square distance $d_{13}^2 = 2$ with $n_{12} = 1$ erroneous bit. Consequently, the BEP is upper-bounded by

$$P_b = P_{12} + P_{13},$$

(BPSK, $n_b = 1$) (C.42)

$$\Lambda_{1j} = \frac{\left(\Gamma_b J_0(4\pi f_d T)\right)^2}{\left[2\Gamma_b\left(1+J_0(4\pi f_d T)\right)+1\right]\left[2\Gamma_b\left(1-J_0(4\pi f_d T)\right)+1\right]} d_{1j}^2,$$

The dominant error event has an effective SNR of $\Lambda_{13} = \Gamma_b / 2$ in the static fading channel. So this BPSK code is also approximately 3 dB worse than BPSK with ideal CSI.

C. 3. 3 QPSK, $n_b = 3/2$

The transmitted symbol set and the data symbol set are respectively

$$S_b \to \left\{ \begin{array}{l} \mathbf{B}_1 = \begin{bmatrix} +1 & 0 \\ 0 & +1 \end{bmatrix}, \mathbf{B}_2 = \begin{bmatrix} -1 & 0 \\ 0 & -1 \end{bmatrix}, \mathbf{B}_3 = \begin{bmatrix} 0 & -1 \\ +1 & 0 \end{bmatrix}, \mathbf{B}_4 = \begin{bmatrix} 0 & +1 \\ -1 & 0 \end{bmatrix} \\ \mathbf{B}_5 = \begin{bmatrix} +j & 0 \\ 0 & -j \end{bmatrix}, \mathbf{B}_6 = \begin{bmatrix} -j & 0 \\ 0 & +j \end{bmatrix}, \mathbf{B}_7 = \begin{bmatrix} 0 & -j \\ -j & 0 \end{bmatrix}, \mathbf{B}_8 = \begin{bmatrix} 0 & +j \\ +j & 0 \end{bmatrix} \end{array} \right\} \quad \text{(C.43)}$$

The transmitted symbol, $\mathbf{a}[k] = \mathbf{b}[k]\mathbf{a}[k-1]$, is from the set

$$S_a \to \left\{ \begin{array}{l} \mathbf{A}_1 = \begin{bmatrix} +1 & +1 \\ -1 & +1 \end{bmatrix}, \mathbf{A}_2 = \begin{bmatrix} +1 & +j \\ +j & +1 \end{bmatrix}, \mathbf{A}_3 = \begin{bmatrix} +1 & -1 \\ +1 & +1 \end{bmatrix}, \mathbf{A}_4 = \begin{bmatrix} +1 & -j \\ -j & +1 \end{bmatrix} \\ \mathbf{A}_5 = \begin{bmatrix} +j & +1 \\ -1 & -j \end{bmatrix}, \mathbf{A}_6 = \begin{bmatrix} +j & +j \\ +j & -j \end{bmatrix}, \mathbf{A}_7 = \begin{bmatrix} +j & -1 \\ +1 & -j \end{bmatrix}, \mathbf{A}_8 = \begin{bmatrix} +j & -j \\ -j & -j \end{bmatrix} \\ \mathbf{A}_9 = \begin{bmatrix} -1 & +1 \\ -1 & -1 \end{bmatrix}, \mathbf{A}_{10} = \begin{bmatrix} -1 & +j \\ +j & -1 \end{bmatrix}, \mathbf{A}_{11} = \begin{bmatrix} -1 & -1 \\ +1 & -1 \end{bmatrix}, \mathbf{A}_{12} = \begin{bmatrix} -1 & -j \\ -j & -1 \end{bmatrix} \\ \mathbf{A}_{13} = \begin{bmatrix} -j & +1 \\ -1 & +j \end{bmatrix}, \mathbf{A}_{14} = \begin{bmatrix} -j & +j \\ +j & +j \end{bmatrix}, \mathbf{A}_{15} = \begin{bmatrix} -j & -1 \\ +1 & +j \end{bmatrix}, \mathbf{A}_{16} = \begin{bmatrix} -j & -j \\ -j & +j \end{bmatrix} \end{array} \right\} \quad \text{(C.44)}$$

The differential encoding rule and bit assignments are shown in Table C.2 on the next page.

It is observed from the Table that the $\mathbf{B}_i$s forms a group under multiplication. However, the sizes of S_a and S_b are NOT identical. There is no signal expansion though, as all the entries in the $\mathbf{A}_j$s are from a QPSK constellation.

Input	Previous Output / Index of Current Output															
	A_1	A_2	A_3	A_4	A_5	A_6	A_7	A_8	A_9	A_{10}	A_{11}	A_{12}	A_{13}	A_{14}	A_{15}	A_{16}
B_1 (000)	1	2	3	4	5	6	7	8	9	10	11	12	13	14	15	16
B_2 (111)	11	12	9	10	15	16	13	14	3	4	1	2	7	8	5	6
B_3 (001)	3	15	11	7	2	14	10	6	1	13	9	5	4	16	12	8
B_4 (110)	9	5	1	13	12	8	4	16	11	7	3	15	10	6	2	14
B_5 (011)	6	7	8	5	10	11	12	9	14	15	16	13	2	3	4	1
B_6 (100)	16	13	14	15	4	1	2	3	8	5	6	7	12	9	10	11
B_7 (010)	8	4	16	12	7	3	15	11	6	2	14	10	5	1	13	9
B_8 (101)	14	10	6	2	13	9	5	1	16	12	8	4	15	11	7	3

Table C.2: Differential encoding rule for ST-QPSK, $n_b = 3/2$.

It can be shown that no matter which data symbol is sent, there is always 1 error event of square distance $d_{12}^2 = 4$ with $n_{12} = 2$ erroneous bits, 3 events of square distance $d_{13}^2 = 2$ with $n_{13} = 1$ erroneous bit, and 3 events of square distance $d_{14}^2 = 2$ with $n_{14} = 2$ erroneous bits. Consequently, the BEP is upper-bounded by

$$P_b = P_{12} + P_{13},$$

(QPSK, $n_b = 3/2$)

$$\Lambda_{1j} = \frac{\left(3\Gamma_b J_0(4\pi f_d T)\right)^2}{4\left[3\Gamma_b\left(1+J_0(4\pi f_d T)\right)+1\right]\left[3\Gamma_b\left(1-J_0(4\pi f_d T)\right)+1\right]} d_{1j}^2,$$

(C.45)

The dominant error event has an effective SNR of $\Lambda_{13} = 3\Gamma_b/4$ in the static fading channel. So this BPSK code is also approximately 1.25 dB worse the BPSK with ideal CSI. Since ideal QPSK has the same BEP as ideal BPSK, so this particular differential ST-QPSK scheme is also 1.25 dB worse than its ideal counterpart.

C. 3. 4 QPSK, $n_b = 2$

The random data symbols are from the set

$$S_b \square \begin{Bmatrix} \mathbf{B}_1, & \mathbf{B}_2, & \mathbf{B}_3, & \mathbf{B}_4, \\ \mathbf{B}_5, & \mathbf{B}_6, & \mathbf{B}_7, & \mathbf{B}_8, \\ \mathbf{B}_9, & \mathbf{B}_{10}, & \mathbf{B}_{11}, & \mathbf{B}_{12}, \\ \mathbf{B}_{13}, & \mathbf{B}_{14}, & \mathbf{B}_{15}, & \mathbf{B}_{16}, \end{Bmatrix}$$

$$\square \begin{Bmatrix} \frac{1}{2}\begin{bmatrix} 1+j & 1+j \\ -1+j & 1-j \end{bmatrix}, \frac{1}{2}\begin{bmatrix} 1+j & 1-j \\ -1-j & 1-j \end{bmatrix}, \frac{1}{2}\begin{bmatrix} 1+j & -1-j \\ 1-j & 1-j \end{bmatrix}, \frac{1}{2}\begin{bmatrix} 1+j & -1+j \\ 1+j & 1-j \end{bmatrix} \\ \frac{1}{2}\begin{bmatrix} 1-j & 1+j \\ -1+j & 1+j \end{bmatrix}, \frac{1}{2}\begin{bmatrix} 1-j & 1-j \\ -1-j & 1+j \end{bmatrix}, \frac{1}{2}\begin{bmatrix} 1-j & -1-j \\ 1-j & 1+j \end{bmatrix}, \frac{1}{2}\begin{bmatrix} 1-j & -1+j \\ 1+j & 1+j \end{bmatrix} \\ \frac{1}{2}\begin{bmatrix} -1-j & 1+j \\ -1+j & -1+j \end{bmatrix}, \frac{1}{2}\begin{bmatrix} -1-j & 1-j \\ -1-j & -1+j \end{bmatrix}, \frac{1}{2}\begin{bmatrix} -1-j & -1-j \\ 1-j & -1+j \end{bmatrix}, \frac{1}{2}\begin{bmatrix} -1-j & -1+j \\ 1+j & -1+j \end{bmatrix} \\ \frac{1}{2}\begin{bmatrix} -1+j & 1+j \\ -1+j & -1-j \end{bmatrix}, \frac{1}{2}\begin{bmatrix} -1+j & 1-j \\ -1-j & -1-j \end{bmatrix}, \frac{1}{2}\begin{bmatrix} -1+j & -1-j \\ 1-j & -1-j \end{bmatrix}, \frac{1}{2}\begin{bmatrix} -1+j & -1+j \\ 1+j & -1-j \end{bmatrix} \end{Bmatrix}$$

(C.46)

The bit-assignments are:

$$\begin{array}{llll} \mathbf{d}_1 = [0,0,0,0] & \mathbf{d}_2 = [0,0,0,1] & \mathbf{d}_3 = [0,0,1,1] & \mathbf{d}_4 = [0,0,1,0] \\ \mathbf{d}_5 = [0,1,0,0] & \mathbf{d}_6 = [0,1,0,1] & \mathbf{d}_7 = [0,1,1,1] & \mathbf{d}_6 = [0,1,1,0] \\ \mathbf{d}_9 = [1,1,0,0] & \mathbf{d}_{10} = [1,1,0,1] & \mathbf{d}_{10} = [1,1,1,1] & \mathbf{d}_{12} = [1,1,1,0] \\ \mathbf{d}_{13} = [1,0,0,0] & \mathbf{d}_{14} = [1,0,0,1] & \mathbf{d}_{15} = [1,0,1,1] & \mathbf{d}_{16} = [1,0,1,0] \end{array}$$

It can be verified that there are 4, 6,4, and 1 error events of square distances $d_{1,2}^2 = 1$, $d_{1,3}^2 = 2$, $d_{1,7}^2 = 3$, $d_{1,10}^2 = 4$, and error counts $n_{1,2} = 1$, $n_{1,3} = 2, n_{1,7} = 3$, $n_{1,10} = 4$ respectively. This means the BEP has the upper-bound:

$$P_b = P_{1,2} + \left(\tfrac{3}{2}\right) P_{1,3} + P_{1,7} + \left(\tfrac{1}{4}\right) P_{1,10},$$

(QPSK, $n_b = 2$)

$$\Lambda_{1j} = \frac{4\left(\Gamma_b J_0(4\pi f_d T)\right)^2}{\left[4\Gamma_b\left(1+J_0(4\pi f_d T)\right)+1\right]\left[4\Gamma_b\left(1-J_0(4\pi f_d T)\right)+1\right]} d_{1j}^2,$$

(C.47)

The worse case effective SNR (with static fading) is $\Gamma_b / 2$. So again, this scheme is 3 dB worse than ideal BPSK and ideal QPSK.

Appendix C-1

Derivation of (C.33)

We show in this Appendix the characteristic function $\Phi_{ij}(s)$ takes the form shown in (C.33) and (C.34). To begin, we note that

$$\begin{aligned}\left|\mathbf{I}_4+2s\boldsymbol{\Phi}_{RR}\mathbf{F}_{ij}\right| &\equiv \left|\left(\mathbf{I}_4+2s\boldsymbol{\Phi}_{RR}\mathbf{F}_{ij}\right)\mathbf{F}_{ij}^H\right| \Big/ \left|\mathbf{F}_{ij}^H\right| \\ &= \left|\begin{pmatrix}\mathbf{0}_2 & \boldsymbol{\Delta}_{ij}\\ \boldsymbol{\Delta}_{ij}^H & \mathbf{0}_2\end{pmatrix}+2sd_{ij}^2\begin{pmatrix}\alpha\mathbf{I}_2 & \beta\mathbf{B}_i\\ \beta\mathbf{B}_i^H & \alpha\mathbf{I}_2\end{pmatrix}\right| \Big/ \left|\begin{pmatrix}\mathbf{0}_2 & \boldsymbol{\Delta}_{ij}\\ \boldsymbol{\Delta}_{ij}^H & \mathbf{0}_2\end{pmatrix}\right| \\ &= \left|\begin{pmatrix}2sd_{ij}^2\alpha\mathbf{I}_2 & 2sd_{ij}^2\beta\mathbf{B}_i+\boldsymbol{\Delta}_{ij}\\ 2sd_{ij}^2\beta\mathbf{B}_i^H+\boldsymbol{\Delta}_{ij}^H & 2sd_{ij}^2\alpha\mathbf{I}_2\end{pmatrix}\right| \Big/ \left|\begin{pmatrix}\mathbf{0}_2 & \boldsymbol{\Delta}_{ij}\\ \boldsymbol{\Delta}_{ij}^H & \mathbf{0}_2\end{pmatrix}\right|\end{aligned} \tag{C.48}$$

But

$$\begin{aligned}&\left|\begin{pmatrix}2sd_{ij}^2\alpha\mathbf{I}_2 & 2sd_{ij}^2\beta\mathbf{B}_i+\boldsymbol{\Delta}_{ij}\\ 2sd_{ij}^2\beta\mathbf{B}_i^H+\boldsymbol{\Delta}_{ij}^H & 2sd_{ij}^2\alpha\mathbf{I}_2\end{pmatrix}\right| \\ &= \left|2sd_{ij}^2\alpha\mathbf{I}_2\right|\cdot\left|2sd_{ij}^2\alpha\mathbf{I}_2-\left(2sd_{ij}^2\beta\mathbf{B}_i^H+\boldsymbol{\Delta}_{ij}^H\right)\left(2sd_{ij}^2\alpha\mathbf{I}_2\right)^{-1}\left(2sd_{ij}^2\beta\mathbf{B}_i+\boldsymbol{\Delta}_{ij}\right)\right| \\ &= \left(2sd_{ij}^2\alpha\right)^2\left|2sd_{ij}^2\alpha\mathbf{I}_2-\frac{\left(2sd_{ij}^2\beta\right)^2\mathbf{I}_2+\boldsymbol{\Delta}_{ij}^H\boldsymbol{\Delta}_{ij}+2sd_{ij}^2\beta\left(\boldsymbol{\Delta}_{ij}^H\mathbf{B}_i+\mathbf{B}_i^H\boldsymbol{\Delta}_{ij}\right)}{\left(2sd_{ij}^2\alpha\right)}\right| \\ &= \left(2sd_{ij}^2\alpha\right)^2\left|2sd_{ij}^2\alpha\mathbf{I}_2-\frac{\left(2sd_{ij}^2\beta\right)^2+d_{ij}^2+\left(2sd_{ij}^2\beta\right)d_{ij}^2}{\left(2sd_{ij}^2\alpha\right)}\mathbf{I}_2\right| \\ &= \left\{4d_{ij}^4\left(\alpha^2-\beta^2\right)s^2-2\beta d_{ij}^4 s-d_{ij}^2\right\}^2\end{aligned} \tag{C.49}$$

and

$$\left|\begin{pmatrix}\mathbf{0}_2 & \boldsymbol{\Delta}_{ij}\\ \boldsymbol{\Delta}_{ij}^H & \mathbf{0}_2\end{pmatrix}\right| = \left|\begin{pmatrix}\mathbf{0}_2 & \boldsymbol{\Delta}_{ij}\\ \boldsymbol{\Delta}_{ij}^H & \mathbf{0}_2\end{pmatrix}\begin{pmatrix}\mathbf{0}_2 & \mathbf{I}_2\\ \mathbf{I}_2 & \mathbf{0}_2\end{pmatrix}\right| \Big/ \left|\begin{pmatrix}\mathbf{0}_2 & \mathbf{I}_2\\ \mathbf{I}_2 & \mathbf{0}_2\end{pmatrix}\right| = \left|\begin{pmatrix}\boldsymbol{\Delta}_{ij} & \mathbf{0}_2\\ \mathbf{0}_2 & \boldsymbol{\Delta}_{ij}^H\end{pmatrix}\right| = d_{ij}^4 \tag{C.50}$$

Substituting (C.49) and (C.50) into (C.48) yields

$$\left|\mathbf{I}_4 + 2s\boldsymbol{\Phi}_{RR}\mathbf{F}_{ij}\right| = \left\{4d_{ij}^2\left(\alpha^2-\beta^2\right)s^2 - 2\beta d_{ij}^2 s - 1\right\}^2 .$$

Consequently,

$$\Phi_{ij}(s) = \left[\frac{-4d_{ij}^2\left(\alpha^2-\beta^2\right)}{s^2 - \dfrac{\beta}{2\left(\alpha^2-\beta^2\right)}s - \dfrac{1}{4\left(\alpha^2-\beta^2\right)d_{ij}^2}}\right]^2 = \left[\frac{p_{1,ij}p_{2,ij}}{\left(s-p_{1,ij}\right)\left(s-p_{2,ij}\right)}\right]^2 \qquad \text{(C.51)}$$

as shown in (C.33) and (C.34).

Bibliography

[1] W. C. Jakes. *Microwave Mobile Communications.* New York: Wiley, 1974,

[2] W. C. Y. Lee. *Mobile Communications Engineering, Second Edition.* New York: McGraw-Hill, 1998,

[3] John G. Proakis. *Digital communications, Fourth Edition,* McGraw-Hill, Inc., New York, 2001

[4] Pooi Yuen Kam. "Binary orthogonal signaling over the Gaussian channel with unknown phase/fading: new results and interpretations", *IEEE Trans. Commun.*, vol. 38, no. 10, pp. 1686 - 1692, Oct. 1990

[5] D. G. Brennan. "Linear Diversity Combining Techniques," *Proc. IEEE,* vol. 91, No 2, Feb. 2003

[6] Thomas Eng, Ning Kong and Laurence B. Milstein. "Comparison of Diversity Combining Techniques for Rayleigh-Fading Channels", *IEEE Trans. Commun.*, vol. 44, No. 9, pp. 1117-1129, September 1996

[7] F. Adachi, K. Ohno and M. Ikura. "Post-detection selection diversity reception with correlated, unequal average power Rayleigh fading signals for pi/4 shift QDPSK mobile radio"*, IEEE Trans. Veh. Techno.,* vol. 41, no. 2, May 1992, pp. 199-210

[8] Pooi Yuen Kam. "Bit Error Probabilities of MDPSK Over the Nonselective Rayleigh Fading Channel with Diversity Reception", *IEEE Trans. Commun*., vol. 39, No. 2, pp. 220-224, Feb., 1991

[9] Pooi Yuen Kam, Thian Ping Soh Chun Sum Ng. "Further Results on the Bit Error Probabilities of MDPSK Over the Nonselective Rayleigh Fading Channel

with Diversity Reception" *IEEE Trans. Commun.*, vol. 43, No. 11, pp. 2732-2741, Nov., 1995

[10] Yao Ma and Teng Joon Lim. "Bit Error Probability for MDPSK and NCFSK over Arbitrary Rician Fading Channels" *IEEE J. on Selected Areas in Commun*. vol. 18, No. 11, Nov. 2000

[11] Ranjan K. Mallik and Moe Z. Win. "Error Probability of Binary NFSK and DPSK with Postdetection Combining over Correlated Rician Channels" *IEEE Trans. On Commun*. vol. 48, No. 12, Dec. 2000

[12] Y. C. Chow, J. P. McGreehan and A. R. Nix. "Simplified Error Bound Analysis for M-DPSK in Fading Channels with Diversity Reception" *IEE Proc. Commun*., vol. 141, No. 5, pp. 341-350, Oct. 1994

[13] Mahesh K. Varanasi. "A Systematic Approach to the Design and Analysis of Optimum DPSK Receivers for Generalized Diversity Communications over Rayleigh Fading Channels" *IEEE Trans. Commun*. vol. 47, No.9 September 1999

[14] Milica S and Zoran Z. "Differentially Coherent Diversity Combing Techniques for DPSK Over Fast Rayleigh Fading Channels" *IEEE Trans. On Veh*. vol. 49, No.5 September 2000

[15] J. W. Craig. "A new, simple and exact result for calculating the probability of error for two-dimensional signal constellations" *IEEE MILCOM'91 Conf. Rec*., Boston, MA, 1991, pp. 25.5.1-25.5.5

[16] Marvin K. Simon and Dariush Divsalar. "Some New Twists to Problems Involving the Gaussian Probability Integral" *IEEE Trans. on Commun*. vol. 46, No. 2, Feb. 1998

[17] Marvin K. Simon. "A New Twist on the Marcum Q-Function and Its Application" *IEEE Commun. Letters*, vol. 2, No. 2, Feb.1998

[18] Marvin K. Simon and Mohamed slim Alouini. *Digital communication over Fading Channels, John Wiley & sons, Inc., New York, 2000*

[19] J. H. Winters. "Optimum combining in digital mobile radio with cochannel interference" *IEEE Trans. Veh. Tech.*, vol. VT-33, pp. 144-155, Aug 1984

[20] M. Chiani, M. Win A. Zanella and J. H. Winter. "Exact symbol error probability for optimum combining in the presence of multiple co-channel interferers and thermal noise," *IEEE GLOBECOM,* vol. 2, pp. 1182 -1186, 2001

[21] C. Chayawan and V. A. Aalo. "On the outage probability of optimum combining and maximal ratio combining schemes in an interference-limited rice fading channel," *IEEE Trans. Common.*, vol. 50, No. 4, pp. 532-535, Apr. 2002

[22] T. D. Pham and K. G. Balmain. "Multipath performance of adaptive antennas with multiple interferers and correlated fading," *IEEE Trans. Veh. Tech.*, vol. 48, No. 2, pp. 342-352. Mar. 1999

[23] Eric Villier. "Performance Analysis of Optimum Combining With Multiple Interferers in Flat Rayleigh Fading" *IEEE Trans. Commun*. vol. 47, No. 10, Oct 1999

[24] Y. Ma, T. J. Lim and S. Pasupathy. "Error probability for coherent and differential PSK over arbitrary Rician fading channels with multiple cochannel interferers," *IEEE Trans. Commun.*, vol. 50, No. 3, pp.429-441, Mar. 2002

[25] V. A. Aalo and J. Zhang. "Performance analysis of maximal ratio combining in the presence of multiple equal-power cochannel interferers in a Nakagami fading channel," *IEEE Trans. Vhe. Tech.*, vol. 50, No. 2, pp. 497-503, Mar. 2001

[26] A. Shah and A. M. Haimovich. "Performance analysis of maximal ratio combining and comparison with optimum combining for mobile radio communications with cochannel interference," *IEEE Trans. Veh. Tech.*, vol. 49, No. 4, pp.1454-1463, July 2000

[27] C. Chayawan and C. A. Aalo. "Performance study of MRC systems with multiple cochannel interference in a non-Gaussian multipath fading environment," *VTC,. Proc*., vol. 3, pp. 24-28 Sep. 2002

[28] J. Cui and A. U. H. Sheikh. "Outage probability of cellular radio systems using maximal ratio combining in the presence of multiple interferers," *IEEE Trans. Commun.*, vol. 47, No. 8, pp.1121-1124, Aug. 1999

[29] M. Chiani. "Analytical distribution of linearly modulated cochannel interferers," *IEEE Trans. Commun*., vol. 45, pp. 73-79, Jan. 1997

[30] M. Chiani. "Performance of BPSK and GMSK with multiple cochannel interferers" *PIMRC. IEEE*, vol. 3, Oct. 1996

[31] M. Chiani. "Statistical analysis of asynchronous QPSK cochannel interference," *GLOBECOM IEEE*, vol. 2, pp. 1855 -1859 Nov., 2002

[32] K. A. Hamdi. "Exact probability of error of BPSK communication links subjected to asynchronous interference in Rayleigh fading environment," *IEEE Trans. Commun.*, vol. 50, No. 10 pp. 1577-1579, Oct. 2002

[33] K. A. Hamdi. "DPSK Exact Bit Error Rates With Unsynchronized Slowly Fading Interferers," *IEEE Trans. Veh. Tech*, vol. 52, No. 6, Nov, 2003

[34] N. C. Beaulieu. "Precise Error Rate Analysis of Bandwidth Efficient BPSK in Nakagami Fading and Cochannel Interference," *IEEE Trans. On Commun*., vol. 52, pp.149-158, Jan. 2004

[35] F. Adachi and M. Sawahashi. "Error Rate Analysis of MDPSK/CPSK with Diversity Reception Under Very Slow Rayleigh Fading and Cochannel Interference" *IEEE Trans. Veh. Tech.*, vol. 43, No. 2, pp.252-262, May 1994

[36] A. A. Abu-Dayya and N. C. Beaulieu. "Diversity pi/4-DQPSK on Microcellular Interference Channels," *IEEE Trans. Commun.*, vol. 44, No. 10, Oct, 1996

[37] V. Tralli and R. Verdone. "Performance characterization of digital transmission systems with cochannel interference," *IEEE Trans. Veh. Tech.*, vol. 48, No. 3, May 1999

[38] S. Verdu . *Multiuser Detection. New York: Cambridge University Press, 1998*

[39] S. J. Grantand and J. K. Cavers. "Performance enhancement through joint detection of cochannel signals using diversity arrays", *IEEE Trans. Commun*, vol. 46, pp.1038 – 1049, Aug. 1998

[40] S. J. Grantand and J. K. Cavers. "Further analytical results on the joint detection of cochannel signals using diversity arrays", *IEEE Trans. Commun*,, vol. 48, pp. 1788 – 1792, Nov. 2000

[41] R. Kwan and C. Leung. "Optimal detection of a BPSK signal contaminated by interference and noise," *IEEE Commun. Lett.,* vol. 6., pp. 225-227, Jun. 2002

[42] T. V. Poon and N. C. Beaulieu. "Jointly and individually optimum receivers for BPSK signals in cochannel interference plus noise," *PACRIM,* vol. 2, pp. 28-30, Aug. 2003

[43] T. V. Poon and N. C. Beaulieu. "Performance analysis of a jointly optimal BPSK receiver in cochannel interference,*" Proc. IEEE GlobeCom. Conf.,* pp. 1721-1725, 2003

[44] T. K. Y. Lo. "Maximum ratio transmission," *IEEE Trans. Commun.*, vol. 47, pp. 1458-1461, Oct. 1999

[45] X. Feng and C. Leung. "A new optimal transmit and receive diversity scheme," in *Proc. PACRIM.* vol. 2, pp. 26-28, Aug. 2001

[46] P. Fan, Z. Cao and X. Xia. "Improved weighting vector selection method in maximum ratio transmission over flat Rayleigh fading channels," *ICSP.* vol. 2, pp. 26-30, Aug. 2002

[47] C.-H. Tse, K.-W. Yip and T. S. Ng. "Performance tradeoffs between maximum ratio transmission and switched-transmit diversity," in *Proc. PIMRC.* pp. 1485-1489, Sep. 2000

[48] P. A. Dighe, R. K. Mallik and S. S. Jamuar. "Analysis of transmit-receive diversity in Rayleigh fading," *IEEE Trans. Commun.*., vol. 51, pp. 694-703, Apr. 2003

[49] M. Kang and M. S. Alouini. "Largest Eigenvalue of complex Wishart matrices and performance analysis of MIMO MRC system," *IEEE J. Sel. Area Commun.*, vol. 21, pp. 418-426, Apr. 2003

[50] V. Tarokh, N. Seshadri, and A. R. Calderbank, "Space-time codes for high data rate wireless communications: Performance analysis and code construction," *IEEE Trans. Inform. Theory*, vol. 44, pp. 744-765, Mar. 1998

[51] V. Tarokh, A. Naguib, N. Seshadri, and A. R. Calderbank, "Space-time codes for high data rate wireless communications: Performance criteria in the presence of channel estimation errors, mobility and multiple paths," *IEEE Trans. Commun*, vol. 47, pp. 199-207, Feb. 1999

[52] S. M. Alamouti, "A simple transmitter diversity scheme for wireless communications," *IEEE J. Select. Areas Commun.* Vol. 16, pp. 1451-1458, Oct. 1998

[53] V. Tarokh, H. Jafarkhani, and A. R. Calderbank, “Space-time block codes from orthogonal designs,” *IEEE Trans. Inform. Theory,* vol. 45, pp. 1456-1467, Jul. 1999

[54] V. Tarokh, and H. Jafarkhani, “A differential detection scheme for transmit diversity,” *IEEE J. Select. Areas Commun.* vol. 18, pp.1169-1174, Jul. 2000

[55] N. C. Beaulieu, C. C. Tan and M. O. Damen. "A "Better than" Nyquist pulse," *IEEE Commun. Lett.*, vol. 5, pp. 367-368, Sept. 2001

[56] Athanasios Papoulis. *Probability, Random Variables, and Stochastic Processes, Third Edition, McGraw-Hill, Inc. New York 1991*

[57] Adnan A. Abu-Dayya and Norman C. Beaulieu. "Diversity MPSK Receivers in Cochannel Interference" *IEEE Trans. Veh. Tech.* vol. 48, No. 6, Nov 1999

[58] J. K. Cavers. "An analysis of pilot symbol assisted modulation for Rayleigh fading channels," *IEEE Trans. Veh. Tech.*, vol. 40, pp. 686-693, Nov. 1991

[59] Pooi Yuen Kam. "Bit-Error Probabilities of 2 and 4DPSK with Nonselective Rayleigh Fading, Diversity Reception, and Correlated Gaussian Interference" *IEEE Trans. Commun.*, vol. 45, No. 4, pp. 400-403, Apr., 1997

[60] T. T. Tjhung F. Adachi. "Distribution of phase angle between two Rayleigh vectors perturbed by Gaussian noise", *Elect. Lett.*, vol. 28, Iss. 10, pp. 923 - 925, 7 May 1992

[61] A. M. Mathai and Serge B. Provost. *Quadratic forms in random variables: theory and applications.* New York : M. Dekker , 1992

[62] K. C. Hwang and K. B. Lee, “Efficient Weight Vector Representation for Closed-Loop Transmit Diversity,” *IEEE Trans. Commons,* vol. 52, No. pp. 9-16, Jan 2004

[63] A. T. James. "Distributions of matrix variates and latent roots derived from normal samples," *Ann. Math. Statist.*, vol. 35, pp. 475-501, 1964

[64] R. A. Horn and C. R. Johnson. *Matrix Analysis,* 1st ed. Cambridge, U.K.: Cambridge Univ. Press, 1985

[65] M. Chiani, M. Z. Win and A. Zanella. "On the capacity of spatially correlated MIMO Rayleigh-fading channels," *IEEE Trans. Info. Theory* vol. 49, pp. 2363-2371, Oct. 2003

[66] Pooi Yuen Kam. "Generalized Quadratic Receivers for Orthogonal Signals Over the Gaussian Channel with Unknown Phase/Fading", *IEEE Trans. Commun.*, vol. 43, no. 6, pp. 2050 - 2059, Jun. 1995

[67] B. L. Hughes, "Differential Space-Time Modulation," *IEEE Trans. Info. Theo*. vol. 46, No. 7 pp. 2567-2578, Nov. 2000

[68] H. Jafarkhani, and V. Tarokh, "Multiple Transmit Antenna Differential Detection From Generalized Orthgonal Design," *IEEE Trans. Info. Theo.* vol. 47, No. 6, pp 2626-2631, Sep. 2001

[69] M. K. Simon, "Single Integral Representations of Certain Integer Powers of the Gaussian Q-Function and Their Application," *IEEE Common. Lett.* vol. 6, pp. 532-534, Dec. 2002

[70] S. Verdú, *Multiuser Detection.* New York: Cambridge University Press, 1998.

[71] P. Ho *et.al* "Performance analysis of differential space-time block codes in fast fading channels", in preparation.